



University
of Glasgow

Williams, Jamie John Lewis (2012) *Identification of substrates for the EPAC1-inducible E3 ubiquitin ligase component SOCS3*. PhD thesis.

<http://theses.gla.ac.uk/4013/>

Copyright and moral rights for this thesis are retained by the author

A copy can be downloaded for personal non-commercial research or study

This thesis cannot be reproduced or quoted extensively from without first obtaining permission in writing from the Author

The content must not be changed in any way or sold commercially in any format or medium without the formal permission of the Author

When referring to this work, full bibliographic details including the author, title, awarding institution and date of the thesis must be given

**Identification of substrates for the Epac1-inducible E3
ubiquitin ligase component SOCS3**

Jamie John Lewis Williams

B.Sc. (Hons) Molecular & Cellular Biology

Submitted in fulfilment of requirements for the Degree of Doctor of Philosophy

Institute of Cardiovascular and Medical Sciences

College of Medical, Veterinary and Life Sciences

University of Glasgow

October 2012

Supervisor: Dr T.M. Palmer

I. Abstract

It is now accepted that there is a link between obesity and several diseases such as cardiovascular disease (CVD), diabetes, rheumatoid arthritis (RA), and atherosclerosis with the common initiating factor in pathogenesis being a state of low grade, chronic inflammation. This state, characterised by elevated levels of pro-inflammatory cytokines such as interleukin (IL) 6, leads to sustained activation of inflammatory signalling pathways such as the Janus kinase/signal transducers and activators of transcription (JAK/STAT) pathway and subsequently pathogenesis. Suppressor of cytokine signalling (SOCS) 3 is inducible by several stimuli including IL6 and 3'-5'-cyclic adenosine monophosphate (cAMP), and *via* these routes has been demonstrated to terminate IL6 signalling thus quenching JAK/STAT signalling and an inflammatory response.

While SOCS3 was primarily characterised as a competitive inhibitor of intracellular signalling, it also functions as specificity factor for an elongin-cullin-SOCS (ECS)-type E3 ubiquitin ligase. In this role, it has been demonstrated to direct ubiquitin-mediated proteasomal degradation of several substrates and lysosomal routing. However, the full spectrum of SOCS3-dependently ubiquitinated substrates is unknown. Given that JAK/STAT signalling is critical in the development of chronic inflammatory disorders, delineating the role of SOCS3 as an E3 ligase might be therapeutically beneficial. However, given the broad range of SOCS3 stimuli, the availability of certain SOCS3 substrates might be conditional on the route of SOCS3 induction. Using a global proteomics approach, this study aimed to identify SOCS3-dependently ubiquitinated substrates in response to cAMP and thus elaborate on the already well-established role of cAMP in inflammation.

Differentially stable isotope labelling of amino acids in cell culture (SILAC)-labelled, tandem affinity purified ubiquitinomes of wild type (WT) murine embryonic fibroblasts (MEFs) and SOCS3^{-/-} MEFs, each expressing epitope-tagged forms of ubiquitin, were compared using mass spectrometry (MS) following cAMP-mediated SOCS3 induction. Using this approach, proteins modified by

SOCS3 with the epitope-tagged form of ubiquitin should be enriched in WT MEFs but not SOCS3^{-/-} MEFs.

MaxQuant analysis of raw mass spectromeric data identified several candidate SOCS3 substrates. Of these, SOCS3 was found to interact with PTRF/cavin-1, a regulator of caveolae formation and stability. Other substrates were tested but with limited success. Co-immunoprecipitation studies showed that SOCS3 could precipitate cavin-1 however the interaction was reduced following the inhibition of protein tyrosine phosphatases (PTPs) using sodium orthovanadate and hydrogen peroxide. This was surprising since all known SOCS3 substrates are tyrosine-phosphorylated prior to interacting with SOCS3 *via* its Src-homology (SH) 2 domain. Consistent with this finding, SOCS3 did not interact with known cavin-1 tyrosine-phosphorylated peptides spotted on a peptide array. However, a full-length cavin-1 peptide array spotted with non-tyrosine-phosphorylated peptides showed specific interactions at multiple sites. It is proposed that this interaction might influence the localisation and stability of either protein.

While SOCS3 was demonstrated to impact cavin-1 ubiquitination, the mechanism by which it does so or the functional consequence is still not clear. Immunoprecipitation of cavin-1 following the introduction of SOCS3 was accompanied by a shift in the polyubiquitin signal from a high molecular weight, seen with cavin-1 alone, to a low molecular weight. Furthermore, an enhanced K48-polyubiquitin signal was detectable in this low molecular weight fraction, which was focused around the molecular weight of cavin-1. It is not known if this ubiquitin signal is SOCS3-dependent.

In conclusion, the project has identified and validated a novel substrate of SOCS3. However, the mechanism by which SOCS3 regulates cavin-1 ubiquitination or the biological function of the interaction is currently unknown.

II. Contents

I. Abstract.....	I
II. Contents	III
III Figures.....	IX
IV. Tables.....	XIII
V. Acknowledgements	XIV
VI. Authors declaration.....	XV
VII. Abbreviations.....	XVI
1.0 Introduction	1
1.1 Project basis: the immune system and disease	2
1.1.1 The immune system and endothelial cell activation.....	2
1.1.2 Chronic inflammation and the immune system	4
1.1.3 Inflammatory disease	5
1.1.4 Targeting inflammatory disorders	9
1.2 Cytokine-mediated JAK/STAT signalling	10
1.2.1 Cytokines.....	10
1.2.2 The IL6 family of cytokines and their receptors	11
1.2.3 IL6-mediated JAK/STAT signalling and its regulation.....	14
1.2.4 Negative regulation of the JAK/STAT pathway	16
1.2.4.1 Extracellular regulation of cytokine signalling.....	16
1.2.4.2 Protein tyrosine phosphatases (PTPs)	16
1.2.4.3 Protein inhibitors of activated STAT	17
1.2.4.4 Suppressors of cytokine signalling.....	17

1.3 SOCS3: the first cAMP-inducible E3 ubiquitin ligase	29
1.3.1 Cyclic AMP: generation and effectors.....	29
1.3.2 SOCS3 and cAMP	32
1.3.3 SOCS3 and inflammation	33
1.4 Ubiquitin-proteasome pathway	37
1.4.1 Ubiquitination: formation and function	37
1.4.2 The canonical NF κ B pathway: a ubiquitin dependent pathway	41
1.4.3 Therapeutically targeting the ubiquitin-proteasome pathway	46
1.5 Project rationale and experimental approach.....	48
1.5.1 Project rationale	48
1.5.2 Experimental approach.....	50
2.0 Materials, methods, and external services	59
2.1 Materials	59
2.2 Methods	64
2.2.1 Cell culture	64
2.2.2 Preparation of puromycin resistant murine embryonic fibroblasts.....	64
2.2.2.1 Production of retrovirus for stable transduction of MEFs	64
2.2.2.2 Production of puromycin resistant MEFs <i>via</i> retroviral transduction.....	65
2.2.3 Plasmid DNA preparation and quantification	65
2.2.4 MTT assay	67
2.2.5 Cell preparation and harvesting	67
2.2.5.1 Preparation of tissue culture dishes	67
2.2.5.2 Harvesting for cell characterisation	68
2.2.5.3 Harvesting for tandem affinity purification	68
2.2.5.4 Harvesting for co-immunoprecipitation	68

2.2.5.5 Harvesting for peptide array	69
2.2.6 Protein quantification by bicinchoninic acid assay	69
2.2.7 Tandem affinity purification	70
2.2.7.1 Preparation of NTA-Ni ²⁺ -Sepharose beads	71
2.2.7.2 Preparation of streptavidin-Sepharose beads	71
2.2.7.3 Nickel affinity chromatography	71
2.2.7.4 Streptavidin affinity purification	72
2.2.8 Immunoblot analysis	73
2.2.9 Sample processing pre-LC-MS/MS analysis	76
2.2.9.1 Concentration of Eluate	76
2.2.9.2 SDS-PAGE and gel slice extraction	76
2.2.9.3 In-gel trypsin digestion	76
2.2.9.4 Reduced-keratin work environment	77
2.2.10 Mass spectrometry data quantitation and analysis.....	78
2.2.10.1 Mascot Daemon.....	78
2.2.10.2 MaxQuant.....	79
2.2.10.3 Analysis for raw mass spectra	80
2.2.11 Production of SOCS3 L189A Mutant	83
2.2.11.1 Primer design and synthesis for site directed mutagenesis	83
2.2.11.2 Site-directed mutagenesis.....	85
2.2.11.3 Sequencing of plasmids	85
2.2.12 Transfection.....	85
2.2.13 Co-immunoprecipitation	86
2.2.13.1 Sepharose beads	86
2.2.13.2 Pre-conjugated anti-Flag M2-agarose beads	87
2.2.14 Denatured immunoprecipitation of ubiquitinated proteins	87
2.2.15 Peptide array	88
2.2.15.1 CelluSpot synthesis of peptide array and overlay.....	88
2.2.15.2 SPOT synthesis of peptide array and overlay	89
2.2.16 Substrate degradation assay	93

2.3 External services.....	93
3.0 Characterisation of experimental cell lines	94
3.1 Introduction	94
3.2 Experimental cell lines and strategy.....	95
3.3 Results and discussion.....	97
3.3.1 HBUb expression does not impact cell viability.....	97
3.3.2 HBUb transgene and endogenous ubiquitin are expressed at comparable levels in control and experimental cell lines	99
3.3.3 HBUb transgene expression does not impair polyubiquitin chain formation and function	101
3.3.4 SOCS3 can be induced in WT but not SOCS3 ^{-/-} MEFs by forskolin, LPS and IL6/IL6R.....	106
3.3.5 Impact of hydrogen peroxide and sodium orthovanadate on global tyrosine phosphorylation, K48-specific ubiquitination, and SOCS3 induction.	110
3.4 Conclusions	115
4.0 Experimental strategy	117
4.1 Introduction	117
4.2 Optimisation of experimental strategy	118
4.3 Results and discussion.....	119
4.3.1 Optimisation of tandem affinity purification.....	119
4.3.1.1 Optimisation of Ni ²⁺ bead volume to maximise recovery of HBUb-modified proteins	119
4.3.1.2 Biotin supplementation is essential for detection of HBUb-modified proteins and does not impact Ni ²⁺ affinity chromatography.	121
4.3.1.3 Nickel affinity chromatography specifically recovers HBUb-modified proteins	125
4.3.1.4 Optimisation of streptavidin bead volume to maximise recovery of HBUb-modified proteins.	129

4.3.1.5 Streptavidin affinity chromatography specifically recovers HBUb-modified proteins	131
4.3.1.6 Specificity of TAP for the specific recovery of K48-linked poly-HBUb-modified proteins	133
4.3.1.7 Tandem affinity purification specifically recovers HBUb-modified proteins	135
4.3.2 Optimisation of stable isotope labelling of amino acids in cell culture	139
4.3.2.1 SILAC media supplemented with dialysed serum does not affect cell viability	139
4.3.2.2 SILAC can achieve full incorporation into MEF proteome over five days	141
4.3.3 Optimisation of sample preparation required for detection LC-MS/MS.....	145
4.3.3.1 Optimisation of preparation of raw material for LC-MS/MS	145
4.3.3.2 The streptavidin-biotin interaction can be disrupted with an aqueous biotin solution and elevated temperature.....	148
4.4 Scaled-up tandem affinity purification specifically enriches sufficient HBUb-modified protein for MS analysis.	151
4.5 Conclusions	153
5.0 Identification of SOCS3-dependently ubiquitinated substrates	156
5.1 Introduction	156
5.1.1 Strategy to identify potential SOCS3-dependently ubiquitinated substrates	157
5.2 Results and discussion.....	158
5.2.1 Selection of HBUb-expressing MEF clones.....	158
5.2.2 Preparation of differentially SILAC-labelled, TAP-isolated ubiquitinome for mass spectrometry	160
5.2.3 Data analysis	164
5.2.3.1 Mascot-based protein identification and mass spectra analysis of raw MS data ...	164
5.2.3.2 MaxQuant: identification of potential SOCS3 substrates using SILAC ratios calculated using raw MS data	171
5.3 Conclusions	178
6.0 <i>In vitro</i> verification of candidate SOCS3 substrates	183

6.1 Introduction	183
6.1.1 Cavin-1: a potential SOCS3-dependently ubiquitinated substrate	184
6.1.2 Hsc70: a potential SOCS3-dependently ubiquitinated substrate	187
6.1.3 Experimental strategy	188
6.2 Results and discussion.....	190
6.2.1 Optimisation of experimental conditions	190
6.2.1.1 Optimisation of co-immunoprecipitation assay	190
6.2.1.2 Optimisation of denatured immunoprecipitation assay	196
6.2.2 A SOCS3-Hsc70 interaction could not be confirmed <i>via</i> co-immunoprecipitation	198
6.2.3 SOCS3 can precipitate cavin-1 but not Abi2	201
6.2.4 Cavin-1 ubiquitination is enriched in the presence of SOCS3.....	207
6.2.5 Peptide array of tyrosine-phosphorylated peptides from SOCS3 candidates supports an interaction between SOCS3 and Hsp70 but not cavin-1	216
6.2.6 SOCS3 specifically interacts with several domains of cavin-1	220
6.2.7 Degradation of cavin-1 could not be detected following the inhibition of protein synthesis.....	223
6.3 Conclusions	226
6.4 Future prospects.....	232
6.4.1 Cavin-1	233
6.4.2 Project summary, conclusions, and perspectives.....	233
7.0 References	236

III Figures

Figure 1.0: Development of atherosclerotic lesions.....	8
Figure 1.1: IL6 cytokine family share receptor subunits.....	13
Figure 1.2: IL6 family cytokine signalling.....	15
Figure 1.3: Elongin-Cullin-SOCS-box (ECS) family of E3 ubiquitin ligases.....	20
Figure 1.4: Structural model of the SOCS3-containing ECS-type E3 ubiquitin ligase.....	21
Figure 1.5: PKA and EPAC domain structure.....	31
Figure 1.6: Ubiquitination.....	39
Figure 1.7: The canonical NF κ B pathway is dependent on K48- and K63-polyubiquitin chain formation.....	43
Figure 1.8: The canonical TNF α -activated NF κ B pathway is dependent on linear (M1-), K48- and K63-polyubiquitin chain formation.....	45
Figure 1.9: Structure and function of the 26S proteasome.....	47
Figure 1.10: SOCS3 induction and function.....	51
Figure 1.11: Experimental strategy.....	52
Figure 1.12: The hexahistidine-biotin tag.....	56
Figure 2.0: Quantitative proteomics using MaxQuant.....	81
Figure 2.1: Mutation of the SOCS-box disrupts the SOCS3-elonginBC interaction.....	84
Figure 3.1: Impact of HBUb expression on cell viability.....	98
Figure 3.2: HBUb transgene and endogenous ubiquitin are expressed at comparable levels in control and experimental cell lines.....	100
Figure 3.3: The K48- and K63-polyubiquitin-dependent NF κ B pathway is not affected by HBUb transgene expression.....	104

Figure 3.4 LPS-dependent activation of the NFκB pathway results in significant phosphorylation and degradation of IκBα.....	105
Figure 3.5: SOCS3 is induced to similar levels by forskolin, LPS or IL6/IL6R in WT but not SOCS3 ^{-/-} MEFs.....	108
Figure 3.6: SOCS3 is significantly induced to comparable levels by forskolin, LPS or IL6/IL6R in WT but not SOCS3 ^{-/-} MEFs	109
Figure 3.7: Impact of H ₂ O ₂ concentration or treatment period on global tyrosine phosphorylation and K48-specific ubiquitination	112
Figure 3.8: Impact of H ₂ O ₂ concentration or treatment period on global tyrosine phosphorylation and K48-specific ubiquitination	114
Figure 4.0: Optimisation of Ni ²⁺ bead volume to maximise recovery of HBUb-modified proteins	120
Figure 4.1: Biotin supplementation is essential for biotin-dependent detection of HBUb-modified proteins	123
Figure 4.2: Biotin supplementation does not impact nickel affinity chromatography ..	124
Figure 4.3: Nickel affinity chromatography specifically recovers HBUb-modified proteins	127
Figure 4.4: Nickel affinity chromatography specifically recovers HBUb-modified proteins	128
Figure 4.5: Streptavidin-Sepharose bead optimisation to maximise recovery of HBUb-modified proteins	130
Figure 4.6: Streptavidin bead optimisation to maximise recovery of HBUb-modified proteins	132
Figure 4.7: Tandem affinity purification recovers K48-linked poly-HBUb-modified proteins	134
Figure 4.8: Specificity of TAP for the recovery of K48-linked poly-HBUb-modified proteins from WT or WT HBUb MEFs.....	137

Figure 4.9: Specificity of TAP for the recovery of K48-linked poly-HBUb-modified proteins from SOCS3 ^{-/-} HBUb MEFs	138
Figure 4.10: SILAC media supplemented with dialysed serum does not affect cell viability	140
Figure 4.11: Incorporation of SILAC isotope ¹³ C6-Arg	143
Figure 4.12: Incorporation of SILAC isotope ¹³ C6-Arg/Lys	144
Figure 4.13: Optimisation of sample preparation required for detection LC-MS/MS	147
Figure 4.14: Optimisation of streptavidin bead elution strategy for the recovery of HBUb-modified proteins	150
Figure 4.15: Scaled-up tandem affinity purification specifically enriches sufficient HBUb-modified protein for MS analysis	152
Figure 5.0: Selection of HBUb expressing clones	159
Figure 5.1: Evaluation of HBUb transgene expression and SOCS3 induction prior to TAP and MS	162
Figure 5.2: Fractionation of concentrated SILAC-labelled, TAP-isolated HBUb-modified proteins prior to MS	163
Figure 5.3: Spectra of pyruvate carboxylase, a protein detectable in differentially labelled WT HBUb and SOCS3 ^{-/-} HBUb MEFs.....	168
Figure 5.4: Spectra of a known SOCS3-dependently ubiquitinated substrate, FAK-1, detectable in heavy-labelled WT but not light-labelled SOCS3 ^{-/-} MEFs	169
Figure 5.5: Spectra of a potential SOCS3-dependently ubiquitinated substrate, PTRF (cavin-1) detectable in heavy-labelled WT but not light-labelled SOCS3 ^{-/-} MEFs ..	170
Figure 5.6: Value-ordered plots of log2-transformed normalised SILAC ratios from forward and reverse SILAC-labelled experiments	172
Figure 5.7: Total ion chromatogram from forward and reverse-labelled experiments .	177
Figure 6.0: Cavin-1, caveolin-1 and the formation of caveolae	185

Figure 6.1: The impact on tyrosine phosphorylation on the interaction between SOCS3 and the E3 scaffold proteins elonginB and cullin5.....	193
Figure 6.2: The impact of the SOCS3-L189A SOCS-box mutation on its interaction with the E3 ligase components elonginB and cullin5	194
Figure 6.3: SOCS3 precipitates known SOCS3-dependently ubiquitinated substrate FAK1	195
Figure 6.4: Expression of Ub-HA and optimisation of denaturing co-immunoprecipitation	197
Figure 6.5: A SOCS3-Hsc70 interaction could not be confirmed <i>via</i> co-immunoprecipitation.....	199
Figure 6.6:SOCS3 precipitates potential substrate cavin-1 but not Abi2.....	202
Figure 6.7: Tyrosine-phosphorylation inhibits the cavin-1-SOCS3 interaction.....	205
Figure 6.8: SOCS3 and the SOCS3 L189A SOCS-Box mutant precipitates cavin-1	206
Figure 6.9: Cavin-1 ubiquitination is enriched in the presence of SOCS3	209
Figure 6.10: Cavin-1 ubiquitination is enriched in the presence of SOCS3	210
Figure 6.11: SOCS3 ubiquitination is enriched in the absence of components of the E3 ligase	212
Figure 6.12: SOCS3 ubiquitination is enriched in the absence of components of the E3 ligase	213
Figure 6.13: Cavin-1 ubiquitination is enriched in the presence of SOCS3	215
Figure 6.14: SOCS3 interacts with several known tyrosine-phosphorylated peptides from candidate proteins	218
Figure 6.15: Degradation of cavin-1 could not be detected following inhibition of protein synthesis	225

IV. Tables

Table 1.0: Ubiquitin-regulated SOCS substrates	25
Table 2.0: Constructs	63
Table 2.1: Primary and secondary antibodies.....	75
Table 2.2: MaxQuant modified settings	82
Table 2.3: Peptide array of tyrosine-phosphorylated peptide from candidate SOCS3 substrates	91
Table 2.4: Peptide array of tyrosine-/non-phosphorylated peptides from candidate SOCS3 substrates	92
Table 5.0: Mascot analysis of the forward SILAC-labelling experiment	167
Table 5.1: MaxQuant analysis of forward labelling experiment	175
Table 5.2: MaxQuant analysis of reverse labelling experiment.....	176
Table 6.0: SOCS3 interacts with several known tyrosine-phosphorylated peptides from candidate proteins	219
Table 6.1: SOCS3 specifically interacts with several domains of cavin-1	221

V. Acknowledgements

I would like to thank the following people who helped me with this project:

Tim Palmer for his supervision and experience. Claire Rutherford for passing on her experience and organising skills. Richard Burchmore (Sir Henry Wellcome Functional Genomics Facility) and Bill Mullen (Proteomics, Biomarkers, and Systems Medicine) for advising me with mass spectrometry. Sara Zanivan (Vascular Proteomics, The Beatson Institute for Cancer Research) and Nick Morrice (Proteomics, The Beatson Institute for Cancer Research) for advising me with mass spectrometric data analysis and MaxQuant. George Baillie and Lucien Gibson (MVLS, University of Glasgow) for the production of peptide arrays. In addition, a special thanks to the BBSRC for funding the project.

VI. Authors declaration

I hereby declare that this thesis, which follows, is my own, original composition and that all work has been performed by me unless otherwise acknowledged. Furthermore, none of this work has been previously presented as part of an application for a higher degree.

Jamie J.L Williams.

October 2012.

VII. Abbreviations

A.

A2AAR	A2A adenosine receptor
ANOVA	Analysis of variance
APC	Antigen-presenting cell
APR	Acute phase response
AR	Adenosine receptor

B.

BCA	Bicinchoninic acid
BSA	Bovine serum albumin
BSC	Biological safety cabinet

C.

cAMP	3'-5'-cyclic adenosine monophosphate
CBD	C-terminal cAMP binding domain
CBP	CREB-binding protein
C/EBP	CCAAT/enhancer-binding protein
cGMP	3'-5'-cyclic guanosine monophosphate
cIAP	Cellular inhibitor of apoptosis
CID	Collision-induced dissociation
CIS	Cytokine-inducible protein with an SH2 domain
CNG	Cyclic nucleotide-gated
CNS	Central nervous system
CP	Cell-penetrating
CPDM	Chronic proliferative dermatitis
CRE	cAMP-response element
CREB	CRE-binding protein
Cul2	Cullin2
Cul5	Cullin5
CVD	Cardiovascular disease

D.

DAG	sn-1,2-diacylglycerol
-----	-----------------------

dCS	Dialysed calf serum
dH ₂ O	Distilled H ₂ O
DMEM	Dulbecco modified Eagle's medium
DMSO	Dimethyl sulphoxide
DTT	Dithiothreitol
DUB	Deubiquitinase
E.	
<i>E.coli</i>	<i>Escherichia coli</i>
ECL	Enhanced chemiluminescence
ECM	Extracellular matrix
ECs	Endothelial cells
ECS	Elongin-cullin-SOCS
EDA-ID	Anhidrotic ectodermal dysplasia with immunodeficiency
EGF	Epidermal growth factor
EPAC	Exchange protein directly activated by cAMP
ERK	Extracellular signal-regulated kinase
ESI	Electrospray ionisation
F.	
FAK	Focal adhesion kinase
FBS	Foetal bovine serum
FDR	False discover rate
FFA	Free fatty acids
FSK	Forskolin
FTMS	Fourier transform mass spectrometry
FWHM	Full width half maximum
G.	
GAP	GTPase-activating protein
GAPDH	Glyceraldehyde 3-phosphate dehydrogenase
GAS	IFN γ -activated sequence
G-CSFR	Granulocyte colony-stimulating factor receptor
GEF	Guanine nucleotide exchange factor
GPCR	G-protein-coupled receptor

Gp130	Glycoprotein 130
Grb	Growth factor receptor-bound
H.	
HBUb	Hexahistidine-biotin
HECT	E6-AP COOH-terminus
HEK293	Human embryonic kidney 293 cells
HLA	Human leukocyte antigen
HOIL	Haem-oxidized IRP2 ubiquitin ligase
HOIP	HOIL-1-interacting protein
HSP	Heat shock protein
HRP	Horseradish peroxidase
HUVEC	Human umbilical vein endothelial cells

I.

IBD	Inflammatory bowel disease
ICAM	Intercellular adhesion molecule
ICAT	Isotope coded affinity tags
IFN	Interferon
Ig	Immunoglobulin
IGF	Insulin-like growth factor
I κ B α	Inhibitor of Nuclear factor- κ B inhibitor α
IKK	I κ B kinase
IL	Interleukin
IL6R α	IL6 receptor α
IPI	International protein index
IRAK	IL1 receptor-associated kinase
IRF	IFN regulatory factors
IRS	Insulin receptor substrate
ISRE	IFN-stimulated response elements

J.

JAK	Janus kinase
JH	JAK homology
JNK	c-Jun N-terminal kinase

K.

KIR Kinase inhibitory region

L.

LB Luria-Bertani

LDL Low-density lipoprotein

LIF Leukaemia inhibitory factor

LIFR Leukaemia inhibitory factor receptor

LPS Lipopolysaccharide

LTQ Linear trap quadrupole

LUBAC Linear ubiquitin chain assembly complex

M.

MAPK Mitogen-activated protein kinase

MALDI Matrix-assisted laser desorption/ionization

MCP1 Monocyte chemotactic protein 1

MEF Murine embryonic fibroblast

MHC Major histocompatibility complex

MMP Matrix metalloproteinases

MS Mass spectrometry

MTT 3-(4, 5-dimethylthiazol-2-yl)-2, 5-diphenyl 2H-tetrazolium bromide

MyD88 Myeloid differentiation primary response protein 88

N.

NEDD8 Neural precursor cell expressed, developmentally down-regulated 8

NEMO NFκB essential modulator

NFκB Nuclear factor kappa B

NK Natural killer

NO Nitric oxide

NTA Nitrilotriacetic acid

NUB NEMO-ubiquitin-binding

O.

O/N Overnight

OSM Oncostatin M

P.

PEP	Posterior error probability
PDE	Phosphodiesterase
PH	Pleckstrin homology
PIAS	Protein inhibitor of activated STAT
PKA	Protein kinase A
PKC	Protein kinase C
PLC	Phospholipase C
PMA	Phorbol myristate acetate
PMSF	Phenylmethylsulphonyl fluoride
PTK	Protein tyrosine kinase
PTM	Post-translational modification
PTP	Protein tyrosine phosphatase

Q.

QTOF	Quadrupole time of flight
------	---------------------------

R.

RA	Rheumatoid arthritis
RIP	Receptor interacting protein
RIPA	Radioimmunoprecipitation assay
RING	Really interesting new gene
ROS	Reactive oxygen species
RT	Room temperature
RTK	Receptor tyrosine kinase

S.

SH2	Src homology2
SHP2	SH2-domain-containing PTP
SHARPIN	SHANK-associated RH domain interacting protein
SIGLEC	sialic-acid-binding immunoglobulin-like lectin
SILAC	Stable isotopic labelling of amino acids in cell culture
SOCS	Suppressor of cytokine signalling
Sos	Son of sevenless
STAT	Signal transducer and activator of transcription

SUMO	Small ubiquitin-like modifier
T.	
TAP	Tandem affinity purification
TAB	TAK1 binding protein
TAK	Transforming growth factor- β -activated kinase
TBS	Tris-buffered saline
TCR	T-cell receptor
TEMED	N,N,N',N'-tetramethylethylenediamine
TGF- β	Transforming growth factor- β
TLR	Toll-like receptors
TNF- α	Tumour necrosis factor- α
TOF	Time-of-flight
TRADD	TNF receptor 1-associated death domain protein
TRAF	TNF receptor associated factor
U.	
Ub	Ubiquitin
UBA	Ub-associated domain
UBD	Ub-binding domain
UBL	Ub-like domain
UBP	Ub-specific processing protease
ULP	Ubiquitin-like proteins
UIM	Ub-interacting motif
USP	Ub-specific protease
V.	
VSMC	Vascular smooth muscle cell
W.	
WT	Wild type

1.0 Introduction

Spiralling levels of obesity has seen a concomitant increase in the cases of inflammatory-related diseases (1). The common initiating factor is a state of low grade, chronic inflammation induced by the elevated secretion of adipocytokines and the subsequent infiltration, into fat tissue, of immune cells that amplify and sustain the effect (2-4). Metabolic and immune systems have a complex relationship being linked by array of pleiotropic signalling molecules. While many adipocytokines might be classified as either protective e.g. adiponectin or damaging e.g. IL6, it is more likely that a balance is necessary for homeostasis. As such, an imbalance created by increased adiposity may result in a local and systemic response leading to the progressive development of several disorders. Adipocytokines up-regulated in obesity such as IL6 (5) can elicit cell and tissue specific responses through activating common intracellular signalling pathways i.e. the JAK/STAT pathway (6). Furthermore, activation of this pathway by multiple stimuli is critical in the development of CVD (7). Therefore, understanding this basic signalling unit and the complex milieu of cell-specific crosstalk may enable specific targeting for therapeutic benefit.

Here, I will introduce the immune system and the interplay between it and the metabolic system, which can result in pathogenesis. I will then introduce the JAK/STAT pathway, its regulation, and consequences of dysregulation. Moreover, I will show how understanding of the negative regulation of the JAK/STAT pathway might be therapeutically beneficial. I aim to show that by targeting SOCS3, a specificity factor for an E3 ubiquitin ligase, it might be possible to elicit a precise response. While several ubiquitinated substrates of SOCS3 are known (8-12), the full spectrum has yet to be identified. As such, I aim to introduce an experimental rational for identifying SOCS3-dependently ubiquitinated substrates. By doing so, it may be possible to therapeutically target specific events while reducing adverse effects.

1.1 Project basis: the immune system and disease

1.1.1 The immune system and endothelial cell activation

Multicellular organisms are constantly exposed to a wide variety of pathogens and foreign particles but evade infection *via* inflammation initiated by the innate immune system. A tightly coordinated system of fast-acting response combined with a slower, long-term response provides an efficient mechanism of detection and removal of potentially damaging infectious agents. These responses, defined as the innate and adaptive immune system respectively, coordinate humoral and cell-mediated defence mechanisms against infectious agents that evade physical barriers e.g. skin, saliva, mucus, and hair. Each system induces an inflammatory response, mediated by a set of soluble proteins such as cytokines and chemo-attractants, which aids the clearance of the infection *via* phagocytosis and destruction of pathogens and infected cells. Inflammatory mediators are usually secreted at the site of infection over periods of hours to days and correlate with negative effects of illness (13). These effects can become exaggerated upon prolonged exposure requiring the inflammatory response to be tightly controlled.

The innate immune response is a rapid and non-specific reaction activated at the site of infection. The elimination of invading agents is mediated by system of conserved circulating proteins, antibodies, and phagocytic cells such as macrophages that recognise pathogen associated molecular patterns (PAMPs) on foreign particles (glycoproteins, lipids, and DNA) *via* conserved, germline-encoded pattern recognition receptors (PRRs). The most well studied PRRs include toll-like receptors (TLRs), NOD-like receptors (NLRs), and RIG-I-like receptors (RLRs) (14). Activation can elicit multiple effects that aid the destruction and phagocytosis of foreign particles and pathogens e.g. complement, activation of inflammatory signalling pathways, and apoptosis (15). For example, TLR4 detects the gram negative bacterial component LPS which leads to activation of the pro-inflammatory nuclear factor kappa B (NF κ B) pathway (16) resulting in the secretion of multiple pro-inflammatory cytokines such as tumour necrosis factor α (TNF α), IL1, and IL6, that initiate the clearance of the infection (17).

Adaptive immunity (13) is a slower, antigen-specific response mediated by B- and T-lymphocytes that detect foreign particles *via* a highly diverse set of antibodies and T-cell receptors (TCRs) respectively (15). Such diversity enables the detection of existing and as yet un-encountered antigens and as such, negative screening of lymphocyte reactivity is necessary to prevent autoimmunity (14). An adaptive response is initiated either *via* the detection of antigen by naïve B-cells or by antigen-presenting cell (APC)-dependent activation of naïve T-cells. APCs express a form of major histocompatibility complex (MHC) molecule on its surface that enables the presentation of internalised, non-self peptides at the plasma membrane. Two forms of MHC, MHCI and MHCII are defined, while MHCI is present on all nucleated cells i.e. all cells with the exception of red blood cells, MHCII is only present on APCs i.e. dendritic cells, macrophages, and B-lymphocytes (13). APCs locally activated by a PAMP/PRR interaction subsequently internalise foreign particles *via* phagocytosis and present them at the surface on MHCII. Directed by chemokines, APCs then move to peripheral lymphoid organs e.g. spleen and lymph nodes where they deliver the foreign cargo to induce an adaptive immune response (13). Activated B- and T-lymphocytes are drawn to sites of infection by chemokines *via* interactions between cell-surface receptors i.e. selectins and integrins, and endothelial cells (13). T-cells are activated by APCs following an MHCII-TCR interaction aided by co-stimulatory molecules which cause them to undergo clonal expansion producing a set of naïve, effector, and memory cells (13). Naïve T-cells differentiate to helper T-cells (T_h cells, CD4+) or cytotoxic T-cells (CD8+), the latter of which induces apoptosis of infected cells upon stimulation with MHCI-bound peptide. MHCII-bound peptides activate CD4+ T-cells to secrete cytokines which amplify the response of specific lymphocyte compartments i.e. T_{h1} elicits a T-cell-mediated response against intracellular bacteria and virus whereas T_{h2} induces a B-cell-mediated humoral response against extracellular pathogens (18). APCs therefore act as the bridge between innate and adaptive systems. Furthermore, T_h cells also differentiate to regulatory (T_{regs}) T-cells that suppress T-cell-induced chronic inflammation and autoimmunity i.e. peripheral tolerance *via* a cytokine-directed mechanism (14). Naïve B-cells also undergo clonal expansion, upon detection of antigen or following activation by T_h cells they differentiate to effector plasma cells that secrete cytokine, chemokine, and antibodies that contribute to complement and phagocytosis (13). Finally, the

generation of both B- and T-cell memory cells preserve the proven antigen detection machinery to enable a quick secondary response to future infection.

The immune system works intimately with the endothelium to enable clearance of infection (19). Healthy vascular endothelial cells (ECs) form an interface between luminal components of the circulatory system and surrounding organs. It functions as a barrier to solutes and cells while maintaining an anti-thrombotic environment. Activation of the immune system results in a cytokine/chemokine-mediated cascade of events where ECs undergo morphological and phenotypic changes enabling them to participate (19). This presents as the common signs of inflammation which includes redness, heat, swelling, pain, increased blood flow, and loss of vascular integrity (20). Vasoconstriction increases blood pressure, producing redness and heat *via* engorgement of the capillary network. Vascular permeability aids infiltration of phagocytic cells but also contributes to swelling from fluid accumulation (20). EC activation causes a reduction in vascular integrity, expression of leukocyte adhesion molecules, increased cytokine/chemokine secretion, up-regulation of human leukocyte antigen (HLA), and generation of reactive oxygen species (ROS) (21,22). These changes enable the recruitment and infiltration of leukocytes to the sub-endothelial space, a process that is promoted by additional cytokine/chemokine secretion from the recruited immune cells. Since such events can be destructive, inflammation must be tightly controlled. EC activation is a graded, tightly regulated response but persistent, increased basal conditions of activating molecules can have a cumulative effect. It is under these conditions that EC activation can result in pathogenesis (23).

1.1.2 Chronic inflammation and the immune system

Adipocytes were initially regarded as a simple lipid store but are now accepted as an endocrine organ. The discovery of leptin provided a mechanism by which adipocytes could communicate the energy status of the organism and thus control body mass (24). Leptin is now considered a pleiotropic signalling molecule involved in energy homeostasis, angiogenesis, and immunity (25). Adipocytes are now accepted to secrete multiple adipocytokines, including leptin, that regulate metabolically active systems including liver, skeletal muscle, and endothelium. Adipocytokines include many pro-inflammatory

signalling molecules such as IL6 and TNF α , which enables cross-talk between metabolic and immune systems (26). For example, IL6 carries out multiple functions such as differentiation of B-cells, T-cell activation and proliferation of vascular smooth muscle cells (VSMCs) (7). IL6 can also induce monocyte chemoattractant protein (MCP) 1, a chemokine that recruits monocytes to sites of infection (27). Furthermore, both TNF α and IL6 induce the expression of adhesion molecules such as selectins, vascular cell adhesion molecule (VCAM) 1, and intercellular adhesion molecule (ICAM) 1 which are necessary for transport, adherence, and infiltration of the endothelium (28,29). Importantly, the secretion of pro-inflammatory adipocytokines correlates with adiposity and as such, IL6 (5) and TNF α (30) are both elevated during obesity. Furthermore, enhanced levels of these adipocytokines are specifically associated with increased visceral fat, as opposed to subcutaneous fat levels (31,32). However, secretion of anti-inflammatory adipocytokines such as adiponectin are reduced under the same condition (26). In support of the involvement of the immune system in obesity, macrophages (4) are sequestered by chemoattractants such as MCP1 and infiltrate adipose tissue to perpetuate and enhance adipocytokine secretion (2). Furthermore, this condition is supported by an imbalance in T-cell compartments (33). An increase in T_{h1} and decrease in T_{h2} and T_{reg} T-cells promotes a pro-inflammatory, macrophage-dependent response which escalates the effect in a vicious feedback cycle (33). In effect, during obesity, adipose tissue enters a nutrient-induced inflammatory state. While this is a simplistic view, it is evident that a complex relationship exists between adipocytes and the immune system, which left unattended, can promote systemic inflammation and *via* EC activation, can promote inflammatory events and pathogenesis (19,23).

1.1.3 Inflammatory disease

It is been discussed how metabolic and immune systems are interrelated and that prolonged high calorie diets and subsequent excess adiposity provoke chronic activation of the immune system. Obesity contributes to a state of systemic low grade inflammation *via* the elevated secretion of adipocytokines (34). An obesity induced imbalance of the metabolic and immune system can lead to a condition referred to as the metabolic syndrome, a state of insulin resistance, high plasma triglyceride, low high-density lipoprotein cholesterol, and hypertension (21). This primes the individual for several inflammatory

related disorders such as type-2 diabetes and atherosclerosis (21,35) and it is of note that the prevalence of these disorders is increasing with rates of obesity (36,37). The link between metabolic and immune systems has enabled the molecular mechanisms of disease to be investigated. However, given the complexity of the relationship between these systems and that disease progression is often multifactorial, involving both genetic and environmental effects, these mechanisms have yet to be fully elucidated.

Insulin resistance and subsequently type-2 diabetes can be induced by several events. Adipose tissue is a source of free fatty acids (FFAs) that are released following lipolysis that can be stimulated by IL6 and TNF α (38). Increased lipolysis during obesity provides elevated levels of circulating FFAs that can activate TLR4 in adipocytes and induce a state of insulin resistance (38) *via* activation of the NF κ B pathway which has well-accepted links to insulin resistance (39). Furthermore, an elevated level of TNF α is associated with insulin resistance in obese mice while genetic impairment of TNF α signalling increases insulin sensitivity with a concomitant decrease in FFAs (40). Both FFA and TNF α can activate one of the pro-inflammatory mitogen-activated protein kinase (MAPK) pathways, the c-Jun N-terminal kinase (JNK) pathway, which is hyperactive in obese mice (35). Subsequently, activation of JNK1 was found to result in an inhibitory phosphorylation on the insulin receptor substrate (IRS) 1 (S³⁰⁷) blocking its interaction with the insulin receptor and thus downstream signalling (35). In contrast, deletion of JNK1 is protective against insulin resistance (35).

It is now well established that obesity-related increases in adipocytokine secretion contributes to the development of atherosclerosis-induced cardiovascular disease which is one of the leading causes of deaths worldwide (41). It has been recognised for years that high fat/cholesterol diets are associated with cardiovascular disease (42). Combining knowledge from a wide variety of inflammation-related events, the progression of atherosclerotic lesion development has been described. It is likely initiated by hyperlipidaemia, hypertension, and elevated cytokine release. The systemic nature of these events combines, resulting in uncontrolled EC activated and pathogenesis.

Atherosclerosis is the formation of lesions within the arterial intima due to the accumulation of lipid, connective tissue, leukocytes, and the proliferation and infiltration of smooth muscle cells (Figure 1.0). Narrowing of the artery precedes plaque rupture that can cause coronary thrombosis (43). Lesions do not always precede pathogenesis since stable lesions can be formed that are compensated for by arterial wall dilation (18). Lesions preferentially localise to areas of haemodynamic strain such as arterial bifurcations, branch ostia, and curvatures (43). Oscillating shear stresses in these regions tends to be accompanied by expression of leukocyte adhesion molecules, pro-inflammatory genes including multiple cytokines, and angiotensin-II which itself promotes a vasoconstriction and a pro-thrombotic environment (23). Increased circulating pro-inflammatory cytokines and accumulation of ROS tend to further activate ECs allowing lipids such as LDL to be oxidised (ox-LDL) upon infiltration into the sub-endothelial space. Sequestered macrophages phagocytose ox-LDL *via* scavenger receptors and develop into foam cells producing a fatty streak, characteristic of early stage atherosclerosis (44). Foam cells, macrophages, and APCs then contribute to the increased production of pro-inflammatory factors that accelerate formation of unstable lesions (Figure 1.0). For example, necrosis and destabilisation of the lesion by macrophage-derived matrix metalloproteinases (MMPs) can lead to rupture and potentially thrombosis, arterial blockage, and myocardial infarction or stroke (44). Furthermore, while high haemodynamic stress induces the release of nitric oxide (NO) and vasodilatation which can compensate for lesion formation, increased flow can also contribute to plaque damage (23).

Chronic inflammatory disorders can be differentiated by individual phenotypes due to tissue specific responses although the underlining cause remains common. For example, atherosclerosis and cirrhosis involve the same leukocyte compartments but whereas cirrhosis is defined by parenchymal-cell injury producing fibrotic scarring, atherosclerosis is induced by endothelial-cell injury that causes fibrosis and smooth muscle proliferation resulting in stenosis, rupture, and thrombosis (45). Chronic inflammatory diseases might therefore be treated by understanding and targeting of common regulatory mechanisms of the immuno-inflammatory response.

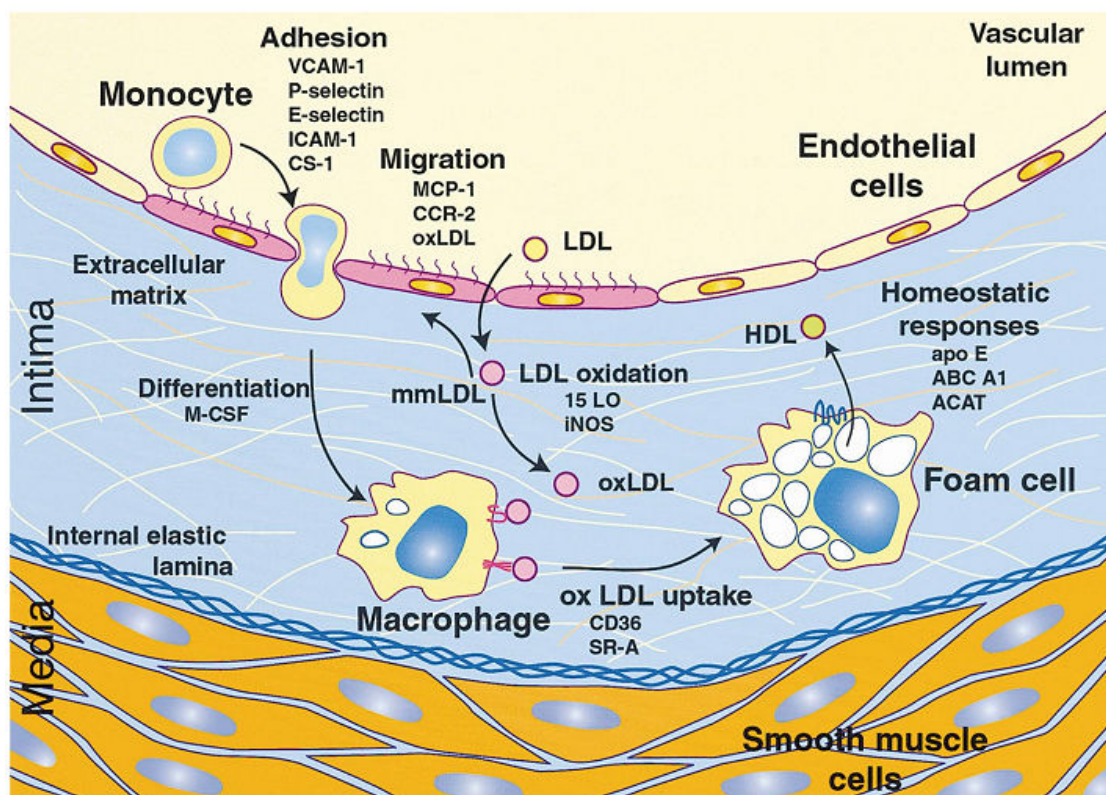


Figure 1.0: Development of atherosclerotic lesions

Atherogenesis is initiated by endothelial cell inflammation, activation, and dysfunction. Loss of vascular integrity allows access to monocytes and the diffusion of solutes such as LDL into the arterial intima. LDL is acted upon by oxidative and enzymatic modification which initiates EC activation. Expression of adhesion molecules, production of reactive oxygen species (ROS), and the secretion of cytokines and chemokines contributes to attraction, activation, and infiltration of macrophages that form foam cells upon uptake of ROS-modified lipids *via* scavenger receptors. Lesions mature following foam cell breakdown and accumulation of cholesterol, calcium, and collagen. Necrosis and destabilisation of the lesion by macrophage-derived matrix metalloproteinases can lead to rupture and potentially thrombosis, arterial blockage, myocardial infarction or stroke. Image adapted with permission from (44).

1.1.4 Targeting inflammatory disorders

It is clear that pathogenesis results due to the sustained, uncontrolled elevation of adipocytokine levels that activate the ECs. Furthermore, *via* positive feedback loops these molecules can interact with the immune system to sustain a pro-inflammatory state that drives pathogenesis. While multiple stimuli are involved, the intracellular signalling pathways activated are often common. It has been described how both FFA and TNF α can stimulate the NF κ B pathway to promote insulin resistance (35). NF κ B also drives transcription of matrix metalloproteinases (MMP1, 3, 9), pro-inflammatory cytokines (TNF- α , IL6), chemokines (IL8), leukocyte adhesion molecules, and growth factors (18,22). It is thus not surprising that numerous other studies have implicated NF κ B in the development inflammatory diseases (39). However, the NF κ B pathway also provides protective, anti-apoptotic effects required for clearance of pathogens (18).

Several events in the progression of atherosclerosis have been shown to be regulated directly or indirectly by the JAK/STAT pathway including vascular tone, mechanical and oxidative stress, and pro-inflammatory gene expression (7). Most notably of course is the direct activation of the JAK/STAT pathway by IL6, a pleiotropic adipocytokine elevated in the obese (5), that can induce acute phase proteins, cytokines, chemokines, activate T-cells and the proliferation of smooth muscle cells (7,27-29). Furthermore dysregulation of the JAK/STAT pathway is also integral to the development of other chronic inflammatory disorders such as Crohn's disease (46) and certain cancers (47).

Targeting of these pleiotropic signalling molecules might therefore be therapeutically beneficial. Several disorders have been targeted using anti-TNF α inhibitors including Crohn's disease (infliximab) and rheumatoid arthritis (etanercept, adalimumab) (48). Treatments that mop-up and inhibit the action of pro-inflammatory cytokines such as anti-IL6 mAbs e.g. elsilimomab, and anti-IL6R mAbs e.g. tocilizumab, have also been successful in reducing disease progression (47).

Inhibition of IL6 signalling might be beneficial in certain cases i.e. to prevent the progression of cancer. However, global inhibition of IL6 signalling might be detrimental since minimum activation might be necessary for protection. For example, Schieffer et al found that atherosclerotic lesion formation was greater in $\text{Apoe}^{-/-} \text{IL6}^{-/-}$ mice and was accompanied by a reduction in levels IL10 compared to $\text{Apoe}^{-/-}$ mice (49). This suggested that lesion formation is dependent on the balance of anti- (IL10) and pro-inflammatory (IL6) cytokines and that IL6 is required to maintain IL10 levels. As such, it would be better to therapeutically target downstream IL6 signalling events, while preserving its protective effects.

This study aims to investigate SOCS3, which was initially described as a cytokine-inducible negative regulator of JAK/STAT signalling (50). At present, inducers of SOCS3 include, but are not limited to, cytokines (IL1, IL6, LIF, OSM, $\text{IFN}\gamma$, $\text{TNF}\alpha$, EPO, and prolactin), chemo-attractants (IL8, N-formyl-Met-Leu-Phe), bacterial components (LPS, unmethylated CpG DNA), leptin, insulin, and the intracellular second-messenger cyclic AMP. SOCS3 can suppress signalling from a diverse set of receptors either by directly binding the receptor itself or by initiating ubiquitin-mediated proteasomal degradation (51). In the case of the latter, SOCS3 acts as a specificity factor for an ECS-type of E3 ubiquitin ligase of which only a few targets are known (8-12). While the ubiquitin-proteasome pathway consists of only a few E1 activation and E2 conjugation proteins (Section 1.2.5), several hundred E3 ligases have been defined (52). Thus, it may be therapeutically beneficial to specifically target SOCS3 in this role.

1.2 Cytokine-mediated JAK/STAT signalling

The following sections review current knowledge on the JAK/STAT pathway and its regulation. The JAK/STAT pathway can be activated by multiple stimuli, however the emphasis here will be on cytokine signalling, specifically IL6.

1.2.1 Cytokines

Cytokines are extracellular proteins secreted by many cell types that function as autocrine, paracrine, juxtacrine, and endocrine hormones. They act pleiotropically and synergistically to regulate survival, proliferation,

differentiation, and the function of many cell types (18). Importantly they are transiently expressed (hours to days) to elicit a pro- or anti-inflammatory response in a cell-specific fashion to activate/amplify the action of specific leukocyte compartments (18). They have the positive effect of co-ordinating the clearance of infection but are also responsible for the negative effects of illness such as fever, lethargy, sleep, allergy, and anorexia. Persistent cytokine generation can result in several chronic inflammatory disease states such as CVD (46).

To date around 50 cytokines have been defined including interleukins (IL), tumour necrosis factors (TNF), interferons (IFN), colony stimulating factors (CSF), and transforming growth factors (TGF) (18). More than 70 further candidates have been identified *via* sequence comparisons (53). Cytokines are characterised by the structure of the receptors that they activate and include: hematopoietin/type 1, interferon/type 2, TNF, and IL1/TLR. IL6 mediates its effects by targeting the largest family of cytokine receptors, the haematopoietin/type 1 receptors, of which the membrane-bound receptor gp130 is the most common signalling unit (54).

1.2.2 The IL6 family of cytokines and their receptors

The IL6 family of four- α -helical cytokines includes IL6, IL11, leukaemia inhibitory factor (LIF), oncostatin M (OSM), cardiotrophin-1 (CT-1), ciliary neurotrophic factor (CNTF), and cardiotrophin-like cytokine (CLC) (55). Most IL6 family members transduce signals *via* gp130 either as a homodimer, as in the case of IL6, or as a heterodimer of gp130 and a second signalling receptor protein (Figure 1.1). Although each ligand-receptor partnership imparts a specific response, in common is the activation of the JAK/STAT and extracellular signal-regulated kinase (ERK) pathways (Figure 1.2). Increased signalling diversity is achieved from their interaction with membrane-bound, soluble and associated isoforms of both IL6R α and gp130 subunits. As well as binding and interacting with membrane-localised IL6R α to trigger signalling *via* gp130, termed “classical” IL6 signalling, IL6 is unique in that it can also function *via* a so-called trans-signalling mechanism. This is achieved because gp130 does not recognise IL6 directly. Instead, IL6 must first form a low affinity complex with the 80kDa non-signalling α -receptor, IL6R α (CD126), which then forms a high affinity

tetramer with a homodimer of gp130. Gp130 is ubiquitously and constitutively expressed whereas membrane bound/non-signalling IL6R α is restricted to hepatocytes, leukocytes, and lymphocytes. However soluble IL6R (sIL6R) variants can also be generated either *via* alternate splicing of the IL6R α primary transcript (56) or by limited proteolysis of the membrane-localised IL6R α protein by metalloproteases ADAM10 or ADAM17, resulting in soluble IL6R α (sIL6R α) being shed from hepatocytes or macrophages (57). This enables signalling in non-IL6R α -expressing cells, thus increasing the repertoire of IL6-responsive cells during an inflammatory response (55).

IL6 is a 22-28 kDa protein, depending on its glycosylation state, secreted by leukocytes, fibroblasts, endothelial cells, keratinocytes, hepatocytes, and bone marrow cells. Five isoforms exist in humans (IL6, IL6alt, IL6 Δ 2, IL6 Δ 2,4, and IL6 Δ 4) due to alternative splicing (58,59). IL6 is a multifunctional mediator of numerous complex biological responses, including hepatic induction of acute phase proteins, differentiation of B cells, as well as T-cell activation, growth, and differentiation. In a pro-inflammatory role, IL6 initiates inflammation *via* the activation of endothelial cells by upregulating expression of the adhesion molecules ICAM1, E-selectin, and VCAM1, chemokine MCP1/CCL2, and by induction of smooth muscle cell proliferation and migration (27-29). IL6 is also involved in the generation of T_{h17} cells from naïve T-cells and the inhibition of T_{reg} development (60). T_{h17} cells provide protection against fungi and extracellular bacteria, while T_{regs} limit this response. In a state of sustained, elevated levels of IL6, the fine balance between T_{h17} cells and T_{regs} is lost. Through this disruption, T_{h17} cells are critical in the development of inflammatory disorders such as rheumatoid arthritis (60). IL6 also mediates anti-inflammatory responses including the negative regulation of IL1 and TNF α synthesis as well as quenching of the pro-inflammatory effects of IL1 by up-regulation of IL1R antagonist IL1ra (61) and maintenance of IL10 (49).

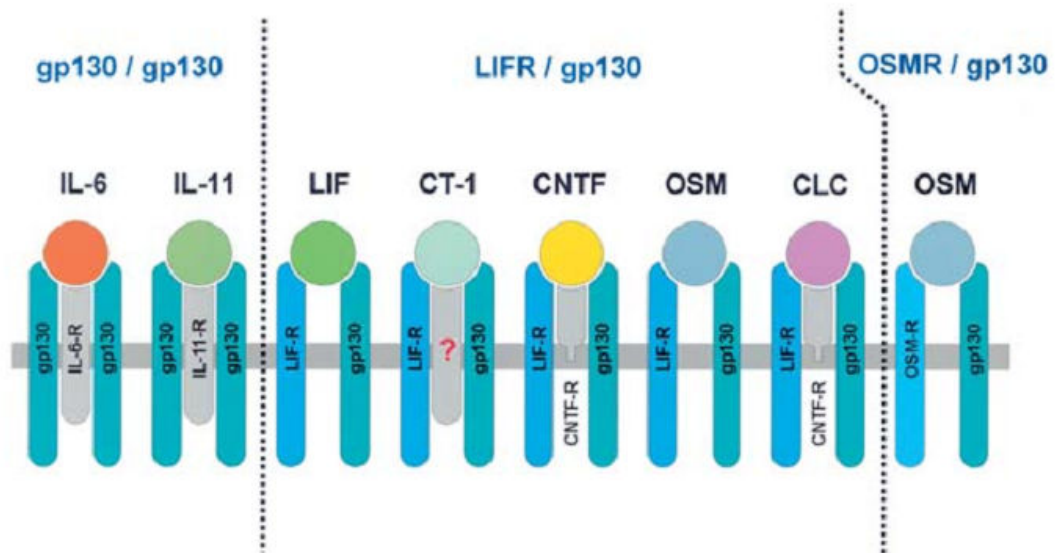


Figure 1.1: IL6 cytokine family share receptor subunits

Gp130, a 130 kDa glycoprotein, forms homo- or hetero-dimers with the IL6 cytokine family of receptors. IL6 and IL11 both require a gp130 homodimer whereas others require hetero-dimers. OSM can bind two forms of heterodimer whereas LIF, CT-1, CNTF and CLC all require a LIFR-gp130 complex, a further non-signalling receptor might also be necessary. Slight structural differences within the α -helical domains of each cytokine might determine the receptor-dimer format. Gp130 does not recognise IL6 directly. IL6 first forms a low affinity complex with the 80kDa, non-signalling α -receptor, IL6R α , which then binds gp130 with high affinity. A similar series of events also applies to IL11, CNTF, CLC and possibly CT-1. IL6 receptor (IL6-R), IL11 receptor (IL11R), leukaemia inhibitory factor receptor (LIFR), oncostatin M receptor (OSMR), ciliary neurotrophic factor receptor (CNTF-R). Adapted with permission from (55).

1.2.3 IL6-mediated JAK/STAT signalling and its regulation

The gp130 signalling receptor lacks intrinsic kinase activity but is constitutively associated with JAK family tyrosine kinases (Figure 1.2). Cytokine-receptor ligation brings gp130-JAK into close proximity allowing trans-phosphorylation and activation of JAKs which then tyrosine phosphorylate gp130 producing docking sites for the SH2-domain-containing signalling mediators STATs and SH2 domain-containing protein-tyrosine phosphatase 2 (SHP2). IL6-family cytokines predominantly signal from gp130 through JAK1/STAT3 and to a lesser extent JAK2/STAT1 (55). JAK1-mediated phosphorylation of gp130 at Y⁷⁶⁷, Y⁸¹⁴, Y⁹⁰⁵ and Y⁹¹⁵ at a pYXXQ consensus sequence enables binding of STAT3 that competes with STAT1 binding at Y⁹⁰⁵ and Y⁹¹⁵ at a more constrained pYXLQ consensus sequence (55,62). This could account for the more potent activation and dimer formation of transcriptionally active STAT3 compared to STAT1. Docked STATs are tyrosine-phosphorylated by JAKs within their SH2 domains (STAT1, Y⁷⁰¹ and STAT3, Y⁷⁰⁵) which enables receptor dissociation and formation of homo- or hetero- dimers, *via* their SH2 domain, or trimers with DNA-binding adapter proteins such as the IFN regulatory factors (IRFs) before translocating to the nucleus where they drive cytokine-inducible gene transcription from palindromic DNA elements with a TTN₄₋₆AA consensus sequence (63) as well as IFN-stimulated response elements (ISRE sites, AGTTTN₃TTTC) and IFN γ -activated sequence (GAS sites, TTCN₃GAA). The exact preference depends on STAT dimer composition, adapter protein interaction, IFN type as well as STAT-specific sequence variations (64). Formation of dimers and trimers further increases the functional capacity of STATs to modulate gene expression patterns in a cytokine dependent fashion. JAKs also activate SHP2 *via* tyrosine phosphorylation of Y⁵⁴² and Y⁵⁸⁰ and at Y⁷⁵⁹ on gp130, all of which overcome the auto-inhibitory mechanism of the internal SH2 domains within SHP2. JAK-phosphorylated SHP2 then induces ERK-mediated gene transcription *via* the recruitment of the Growth factor receptor-bound 2-Sos of sevenless (Grb2-Sos) complex *via* pY⁵⁴² and pY⁵⁸⁰ (55). Grb2 functions as an adaptor protein for Sos, a Ras guanine nucleotide exchange factor (GEF). Co-localisation of Sos with Ras at the plasma membrane enables activation of Ras and initiation of the ERK signalling pathway (55).

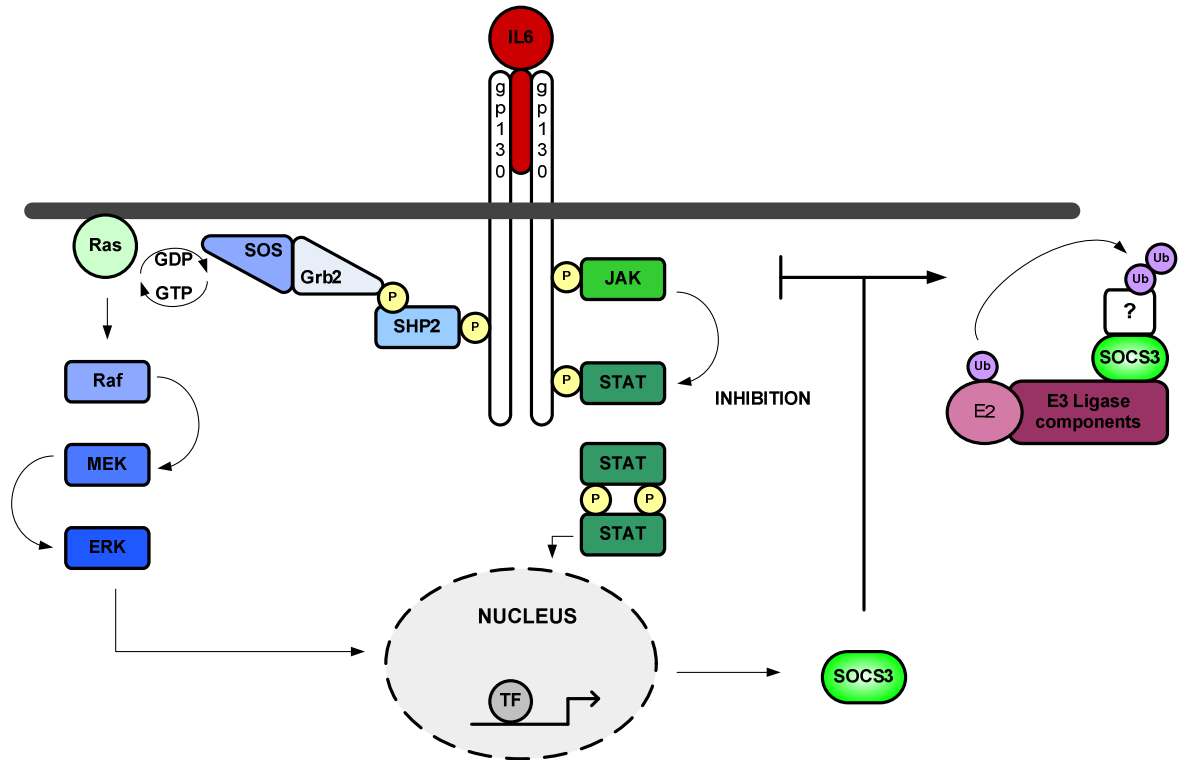


Figure 1.2: IL6 family cytokine signalling

IL6-family cytokine signalling. IL6-family cytokines activate JAK/STAT and ERK pathways. IL6 binds either soluble or membrane-associated IL6 receptor alpha chains followed by binding a gp130 receptor which itself lacks kinase activity but is constitutively associated with JAKs. Cytokine-receptor ligation forms receptor dimers which brings JAKs into close proximity. Following trans-phosphorylation and activation of JAKs, the receptor subunits are phosphorylated producing docking sites for SH2-domain containing proteins, STATs and SHP2. Activation of STATs by JAKs results in receptor dissociation, dimerisation, and translocation to the nucleus where they drive cytokine-induced gene transcription. STAT-induced SOCS3 negatively regulates cytokine signalling either by direct inhibition of JAKs or *via* the degradation of signalling intermediates in its role as a specificity factor for the ECS family of E3 ubiquitin ligases. In a similar fashion to STATs, bound, phosphorylated SHP2 induces gene transcription by activation of the MAPK pathway *via* the recruitment of the Growth factor receptor bound protein 2-Son of sevenless (Grb2-Sos) complex *via* phosphorylated tyrosine residues pY^{542} and pY^{580} . Grb2 is an adaptor protein required for SHP2 association and Sos is a Ras guanine nucleotide exchange factor (GEF). SHP2 is a phosphatase so might act on gp130 and associated factors to negatively regulate signalling.

1.2.4 Negative regulation of the JAK/STAT pathway

Chronic activation of the JAK/STAT pathway can initiate and perpetuate chronic inflammatory diseases such as rheumatoid arthritis and Crohn's disease as well as certain forms of cancer (46,47,65,66). Negative regulation occurs through multiple routes within both extracellular and intracellular domains *via* inhibitory and degradative mechanisms. For example, soluble gp130 (sgp130) can trap circulating sIL6R α /IL6 complexes and thus quench trans-signalling. Furthermore, active phagocytic cells, such as neutrophils at sites of inflammation, secrete proteases that degrade cytokines including IL6 (65,67). Intracellular signalling intermediates can be made functionally mute by protein tyrosine phosphatases such as SHP2, and also by direct inhibition by protein inhibitors of activated STAT (PIAS) (68,69) and suppressor of cytokine signalling (SOCS) proteins (70), the latter of which can also drive ubiquitin-directed proteasomal degradation (10).

1.2.4.1 Extracellular regulation of cytokine signalling

Cytokine-dependent signalling can be suppressed by inhibition or degradation of cytokines. Soluble forms of IL6R (sIL6R) is shed from macrophages and is essential for IL6 trans-signalling through gp130 (57). However, sIL6R and soluble gp130 (sgp130) is detectable in human serum (67). As such, sgp130 can antagonise IL6-IL6R-induced signalling and modulate the effects of circulating IL6 (67,71).

Elevated levels of IL6 present during inflammation are also removed following degradation by serine proteases elastase, proteinase 3, and cathepsin G secreted from neutrophils (65). However, it is not clear if these are expressed in response to IL6 *i.e.* as a regulatory feedback loop. It is also possible that other cells are involved including those of the invading pathogen which might secrete proteases as a protective mechanism (65).

1.2.4.2 Protein tyrosine phosphatases (PTPs)

While SHP2 can activate the ERK pathway, it can also negatively regulate the JAK/STAT pathway *via* its protein tyrosine phosphatase activity against gp130, JAK, and STAT proteins. SHP2 is ubiquitously expressed and consists of two N-

terminal SH2 domains and a C-terminal catalytic phosphatase domain. In its inactive state, the SH2 domains bind to the phosphatase domain to block substrate interaction. This inhibitory action is removed upon tyrosine phosphorylation by cytokine-activated JAKs (see above). Other phosphatases might also have roles in JAK/STAT regulation such as PTP ϵ C, PTP1B, CD45, SHP1 and nuclear-localised phosphatase TCPTP (55).

1.2.4.3 Protein inhibitors of activated STAT

Protein inhibitors of activated STAT (PIAS), as their name suggests, block the function of active/phosphorylated STATs but they also interact with a wide range of non-STAT proteins, most of which are transcription factors such as NF κ B, and so have wider actions as transcriptional regulators (69). Five PIAS family members (PIAS1, PIAS3, PIAS α , PIAS β , and PIAS γ) have been defined. All PIAS bind to active/tyrosine-phosphorylated, nuclear-localised STAT proteins although the inhibitory mechanism appears to be PIAS-specific. All PIAS proteins also have E3 SUMO ligase activity enabling the reversible covalent attachment of “small ubiquitin-related modifier” (SUMO) to the ϵ -amino groups of lysine residues residing within a Ψ -K-x-D/E consensus sequence for SUMOylation on target proteins (Ψ =hydrophobic residue) (69). This post-translational modification modulates cellular localisation, function, and protein-protein interactions, thus altering the composition and activity of transcription factor complexes. IFN γ -induced STAT1 and IL6-induced STAT3-dependent gene transcription are suppressed by PIAS1 and PIAS3 respectively *via* inhibition of transcription factor-DNA binding. Furthermore, STAT1-dependent gene transcription is also inhibited *via* SUMOylation at K⁷⁰³ (72). In contrast, PIAS α and PIAS γ inhibit gene transcription by acting as transcriptional co-repressors. Regulation by PIAS proteins is complex with certain regulatory roles being SUMOylation independent and others relying on specific PIAS domains(68).

1.2.4.4 Suppressors of cytokine signalling

SOCS proteins negatively regulate multiple pathways involved in immune, growth, and metabolic responses. Eight SOCS family members are defined (SOCS1-7 and cytokine-inducible SH2 domain-containing protein (CIS)) of which CIS and SOCS1-3 are best characterised (73). SOCS proteins were discovered

following a search for early cytokine-induced genes in haematopoietic cells (74). In general, SOCS proteins have low basal expression levels that are rapidly elevated by several inflammatory mediators. In a classical negative feedback loop, STAT-induced SOCS proteins ablate intracellular pro-inflammatory signalling by either direct inhibition of signalling components or by ubiquitin-mediated receptor internalisation and proteasomal degradation of signalling intermediates *via* its action as the specificity factor for E3 ubiquitin ligases (62,75). However, sequence deviations between family members bring about different mechanisms of action, and combined with differential expression kinetics, suggest that SOCS family members might each provide non-redundant functionality.

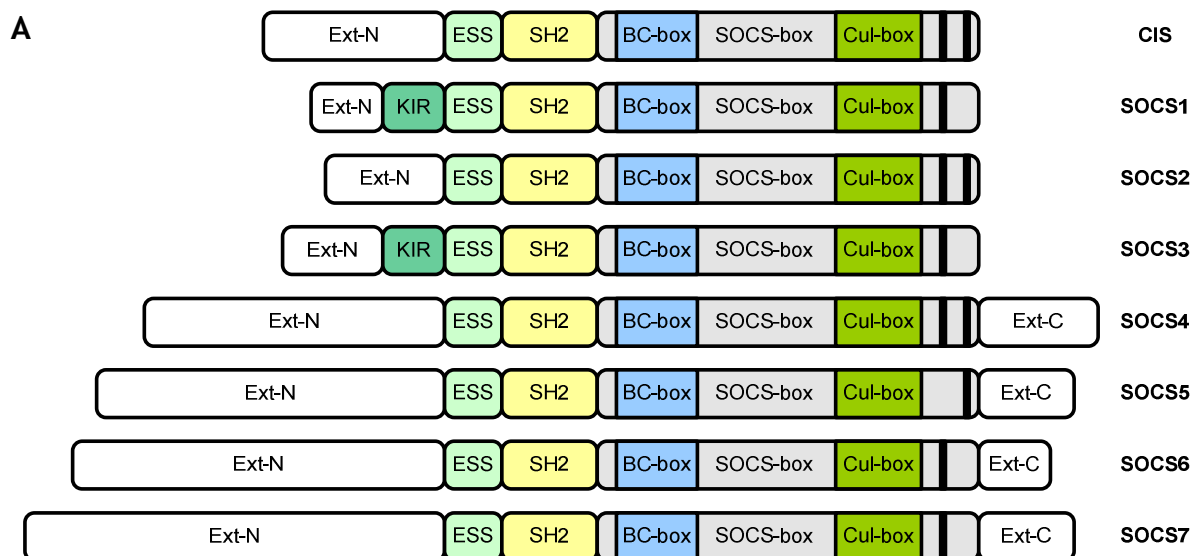
Induction of SOCS proteins occurs *via* multiple routes and the variety of SOCS-regulated pathways is becoming more diverse. Moreover, differing expression kinetics and the potential for cross-regulation within the SOCS family adds a further layer of complexity. At present, inducers of SOCS include, but are not limited to, cytokines (IL1, IL6, LIF, OSM, IL3, IFN γ , TNF α , EPO, prolactin), chemo-attractants (IL8, formyl-Met-Leu-Phe), bacteria-derived components (LPS, unmethylated CpG DNA), hormones (leptin, insulin), and the second-messenger cAMP. Receptor tyrosine kinases (RTK) such as EGFR and PDGFR activated by their cognate ligands might also induce and be regulated by SOCS proteins (51). SOCS proteins bind tyrosine-phosphorylated receptors that have immunoreceptor tyrosine-based inhibitory motif (ITIM)-like sites such as gp130, EpoR, ObR, and others such as CD33 of the SIGLEC glycoprotein family (12). Due to the requirement for tyrosine phosphorylation, it is possible that in certain circumstances inhibition of signalling by SOCS might be indirect i.e. cross-talk between related signalling pathways (51).

Structurally, each SOCS family member consists of a conserved central SH2 domain, an extended SH2 subdomain (ESS), a variable-length, non-conserved N-terminal domain, and a 40 amino acid C-terminal domain SOCS-box (Figure 1.3, panel A). The SOCS-box is considered a multi-functional region. It can regulate stability and the cross-regulation of SOCS proteins as well as SH2-dependent SOCS/substrate recognition and regulation i.e. CIS/ERK regulation. In its role as an E3 ligase, the SOCS-box is required for interaction with the ubiquitin

machinery (cullin5, elonginB, and elonginC) *via* cullin-binding and B/C-box subdomains while tyrosine-phosphorylated substrates are specifically targeted *via* the SH2 domain (Figure 1.3 and 1.4). SOCS1 and SOCS3 are unique in that they also contain an N-terminal kinase inhibitory region (KIR) that shares homology with the pseudosubstrate domain of JAKs. SOCS4-7 also have extended C-terminal domains that have no known functional motifs.

Crystal structures of elongin-bound SOCS2 and SOCS4 suggest that extended N- and C-terminal regions might function to stabilise the tertiary structure (75). SOCS2 has a conserved C-terminus that is predicted to stabilise the SH2-SOCS-box interaction allowing exposure of the N-terminal ESS and KIR. The SOCS4 SH2-SOCS-box interaction is stabilised by the extended N-terminal domain, the extended C-terminus then interacts with the N-terminal domain to further stabilise the structure (75). These structural characteristics are thought to apply to similar SOCS family members i.e. SOCS1, SOCS3, CIS, and SOCS5-7 respectively. Over the full length of the protein, SOCS family members have sequence homology with SOCS4-5 being most similar (92%) followed by SOCS6-7 (57%), CIS and SOCS2 (45%), and finally SOCS1 and SOCS3 (35%) although certain domains are more conserved than others (76) (Figure 1.3, panel B). For instance, the elongin binding site is the most conserved site on all SOCS proteins which points to its importance (75). Consistent with this, mutation of a single leucine within the B/C-box has been demonstrated to completely block elongin interaction and substrate degradation (77).

Direct inhibition of substrates requires the SH2 domain, ESS, and KIR, but uniquely, CIS also requires the SOCS-box and pY^{253} (75). Furthermore, interaction of the CIS-SH2 domain with pY^{253} is hypothesised to regulate CIS by keeping it in an inactive state until tyrosine-phosphorylated substrates are available. SOCS1 and SOCS3 are the only family members that can inhibit IL6-gp130 signalling *via* a SOCS-box independent route. Both inhibit JAK catalytic activity by acting as pseudosubstrates and thus blocking STAT1 and STAT3 activation. SOCS1 binds to the tyrosine-phosphorylated activation loop of JAK2 *via* its KIR, SH2, and ESS. SOCS3 similarly binds JAK1 but its interaction is weaker and requires further interaction with tyrosine-phosphorylated receptors such as gp130 at pY^{759} *via* its



B

	BC-box	Cul5-box
CIS	VQPFVRRSSARSLQHLCLRLVINRLVA--	DVDCLPLPRRMADYLRQYPFQL
SOCS1	LGAPLRQRRVRPLQELCRQRIVAAVGREN	LARIPLNPVLRDYLSSFPFQI
SOCS2	TKPLY--TSAPSLQHLCLRLTINKCTG--	AIWGLPLPTRLKDYLEEYKFQV
SOCS3	VLSRPLSSNVATLQHLCRKTVNGHLDS-	YEKVTQLPGPIREFLDQYDAPL
SOCS4	LSTPLIRTFPFSLQHICRTVICNCTTYDG	IDALPIPSSMKLYLKEYHYKS
SOCS5	LTISLNRTFPFSLQYICRAVICRCCTTYDG	IDGLPLPSMLQDFLKEYHYKQ
SOCS6	TNPVSRFMQVRSLQYLRCRFVIRQYTRIDL	IQKLPLPNKMKDYIQEKHY--
SOCS7	LYPVSRFNSNVKSLQHLRCFRIRQLV	LRIDHLPDLPLPKPLISYIRKFYYD

Figure 1.3: Elongin-Cullin-SOCS-box (ECS) family of E3 ubiquitin ligases

A. Organisation of domains within the SOCS protein family, see text for description. **B.** Sequence alignment of the SOCS-box for all SOCS family members. The alignment was performed using the clustalW2 multiple sequence alignment tool available at <http://www.ebi.ac.uk/Tools/msa/clustalw2/>. Highlighted sections indicate the BC-box and Cul5-box.

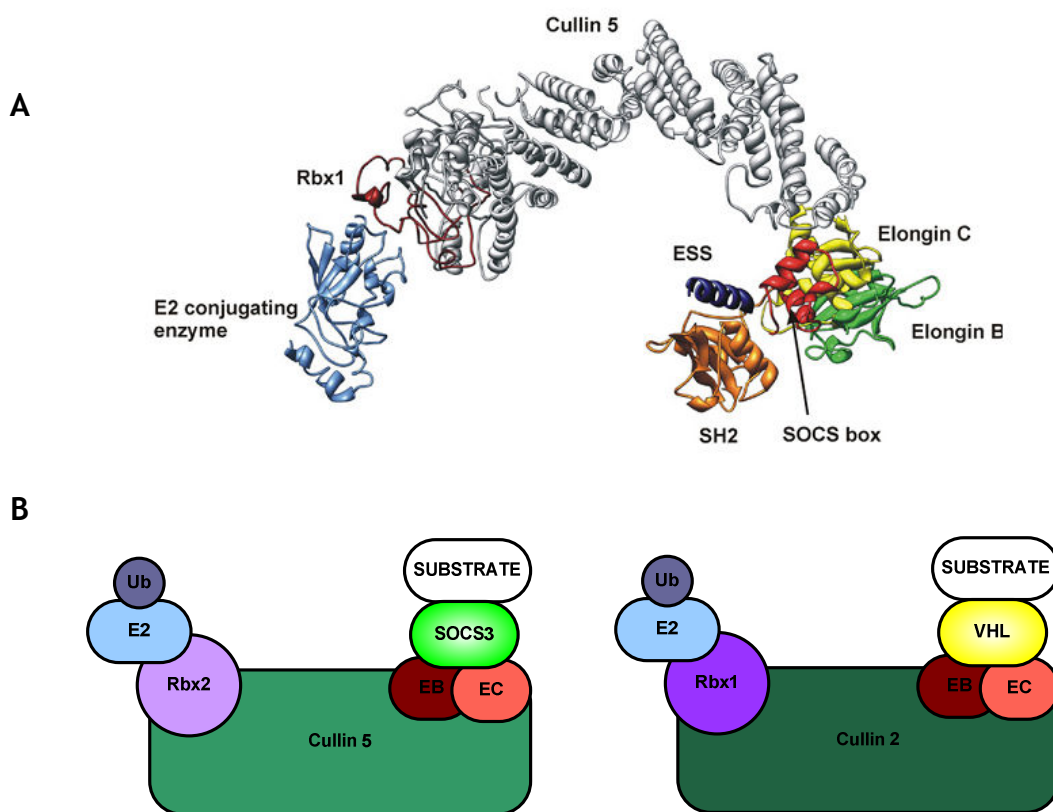


Figure 1.4: Structural model of the SOCS3-containing ECS-type E3 ubiquitin ligase

A. The central cullin5 scaffold protein positions the E2 conjugating enzyme in close proximity to SOCS3, which binds a target substrate (not shown) *via* its SH2 domain. SOCS3 is attached to cullin5 *via* a complex of elonginB and elonginC. The triple α -helix structure of the C-terminal domain SOCS-box forms a 4-helix bundle with a single helix, helix 4, of elonginC. Diagram reproduced with permission from (75). **B.** Basic E3 ubiquitin ligase architecture. VHL and SOCS proteins act as specificity units for the ECS family of E3 ubiquitin ligases. SOCS proteins bind specific tyrosine-phosphorylated substrates or phosphodegrons *via* an SH2 domain. The SOCS-box motif enables interaction with components an E3 ubiquitin ligase. SOCS binds to the N-terminal of the cullin5 scaffold protein *via* the adaptor proteins elonginB, elonginC. Cullin5, *via* its C-terminus, also binds the RING finger-containing protein Rbx2 that enables interaction with the E2 conjugation protein. In complex with the E3 ligase scaffold, the substrate and E2-bound ubiquitin are in close proximity thus facilitating the transfer of ubiquitin to the substrate.

SH2 domain and as such, mutation of Y⁷⁵⁹ (Y⁷⁵⁷ on murine gp130) reduces the inhibitory effect of SOCS3 but not SOCS1 (51,78). This is thought to explain why SOCS1 is a more potent inhibitor of JAK/STAT signalling. IL6 and IFN γ both induce SOCS1 and SOCS3 in a STAT-dependent fashion. Furthermore, overexpression of SOCS1 or SOCS3 is sufficient to terminate JAK/STAT signalling. In contrast, *in vivo* studies indicate that SOCS1 specifically targets IFN γ -dependent JAK2/STAT1 signalling whereas SOCS3 targets IL6-dependent JAK1/STAT3 signalling. Interestingly, in conditional SOCS3 knockout mice, IL6 has a similar response and gene expression profile as IFN γ due to prolonged STAT1 signalling suggesting that SOCS3 might be required prevent generation of a IFN γ -type response by IL6 (51).

The SOCS3 SH2 domain shares 41% homology with that of SHP2 (12). Furthermore, SOCS3 binds at an overlapping sequence and as such can compete with SHP2 to ablate SHP2-induced ERK activation by gp130. SHP2 itself might also contribute to signal suppression *via* the dephosphorylation of receptor tyrosine residues or receptor-bound substrates such as JAK. SOCS3 can also prolong ERK signalling by binding, and thus inhibiting, the Ras inhibitor p120 RasGAP. Upon SOCS3 induction by IL2, IL6, Epo, insulin, EGF, and PDGF, SOCS3 is tyrosine-phosphorylated within the SOCS-box domain enabling binding to p120 RasGAP. This function does not affect SOCS3-dependent inhibitory effects such as its ability of block STAT5 activation. Unregulated Ras-mediated ERK activation is an initiator of tumourigenesis and Ras is mutationally activated in over 15% of all cancers (79). Since IL6 activates ERK signalling but also maintains ERK activation *via* SOCS3, sustained JAK/STAT signalling due to chronic inflammation might also contribute to tumourigenesis.

CIS is thought to compete with STAT5 for phosphotyrosine residues on active erythropoietin (Epo) and growth hormone (GH) receptors (51,74). However, this is disputed in the case of GHR due to non-overlapping binding sites of STAT5 and CIS (75). However, CIS may disrupt STAT5 binding *via* steric hindrance (80). A degradation-dependent regulatory mechanism is now preferred since CIS can only bind its substrates when in complex with elonginB/C. SOCS2, being most similar to CIS with which it shares 35% identity, has been shown to function by

inhibiting GH-stimulated STAT5 activation in a SOCS-box dependent fashion. Furthermore, SOCS2^{-/-} mice have an overgrown phenotype (75,81) which indicates its importance in GH regulation. Inhibitory mechanisms and functional relevance of SOCS4-7 are as yet undefined. However, both SOCS4 and SOCS5 have been reported to increase EGF-dependent EGFR degradation (75) while SOCS5, being specifically expressed in T_{h1} but not T_{h2} cells, might affect T-helper cell equilibrium by repressing T_{h2} cell differentiation (51). This is relevant in the study of allergic diseases such as asthma where T_h cell imbalance, specifically an increase in the T_{h2} compartment due to atopic SOCS protein expression, is thought to be an initiating factor (82). Furthermore, SOCS5 might also regulate IL4 signalling by inhibiting IL4R-bound JAK1 (80). SOCS6 and SOCS7 are most similar in relation to SH2 and SOCS-box domains and both bind tyrosine-phosphorylated insulin receptors to suppress signalling following insulin treatment, suggesting similar or redundant functions.

Suggestions of E3 ligase functionality resulted from analysis of SOCS3 which identified a conserved C-terminal domain, the SOCS-box, also present in a known E3 ligase Von-Hippel-Lindau (VHL) and others MUF-1, and elonginA (51). SOCS-box domains have been identified within over 70 human proteins conjugated to a variety of protein-protein interaction domains including SH2 domains, WD-40 repeats, SPRY domains, leucine rich repeats, and ankyrin repeats that are thought to add target specificity and diversity (75,83).

Most SOCS members form ECS-type E3 ligases and as such specifically bind E3 ligase components elonginB/C, cullin5 and the RING finger-containing protein Rbx2 *via* the SOCS-box (Figure 1.4, panel B). SOCS binds the cullin5 scaffold protein *via* the elonginB/C dimer that binds the N-terminal region of cullin5. Cullin5 also binds Rbx2 *via* its C-terminus and enables interaction with the E2 conjugation protein. SOCS1 has also been found in complex with cullin5/Rbx1 (51). Both Rbx1 and Rbx2 bind cullin2 and cullin5 when overexpressed but under physiological conditions preferentially binds cullin2 and cullin5 respectively (84). Interestingly, SOCS6 might regulate proteasomal degradation *via* a non-ECS E3 ubiquitin ligase since it has been reported in complex with haem-oxidized IRP2 ubiquitin ligase1 (HOIL1) (85).

Unbound SOCS-box exists in a disordered state and only becomes organised upon binding elonginB/C, requiring that this interaction precede the binding of cullin5 and E3 ligase complex formation (77). This was initially hypothesised from observations of crystal structures of VHL, SOCS2 and SOCS4 that were found to interact with elongins through mainly (+70%) hydrophobic interactions. Uncoupling of these proteins vastly increases exposure of non-polar residues and as such was expected to contribute to unfolding and also increase the difficulty in producing unbound crystal structures (75). Two subclasses of SOCS proteins can be defined based on their differing affinity for cullin5 (86). SOCS1 and SOCS3 binds elonginB/C-cullin5-Rbx2 weakly ($K_d=10^{-6}$ M (SOCS1), 10^{-7} M (SOCS3)) compared to all other family members ($K_d=10^{-8}$ M) due to slower off rates and they also have shorter half-lives. As such, it is thought that SOCS2, SOCS4-7 and CIS regulate signalling *via* a solely ubiquitin dependent pathway.

E3 ligase functionality has been demonstrated for SOCS1 and SOCS3 but has yet to be confirmed for other SOCS family members (86). As such, studies on mice that have been genetically manipulated to remove the SOCS3 SOCS-box i.e. SOCS3 SOCS-box knockout mice, have immunological defects suggesting important proteasome-dependent regulatory roles (see below). The SOCS proteins act as a specificity unit within the elonginBC-cullin5-Rbx2 E3 ligase complex. Binding to the E3 ligase scaffold is *via* the SOCS box domain. SOCS proteins associate with tyrosine-phosphorylated substrates *via* a conserved central SH2 domain. It is currently regarded as a multifunctional domain implicated in SOCS stability, adaptor protein interaction, proteasomal degradation, receptor binding, and regulation of MAPK pathway. In relation to JAK/STAT signalling, SOCS1 has been shown to direct proteasomal degradation of active/tyrosine-phosphorylated JAK2 (87). JAK2 is monoubiquitinated in unstimulated cells but becomes polyubiquitinated following tyrosine phosphorylation (Y^{1007}) and subsequent association with SOCS1. It is possible that SOCS3 similarly regulates JAK1 (73) but this has yet to be demonstrated. The full spectrum of ubiquitin-regulated SOCS substrates is unknown; those identified so far are shown in Table 1.0.

Table 1.0: Ubiquitin-regulated SOCS substrates

Table of proteins known to be targeted for ubiquitin-mediated proteasomal degradation by SOCS family members.

Substrate	Reference	SOCS Family Member
CD33	(11)	SOCS3
Siglec-7	(12)	
IRS-1/2	(9)	
JAK2	(87)	SOCS1
Tel-JAK2	(88)	
Vav	(89)	
NF κ B subunit p65/Rel A	(90)	
Mal	(91)	
HPV, E7	(92)	
FAK	(10)	

The importance of the SOCS-box component of individual SOCS proteins has been demonstrated using animal models. Zhang et al (2001) showed SOCS1-SOCS-box-deleted ($\text{SOCS1}^{\Delta\text{SB}/\Delta\text{SB}}$) knock-in mice developed a less severe phenotype than SOCS1 knockout mice suggesting an essential role for the SOCS-box domain (93). The severity of phenotype has been linked to prolonged hyper-responsiveness to $\text{IFN}\gamma$ that prolongs STAT1 signalling in $\text{SOCS1}^{\Delta\text{SB}/\Delta\text{SB}}$, but intermediate to that observed for the WT and conditional $\text{SOCS1}^{-/-}$ mice. Similarly, $\text{SOCS3}^{\Delta\text{SB}/\Delta\text{SB}}$ mice, although viable, have prolonged STAT3 signalling that is intermediate to that of conditional $\text{SOCS3}^{-/-}$ and WT mice. Hyper-responsiveness to G-CSF, in $\text{SOCS3}^{\Delta\text{SB}/\Delta\text{SB}}$ mice, resulted in enhanced granulopoiesis, tissue infiltration, and arthritis, although the phenotype was reduced compared to the conditional $\text{SOCS3}^{-/-}$ mice (94). The increased half-life of active pJAK1 found in $\text{SOCS3}^{\Delta\text{SB}/\Delta\text{SB}}$ embryonic stem cells (ES) suggests that SOCS3 can regulate JAK1 *via* ubiquitin ligase activity (73). Furthermore, comparison of WT, $\text{SOCS3}^{-/-}$ and $\text{SOCS3}^{\Delta\text{SB}/\Delta\text{SB}}$ ES cells has shown that the SOCS-box is specifically required to target LIF-induced pJAK for proteasomal degradation. These results indicated that in ES cells, pJAK dissociates from gp130 and is cleared *via* proteasomal degradation by SOCS3 and not simply inhibited by the KIR domain (73).

SOCS3 negatively regulates IL6-induced JAK/STAT signalling *in vitro* and *in vivo* (95). This is supported from the finding that IL6-activated STAT1 and STAT3 signalling is prolonged in conditional $\text{SOCS3}^{-/-}$ mice. *In vitro* studies have found that over-expressed SOCS1, SOCS3, or CIS can inhibit JAK/STAT signalling although *in vivo* function is more specific. If over-expressed, SOCS1 and SOCS3 inhibits IL6 and $\text{IFN}\gamma$ signalling although in conditional $\text{SOCS3}^{-/-}$ mice IL6 signalling is prolonged whereas $\text{IFN}\gamma$ is unaffected. The opposite occurs in $\text{SOCS1}^{-/-}$ mice i.e. $\text{IFN}\gamma$ signalling is prolonged whereas IL6 is unaffected suggesting that SOCS1 and SOCS3 have reciprocal roles. Interestingly, IL6-induced gene products from $\text{SOCS3}^{-/-}$ mice matched that of $\text{IFN}\gamma$ -induced genes. This observation might be explained by the extended activation period of the STAT1, since it is potently activated by $\text{IFN}\gamma$ but minimally activated by IL6 in the presence of SOCS3. Suppression of the IL6-activated JAK/STAT pathway by SOCS3 might therefore prevent an $\text{IFN}\gamma$ -induced response by IL6 (95).

Tyrosine residues within the SOCS-box (70%) are conserved across all SOCS family member and are thought to regulate substrate binding, SOCS protein stability, ERK pathway regulation or auto-regulation in complex with the ESS or SH2 domains (75). The interaction of the CIS SH2 domain with pY²⁵³ has already been mentioned with regard to the potential for auto-regulation. Furthermore, SOCS3 SOCS-box-dependent maintenance of ERK signalling has also been discussed. Other phosphorylation events are thought to regulate the interaction of SOCS with the ubiquitination machinery and also modulate SOCS stability. In these cases, phosphorylation is thought to affect auto-ubiquitination or interaction with other E3 ligase complexes including those constructed from other SOCS family members. A complete list of protein kinases responsible for SOCS phosphorylation has yet to be documented although cytokine-induced kinases such as the Pim serine/threonine family kinases are thought to stabilise SOCS1 (96). In support of this, all Pim family members (Pim1-Pim3) interact and phosphorylate SOCS1, while reduced SOCS1 levels were detected in Pim1/2 knockout mice. It should be noted that not all phosphorylation events are sufficient to affect stability since hyperphosphorylation of SOCS3 by a constitutively active JAK2 mutant (V617F) is insufficient to cause destabilisation (8,73).

Ubiquitin-directed proteasomal degradation of SOCS proteins, which is intimately linked to phosphorylation, might occur in an auto-regulatory fashion or *via* another SOCS protein or E3 ligase. Ubiquitination occurs within non-conserved sequences at specific lysine residues on target proteins. As such, SOCS3 stability was increased, following an N-terminal domain truncation that resulted in the loss of Lys6 (97). Furthermore SOCS2, 6 and 7 can bind all other SOCS proteins and have been implicated in their regulation *via* proteasomal degradation (75). Ubiquitin-dependent SOCS regulation is yet to be resolved, with literature painting a complex picture of both auto- and cross-regulation, mainly from the finding that formation of SOCS E3 ligases, specifically the SOCS-elongin interaction, has been shown to both stabilise and destabilise SOCS proteins. Furthermore, RING E3 ligases often perform auto-ubiquitination but are also found in complex with other E3 ligases (98) and so both mechanisms of regulation are equally possible. For example, concomitant degradation of CIS and SOCS3 with their target proteins, GHR and SIGLEC 7 respectively (75) as well

as the observation that disruption of the elonginB/C interaction leads to stabilisation, suggests that CIS/SOCS3-E3 ligases perform auto-ubiquitination. Conversely, a similar disruption to SOCS1 has been reported to *destabilise* the protein (99) suggesting that the elonginB/C interaction is protective. Additionally, SOCS3 is phosphorylated within the SOCS-box at Y²⁰⁴ and Y²²¹ upon induction in response to IL2, IL3, Epo, EGF, PDGF, and IL6. Such phosphorylation events fail to block binding to gp130 or JAK inhibition but blocks binding to elonginB/C and reduce protein stability (100). In MEFs, IL6-induced SOCS3 is phosphorylated independently from IL6 stimulation, gp130 recruitment, and JAKs. Src receptor tyrosine kinases (RTK) were shown to be involved although residual SOCS3 phosphorylation suggested the involvement of additional kinases. It might therefore be speculated that SOCS3 could be regulated *via* crosstalk from other signalling pathways (62). Furthermore, SOCS3 was found to be stabilised in SOCS3^{ΔSB/ΔSB} cells suggesting that SOCS-box or SOCS-box phosphorylation is necessary for its degradation (94).

Different expression kinetics of SOCS proteins suggests the potential for additional regulation. SOCS1, 3, and CIS are rapidly and transiently induced, whereas SOCS2, 6, and 7 are expressed later and, in the case of SOCS2, expression in more prolonged (75). For example, Tannahill et al (2005) (55) showed that SOCS3 is induced after 30 minutes in IL2-treated peripheral blood mononuclear cells (PBMC) whereas SOCS2 was only detectable after 4 hours. Furthermore, whereas SOCS3 expression is transient and undetectable after 4 hours, SOCS2 could still be detected after 24 hours (55). All SOCS proteins interact with E3 ubiquitin machinery although SOCS1 and SOCS3 do so more weakly (101). Thus a situation is possible where stronger interacting members could potentially out-complete weaker members for the ubiquitin machinery and thus induce their proteasomal degradation. For example, SOCS2 is expressed later than SOCS1/3, and overexpression was found to have the unexpected effect of restoring JAK/STAT signalling following GH stimulation (51). This would suggest a role for SOCS2 in the negative regulation of SOCS1/3. Although new data dispute such a mechanism (102), SOCS2 has been demonstrated to regulate CIS in this fashion (75). Furthermore, different expression kinetics might allow temporal regulation of signalling. For example, delayed expression of SOCS proteins would prolong the action of target signalling intermediates by delaying

their inhibition/degradation. SOCS2-mediated regulation is further complicated since low levels of SOCS2 can suppress GH signalling indicating a dual function (103). As well as ubiquitination, specific regions such as PEST (proline, glutamate, serine, and threonine-rich) motifs are also associated with the regulation of stability *via* proteasomal degradation. An unstructured PEST motif is found within the SH2 domain of SOCS3. Mutation of the PEST motif does not impact SH2 binding of phospho-tyrosine residues and complete removal of the motif does not prevent STAT3 inhibition. However, it does seem to impact stability since removal of the domain increases the half-life of SOCS3, suggesting a destabilising role (77).

1.3 SOCS3: the first cAMP-inducible E3 ubiquitin ligase

1.3.1 Cyclic AMP: generation and effectors

Cyclic-AMP is a second messenger produced following the activation of $G_{\alpha s}$ -coupled GPCRs e.g. activation of EP₂ and EP₄ receptors by prostaglandin E₂ or by direct activation the $G_{\alpha s}$ effector protein adenylyl cyclase by forskolin (70). Adenylyl cyclase generates cAMP from cellular ATP, which rapidly diffuses throughout the cell. Efficient cAMP-dependent signalling is achieved by co-localisation of cAMP effectors at typically at A-kinase anchoring proteins (AKAPs) (104). Furthermore, compartmentalisation and negative regulation of cAMP signalling is mediated by a family of phosphodiesterases (PDEs) such as the cAMP-specific PDE4 family which catalyses the hydrolysis of cAMP to AMP (104). Four cAMP effectors are defined namely cyclic nucleotide-gated (CNG) ion channels (105), protein kinase A/cAMP-dependent protein kinase (PKA) (106), exchange protein directly activated by cAMP (EPAC) (107,108), and potentially CNRASGEF1 (109,110). The latter is controversial since the direct binding of cNMP has yet to be confirmed. While CNG ion channels are well characterised for photoreceptor, olfactory, and neuronal cells (105), functions within other cells types are not well characterised. As such, CNRASGEF1 and CNG ion channels will not be considered further.

PKA, a serine/threonine kinase, is a multi-subunit protein consisting two regulatory (R) and two catalytic (C) units (Figure 1.5). Genes encoding four R

units RI α , RI β , RII α , and RII β and three C units C α , C β , and C γ are defined. PKA can be targeted to specific substrates by precise cellular localisation by AKAPs that bind PKA preferentially *via* the RII subunit although some also interact with RI subunits (111,112). Classically, cAMP drives gene transcription in a PKA/cAMP response element-binding protein (CREB)-dependent manner (113). Activation of PKA follows threonine phosphorylation at Thr¹⁹⁷ within the activation loop of the catalytic unit and cAMP binding at two locations on each regulatory unit at the C-terminal cAMP-binding domain (CBD)(112). Conformational changes induced by cAMP binding allow dissociation of catalytic units and translocation to the nucleus. Within the nucleus, PKA catalytic domains phosphorylate CREB at S¹³³, which enables association with CREB-binding protein (CBP) and gene transcription from cAMP-response elements (CREs) (113).

Exchange protein directly activated by cAMP (EPAC) is a second form of cAMP sensor that changed the landscape of cAMP-mediated signalling (Figure 1.5). Until their discovery, PKA was the only accepted cAMP-activated protein (107,108) EPACs are cAMP-activated guanine nucleotide exchange factors (GEF) for the Rap family of GTPases (107). Two isoforms of EPAC are defined; EPAC1 is ubiquitously expressed while EPAC2 is restricted to brain tissue and adrenal glands (107,108). EPACs have diverse functions including cell adhesion, exocytosis, cell differentiation and proliferation, gene expression, and apoptosis (114). Cyclic AMP is a well defined anti-inflammatory mediator (115) and several of its responses are elicited *via* EPAC. For example, cAMP/EPAC-mediated SOCS3 induction is sufficient to terminate IL6 signalling (70). Furthermore, to protect against infiltration of pro-inflammatory mediators, vascular permeability is reduced following EPAC1 activation by vascular endothelial (VE)-cadherin-dependent cell junction formation and actin remodelling (116). The development of cAMP analogues that selectively activate EPACs such as 8CPT-2'O-Me-cAMP(007) has enabled PKA- and EPAC-specific pathways to be delineated (116).

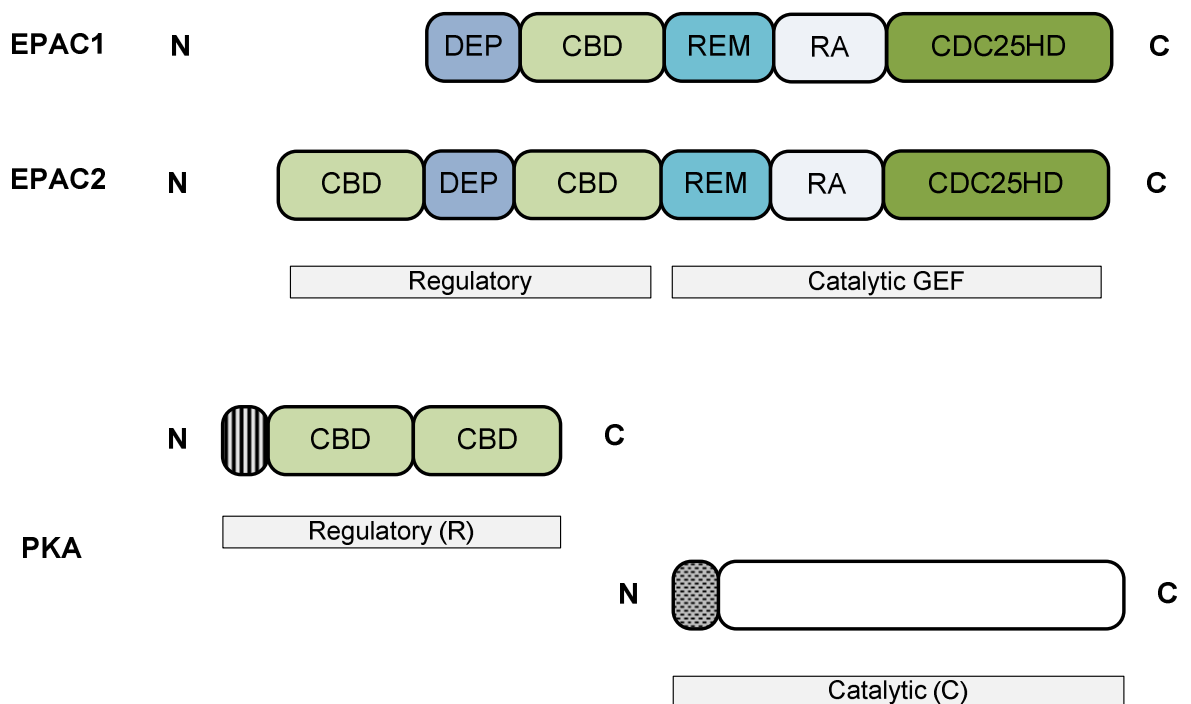


Figure 1.5: PKA and EPAC domain structure

PKA is a cAMP-activated serine/threonine protein kinase. It exists as a complex of two regulatory (R) and two catalytic (C) units when inactive. Binding of cAMP at two cAMP-binding domains (CBD) on each regulatory unit leads to activation and dissociation of catalytic units and phosphorylation of multiple substrates at serine and threonine residues. EPACs are GEFs for the Rap family of small GTPases. They share a conserved central CBD with PKA although EPAC2 also has an additional low affinity N-terminus CBD of unknown function. The Dishevelled/Egl-10/Pleckstrin (DEP) domain mediates membrane attachment while the Ras exchange motif (REM), found in all known Rap GEFs, is important for structural stability (107). GEF activity is provided by the CDC25 homology domain (CDC25HD) aided by the REM and the Ras association domain (RA).

1.3.2 SOCS3 and cAMP

As previously stated, SOCS proteins are each induced by a variety of stimuli but importantly, SOCS3 is also inducible by cAMP (117). How cAMP leads to SOCS3 induction is yet to be fully described. Unlike IL6 which induces SOCS3 *via* the JAK/STAT pathway, cAMP-induced SOCS3 is *via* an EPAC/CAATT enhancer binding protein (C/EBP) (70) and a PKA-independent ERK-mediated route (118). Whereas the former is dependent on STAT-mediated gene transcription the latter is dependent on the C/EBP transcription factor family, specifically the C/EBP β and C/EBP δ isoforms (119). Sustained cAMP elevation is thought to result in at least two distinct events leading to SOCS3 induction: EPAC1 activation and transient PKA-independent ERK activation (118). EPAC1 activation increases recruitment of C/EBP at the SOCS3 promoter (119) whereas ERK-dependent phosphorylation of C/EBP β at Thr²³⁵ fully activates SOCS3 expression (70). While downstream events following EPAC activation are unclear, it has been shown that SOCS3 induction is Rap1-dependent (119), *via* the activation of its downstream effector PKC α through PLC ϵ (120). Activation of PKC by the sn-1,2-diacylglycerol (DAG) analogue phorbol myristate acetate (PMA) leads to ERK-dependent phosphorylation of the transcription factors STAT3 (S⁷²⁷), SP3 (S⁷³), and the component of the AP-1 complex c-Jun (S⁶³) within their transactivation domains in HUVECs (121). Furthermore, AP-1, STAT, and SP1/SP3 consensus sites within SOCS3 promoter (-107 nucleotides from the transcription start site) are necessary for PMA and cAMP-mediated SOCS3 induction. Inhibition of ERK signalling using the MEK inhibitor U0126 does not completely ablate SOCS3 induction in COS1 cells suggesting the involvement of another MAPK such as JNK (121). Indeed, JNK inhibition blocks PMA-dependent phosphorylation of c-Jun and cAMP-mediated induction of SOCS3 (121). A further study by the same group also showed that the p38 MAPK pathway is also involved in the maintenance of basal activity of the SOCS3 promoter (122).

It has been demonstrated that EPAC1 activation is sufficient to terminate IL6 signalling following SOCS3 induction (70). The SOCS3 SH2 and KIR domains have been shown to be essential for this inhibitory role (123). However, the increased half-life of active pJAK1 found in SOCS3 ^{Δ SB/ Δ SB} embryonic stem cells (ES) suggests

that SOCS3 can regulate JAK1 *via* ubiquitin ligase activity (73). The identification of several SOCS3 ubiquitin-regulated substrates has marked SOCS3 as the first cAMP-inducible E3 ubiquitin ligase (8-12). However, the full spectrum of SOCS3-dependently ubiquitinated substrates has yet to be identified necessitating this study.

1.3.3 SOCS3 and inflammation

The importance of STAT3/SOCS3 signalling has been demonstrated in several chronic inflammatory disorders such as atherosclerosis (66) and Crohn's disease (46,124). SOCS3 inhibits pro-inflammatory IL6-stimulated signalling in ECs (70,118). Furthermore, prolonged IL6 signalling is detected in macrophages and liver cells from conditional SOCS3^{-/-} mice (95). Moreover, while IL6 can inhibit macrophage colony-stimulating factor (M-CSF)-mediated proliferation of bone marrow-derived macrophages, IL6 has a greater inhibitory effect on SOCS3^{-/-} macrophages (95). Sustained IL6 signalling in the absence of SOCS3 led to an IFN γ -type response, probably due to extended STAT1 signalling, suggesting that SOCS3 is required to direct the appropriate cytokine response (95). Together, these data not only demonstrate the ability SOCS3 to suppress and regulate the duration of cytokine signalling but also to regulate macrophage proliferation. Furthermore, the specific loss of SOCS3 in macrophages has been shown to produce an IL6-mediated IL10-like anti-inflammatory response (125). Similar to IL10-treated WT macrophages, treating SOCS3^{-/-} macrophages with LPS plus IL6 resulted in sustained STAT3 activation that suppressed secretion of the pro-inflammatory cytokines TNF α and IL12 (125).

Chronic IL6 signalling contributes to the onset of atherosclerosis, which is associated with the upregulation of adhesion molecules, chemokines, and proliferation of vascular smooth muscle cells (VSMCs) (Section 1.1.3). Furthermore, SOCS3 is found to be elevated in the shoulder regions of atherosclerotic plaques (66). The shoulders are weak, vulnerable regions associated with inflammatory gene expression, macrophage infiltration, and strong haemodynamic stress, it is here where rupture frequently occurs (66,126). Overexpression of SOCS3 has been demonstrated to negatively regulate IL6-mediated STAT3 signalling and reduce proliferation of VSMCs and monocytes

(66). Furthermore, this was accompanied by a reduction in ICAM1 and MCP1 expression thus supporting its role as a negative regulator of inflammation (66). SOCS3 is also a negative regulator of G-CSF mediated granulopoiesis, the development of progenitor stem cells to granulocytes such as neutrophils. A targeted, conditional deletion of SOCS3 in haematopoietic cells resulted in splenomegaly and neutrophil leukocytosis followed by inflammation of the plural and peritoneal cavities (127). Increase response to G-CSF was linked to sustained STAT3 activation but not STAT1, STAT5, or ERK1/2, which are also G-CSFR effectors. This study showed that SOCS3 could inhibit STAT3 signalling *via* inhibition of JAK, which was dependent on G-CSFR pY^{729} (pY^{728} in mouse). However, a more recent study found that negative regulation of G-CSFR might also be dependent on the E3 ligase functionality of SOCS3. A specific SOCS3 SOCS-box deletion ($SOCS3^{\Delta SB/\Delta SB}$) in mice produced a similar but milder phenotype compared to the conditional $SOCS3^{-/-}$ mice (94). Furthermore, $SOCS3^{\Delta SB/\Delta SB}$ mice had prolonged STAT3 signalling that was intermediate to that of conditional $SOCS3^{-/-}$ and WT mice (94). Furthermore, SOCS3 has been shown to target G-CSFR for SOCS-box-dependent ubiquitination and lysosomal degradation (8). As such, SOCS3 regulates this pathway *via* both SOCS-box dependent and independent mechanisms. As an E3 ligase, SOCS3 might more broadly impact inflammatory signalling by targeting effectors of JAK/STAT signalling. A $SOCS3^{\Delta SB/\Delta SB}$ in embryonic stem cells (ES) resulted in an increased half-life of active pJAK1 suggests that SOCS3 can regulate JAK1 *via* ubiquitin ligase activity (73). Furthermore, comparison of WT, $SOCS3^{-/-}$, and $SOCS3^{\Delta SB/\Delta SB}$ ES cells has shown that the SOCS-box is specifically required to target LIF-induced pJAK for proteasomal degradation. These results indicated that in ES cells, pJAK dissociates from gp130 and is cleared *via* proteasomal degradation by SOCS3 and not simply inhibited by the KIR domain (73).

The role of SOCS3 in adaptive immunity is less well understood. However, SOCS3 has been shown to be important in the development and maintenance of allergy (82) and the development of autoimmune disorders such as multiple sclerosis (128). SOCS3 is differentially expressed in naïve CD4⁺ T-cells following differentiation to T_h cells with SOCS3 being exclusively expressed in T_{h2} cells. Elevated SOCS3 expression during differentiation, which is dependent on IL4/STAT6 signalling, correlates with the development and severity of atopic

dermatitis and asthma (82). SOCS3 transgenic mice, which constitutively express elevated levels of SOCS3 in T-cell subsets, have an increased T_{h2} response (82). SOCS3 expression was found to inhibit IL12-mediated STAT4 signalling thus inhibiting T_{h1} differentiation. As such, increase SOCS3 levels leads to pathogenesis due to an excessive T_{h2} -activated granulocyte response (82). Increased levels of SOCS3 seem to be driven by IL4 which is also secreted by T_{h2} cells and in a positive feedback loop maintains SOCS3 expression. A further study implicated SOCS3 in the development of T_{h17} cells (129). T_{h17} cells provide protection against fungi and extracellular bacteria, while T_{regs} limit this response. Sustained IL6 signalling disrupts the T_{h17}/T_{reg} balance leading to T_{h17} cell-mediated development of inflammatory disorders such as rheumatoid arthritis (60). In the absence of SOCS3, IL23-mediated STAT3 signalling is enhanced which drives STAT3 mediated IL17A/F gene expression and subsequent generation of T_{h17} cells; this effect is enhanced in the presence of IL6 (129).

The effects of SOCS3 therefore seem to be cell/context specific and thus therapeutic benefits might require precise targeting of SOCS3. For example, in the case of G-CSFR signalling, inhibition of SOCS3 might aid recovery from neutropenia such as following chemotherapy while activation of SOCS3 might aid treatment of chronic inflammation associated with neutrophil accumulation such as inflammatory bowel disease (IBD) (127). Furthermore, while upregulation of SOCS3 might be anti-inflammatory by reducing atherosclerotic lesion formation (66), upregulation in macrophages might be pro-inflammatory (125).

Exogenous delivery of recombinant SOCS3 through various routes has been used to reduce the severity of phenotype of several chronic inflammatory disorders such as rheumatoid arthritis (130) and acute systemic inflammatory responses such as endotoxic shock (131). Adenoviral delivery of SOCS3 cDNA into joints of arthritic mouse models (antigen/collagen-induced arthritis) suppressed proliferation of synovial fibroblasts, pannus formation, monocyte infiltration, secretion of IL6, and a generally milder arthritic phenotype (130). Furthermore, liposomal delivery of SOCS3 cDNA into mice peritoneum prior to challenge with LPS increased mouse survival and reduced serum TNF α levels (131). Moreover, a cell penetrating (CP) form of SOCS3 has been produced that strongly targets leukocyte and lymphocyte subsets in blood, spleen, and liver but also kidney and

liver cells and to a lesser degree lung, spleen, and heart (132). Intraperitoneal delivery of CP-SOCS3 has been demonstrated to reduce IL6, TNF α , and MCP1 expression. CP-SOCS3 also reduced MHCII induction possibly *via* inhibition of IFN γ /STAT1 signalling. Interestingly, a CP-SOCS3 mutant lacking a SOCS-box had an impaired ability to inhibit STAT1 signalling thus demonstrating the importance of this region of SOCS3 to negatively regulate inflammatory signalling. Additionally, CP-SOCS3 administered to a mouse model of acute liver injury (staphylococcal enterotoxin B + D-galactosamine) resulted in a 100% survival rate with no visible liver injury (132).

Recently, statins have been used to combat multiple sclerosis, an autoimmune disease associated with autoreactive T-cells, likely T_{h17} cells, which migrate to the central nervous system (CNS) and cause neuronal demyelination and conduction dysfunction amongst many other things (128). Statins have lots of anti-inflammatory effects besides their ability to lower cholesterol such as reducing expression of adhesion molecules (ICAM, VCAM), cytokines (TNF α , IL6), chemokines (MCP1), and inhibition of the NF κ B pathway (133,134). With regards to T-cell response, the anti-inflammatory effects of statins are thought to stem from manipulation of SOCS3 expression (128). For example, simvastatin is thought to activate STAT3 in dendritic cells to induce SOCS3 which blocks IL23 production thus inhibiting T_{h17} cell differentiation (128). However, this might also be accompanied by several other anti-inflammatory effects of statins such as reducing T_{h1} pro-inflammatory cytokines (TNF α , IFN γ) and elevating T_{h2} anti-inflammatory cytokines (IL10) (128).

It can be seen that SOCS3 is integral to the regulation of both innate and adaptive immune systems. Furthermore, manipulation of SOCS3 has been shown to be successful in the treatment of chronic inflammatory disorders. However, the involvement of SOCS3 as an E3 ubiquitin ligase in the regulation of these disorders is incompletely understood. Given that the disruption of E3 ligases are expected to have specific effects (Section 1.4), targeting of SOCS3 in this capacity might be therapeutically beneficial.

1.4 Ubiquitin-proteasome pathway

1.4.1 Ubiquitination: formation and function

Ubiquitination is a reversible post-translational modification that parallels the phosphorylation system by modulating location, activity and protein interactions (98). Ubiquitin is a 76 amino-acid protein which is thought to be involved in the regulation of most cellular events (98). Covalent attachment of mono-, multi-, or polyubiquitin chains provides a diverse set of signals from which signalling pathways can be fine-tuned. Ubiquitination typically involves the formation of an isopeptide bond between the ϵ -amino-group on an internal lysine residue within the target protein and the C-terminal glycine residue (G⁷⁶) of ubiquitin. A modification of the N-terminal methionine residue of ubiquitin has also been reported (135). Attachment of ubiquitin is mediated by the individual actions of E1 activating, E2 conjugating, and E3 ligase proteins where substrate specificity is determined by the latter (Figure 1.6). Furthermore, an additional protein termed the E4 enzyme (ubiquitin chain elongation factor) has also been reported that serves to elongate mono- or oligoubiquitin chains (136). By doing so, proteins activated by monoubiquitination might be targeted for polyubiquitin-dependent degradation. E3 ubiquitin ligases comprise two main forms, the homologous to E6-AP COOH-terminus (HECT)-domain and really interesting new gene (RING)-finger-motif. RING-finger E3s are the largest family of ubiquitin ligases and include the elongin-cullin-SOCS family (52). The main functional difference being that, while RING-finger E3s indirectly bind ubiquitin *via* an E2 conjugation enzyme, HECT-domain E3s become covalently attached to ubiquitin at conserved a cysteine residue *via* a thiol-ester bond and are therefore directly involved in ubiquitin transfer (Figure 1.6).

Ubiquitin has seven lysine residues (K6, K11, K27, K29, K33, K48, and K63) (98) and all can be used to form polyubiquitin chains although most is known about the K48- and K63-linked moieties. K48-linked chains are the most understood and direct proteasomal degradation (137) (Figure 1.8) whereas K63-linked chains can function as scaffolds and activators of ubiquitin-interacting domain-bound complexes (16).

While the functions of chains produced using non-K48/K63 lysine residues are not well understood (see figure 1.6 for examples), recent studies suggest that all non-K63-polyubiquitin chains might have a role in targeting proteins to the proteasome (138). SOCS3 has been shown to direct ubiquitin-mediated proteasomal degradation and lysosomal routing of its substrates and so it is predicted to form K48-polyubiquitin chains (8-12). A difference in structure of polyubiquitin chains has been suggested to be responsible for the functional variation. NMR has been used to show that K48-polyubiquitin produces a closed conformation whereas K63-linked chains produce a more extended linear structure (98). Adding to the complexity of the ubiquitin signal, chains can have mixed linkages and branches although their significance has not yet been explained(138). Furthermore, proteasomal degradation has also been reported following generation of novel linear ubiquitin chains i.e. C-terminal glycine of ubiquitin to the N-terminal methionine of ubiquitin (85).

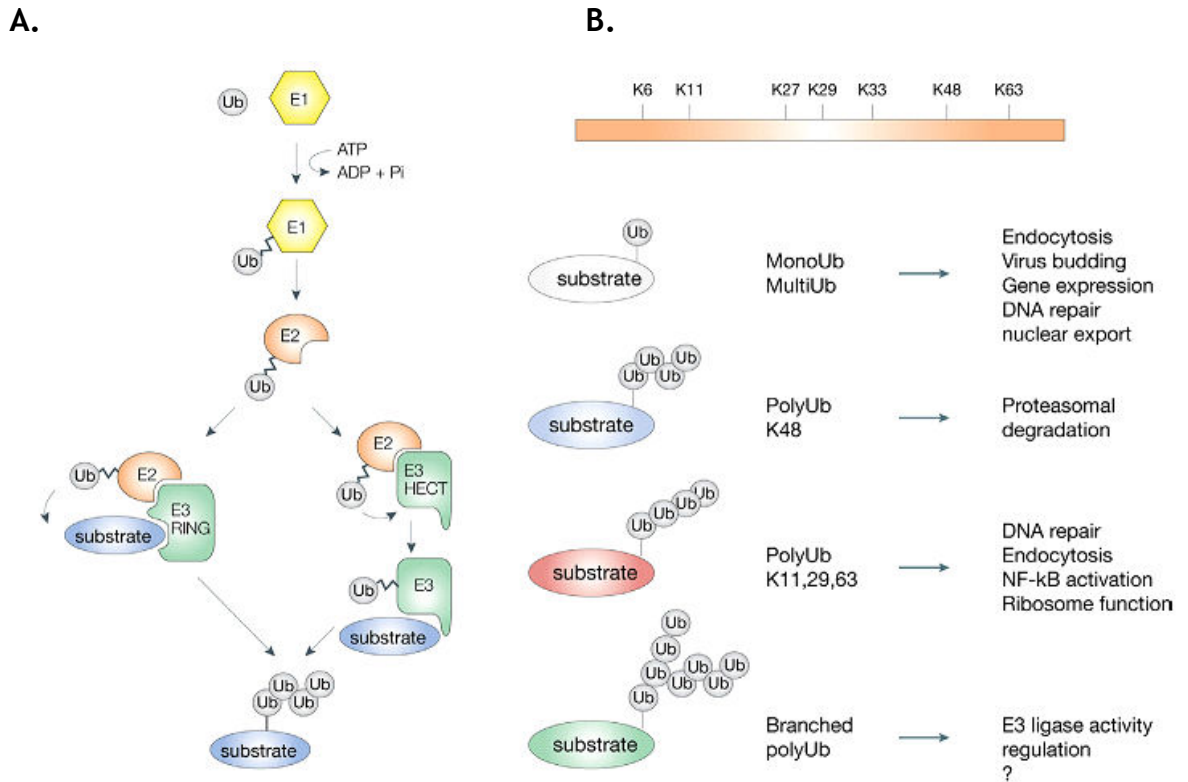


Figure 1.6: Ubiquitination

Ubiquitin is a 76-residue protein that is covalently bound to a target protein to direct multiple functions (5). **A.** Attachment of ubiquitin is *via* a three-step hierarchical process of activation (E1), conjugation (E2), and ligation (E3). In human, two E1, 50 E2 and over 600 E3 ubiquitin ligases have been defined along with 90 DUBs and 20 UBDs (14). In an ATP dependent step, ubiquitin is attached to an E1 activating enzyme *via* a high energy thio-ester bond. This charged complex then transfers ubiquitin to another cysteine in the active site of the E2 conjugating enzyme. Finally, ubiquitin is transferred to a substrate lysine residue *via* an isopeptide bond between the ϵ -amino group of the lysine within the substrate and the C-terminal carboxyl of ubiquitin *via* the E2-E3 interaction. The E3 ligase, itself a multi-subunit protein complex, brings together the E2 linked ubiquitin and the target protein and so acts as a specificity unit. The mechanism of ubiquitin ligation differs between E3 ligase families. HECT E3 ligases are directly covalently attached to ubiquitin whereas E3 RING ligases indirectly bind ubiquitin *via* the E2 conjugation enzyme. **B.** Ubiquitin has seven lysine residues and chains can be produced from each of them. Variations direct different functions as shown although not all possible ubiquitin combinations have defined functions. Reproduced with permission from (98).

Ubiquitin is not alone in its ability to modulate the proteome. Ubiquitin-like proteins (ULP) have also been characterised which include small ubiquitin-like modifier (SUMO) and neural precursor cell expressed, developmentally down-regulated 8 (NEDD8). They are structurally similar in that they have a conserved 'ubiquitin fold'. In a similar three-step fashion to ubiquitin, they are covalently attached to target proteins to facilitate a number of functions such as regulating protein interactions, localisation, activity, and stability. SUMOylation might be more specific than ubiquitination due to the use of a single E2 conjugation enzyme, Ubc9 (69). Furthermore, unlike ubiquitination SUMOylation takes place at ΨKxE (Ψ is I, L or V; x is any residue) consensus motif (69). Mono- and poly-SUMOylation are possible where mono-SUMOylation regulates interaction, activity, and localisation whereas poly-SUMOylation is thought to initiate polyubiquitination and proteasomal degradation thus linking the SUMO and ubiquitin systems (69). PIAS members are thought to be regulated by SUMOylation and that they themselves have SUMO-E3 ligase function (69). All known cullins are mono-neddylated at an internal lysine residue within the consensus sequence IVRIMKMR (139). Neddylation is thought to be essential for E3 ligase formation and increased catalytic activity (52,98). Both modifications occur *via* an isopeptide bond with the C-terminal G⁷⁶ of the ULP and are therefore indistinguishable from ubiquitin following trypsin digestion i.e. both modifications leave a GlyGly remnant important for determining the modified lysine residues *via* mass spectrometry.

Ubiquitination is reversible *via* the action of deubiquitinases (DUBs). Around 100 DUBs have been identified, however their substrates have not been fully described (140). DUBs regulate signalling events by cleaving and disassembling ubiquitin and polyubiquitin chains from affected substrates and so aid the recycling of free ubiquitin (141). Specificity is conveyed by protein-protein interaction motifs that enable binding to proteins with specific ubiquitin modifications e.g. K63/K48 polyubiquitin chains. DUBs like A20 and CYLD are integral to the regulation of the innate immune response by ablating NF κ B signalling (141). CYLD also regulates the adaptive immune response *via* its role in the development, tolerance, and activation of T-Cells (142). As such, DUBs are associated with several immune-related disorders (see below).

Covalent attachment of ubiquitin can modulate protein function and localisation but other proteins can also interact non-covalently with ubiquitin with similar results. For example, the K63-polyubiquitination is essential for the localisation of activation of NF κ B essential modulator (NEMO/IKK γ) during NF κ B signalling (16). Around 16 UBDs have been characterised which enable a weak ($K_d > 100 \mu\text{M}$) interaction with monoubiquitin which is strengthened by several mechanisms such as cooperative binding with other proteins/lipids and by having multiple UBDs (143). Different UBDs interact with ubiquitin at different sites resulting in a diverse range of proteins and protein folds that interact with ubiquitin. Furthermore, the diversity of linkages/branching of polyubiquitin chains has complicated the characterisation of the UBDs (143). As such, delineating ubiquitin-binding code is in its infancy. For instance, NEMO binds to polyubiquitin chains *via* a novel UBD termed NEMO-ubiquitin-binding (NUB) domain that partly includes a coiled-coiled domain and leucine zipper motif and the intermediate linker region (16).

1.4.2 The canonical NF κ B pathway: a ubiquitin dependent pathway

Ubiquitination is recognised as a regulator of the immune system where it plays a central role in the activation, amplification, and termination of the innate and adaptive immune system (14). Ubiquitination is central to the regulation of the pro-inflammatory NF κ B pathway and requires functional K48- and K63-polyubiquitin chains (16). Different stimuli initiate distinct sequences of events that eventually activate NF κ B, although in each case several ubiquitin-mediated events such as protein localisation, activation, and proteasomal degradation are shared (16). Lipopolysaccharide (LPS) activates toll-like receptor 4 (TLR4) resulting in the recruitment of adaptor proteins myeloid differentiation primary response protein 88 (MyD88) and interleukin-1 receptor-associated kinase 1 (IRAK1) to its cytoplasmic face (Figure 1.7). The activated E3 ubiquitin ligase, TNF receptor associated factor 6 (TRAF6), catalyses the formation of K63-polyubiquitin chains which binds multiple factors *via* their ubiquitin-interacting domains. The K63-polyubiquitin-dependent localisation of kinase regulatory unit TAK1 binding protein 2 (TAB2) binds and enables the autophosphorylation and activation of transforming growth factor- β -activated kinase-1 (TAK1). Subsequently, a further K63-polyubiquitin-bound kinase complex I κ B kinase (IKK)

is activated following the phosphorylation of IKK β by TAK1. IKK consists of the catalytic subunits I κ B kinase α (IKK α) and I κ B kinase β (IKK β) which are bound to the K63-polyubiquitin chains *via* the regulatory subunit NEMO/IKK γ . This phosphorylation cascade concludes with the phosphorylation of I κ B α by IKK α at S³² and S³⁶. Phosphorylated I κ B α is then recognised and K48-polyubiquitinated by its cognate E3 ubiquitin ligase (SCF ^{β -TRCP}, not shown). I κ B α is subsequently degraded *via* the 26S proteasome allowing the p65 (REL-A)/p50 subunits of NF κ B to translocate to the nucleus to drive gene transcription. Other PRRs (RLRs, NLRs) can also activate the NF κ B pathway *via* distinct receptor-activated ubiquitin-dependent mechanisms (144).

The NF κ B pathway is negatively regulated *via* several mechanisms. I κ B α is a gene target of NF κ B and so acts as part of a classical feedback loop to suppress NF κ B-directed gene transcription *via* its sequestration back to the cytoplasm. In addition to nuclear export, REL-A is also targeted for ubiquitin-mediated proteasomal degradation *via* a COMMD1/ECS^{SOCs1} complex within the nucleus (145). This pathway is also negatively regulated by the DUBs CYLD and A20 that degrade K63-polyubiquitin chains thus blocking downstream signalling events (146). CYLD is inducible by LPS after which it depolymerises K63-polyubiquitin chains on NEMO to ablate NF κ B signalling (147). A20, a TNF α -inducible DUB, targets receptor interacting protein (RIP), part of the TNF receptor 1 (TNFR1) signalling complex, to ablate NF κ B signalling. However, A20 is unique in that it has both DUB and E3 ligase domains and following K63-specific deubiquitination of RIP, A20 ubiquitinates RIP with a K48 polyubiquitin chain thus targeting it for degradation (146).

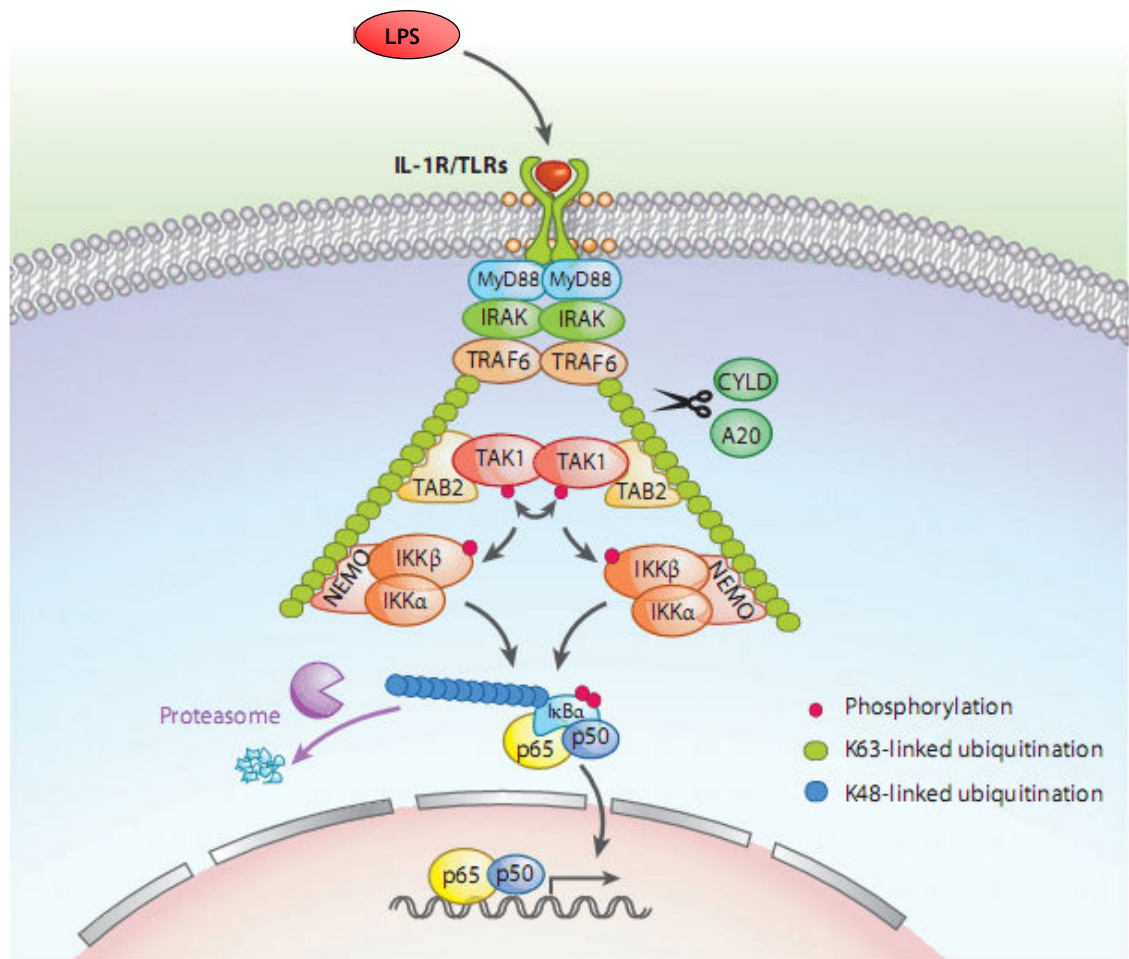


Figure 1.7: The canonical NF κ B pathway is dependent on K48- and K63-polyubiquitin chain formation

Briefly, lipopolysaccharide (LPS) activates toll-like receptor 4 (TLR4) resulting in the binding and activation of multiple signalling mediators to its cytoplasmic face. The activated E3 ubiquitin ligase, TNF receptor associated factor 6 (TRAF6), catalyses the formation of K63-polyubiquitin chains which binds multiple factors *via* their ubiquitin-interacting domains. These factors initiate a phosphorylation cascade that leads to the phosphorylation of I κ B α by IKK α . This phosphorylation event allows I κ B α to be recognised and K48-polyubiquitinated by its E3 ubiquitin ligase (SCF^{B-TRCP}, not shown). I κ B α is subsequently degraded *via* the 26S proteasome allowing the p65 (REL-A)/p50 subunits of NF κ B to translocate to the nucleus to drive gene transcription. I κ B α is a gene target of NF κ B and so acts in a classical feedback loop to suppress NF κ B-directed gene transcription. Image adapted with permission from (16).

NF κ B signalling is integral to the activation of the innate immune response such as the TLR4-mediated activation of macrophages which then secrete pro-inflammatory cytokines to amplify/maintain the innate response but also activate an adaptive T-Cell response (39). Given the importance of ubiquitin in NF κ B signalling it is not surprising that dysregulation is associated with severe inflammatory and immunological disorders. For example, a mutation within the NUB domain of NEMO, which impairs the binding of K63-polyubiquitin chains and thus localisation and activation of the IKK complex, is associated X-linked recessive syndrome anhidrotic ectodermal dysplasia with immunodeficiency (EDA-ID). Patients with EDA-ID have poor inflammatory response, impaired NF κ B signalling such as in response to LPS, and die prematurely from multiple infections (148). Dysregulation of DUBs or mutations of ubiquitin attachment sites in target proteins also cause dysfunction. Mouse models lacking the DUB A20 die prematurely from severe inflammation due to hyperactive NF κ B signalling (146,149). However, mice lacking CYLD, while having normal TNF α -mediated NF κ B signalling in bone-marrow-derived macrophages, have impaired levels of CD4⁺ and CD8⁺ T-Cells (142).

In a similar way to LPS, TNF α also activates the canonical NF κ B pathway (Figure 1.8). However, full activation is conditional on the recruitment of the E3 ligase linear ubiquitin chain assembly complex (LUBAC), a trimeric complex consisting of HOIL1, HOIL-1-interacting protein (HOIP), and SHANK-associated RH domain interacting protein (SHARPIN). LUBAC catalyses the formation of linear (M1-) polyubiquitin chains on RIP1 and NEMO, which is thought to result in a more stable IKK complex (136,150,151). In the absence of LUBAC, NF κ B signalling is impaired leading to TNF α -induced cell death (150). Furthermore, mice deficient in SHARPIN develop chronic proliferative dermatitis (CPDM), a multi-organ inflammatory disorder (150).

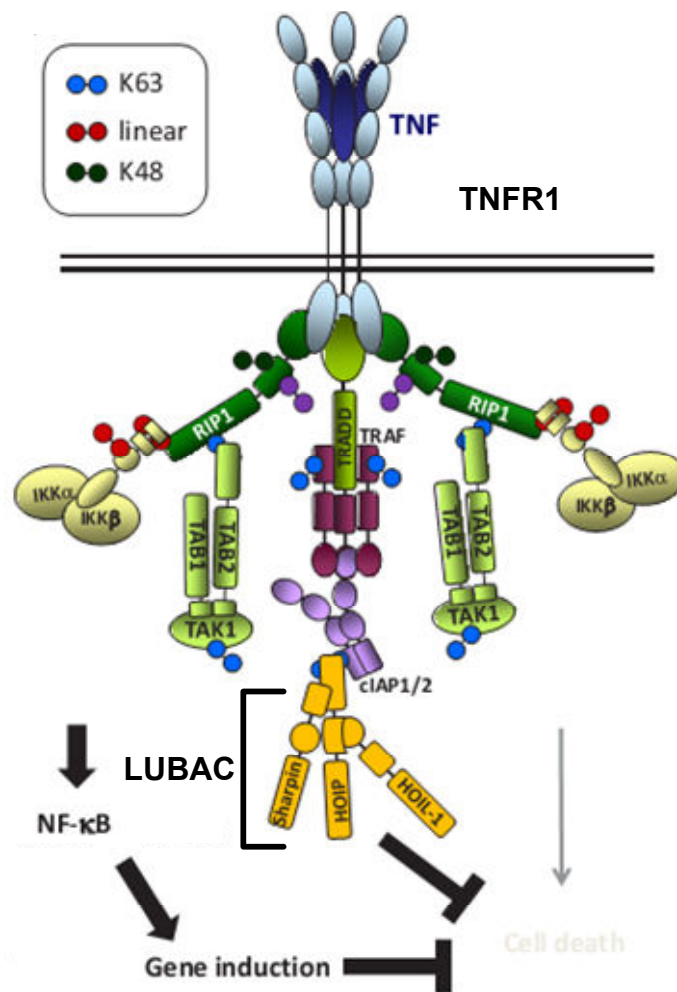


Figure 1.8: The canonical TNF α -activated NF κ B pathway is dependent on linear (M1-), K48- and K63-polyubiquitin chain formation

Briefly, a trimer of tumour necrosis factor alpha (TNF α) cross-links and activates the TNF-receptor 1 (TNFR1) monomers resulting in the binding and activation of multiple signalling mediators to its cytoplasmic face. The adaptor protein TNF receptor 1-associated death domain protein (TRADD) recruits the E3 ubiquitin ligases, TNF receptor associated factor 2 (TRAF2) and cellular inhibitor of apoptosis 1/2 (cIAP1/2) which catalyses the formation of K63-polyubiquitin chains on receptor-interacting protein kinase 1 (RIP1). Multiple factors are then recruited *via* their ubiquitin-interacting domains. These factors initiate a phosphorylation cascade that leads to the phosphorylation, ubiquitination, and degradation of I κ B α allowing NF κ B to translocate to the nucleus to drive gene transcription. Full activation of the NF κ B is conditional on the recruitment of the E3 ligase linear ubiquitin chain assembly complex (LUBAC), a trimeric complex consisting of HOIP, SHARPIN, and HOIL-1. LUBAC catalyses the formation of linear (M1) polyubiquitin chains on RIP1 and NEMO (not shown) which is thought to result in a more stable IKK complex. Image adapted with permission from (151).

Together it seems that ubiquitination and canonical NF κ B signalling is critical for protection against infection due to its role in the activation and development of the immune system but dysregulation can result in severe inflammation. As such, tight control is necessary to maintain homeostasis.

1.4.3 Therapeutically targeting the ubiquitin-proteasome pathway

The ubiquitin proteasome pathway has been therapeutically exploited by targeting both the ubiquitin protein cascade and the proteasome. With structural knowledge of the ubiquitin cascade proteins (E1, E2, and E3), it might be possible to disrupt the interaction of these proteins with each other or their substrates. In human, two E1, 50 E2s, and over 600 E3 ubiquitin ligases have been defined (14). As such, disruption of E1 function might be valuable where a global effect might be achievable. However, targeting at the level of the E3, which determines the specificity of ubiquitination, would be more precise with potentially less adverse effects. However, a potential problem with disruption of E3 ligases is the lack of knowledge of E3 targets. Inhibition of a single E3 could affect multiple unknown targets and pathways. If this could be overcome, targeting of substrate-E3 complex would allow a highly specific functional inhibition *via* selective targeting of substrates. So far, small molecule disruption of E3-E2 has not been reported. Targeting of a RING-finger based E3-substrate interaction has been successful such as in the case of MDM2-p53 with the MDM2 antagonist Nutlin, which targets the p53-binding pocket on MDM2 (52,152). This strategy might also be possible in treatment of inflammation. It is known that β -transducin repeat-containing protein (β -TRCP), the specificity factor for a further RING-finger based E3 ligase, SCF ^{β -TRCP}, targets NF κ B signalling *via* ubiquitination of its inhibitor I κ B α (153). Inhibition could have potential anti-inflammatory effects. However, since SCF ^{β -TRCP} also regulates the pro-oncogenic transcription factor β -catenin, inhibition of SCF ^{β -TRCP} might result in tumourigenesis (52). Interestingly, a small molecule inhibitor of I κ B α ubiquitination, Ro106-9920, has been identified (154). This novel, but yet unidentified E3 is distinct from SCF ^{β -TRCP} and inhibits NF κ B signalling without affecting levels of β -catenin (154).

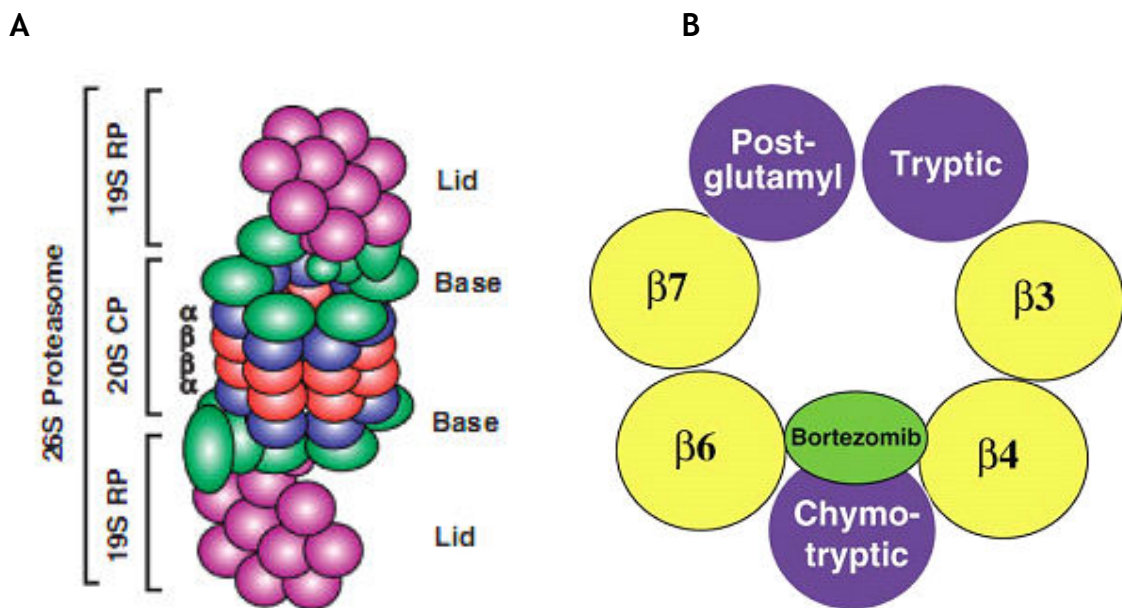


Figure 1.9: Structure and function of the 26S proteasome

The 26S proteasome is a 2000 kDa multi-subunit protein that performs ATP-dependent, ubiquitin-dependent degradation of a vast range of cellular proteins. **A.** The 26S proteasome is constructed from two 19S regulator units and one 20S catalytic unit. Only the structure of the 20S unit has been determined (155). Ubiquitinated proteins are recognised by the 19S units which deubiquitinate and denature the proteins before feeding them into a cylindrical chamber of the 20S subunit. Three broad-spectrum proteolytic sites within the 20S core, chymotrypsin-like, trypsin-like, and post-glutamyl peptide hydrolase-like (PGPH), cleave the peptides at C-terminal hydrophobic, basic, and acidic residues respectively as it is fed through producing 3-26 residue peptides(156). The 20S subunit can exist in a latent form but requires additional units to aid entry of the peptide into the catalytic core i.e. 19S subunit. **B.** The β catalytic rings are made of 7 subunits with β 1, β 2, and β 5 having catalytic activity. Chymotrypsin-like, trypsin-like, and capsase-like/post-glutamyl peptide hydrolase-like (PGPH), cleave the peptides at C-terminal hydrophobic, basic, and acidic residues. Inhibition of the chymotrypsin-like domain by the drug Bortezomib is a successful anti-cancer treatment. RP, regulatory protein; CP, catalytic protein. Adapted with permission from (155,156).

Neddylation is important in the construction and regulation of catalytic activity of E3 ligases including cullin5, a component of the elongin-cullin-SOCS3 type E3. Inhibition of neddylation is a further potential strategy that could be implemented to sustain the functional effects of ubiquitinated proteins. Inhibition of this process might be therapeutically beneficial although non-specific effects are expected since it regulates all cullins (157).

Inhibition of the proteasome (Figure 1.9) has been exploited in cancer treatments. The chymotrypsin-like inhibitor Bortezomib specifically targets cancer cells possibly since these cells have higher rates of protein expression and so are more sensitive to proteasome inhibition. However, the mechanism of growth inhibition and cell death of cancer cell lines due to proteasome inhibition is unknown (156).

Currently there is a lack of knowledge of structure and protein interaction that make the design of a specific E3-substrate disruptors challenging, although some progress has been made *via* functional screening programs (152). In the case of SOCS3, few substrates are known. By performing a global screen for SOCS3-dependently ubiquitinated substrates, it is hoped that the impact of SOCS3 on inflammation can be better understood. Discovery of new SOCS3 substrates through this study might therefore provide targets that when correctly targeted produce specific therapeutically beneficial effects.

1.5 Project rationale and experimental approach

1.5.1 Project rationale

Currently, it is accepted that there is a link between obesity and several diseases such as CVD, diabetes, RA, and atherosclerosis with the common initiating factor in pathogenesis being a state of low grade, chronic inflammation (1,3). Such a state is characterised by elevated levels of pro-inflammatory cytokines such as IL6 (5). Sustained activation of inflammatory signalling pathways following ligand-cytokine-receptor ligation can result in pathogenesis if not properly regulated (46). One such pathway, the JAK-STAT pathway, is found to be hyperactive in several chronic inflammatory disorders (46,66,130). An IL6-inducible protein, SOCS3, has been demonstrated to terminate IL6-

mediated STAT signalling thus suppressing an inflammatory response (Section 1.3.3) (118). Furthermore, SOCS3 is induced by, and regulates several signalling pathways including, but not limited to, IL6 (Figure 1.2) (70), LPS (158), TNF α (159), and insulin (160). As such, SOCS3 might simultaneously control a diverse set of intracellular signalling events. Supporting its role as an anti-inflammatory mediator, SOCS3 is also inducible *via* cAMP (70), an accepted global anti-inflammatory agent (Figure 1.10) (115).

While SOCS3 was primarily characterised as a competitive inhibitor of intracellular signalling (70,158,159), it also functions as specificity factor for an ECS-type E3 ubiquitin ligase. In this role it has been demonstrated to direct ubiquitin-mediated proteasomal degradation of several substrates (9-12) and lysosomal routing (8). However, the full spectrum of SOCS3-dependently ubiquitinated substrates is unknown. It is possible that SOCS3 might regulate cytokine signalling *via* the targeted degradation of specific pro-inflammatory mediators. Indeed, SOCS1 has been shown to target JAK2 for proteasomal degradation (87). Moreover, the increased half-life of active pJAK1 following genetic impairment of SOCS3 E3 ligase functionality in embryonic stem cells (ES) suggests that SOCS3 might similarly regulate JAK1 (73). Interestingly, JAK3 is also downregulated following elevation of cAMP levels in antigen-primed T-lymphocytes, however the mechanism of how this occurs is unclear (161). Given that JAK/STAT signalling is critical in the development of inflammatory disorders, delineating the role of SOCS3 as an E3 ligase might be therapeutically beneficial. However, given the broad range of SOCS3 stimuli, the availability of certain SOCS3 substrates might be conditional on the route of SOCS3 induction and target phosphorylation. Using a global proteomics approach, this study aimed to identify SOCS3-dependently ubiquitinated substrates in response to cAMP and thus elaborate on the already well-established role of cAMP in inflammation.

Differentially SILAC-labelled, tandem affinity purified ubiquitinomes of WT MEFs and SOCS3^{-/-} MEFs each expressing epitope-tagged forms of ubiquitin were compared using mass spectrometry following cAMP-mediated SOCS3 induction (Figure 1.11). Using this approach, proteins modified by SOCS3 with the epitope-tagged form of ubiquitin should be enriched in WT MEFs but not SOCS3^{-/-} MEFs.

1.5.2 Experimental approach

SOCS3 regulates several pathways in part by acting as a specificity factor for an ECS-type E3 ubiquitin ligase (9-12). E3 ligases do not recognise a consensus ubiquitinated sequence. Furthermore, SOCS3 does not ubiquitinate all its binding partners (162). Therefore, analysis of SOCS3 protein-protein interactions *via* microarray, immunoprecipitation, or GST pull-down is insufficient for identification of SOCS3-dependently ubiquitinated substrates. Direct analysis of the ubiquitinome is necessary. Identification of substrates of cAMP-dependent, SOCS3-specific ubiquitination will instead be performed *via* a comparison of purified ubiquitinomes from WT and SOCS3^{-/-} MEFs (Figure 1.11). As such, SOCS3-dependently ubiquitinated proteins should be detectable in WT but not SOCS3^{-/-} MEFs.

Currently, all known SOCS3-dependently ubiquitinated targets are tyrosine-phosphorylation prior to binding SOCS3 and ubiquitination (9-12). While it is understood that the impact of ubiquitination on cell signalling events is growing ever more important, the ubiquitinome might still only make up only a small fraction of the proteome. As such, detection of potentially low abundance signalling intermediates with transient, labile PTMs are not without their challenges. The probability of detecting SOCS3-dependently ubiquitinated substrates might be improved by preserving tyrosine-phosphorylated, ubiquitinated proteins *via* the inhibition of PTPs, the proteasome, and by blocking the action of DUBs. As such, the pool of tyrosine-phosphorylated proteins will be enriched by the use of PTP inhibitors Na₃VO₄ and H₂O₂ while the ubiquitinome will be preserved *via* the use of the proteasome inhibitor MG132. Furthermore, the use of highly denaturing conditions during ubiquitinome isolation will contribute to the preservation of ubiquitinated proteins by denaturing and deactivating DUBs. Forskolin, the direct activator of adenylyl cyclase, will facilitate the elevation of intracellular cAMP levels and SOCS3 induction.

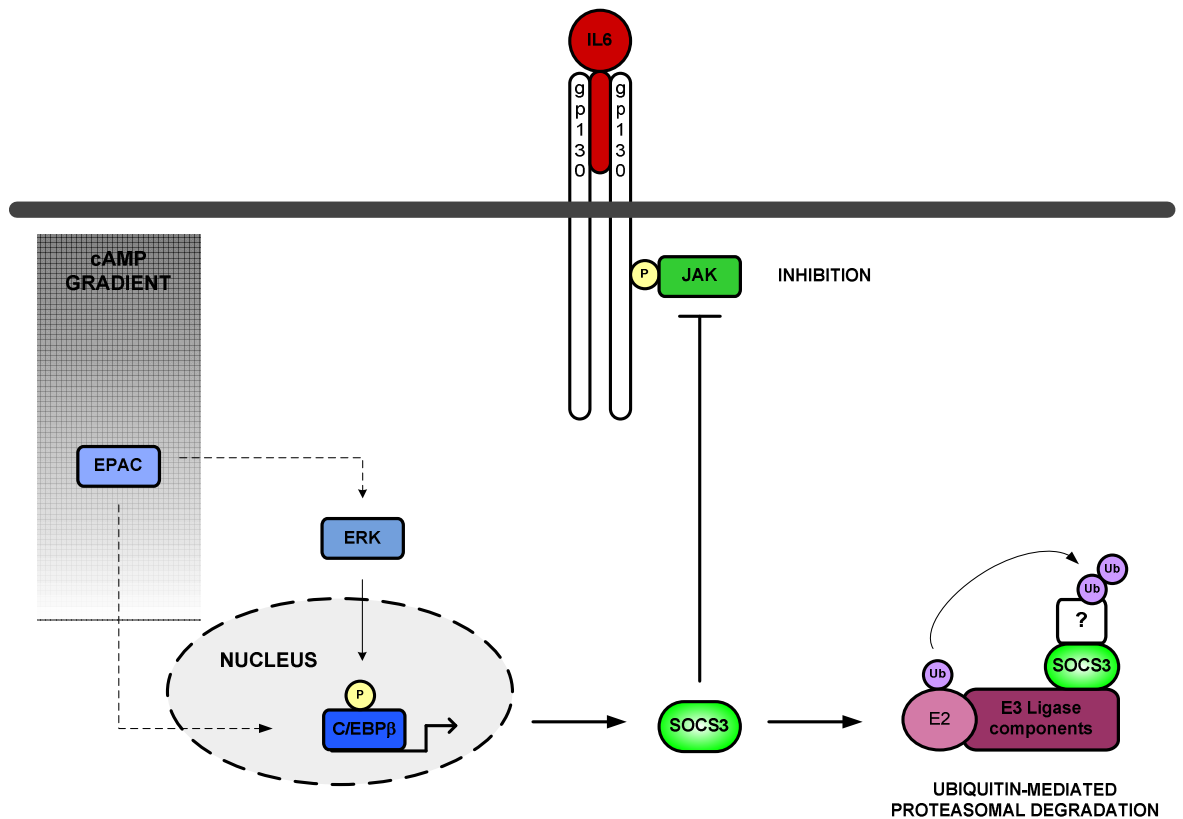


Figure 1.10: SOCS3 induction and function

SOCS3 is rapidly induced upon sustained, elevated levels cAMP *via* EPAC1 activation and transient PKA-independent ERK activation. SOCS3 is induced *via* C/EBP β -dependent gene transcription. EPAC1 activation increases recruitment of C/EBP at the SOCS3 promoter (119) whereas ERK-dependent phosphorylation of C/EBP β at Thr²³⁵ fully activates SOCS3 expression (70). SOCS3 induction is sufficient to terminate IL6 signalling (70). SOCS3 has also been identified as a component of E3 ligases that direct ubiquitin-dependent protein degradation *via* the 26S proteasome(9-12). SOCS3 might further regulate the inflammatory response *via* this mechanism.

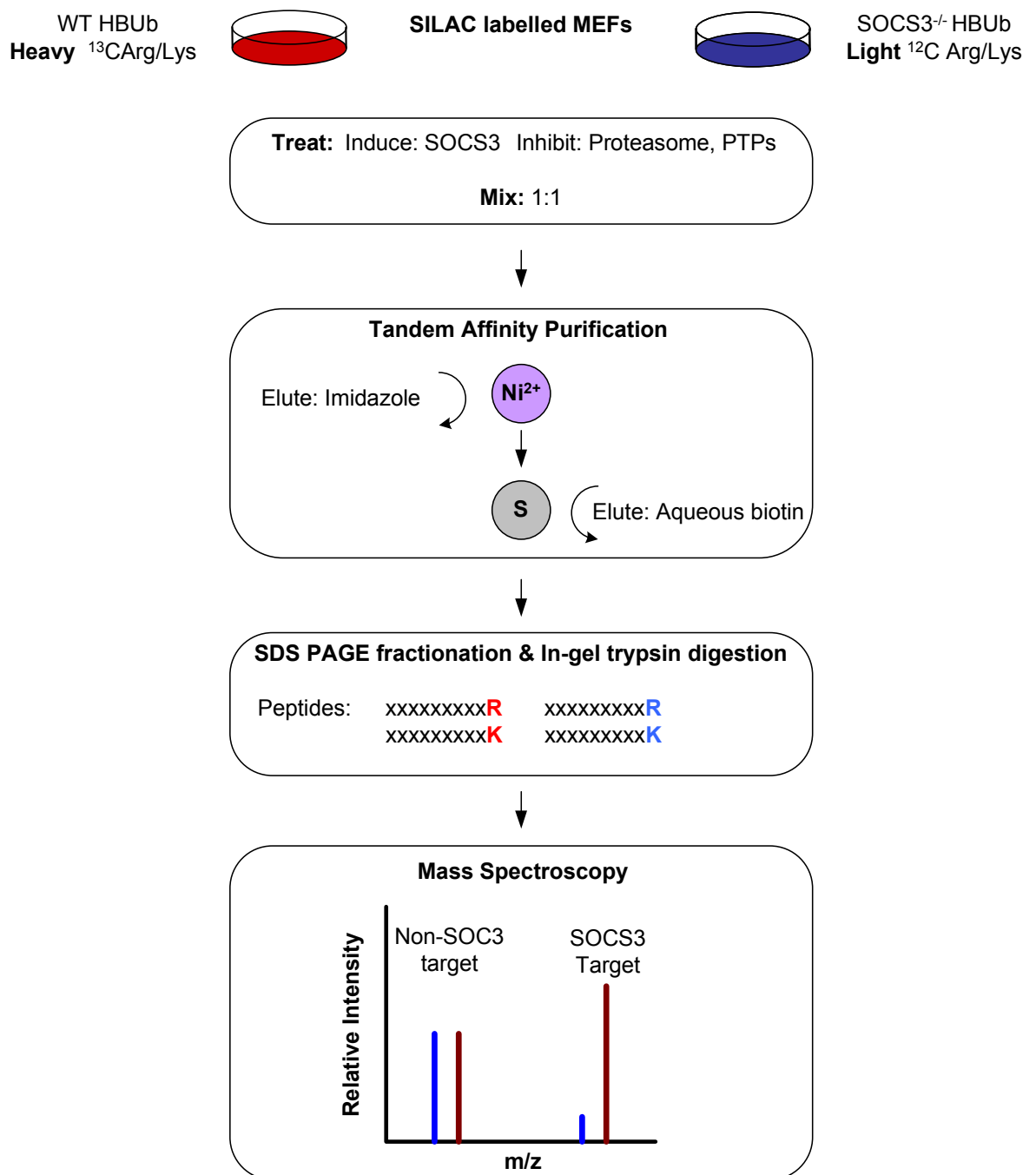


Figure 1.11: Experimental strategy

The aim of this study was to identify SOCS3-dependently ubiquitinated substrates from differentially SILAC-labelled ubiquitinomes, tandem affinity purified from WT and SOCS3^{-/-} MEFs aided by (His)₆-biotin-tagged ubiquitin (HBUb). SILAC ratios of C-terminal arginine- or lysine-labelled peptides were assessed following mass spectrometry. Peptides from SOCS3-specific HBUb-modified proteins should only be detectable in WT HBUb but not SOCS3^{-/-} HBUb MEFs. See text for details.

I have chosen SILAC to enable the discrimination of WT HBUb and SOCS3^{-/-} HBUb MEF-isolated ubiquitinomes. SILAC is an efficient, reproducible, metabolic process of incorporating stable isotopes of amino acids into the proteome. Labelling coverage is dependent on the purity and composition of the SILAC media as well as the incubation period. It has been shown that it is possible to achieve almost 100% coverage of even low abundance proteins over five cell doublings (163). Owing to a low level of the natural, light amino acid that is usually present in SILAC media, 98.5% incorporation is typical (verbal communication, Biochemical Society conference). Here, SILAC media (Dundee Cell Products) with a purity >99% is used thus establishing the limit of maximum incorporation. Furthermore, growth media supplements may contribute to contamination from the natural amino acid. As such, the use of dialysed serum is necessary, although its use could potentially impact on cell proliferation (163). There is no chemical difference between the natural amino acid and its isotope and so cells can be grown and handled as normal. Since labelling occurs within live cells, samples can be differentiated, mixed, and treated as one sample directly following cell harvesting. As such, the chance of introducing handling errors is reduced. In contrast, other chemical incorporation techniques such as isotope coded affinity tags (ICAT) are multi-step, require post-harvest processing, and do not achieve complete incorporation (163,164).

Standard mass spectrometry protocols begin with digestion of proteins to peptides of manageable size (8-20 amino acids). Liquid chromatography (LC) then focuses peptides into bands of similar mass prior to ionisation and MS. This not only reduces the complexity of the peptide mixture but also enables accurate quantitation of the co-eluting peptides. Sequencing of peptides is achieved *via* mass analysis of fragmented, ionised peptides. As such, the choice of amino acid(s) and isotope are important considerations for mass spectrometric analysis. The most frequently used stable isotopes include ²H, ¹³C, and ¹⁵N. While deuterium is the cheaper isotope, it is problematic in that it resolves from its light-labelled counterpart during reverse phase liquid chromatography and as such affects quantitation (165). To achieve maximum coverage, common essential amino acids such as lysine, leucine, and arginine are used. Arginine is non-essential *in vivo* but has been demonstrated to be essential under cell-culture conditions (166). Trypsin, a commonly used protease

for MS-based studies, cleaves C-terminally to arginine and lysine and thus all tryptic peptides, apart from C-terminal fragments, will be labelled (167). Furthermore, due to the frequency and abundance of these amino acids within the proteome (~5%)(165), trypsin produces several peptides around 8-10 amino acids in length per protein. Such peptides are small enough to be accurately sequenced *via* MS but large enough to be unique which is important for protein identification. Moreover, the detection of several peptides from a single protein will improve protein assignment and calculation of a SILAC ratio. Additionally, since lysine and arginine have basic side-chains, they retain a positive charge, which is a prerequisite for ionisation and detection by mass spectrometry. Differential-SILAC labelling (168) using these amino acids effectively produces two separate proteomes distinguishable *via* a mass shift imparted by the heavy isotope. Heavy $^{13}\text{C}_6$ -arginine and $^{13}\text{C}_6$ -lysine will produce a mass difference of 6Da (6 carbons per amino acid) compared to the natural $^{12}\text{C}_6$ species, for each arginine or lysine residue replaced. This shift is sufficient to discriminate between differentially labelled peptides (165) and thus enable further processing by data analysis software. Taken together, these qualities make arginine and lysine well suited to this project.

The disadvantage of using arginine is that it can be metabolised from $^{13}\text{C}_6$ -arginine to an isotope of the non-essential amino acid $^{13}\text{C}_5$ -proline *via* the arginase pathway (169). Incorporation of the heavy proline isotope will result in a second set of peaks shifted by 5Da from the unaffected, heavy-labelled species for each proline present. Although this makes quantitation difficult, it can be corrected for by the addition of the different MS peak clusters using software such as MaxQuant (Section 2.2.10.2) (170). However, since mathematical corrections can be time consuming and inaccurate, several non-computer-based solutions have been suggested. These include modifications of the SILAC media to either reduce (171), prevent (169), or compensate (172) for arginine metabolism or to genetically modify cells (173) to prevent arginine conversion. Of these, the most simplistic approach was suggested by Bendall et al (169). In this system, successfully implemented in ECs, HeLa, and MCF7 cell lines, media was merely supplemented with L-proline (200mg/L). The L-arginine metabolic pathway is bidirectional and dependent on the bioavailability of precursors (169). As such, the presence of proline, an essential amino acid usually omitted

from DMEM or present in reduced concentrations, prevents conversion of arginine to proline. Although proline can be metabolised back to arginine, no significant back-conversion was detected, probably due to its presence in the media. Given its simplicity, this method was favoured for this project.

Mass spectrometry is very sensitive (peptide detection limit $\sim 10^{-15}$ mol) and thus commonly used for the detection of low abundant proteins. However, a high background of contaminant e.g. keratin, can mask weak signals. Preparation of samples is therefore a limiting factor in MS-based studies (Section 2.2.9.4) (174). Importantly, detection of low abundant proteins can be improved following the isolation of the relevant subproteome i.e. the ubiquitinome. Tandem affinity purification (TAP) strategy is relatively quick and achieves high levels of purity necessary for MS. General TAP strategies involve the production of a fusion protein where a TAP tag is conjugated to the N- or C-terminus of the protein of interest. Employing multiple structurally distinct tags theoretically allows for the selection of specific complexes and the removal of others. TAP strategies typically involve two purification stages allowing reduction of non-specifically bound proteins and contaminants. Since most approaches are performed under native/non-denaturing conditions, post-translational modifications can be vulnerable. I have chosen to perform TAP under fully denaturing conditions as doing so might protect PTMs such as ubiquitinated proteins from DUBs. Such conditions would also reduce background from non-specifically bound proteins and ubiquitin binding proteins that bind ubiquitin but are not ubiquitinated themselves.

This study employs the (His)₆-biotin (HBUb) tag to isolate proteins following sequential application of nickel and streptavidin affinity chromatography. The HBUb tag (168,175) (Figure 1.12) is able to facilitate purification under extreme denaturing conditions (8M urea/6M guanidinium chloride) and consists of a hexahistidine domain that reversibly binds nickel, and a biotinylation signal peptide. The latter is a 75 amino-acid region from the *Propioni-bacterium shermanii* 1.3S transcarboxylase subunit which can be covalently linked *via* Lys41 to the carboxyl group of biotin by endogenous biotin ligases (176).

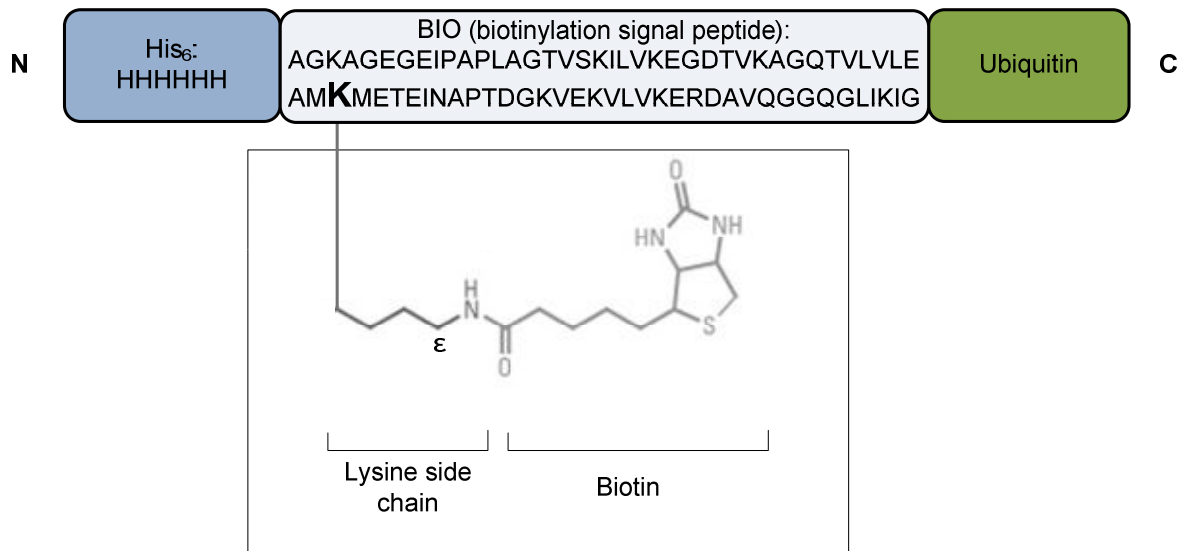


Figure 1.12: The hexahistidine-biotin tag

The (His)₆+biotin-tagged Ub (HBUb) allows purification under highly denaturing conditions. This accommodates the preservation of ubiquitinated proteins *via* the inactivation of DUBs and prevents purification of ubiquitin binding proteins (UBP), proteins that bind ubiquitin but are not ubiquitinated themselves. HBUb-tagged proteins are first purified using the hexahistidine domain that reversibly binds nickel (Ni²⁺). The second round of purification involves the BIO domain that irreversibly binds ($K_d = 10^{-15}$ M) streptavidin. The BIO domain has been shown to be biotinylated at K⁴¹ in yeast and mammalian cells.

The first stage of TAP, Ni²⁺ affinity chromatography, removes non-specifically bound proteins along with endogenously biotinylated proteins that might otherwise be purified in the following stage. The tight binding of biotin to streptavidin ($K_d = 10^{-15}M$) during streptavidin affinity chromatography allows very stringent wash conditions and enables the removal of most non-specifically and non-covalently associated proteins. However, a low level of background should always be expected. Using the HBUb system the second purification step can achieve a 6-fold reduction in non-specific purification over the first (175). Since ubiquitin is N-terminally tagged, linear (M1) polyubiquitin chains cannot be constructed (151). While SOCS3 has not been shown to be able to form this type of polyubiquitin chain, it cannot be ruled-out. However, if this is the case then this strategy would be limited to the identification of non-M1 polyubiquitinated substrates.

Mass spectromeric analysis combines the several systems to fractionate, ionise, fragment, and analyse the mass of peptides (177). The choice of system depends on requirements of cost, speed, sensitivity, resolution, and mass accuracy etc. A matrix-assisted laser desorption/ionization time-of-flight (MALDI-TOF) was used for optimisation experiments such as SILAC-label incorporation (Section 4.3.2). MALDI ionises dried peptides from a solid matrix using several laser pulses (177). Given that peptides of various sizes are ionised simultaneously, this system is limited to simple peptide mixtures. Furthermore, mass analysis is dependent on the time-of-flight ($t \propto m/z$) over a known distance where smaller molecules take less time than larger molecules to reach a detector module (177). The device-dependent distance is a major limiting factor of the resolution of the mass spectrometer. In contrast, a linear trap quadrupole (LTQ)-Orbitrap system incorporating an electrospray ionisation (ESI) technique was used to identify SOCS3 substrates (Section 5.0). ESI involves ionising samples out of solution, a milder method to MALDI that reduces the possibility of peptide fragmentation. As such, samples can be pre-fractionated by liquid chromatography, enabling the analysis of more complex peptide mixtures. Furthermore, by using an LTQ-Orbitrap, distance is not limiting since ions are trapped within an electromagnetic field and allowed to oscillate repeatedly around a central axis (177,178). Here, peptides are not separated by their mass-dependent velocity, the mass is now dependent on the frequency of axial oscillations (ω , where $\omega \propto$

1/m/z) and gives the Orbitrap superior mass accuracy (sub ppm vs. 10s ppm) and resolution (100,000s vs. 1000s, full width half maximum (FWHM)) over the TOF (177). Both systems employ tandem mass spectrometry (MS/MS) where two mass spectrometers are coupled. While the first measures the mass and abundance of the primary peptide, the second measures the mass and abundance of peptides that have been fragmented by collision with an inert gas i.e. collision-induced dissociation (CID). Fragmentation, occurs at the weakest point in the peptide and most commonly at the peptide bond (179). Fragmentation of multiple copies of the same peptide produces a sequence of daughter ions differing by a single amino acid i.e. a known mass, and as such, the peptide sequence can be predicted. Fragmentation can occur leaving the C-terminal (y-ions) or the N-terminal (b-ions) intact. The former are most common and are therefore more likely to produce a complete sequence of daughter y-ions (167). As such, it is advantageous to analyse trypsin-digested, C-terminally SILAC-labelled peptides. Furthermore, y-ions from heavy labelled peptides are less likely to be confused with those of the unlabelled moiety (167). Loss of low abundant proteins during TAP or loss of peptides during ionisation may lead to partial sequence coverage. Moreover, CID favours and thus fragments at the weakest bond, thus PTMs including phosphorylation are frequently lost (179). This information would be of value since known SOCS3-ubiquitinated substrates are tyrosine-phosphorylated before binding SOCS3 (9-12). However, it is not the focus of the project and so not critical to its success.

A major disadvantage of MS is the amount of data that is generated. While manual analysis of the mass spectra must be performed to assess the quality of the data, the most analysis can be performed automatically. For this study, post-MS data analysis will be performed using the free quantitative proteomics software MaxQuant (Section 2.2.10.2) (170) but also using the commercially available Mascot search engine (180) (Section 2.2.10.1).

Using a strategy that combines SILAC, TAP, MS, and subsequent MaxQuant data analysis will be exploited for the identification of SOCS3-dependently ubiquitinated substrates.

2.0 Materials, methods, and external services

2.1 Materials

Abcam, UK:

Anti-PTRF antibody (cat. no. ab48824)

Agilent, UK:

Quikchange II Site-Directed Mutagenesis kit (cat. no. 200523)

Bio-Rad Laboratories Ltd, UK:

Precision Plus Protein Kaleidoscope Standards (cat. no. 161-0375)

Cell Signaling Technology, US:

Anti-poly-His, rabbit polyclonal IgG (cat. no. 2365)

Anti-I κ B α , (44D4) rabbit monoclonal IgG (cat. no. 4812)

Anti-plkB α , (ser32/36) (5A5) mouse monoclonal IgG (cat. no. 9246)

Corning

15cm diameter TC treated culture dish (cat. no. 430599)

Dundee Cell Products, UK:

Ready to use SILAC DMEM media containing 13C labelled arginine and lysine amino acids (R6K6) (cat. no. LM010)

Control SILAC DMEM media containing unlabelled arginine and lysine amino acids (R0K0) (cat. no. LM014)

SILAC dialysed calf serum (cat. no. DS1003)

Expedeon:

InstantBlue single step Coomassie based gel stain (cat. no. ISB1L)

GE Healthcare:

Ni-Sepharose beads, 6 Fast Flow (cat. no. 17-5318-01)

Streptavidin-Sepharose beads, High Performance (cat. no. 17-5113-01)

Inverclyde Biologicals, UK:

Whatman Protran Nitrocellulose Membrane (cat. no. 10401396)

Invitrogen, UK:

D-biotin 50mM aqueous solution (cat. no. B-20656)
Cell Dissociation Buffer, enzyme free, PBS-based (cat. no. 13151-014)
Endotoxin-free phosphate buffered saline (PBS) (cat. no. 14140-094)
Dulbecco's Modified Eagle Medium (DMEM) (cat. no. D6546)
NuPAGE 4-12% Bis-Tris Gel (1.0mm x 10 well) (cat. no. NP0321BOX)
NuPAGE MOPs SDS Running Buffer(20x) (cat. no. NP0001)
NuPAGE LDS Sample Buffer(4x) (cat. no. NP0007)
XCell SureLock Mini-Cell (cat. no. EI0001)

Jencons, UK:

Sleeve Protectors, PP/PE (cat. no. 114-3437)

Merck Biosciences, UK:

MG-132 (cat. no. 474790)
Forskolin (cat. no. 344270)

Millipore,UK:

Anti-Ub, Lys48-specific, (Apu2), rabbit monoclonal IgG (cat. no. 05-1307)
Anti-Phosphotyrosine, clone 4G10 (cat. no. 05-321X)
Amicon Ultra Pre-Launch Centrifugal Filter Devices (cat. no. UFC201024PL)

Kodak, UK:

Medical X-ray Film General Purpose Blue (cat. no. 8143059)

Perkin-Elmer Life Sciences, UK:

Enhanced chemiluminescence (ECL) reagents (cat. no. NEL 104)

Pierce Thermo Scientific:

High sensitivity streptavidin-HRP (cat. no. 21130)

Promega:

Wizard Plus SV minipreps (cat. no. A1330)

Qiagen, UK:

Endofree plasmid Maxi kit (cat. no. 12362)

Roche Applied Science, UK:

Complete, EDTA-free protease inhibitor cocktail tablets (cat. no. 11836170001)

Santa Cruz Biotechnology, US:

Anti-SOCS3, (M-20) goat polyclonal IgG (cat. no. sc-7009)

Anti-Ub, (P4D1), mouse monoclonal IgG (cat. no. sc-8017)

Sartorius Stedim Biotech, DL:

Minisart syringe end filter, 0.45µm (cat. no. 16555)

Minisart syringe end filter, 0.20µm (cat. no. 16534)

Sigma-Aldrich, UK:

Anti-FLAG M2 agarose from mouse (cat. no. A2220)

Protein G-Sepharose 4B Fast Flow recombinant protein (cat. no. P3296)

Trypsin, Proteomics grade (cat. no. T6567)

Sterile filtered cell culture water (cat. no. W3500)

Trypsin - EDTA (cat. no. T4299)

Tween - 20 (cat. no. P5927)

30% (w/v) acrylamide/0.8% (w/v) bis-acrylamide (cat. no. A3699)

L-glutamine (cat. no. G7513)

Penicillin-streptomycin (cat. no. P0781)

Anti-mouse IgG (peroxidase-conjugated) (cat. no. A4416)

Anti-rabbit IgG (peroxidase-conjugated) (cat. no. A6154)

Anti-Goat IgG (peroxidase-conjugated) (cat. no. A5420)

Anti-poly-His, (HIS-1), mouse monoclonal IgG (cat. no. H1029)

Soybean trypsin inhibitor (cat. no. T9003)

Benzamidine (cat. no. 12072)

Bovine serum albumin (cat. no. A7030)

Bromophenol blue	(cat. no. B7021)
Ampicillin	(cat. no. A9393)
N, N, N',N'-tetramethylethylenediamine (TEMED)	(cat. no. T9281)
Phenylmethanesulphonyl fluoride (PMSF)	(cat. no. P7626)
Nonidet P-40	(cat. no. N6507)
Tissue culture bovine serum albumin	(cat. no. A1595)
Puromycin	(cat. no. P8833)
L-Proline BioUltra, ≥99.5%	(cat. no. 81709)
Imidazole	(cat. no. I5513)
Monoclonal anti-HA agarose conjugated clone HA-7	(cat. no. A2095)

Sino Biological Inc.:

Recombinant Human SOCS3 / CIS3	(cat. no. 11315-H30E)
--------------------------------	-----------------------

Sarstedt:

Tissue culture cell scraper 25cm	(cat. no. 83.183)
----------------------------------	-------------------

Thermo-Scientific:

Rectangular Dishes 4-well dishes	(cat. no. 267061)
----------------------------------	-------------------

Cell lines:

MEFs: WT (SOCS3^{+/+}) and SOCS3^{-/-} (Kawaguchi et al., 2004, (9)), initially provided by Prof. Akihiko Yoshimura (Kyushu University, Japan) were available as liquid nitrogen-frozen laboratory stocks.

Table 2.0: Constructs

Donor		cDNA	Vector	Tag	A ^R	Reference
Peter Kaiser	University of California	HBUb	pQCXIP	-	P	(168)
Merry Mclaird	Stowers Institute for Medical Research	Elongin B	pCDNA3	Myc-5xHis	A	(181)
		Elongin C	pCDNA3-HSV	-	A	(181)
		Cullin 5	pCDNA3	-	A	(181)
		Rbx1	pRSETB	Myc	A	(181)
Stephen Yarwood	University of Glasgow	FAK1	-	Myc	A	-
Paul Pilch	University of Boston	Cavin-1	pEGFP-N1 pEGFP-C1	C-eGFP	K	(182)
				N-eGFP	K	
Gunter Schmidtko	Universität Konstanz	UBE1	pcDNA3.1	HA	A	(183)
Cam Patterson	Division of Cardiology University of North Carolina	Hsc70	pcDNA3.1	Myc	A	(184)
Eric Wanker	Max-Delbrück Centrum für mol. Medizin	Vcp/p97	pTC10	Flag	A	(185)
Pier Paolo Di Fiore	University of Milan	EPS15L1	pcDNA1	HA	A	(186)
Paul van Bergen en Henegouwen	Utrecht University	EPS15L1	pcDNA3	Myc	A	(187)
Elisabetta Citterio	Netherlands cancer centre	USP5	pcDNA3.1	Myc	A	(188)
Philip A. Robinson	University of Leeds	UCHL1	?	HA	A	(189)
Anne-Marie Pendergast	Duke University Medical Center	Abi2	?	eYFP	K	(190)
Laboratory Stocks		Puromycin	pBabe	-	P	-
		SOCS3	pcDNA3.1(+)	Flag	A	-
Antibiotic resistance (A ^R): A= ampicillin; K=kanamycin; P=puromycin.						

2.2 Methods

2.2.1 Cell culture

Murine embryonic fibroblasts stably expressing a puromycin-resistance and (His)₆+biotin-tagged Ub (HBUb) transgene or puromycin-resistance transgene alone were maintained in Dulbecco's modified Eagle's medium (DMEM) supplemented with 10% (v/v) foetal bovine serum (FBS), 1mM L-glutamine and 100U/ml penicillin, 100 μ M streptomycin, and 4 μ g/ml puromycin. For experiments requiring stable isotopic labelling of amino acids in cell culture (SILAC), the same cells were maintained in either SILAC DMEM (R6K6) or control SILAC DMEM (R0K0) supplemented with 10% (v/v) dialysed calf serum (dCS), 100U/ml penicillin, 100 μ M streptomycin, and 4 μ g/ml puromycin.

Plat-E retroviral packaging cells were maintained in DMEM supplemented with 10% (v/v) FBS, 100U/ml penicillin, 100 μ M streptomycin, 1 μ g/ml puromycin, 10 μ g/ml blasticidin, and 1mM glutamine.

HEK293 cells were maintained in DMEM supplemented with 10% (v/v) FBS, 100U/ml penicillin, 100 μ M streptomycin, and 1mM glutamine.

All cell lines were maintained at 37°C in a humidified 5% (v/v) CO₂ atmosphere. Passaging of cells was performed at ~80% confluency by washing cells in tissue grade PBS followed by incubation with trypsin or cell dissociation buffer for 2-3 minutes at room temperature (RT) after which the reaction was neutralised *via* the addition of fresh media. Cells were finally resuspended *via* gentle pipetting before transferring to 10-12ml of fresh media.

2.2.2 Preparation of puromycin resistant murine embryonic fibroblasts

2.2.2.1 Production of retrovirus for stable transduction of MEFs

Plat-E retroviral packaging cells were seeded on 10cm dishes to be 80% confluent the following day when cells were transfected with the relevant plasmid vector using Lipofectamine 2000 transfection reagent as per manufacturer's instructions. Briefly, on the day of transfection, either DNA (20 μ g) or

Lipofectamine 2000 reagent (60 μ l) were added to Optimem serum-free media (1.5ml) and mixed thoroughly *via* gentle pipetting prior to the individual solutions being mixed together, again *via* gentle pipetting. The solution was then incubated for 15 minutes at room temperature to allow formation of lipid-DNA complexes. During this time, the target cells were washed twice with Optimem before addition of the necessary transfection volume of Optimem (15ml). The Lipofectamine 2000 reagent-DNA-Optimem solution was then added to the target cells in a drop-wise fashion and mixed *via* gentle rocking. Cells were incubated at 37°C for 3 hours to allow transfer of DNA into the target cells after which time the transfection media was replaced with growth media containing no antibiotics before incubating overnight (O/N) at 37°C. Retrovirus-containing media was collected following two sequential incubation periods, one of 24 hours at 37°C and a second of 24 hours at 32°C at which point the retrovirus-containing media was stored at -80°C to maintain stability.

2.2.2.2 Production of puromycin resistant MEFs *via* retroviral transduction

MEFs were seeded in 10cm dishes to be 40% confluent the following day for transduction with retrovirus-containing media (section 2.2.2.1). At this time, the media was refreshed with 2ml DMEM supplemented with 10% (v/v) FCS, 1mM glutamine, and the cells transduced with the addition of 10 μ g/ml polybrene and 2ml of retrovirus-containing media. After 12 hours, the media was replaced with DMEM supplemented with 10% (v/v) FBS, 1mM L-glutamine and 100U/ml penicillin, 100 μ M streptomycin, and 1 μ g/ml puromycin. Individual puromycin resistant clones were picked in 50 μ l of media and expanded sequentially in 24 well plates, 6cm dishes, and T75 flasks.

2.2.3 Plasmid DNA preparation and quantification

Expression DNA plasmids were either received from donors in solution, as filter-paper spots, or prepared from glycerol laboratory stocks. Donated plasmids (Table 2.0) were first amplified by transforming XL1-Blue *E.coli* *via* heat pulse treatment. Briefly, 50 μ l of cells were aliquoted into pre-cooled microfuge tubes before the addition of 50ng of DNA and incubation on ice for 15 minutes. The mixture was then heat-shocked for 90 seconds in a 42°C water bath followed by recovery on ice for 2 minutes. The cells were then allowed to recover for a

further 45 minutes in a 37°C shaker following the addition of 450µl pre-heated, 37°C, Luria Bertani (LB) broth (1% (w/v) bactotryptone, 0.5% (w/v) yeast extract, 1% (w/v) sodium chloride) with no selection antibiotic. Cells were then concentrated by centrifugation at 1000g for 5 minutes after which the volume of LB-broth was reduced to 100µl. The cells were then resuspended, spread onto dry LB-agar (1% (w/v) bactotryptone, 0.5% (w/v) yeast extract, 1% (w/v), 1.5% (w/v) agarose) plates supplemented with the relevant selection antibiotic (ampicillin, 50µg/ml; kanamycin, 10µg/ml) and allowed to proliferate overnight in a 37°C incubator. The following day, the plates were either stored at 4°C or a starter-culture was prepared by picking off a single colony and inoculating 5ml of selection LB-broth that was incubated for 8 hours at 37°C with shaking. In the case of laboratory stocks, 5ml of LB supplemented with the relevant selection antibiotic was inoculated with a stab from a glycerol stock and incubated for 8 hours at 37°C with shaking.

The plasmid DNA was extracted from the starter-culture using a Wizard *Plus* miniprep DNA purification system (Promega) following the manufacturer's instructions or further amplified for a maxiprep DNA extraction procedure. In the latter case, the full 5ml starter-culture was used to inoculate 250ml of selection LB-broth that was incubated for a further 16 hours at 37°C with shaking. The plasmid DNA was then extracted using a maxiprep DNA purification system (Qiagen) following the manufacturer's instructions.

DNA yields were measured using a *NanoDrop*[™] 1000 Spectrophotometer. Absorption of ultraviolet light by DNA peaks at 260nm whereas that of protein peaks at 280nm. Absorption measurements were performed directly on 2µl of eluted DNA in either distilled H₂O (dH₂O) or TE buffer (1M Tris-HCl pH7.5, 0.25M EDTA) with the same solvent also being used as reference. Purity of nucleic acids was assessed from the resulting 260nm/280nm (protein contamination) and 260nm/230nm (chemical contamination e.g. phenol, EDTA) ratios where a value greater than 1.8 and >2.0 respectively is deemed to be of sufficiently high purity.

2.2.4 MTT assay

Cell death or apoptosis can be caused by unexpected side effects resulting from drug treatment or transgene overexpression. Cell survival can be assessed *via* a cell viability assay such as the MTT assay (191). Briefly, yellow MTT (3-(4,5-dimethylthiazol-2-yl)-2,5-diphenyltetrazolium bromide) reagent is converted to purple formazan crystals upon reduction within the mitochondria of living cells. Formazan concentration, measured as a function of its absorbance at 590nm, is directly related to the cell density and therefore a good indicator of viability. Proliferation of each cell line was compared to controls consisting of a dish containing no cells (blank) and cells pre-killed with 50% (v/v) DMSO for one hour. Since the mitochondria are no longer functioning, the reduction of MTT and therefore a colour change cannot take place.

WT, WT HBUb, SOCS3^{-/-} HBUb and SOCS3^{-/-} MEFs were seeded in 12 well plates at a density of 5×10^4 cells/well so that they would be ~60-70% confluent the next day. After this time, the media was refreshed and MTT reagent (100 μ M) directly added to cells before incubating at 37°C for 3 hours. The media was then removed and cells lysed with 500 μ l of neat DMSO, which also solubilises the formazan crystals. Proliferation was assessed by measuring the absorbance of 200 μ l aliquots of DMSO-solubilised crystals at 590nm.

2.2.5 Cell preparation and harvesting

2.2.5.1 Preparation of tissue culture dishes

Most cells adhere and grow on untreated tissue culture dishes without difficulty. Where adherence is a problem such as in the case of HEK293 cells which weakly adhere to untreated dishes, a coating can be applied to strengthen the cell-plastic interaction e.g. poly-D-lysine. The overall positive charge provided by the amino group of the lysine side chain increases the electrostatic interaction with the negatively charged plasma membrane of the HEK293 cells. Here, cell attachment was enhanced by briefly washing the dishes with neat aqueous poly-D-lysine and leaving to dry following the removal of all residual solution.

2.2.5.2 Harvesting for cell characterisation

MEFs grown on the appropriately sized dishes were placed on ice and washed twice with ice cold tissue culture grade PBS before harvesting with the addition of an appropriate volume (50µl, 6-well plate; 250µl, 6cm diameter dish; 500µl, 10cm diameter dish) of RIPA buffer (50mM HEPES pH 7.4, 150mM sodium chloride, 1% (v/v) Triton x100, 0.5% (v/v) sodium deoxycholate, 0.1% (w/v) SDS, 10mM sodium fluoride, 5mM EDTA, 10mM sodium phosphate, 0.1mM PMSF, 10µg/ml benzamidine, 10µg/ml soybean trypsin inhibitor, 2% (w/v) EDTA-free complete protease inhibitor cocktail). Cell lysis was completed by incubating for one hour at 4°C with rotation. Supernatant, (~45µl, 6-well plate; ~230µl, 6cm diameter dish; ~450µl, 10cm diameter dish) was then isolated, taking care not to disturb the pellet, following centrifugation at 21000g for 15 minutes at 4°C.

2.2.5.3 Harvesting for tandem affinity purification

MEFs grown on the appropriately sized dishes were placed on ice and washed twice with ice cold tissue culture grade PBS before harvesting with the addition of an appropriate volume (250µl, 6cm diameter dish; 500µl, 10cm diameter dish; 1ml, 20cm diameter dish) of lysis buffer A (8M urea, 300mM NaCl, 50mM NaH₂PO₄, 0.5% (v/v) NP-40, pH 8.0) supplemented with 1mM PMSF. Lysate was sonicated for three 10 second pulses, with a 10 second rest phase, at 40% amplitude with a 2mm diameter stepped micro-tip (150µl-1ml) or 6mm tapered micro-tip (>5ml) to fragment the precipitated DNA. Supernatant (~230µl, 6cm diameter dish; ~450µl, 10cm diameter dish) was then isolated, taking care not to disturb the pellet, following centrifugation at 21000g for 30 minutes at RT.

2.2.5.4 Harvesting for co-immunoprecipitation

HEK293 cells grown on the appropriately sized, poly-D-lysine-treated dishes were placed on ice and media completely removed. Since certain treatments i.e. H₂O₂ exacerbate cell dissociation, cells were harvested in ice cold PBS which was removed following centrifugation at 1000g for 5 minutes at 4°C and replaced with an appropriate volume (250µl, 6cm diameter dish; 500µl, 10cm diameter dish) of co-immunoprecipitation buffer (50mM HEPES, pH 7.4, 120mM NaCl, 5mM EDTA, 10% (v/v) glycerol, 1% (v/v) Triton X-100, supplemented with

phosphatase inhibitors 5mM NaF, 1mM Na₃VO₄, and protease inhibitors 10µg/ml benzamidine, 0.1mM PMSF, 10µg/ml soybean trypsin inhibitor, 2% (w/v) EDTA-free complete protease inhibitor cocktail). Cells were resuspended *via* gently pipetting and lysis completed by incubating for one hour at 4°C with rotation. Supernatant (~230µl, 6cm diameter dish; ~450µl, 10cm diameter dish) was isolated, taking care not to disturb the pellet, following centrifugation at 21000g for 15 minutes at 4°C.

2.2.5.5 Harvesting for peptide array

HEK293 cells grown on 10cm diameter, poly-D-lysine-treated dishes were placed on ice and the media completely removed. Cells were harvested in ice cold PBS which was removed following centrifugation at 1000g for 5 minutes at 4°C. Cell lysates were prepared to be highly concentrated by lysing cells in a small volume (250µl/10cm diameter dish) of peptide array buffer (50mM HEPES, pH 7.4, 150mM NaCl, 5mM EDTA, 1% (v/v) Triton X-100, supplemented with phosphatase inhibitors 5mM NaF, 1mM Na₃VO₄, and protease inhibitors 10µg/ml benzamidine, 0.1mM PMSF, 10µg/ml soybean trypsin inhibitor, 2% (w/v) EDTA-free complete protease inhibitor cocktail). This allowed the concentration of the detergent Triton X-100 to be diluted, prior to incubation with the peptide array, with TBS-Tween (50mM Tris pH 7.5, 150mM NaCl, 0.05% (v/v) Tween-20) to below 0.05% preventing it from effecting interactions.

2.2.6 Protein quantification by bicinchoninic acid assay

The bicinchoninic acid (BCA) assay (192) is an accurate, sensitive, stable technique for quantification of proteins i.e. high tolerance to non-ionic detergent and salts usually found in buffers. It is based on the coupling of two reactions, the reduction of alkaline Cu²⁺ to Cu¹⁺ (biuret reaction) by peptide bonds and the formation of a purple complex between Cu¹⁺ and two molecules of BCA. The intensity of the purple complex, measured as a function of its absorbance at 630nm (A₆₃₀), is directly proportional to the amount of protein in solution and as such, is a good indicator of protein concentration.

Protein standards (0.0 to 2.0µg/µl) of bovine serum albumin (BSA) prepared in the appropriate lysis buffer along with appropriate dilutions of protein lysate in

lysis buffer (total volume, 10 μ l) were arranged on a 96 flat-well plate. A 200 μ l 1:50 dilution of copper sulphate (4% (v/v)) to BCA reagent (1% (w/v) 4,4 dicarboxy-2,2 biquinoline disodium salt, 2% (w/v) sodium carbonate anhydrous, 0.16% (w/v) sodium potassium tartrate, 0.4% (w/v) sodium hydroxide, 0.95% (w/v) sodium bicarbonate, pH 11.25) was then added to each well before incubating at RT for the appropriate time period until a linear standard curve ($r^2 \sim 0.98$) standard curve was produced. Absorption measurements were taken at 630nm using a POLARstar OPTIMA (BMG LabTech) microplate reader. Protein concentrations were quantified using POLARstar OPTIMA MARS data analysis package v.1.20 and GraphPad Prism v.4.

2.2.7 Tandem affinity purification

Tandem affinity purification (TAP) (174) is a facile strategy to achieve high levels of purity necessary for post-analysis *via* LC-MS/MS. General TAP strategies involve the production of a fusion protein where a TAP tag is attached to the N- or C-terminus of the protein of interest. Employing multiple structurally distinct tags theoretically allows for the selection of specific complexes and the removal of others. TAP strategies typically involve two purification stages allowing reduction of non-specific purification and contaminants. It has been shown that using the HBUb-tag system the second purification step can achieve a 6-fold reduction in non-specific purification over the first (175). The majority of TAP strategies allow purification under native conditions but this leaves the majority of post-translational modifications (PTMs) vulnerable. The HBUb tag (168,175) is able to facilitate purification under extreme denaturing conditions (8M urea/6M guanidinium chloride) thus protecting PTMs, in this case, ubiquitinated proteins from deubiquitinases (DUBs) and reduce background from non-specifically bound proteins and ubiquitin binding proteins which bind ubiquitin but are not themselves ubiquitinated. The tight binding of biotin to streptavidin ($K_d=10^{-15}$ M) also facilitates very stringent wash conditions to further reduce background *via* the removal of all non-covalently associated proteins. Overall, TAP using the HBUb tag provides high purity and low background from non-specifically bound proteins facilitating the detection of proteins, even those in low abundance.

2.2.7.1 Preparation of NTA-Ni²⁺-Sepharose beads

The appropriate volume of nitrilotriacetic acid (NTA)-Ni²⁺-Sepharose beads was aliquoted and the supernatant removed using a Hamilton syringe following centrifugation at 500g for 30 seconds. The pellet was washed, to remove the ethanol storage media, in 5 bead volumes of autoclaved distilled water and rotated for 3 minutes at RT. Following centrifugation at 500g for 30 seconds at RT, the supernatant was removed using a Hamilton syringe and the process repeated with buffer A (8M urea, 300mM NaCl, 50mM NaH₂PO₄, 0.5% (v/v) NP-40, pH 8.0) supplemented with 1mM PMSF and 10mM imidazole to reduce non-specific binding. Finally, one bead volume of buffer A was added to the beads to produce a 50% (v/v) bead slurry.

2.2.7.2 Preparation of streptavidin-Sepharose beads

The appropriate volume of streptavidin-Sepharose beads was aliquoted and the supernatant removed using a Hamilton syringe following centrifugation at 500g for 30 seconds. The pellet was then re-suspend and washed, to remove the ethanol storage media, in 5 bead volumes of elution buffer (8M urea, 200mM NaCl, 50mM NaH₂PO₄, 2% (w/v) SDS, 10mM EDTA, 100mM Tris, pH 8.0) supplemented with 1mM PMSF. Following centrifugation at 500g for 30 seconds, the supernatant was removed using a Hamilton syringe and the process repeated. Finally, one bead volume of elution buffer was added to beads the beads to produce a 50% (v/v) bead slurry.

2.2.7.3 Nickel affinity chromatography

Soluble protein lysates were prepared in buffer A supplemented with 1mM PMSF. Lysates were equalised to 1mg/ml and incubated with 30µl of 50% (v/v) Ni²⁺-NTA-Sepharose beads per milligram of protein and rotated overnight at RT. Optimisation experiments were performed in microfuge tubes whereas for scaled-up experiments the larger volumes (~400ml) of lysates were aliquoted to 15ml conical tubes. The next day, the flow-through was removed following centrifugation at 100g for 1 minute. The beads were then washed sequentially, once with 20 bead volumes of buffer A (8M urea, 300mM NaCl, 50mM NaH₂PO₄, 0.5% (v/v) NP-40, pH 8.0) supplemented with 1mM PMSF and 10mM imidazole and twice with 20 bead volumes of buffer B (8M urea, 300mM NaCl, 50mM

NaH₂PO₄, 0.5% (v/v) NP-40, pH 6.3) supplemented with 10mM imidazole and 1mM PMSF. The supernatant was then removed with a Hamilton syringe following centrifugation at 100g for 1 minute. Elution was performed in two steps. Bound proteins were eluted from the Ni²⁺-NTA-Sepharose beads with 5 bead volumes of elution buffer (8M urea, 200mM NaCl, 50mM NaH₂PO₄, 2% (w/v) SDS, 10mM EDTA, 100mM Tris, 500mM imidazole, pH 8.0) supplemented with 1mM PMSF. The supernatant was then isolated following centrifugation at 100g for 1 minute and the process repeated.

2.2.7.4 Streptavidin affinity purification

Eluate from nickel affinity chromatography was directly added to 10µl of 50% (v/v) streptavidin-Sepharose beads per milligram of initial protein lysate and rotated overnight at RT. The next day, the flow-through was removed following centrifugation at 100g for 1 minute. The beads were then washed sequentially, twice with 25 bead volumes of buffer C (8M urea, 200mM NaCl, 2% (w/v) SDS, 100mM Tris, pH 8.0) and twice with 25 bead volumes of buffer D (8M urea, 1.2M NaCl, 0.2% (w/v) SDS, 100mM Tris, 10% (v/v) ethanol, 10% (v/v) isopropanol, pH 8.0). In each case, the supernatant was removed following centrifugation at 100g for 1 minute. After the final wash, the supernatant was removed using a Hamilton syringe. Elution was performed using two methods.

Method one: optimisation of experimental strategy:

For SDS-PAGE analysis of eluate, bound proteins were eluted from the streptavidin-Sepharose beads *via* the addition of one bead volume of 12% (w/v) SDS sample buffer (50mM Tris, PH 6.8, 10% glycerol (v/v), 12% (w/v) SDS, 0.02% (w/v) bromophenol blue, 1.6mg/ml dithiothreitol (DTT)) and heating to 95°C for 5 minutes. The supernatant was then isolated, using a Hamilton syringe, following centrifugation at 100g for 1 minute.

Method two: LC-MS/MS: In-gel trypsin digestion

Optimum sample preparation following SDS-PAGE fractionation for LC-MS/MS requires the use of thin, narrow lane pre-cast gels (see section 2.2.9.2). This requirement reduces acrylamide levels and trypsin volume resulting in improved

digest efficiency. The main caveat is that the gels have small wells and thus small loading volumes (25 μ l). To increase probability of detecting low-abundant proteins, a large initial volume (~40ml) of protein lysate was prepared and so a large volume (~2ml) of eluate was produced that needed to be concentrated to ~25 μ l before SDS-PAGE fractionation. SDS sample buffer is not compatible with protein concentration spin-columns. Bound proteins were eluted from the streptavidin-Sepharose beads *via* the addition of one bead volume of aqueous biotin (50mM) and heating to 95°C for 5 minutes. The supernatant was then isolated, using a Hamilton syringe, following centrifugation at 100g for 1 minute.

2.2.8 Immunoblot analysis

Soluble protein lysates were fractionated *via* SDS-PAGE on 8, 10, or 12% (w/v) resolving gels (see below). Fractionated proteins were transferred to a nitrocellulose membrane and blocked for 1 hour at RT or overnight at 4°C with 5% (w/v) dried milk powder (Marvel) in TBS-Tween (10mM Tris pH 7.6, 150mM NaCl, 0.1% (v/v) Tween-20). Proteins were detected with specific primary antibody followed by the corresponding horseradish peroxidase (HRP)-conjugated antibody (Table 2.1). Membranes were incubated overnight with primary antibody in 5% (w/v) dried milk powder in TBS-Tween. Membranes were incubated with secondary antibody for 1 hour at RT in 5% (w/v) dried milk powder in TBS-Tween. Membranes were then submerged in TBS-Tween and washed three times for ten minutes with shaking. Proteins were visualised using enhanced chemiluminescence using ECL Western Blotting Substrate (Pierce). Excess TBS-Tween was removed and membranes were incubated in 2ml of ECL Western Blotting Substrate for 1 minute. Excess substrate was removed before developing using medical x-ray film (Kodak) and an X-OMAT 2000 processor (Kodak).

Resolving gel: 12%: 28% (v/v) dH₂O, 25% (v/v) Buffer 1 (1.5M Tris pH 8.8, 0.4% (w/v) SDS), 6.5% (v/v) 50% (v/v) glycerol, 0.32% (v/v) APS (0.3mg/ml), 0.08% (v/v) TEMED, 40% (v/v) 30% (v/v) bis/tris acrylamide.

Resolving gel: 10%: 34% (v/v) dH₂O, 25% (v/v) Buffer 1 (1.5M Tris, pH 8.8, 0.4% (w/v) SDS), 6.5% (v/v) 50% (v/v) glycerol, 0.32% (v/v) APS (0.3mg/ml), 0.08% (v/v) TEMED, 33.4% (v/v) 30% (v/v) bis/tris acrylamide.

Resolving gel: 8%: 41% (v/v) dH₂O, 25% (v/v) Buffer 1 (1.5M Tris, pH 8.8, 0.4% (w/v) SDS), 6.5% (v/v) 50% (v/v) glycerol, 0.32% (v/v) APS (0.3mg/ml), 0.08% (v/v) TEMED, 26.7% (v/v) 30% (v/v) bis/tris acrylamide;

Stacking gel: 25% (v/v) Buffer 2 (0.5M Tris, pH 6.8, 0.4% (w/v) SDS), 1% (v/v) APS (0.3mg/ml), 0.1% TEMED, 12% (v/v) 30% (v/v) bis/tris acrylamide)

Table 2.1: Primary and secondary antibodies

Primary Antibodies					
Antibody Reactivity	Linked	Species	Supplier	Cat.no	Dilution
Poly-His (HHHHHH)	-	Mouse	Sigma-Aldrich	H1029	1:1000
Poly-His (HHHHHH)	-	Rabbit	Cell Signaling	2365	1:1000
HA (YPYDVPDYA)	-	Rabbit	Sigma-Aldrich	F3165	1:1000
MYC (9e10, EQKLISEEDL)	-	Mouse	In-House	-	1:1000
Flag (DYKDDDDK)	-	Mouse	Sigma-Aldrich	F3165	1:2000
IκBa	-	Rabbit	Cell Signaling	4812	1:1000
pIκBa	-	Mouse	Cell Signaling	9246	1:1000
SOCS3	-	Goat	Santa Cruz Biotechnology	sc-7009	1:1000
GFP	-	Goat/Sheep	In-House	-	1:2000
Ub	-	Mouse	Santa Cruz Biotechnology	sc-8017	1:1000
K48-Ub	-	Rabbit	Millipore	05-1307	1:1000
pTyr (4G10)	-	Goat	Millipore	05-321x	1:1000
PTRF (cavin-1)	-	Rabbit	Abcam	ab48824	1:1000
Streptavidin	HRP	Rabbit	Pierce Thermo Scientific	21134	1:500
Secondary Antibodies					
Rabbit	HRP	Goat	Sigma-Aldrich	A6154	1:1000
Mouse	HRP	Goat	Sigma-Aldrich	A4416	1:1000
Goat	HRP	Rabbit	Sigma-Aldrich	A5420	1:2000
Mouse	IRDYE 800CW	Donkey	Licor	926-32212	1:2500
Rabbit	IRDYE 680LT	Goat	Licor	926-68021	1:2500

2.2.9 Sample processing pre-LC-MS/MS analysis

2.2.9.1 Concentration of Eluate

Eluate was concentrated using Amicon 10K Ultra-2 Centrifugal Filter Devices (Millipore) as per manufacturer's instructions. Briefly, the eluate was transferred into the device before centrifugation using a fixed angle rotor at 7500g for 40 minutes at RT. Immediately after, the flow-through was removed and the concentrated protein eluted by centrifugation for 2 minutes at 1000g after which the sample (~25µl) was isolated to a fresh microfuge tube.

2.2.9.2 SDS-PAGE and gel slice extraction

Concentrated protein (Section 2.2.9.1) was fractionated following the addition of 5µl 4x NuPage LDS sample buffer (Invitrogen) using NuPAGE 4-12% Bis-Tris Gel 1.0mm x 10 well (Invitrogen) on an XCell SureLock Mini-Cell (Invitrogen) using NuPAGE MOPs SDS Running Buffer (Invitrogen) as per manufacturer's instructions. During fractionation, the dye front was only allowed to progress for 2cm into the resolving gel so to reduce acrylamide levels thus improving in-gel digestion efficiency. Protein bands were visualised using a Coomassie-based staining solution InstantBlue (Expedion). A single lane was then segmented on a clean glass plate, under reduced-keratin/contaminant conditions using a fresh scalpel, into ~3mm slices before being transferred individually to fresh microfuge tubes and stored at -80°C before further processing. Care was taken to remove all unstained regions from each 3mm section to further reduce acrylamide levels.

2.2.9.3 In-gel trypsin digestion

SDS-PAGE fractionated proteins must be extracted from the acrylamide gel and trypsin digested prior to LC-MS/MS. Gel pieces were first washed in 500µl (100mM) ammonium bicarbonate for 30 minutes on a shaker before disposing of wash and repeating with 500µl, 50% (v/v) acetonitrile/ammonium bicarbonate (100mM). The samples were then reduced with the addition of 150µl (100mM) ammonium bicarbonate and 10µl (45mM) DTT followed by incubation at 60°C for 30 minutes in a heating block. Samples were allowed to cool to RT before

alkylation using 10 μ l (100mM) iodoacetamide followed by incubation in the dark at RT for 30 minutes. The solvent was then discarded and the gel pieces washed in 500 μ l, 50% (v/v) acetonitrile/ammonium bicarbonate (100mM) for 1 hour on a shaker after which the wash was discarded. The gel pieces were then shrunk by treating with 50 μ l acetonitrile for 10 minutes after which the solvent was discarded and the gel pieces dried using a vacuum centrifuge for 1 hour. A sufficient quantity (~20 μ l) of trypsin suspended in 1ml ammonium bicarbonate (25mM) was used to rehydrate each gel piece. A further amount of trypsin, in 10 μ l volumes, was added if the initial volume was absorbed by the gel slice. This continued until the gel piece reverted to its initial fully rehydrated size. Finally, a sufficient amount of ammonium bicarbonate (25mM) was added to just cover the gel piece. The protein was then allowed to digest overnight at 37°C.

The following day, gel pieces were isolated *via* brief centrifugation after which the supernatant was transferred to a fresh 96 well plate without disturbing the gel pieces. Residual digested protein was then extracted by treating the gel piece with 20 μ l, 5% (v/v) formic acid for 20 minutes at RT with shaking followed by the addition of 40 μ l acetonitrile for a further 20 minutes with shaking at RT. Following brief centrifugation, the supernatant was pooled with the initial supernatant on a 96 well plate. Finally, extracts were dried using a SpeedVac centrifugal evaporator. Samples were then stored at -20°C prior to MALDI-TOF. Due to different requirements of the Orbitrap Velos LC-MS/MS, dried samples were first resuspended in a sufficient volume of dH₂O (10 μ l) beforehand.

2.2.9.4 Reduced-keratin work environment

Accurate MS analysis can be limited by keratin contamination. Keratins are the main components of skin, hair, and nails which makes it the most abundant contaminant under normal laboratory conditions. Keratin contamination becomes significant during MS when attempting to assess proteins with low abundance. As such, it is vital that contamination is kept to a minimum.

For all experimental stages leading up to MS, simple steps were made to reduce keratin contamination. All work, where possible, was performed in a biological safety cabinet (BSC) that was quarantined and cleaned with ethanol and water prior to use. All equipment and reagents contained in paper/lint-free packaging

were sprayed with ethanol prior to use within the BSC. Where necessary, reagents such as lysis buffer were prepared in the BSC and filter sterilised using 0.45µm filters (Sartorius Stedim Biotech) prior to use. Reagent contamination, when outside of BSC i.e. during pH adjustment, was reduced by using facemasks and minimising the time reagent containers were left uncovered. Clothing, being a high source of keratin, was covered with lab coat and disposable clean-room sleeve protectors along with powder-free nitrile gloves to minimise contamination from hands and wrists.

2.2.10 Mass spectrometry data quantitation and analysis

2.2.10.1 Mascot Daemon

An MS/MS ion search was performed using Mascot daemon v2.2 using the mus musculus SwissProt protein database (SwissProt_56.6.fasta). Raw mass spectrometry data (.raw) from the Orbitrap Velos Fourier Transform Mass Spectrometer (FTMS), operated by William Mullen (University of Glasgow, Proteomics Biomarkers and Systems Medicine), was searched for monoisotopic peaks ($z=2+$ and $3+$) with a MS peptide tolerance of 5ppm and a MS/MS tolerance of 0.05Da. Peptides with a charge greater than one was chosen to enable differentiation from simple, non-peptide ions. A maximum of one missed trypsin cleavage site was allowed per peptide to account for non-cleavage of Arg or Lys dipeptides, interspersed dipeptides, and cases where either peptide precedes a proline residue. To account for mass variations of peptides due to PTMs, a set of common variable and fixed modifications were chosen to improved peptide sequencing and identification. Variable modifications, i.e. those which might only occur following treatment or under certain cellular conditions, included phosphorylation (S, T, and Y), a remnant of ubiquitin cleavage, GlyGly (K), and SILAC labels $^{13}\text{C}_6$ -arginine (R6) and $^{13}\text{C}_6$ -lysine (K6). The alkylating agent iodoacetamide was used during in-gel trypsin digestion to prevent oxidation of the SH group of cysteine residues *via* S-carbamidomethylation. Carbamidomethylation along with oxidation of methionine was set as fixed modifications i.e. those which are expected to occur as a result of processing.

Data from a hybrid quadrupole time of flight mass spectrometer (QTOF), operated by Richard Burchmore (University of Glasgow, Sir Henry Wellcome

Functional Genomics Facility), has a lower resolution and accuracy. Raw mass spectrometry data (.wiff) from the QTOF was searched using a peptide tolerance of 1.2Da and a MS/MS tolerance of 0.6Da. All other settings remained unchanged.

2.2.10.2 MaxQuant

Post-MS data analysis will be performed using MaxQuant v.1.1.1.36 (170) (Figure 2.0), a freely available software package that was designed for SILAC-based studies. The software includes its own peptide search engine, Andromeda (193) and operates as a stand-alone, PC-based module. Briefly, MaxQuant takes raw MS data from which it extracts peak information, and performs quantitation of SILAC peptide pairs (170). Data, combined with a set of user defined parameters, are then submitted to the peptide search engine Andromeda (193) after which peptides are assigned to proteins. The parameters defined are important as they can increase the stringency of the search, increase confidence in protein identification, and simplify analysis. However, with any automated proteomics software package, it is also possible to negatively influence protein identification e.g. reducing minimum peptide length, and so default settings were used where possible. Table 2.2 outlines additional MaxQuant settings used, all others settings were unchanged from their default state. The parameters that were altered enabled the software to account for detection of low abundant proteins (identification using single unique peptide), specification of the SILAC isotopes, and variability of mass i.e. due to phosphorylation (S, T, and Y), ubiquitination (GlyGly, trypsin remnant), oxidation (Met, *in vitro* processing) and carbamidomethylation (iodoacetamide alkylation prior to trypsin digestion).

Peptide identification is based on the comparison the MS/MS sequenced peptides with peptides from true and modified/reverse peptide databases (International protein index (IPI), Uniprot) (170). This analysis produces a posterior error probability (PEP) for each peptide. The smaller the PEP, the more certain is the identification of the peptide (170). Proteins are 'identified' by a process of peptide assignment. Peptides are assigned to all proteins in which they are found but are accepted to belong to proteins with the most identified peptides (Razor peptides). At least a single unique peptide is necessary for confident protein identification. Proteins are accepted based on the protein PEP, the

product of the individual peptide PEPs, which is limited by the false discover rate (FDR) which is set at 1% as a default (170). Protein SILAC ratios are calculated as the median of the SILAC ratios of unique or unique and razor peptides based on the stringency required (170). These ratios are then normalised to account for differences in protein abundance. Finally, MaxQuant outputs data into several tab-delimited text files that can be manipulated by standard software packages i.e. Excel.

2.2.10.3 Analysis for raw mass spectra

Raw mass spectra were manually assessed using either Xcalibur v.2.1, Thermo Scientific (Orbitrap Velos FTMS) or Analyst v.1.2, Applied Biosystems (QTOF). Visual inspection allowed assessment of correct peak assignment, SILAC ratios, and the possibility of conversion of $^{13}\text{C}_6$ -arginine to $^{13}\text{C}_6$ -proline. The latter is assessed by the detection satellite peaks that are offset from heavy labelled monoisotopic peaks, relating to proline-containing peptides, by multiples of 5Da.

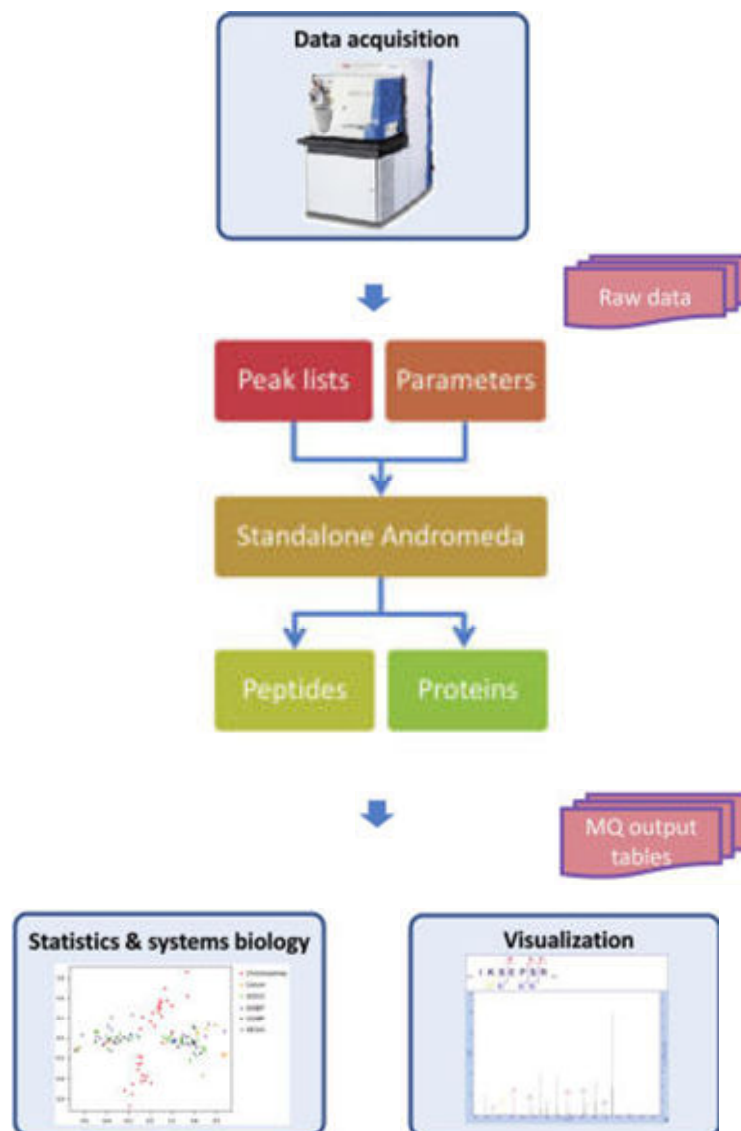


Figure 2.0: Quantitative proteomics using MaxQuant

MaxQuant (170) takes raw MS data from which it extracts peak information, and performs quantitation of SILAC peptide pairs. Data, combined with a set of user defined parameters, is then submitted to the peptide search engine Andromeda (193) after which peptides are assigned to proteins. Peptide identification is based on the comparison the MS/MS sequenced peptides with peptides from true and modified/reverse peptide databases. Proteins are accepted based on a posterior error probability (PEP), the product of the individual peptide PEPs, which is limited by the false discover rate (FDR) which is set at 1%. Protein SILAC ratios are calculated as the median of the SILAC ratios of selected peptides. Finally, MaxQuant outputs data into several tab-delimited text files that can be manipulated by standard analysis software packages i.e. Excel. Adapted with permission from (193). Copyright (2011) American Chemical Society.

Table 2.2: MaxQuant modified settings

Most parameters used were unchanged from their default state. Parameters presented here were altered to account for specific experimental conditions.

Parameter	Value	Comment
Version	1.1.1.36	MaxQuant version used.
SILAC isotope	Arg6, Lys6	Heavy SILAC isotopes
Quantification: Use only unmodified peptides and	TRUE	Modified peptides are rare and variable. Using least modified peptides improves accuracy of protein quantitation.
Modifications included in protein quantification	Oxidation (M); Acetyl (Protein N-term); Phospho (STY); GlyGly (K)	Accounts for more probable experimentally induced modifications.
Peptides used for protein quantification	Unique and razor	Peptides that match several proteins but are assigned to the most abundant and thus most probable protein.
Min. ratio count	1	At least one SILAC-paired peaks used to calculate the SILAC ratio.
Re-quantify	TRUE	Forces MaxQuant to search for SILAC paired peaks where none were previously detected. If peaks are found then they are used to quantify the missing peptide pair. However, this often results in the quantification of the background, which should be very low. In this way, a SILAC ratio is returned which should be a good estimation of the different amounts of the protein in the heavy and light samples
Fasta file	ipi.MOUSE.v3.80.fasta	A database of 59534 protein entries.
First search fasta file	mouse.first.search.fasta	A reduced database use for MaxQuant calibration .
Labelled amino acid filtering	FALSE	Enables MaxQuant to improved us of R6K6 SILAC labelling.
Variable modifications	Oxidation (M); Acetyl (Protein N-term); GlyGly (K); Phospho (STY)	Experimentally induced modifications that could impact peptide identification.
Fixed modifications	Carbamidomethyl (C)	Modifications that arise due to sample processing.

2.2.11 Production of SOCS3 L189A Mutant

2.2.11.1 Primer design and synthesis for site directed mutagenesis

Primers, (forward, 5'-tcc acc gtg gcc acc gcc cag cat ctt tgt cg-3', reverse, 5'-cg aca aag atg ctg ggc ggt ggc cac gtt gga-3') were designed to produce an L189A mutation of the B/C-box within the SOCS3 SOCS-box. This mutation disrupts the essential leucine residue and prevents interaction with elonginC thus blocking E3 ligase function (194) (Figure 2.1).

In brief, primers were designed to be 25 bases in length with the mutation centred with 10-15 bases each side. Primers had a GC content greater than 40%, terminated with a GC and had a melting temperature greater or equal to 78°C where:

$$T_m = 81.5 + 0.41(\%GC) - (675/N) - \%mismatch$$

N = Primer length in bases

%GC and %mismatch are whole numbers

The final design verified using an online tool (Agilent) available at: (<https://www.genomics.agilent.com/CollectionSubpage.aspx?PageType=Tool&SubPageType=ToolQCPD&PageID=15>).

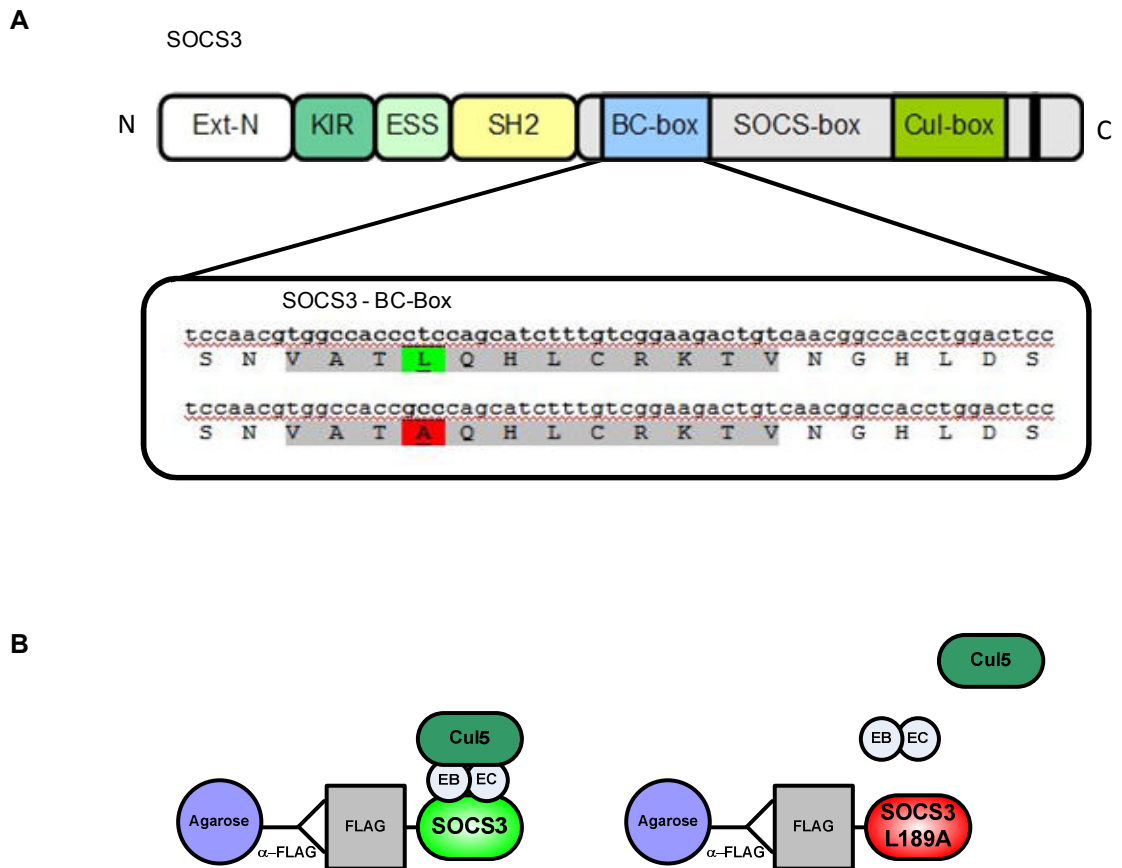


Figure 2.1: Mutation of the SOCS-box disrupts the SOCS3-elonginBC interaction

An L189A mutation of the B/C-box within the SOCS3 SOCS-box disrupts an essential leucine residue (Panel A) and prevents interaction with elonginC and thus blocks E3 ligase function (194) (Panel B). Primers were designed (Section 2.2.11.1) and site-directed mutagenesis performed on SOCS3-cDNA as described (Section 2.2.11.2). The mutation was confirmed *via* DNA sequencing (Section 2.2.11.3) and by co-immunoprecipitation (Panel B, section 6.2.1.1).

2.2.11.2 Site-directed mutagenesis

Site-directed mutagenesis was performed using a Quikchange II Site-Directed Mutagenesis kit as per manufacturer's instructions. Briefly, reaction components (reaction buffer, dsDNA template, primers, dNTP mix, ddH₂O, and DNA polymerase) were mixed and the reaction allowed to proceed for 18 temperature cycles (95°C, 30 seconds; 55°C, 1 minute; 68°C, 6 minutes) following an initial 30 second extended melting period 95°C. Non-mutated, methylated DNA was then digested for 1 hour with the restriction enzyme *Dpn I* prior to nick repair and amplification of mutated dsDNA *via* the transformation of XL1-Blue super-competent cells. Mutant-DNA transformed-cells along with mutagenesis (pWhitescript) and transformation (pUC18) controls were spread on separate LB-ampicillin (50µg/ml) agar plates containing 80µg/ml X-gal and 20mM IPTG. Colonies were allowed to proliferate for 16 hours at 37°C before isolation of transformed colonies prior to mini or maxiprep DNA purification and sequencing.

2.2.11.3 Sequencing of plasmids

Before and after site-directed mutagenesis, candidate SOCS3-FLAG plasmids were sequenced using the DNA sequencing service provided by www.dnaseq.co.uk based at the University of Dundee. Sequencing was performed across the open reading frame (ORF) using T7 (TAATACGACTCACTATAGGG, forward) and SP6 (AGCTATTTAGGTGACACTATAG, reverse) primers that were provided by www.dnaseq.co.uk. The quality of sequencing was visually evaluated using Chromas lite by assessing the intensity and separation of individual base peaks. The location of the epitope tag, the identity, and species of the encoded SOCS3 protein was verified *via* an NCBI BLAST search (<http://blast.ncbi.nlm.nih.gov/Blast.cgi>).

2.2.12 Transfection

HEK293 cells seeded at 80% confluency on poly-D-lysine-coated dishes were transfected with 2µg to 8µg of DNA using Lipofectamine 2000 Reagent (Life Technologies, UK) as per manufacturer's instructions. Briefly, either DNA or Lipofectamine 2000 reagent were added to Optimem serum-free media and mixed thoroughly *via* gentle pipetting prior to the individual solutions being

mixed together, again *via* gentle pipetting. The solution was then incubated for 15 minutes at room temperature to allow formation of lipid-DNA complexes. During this time, the target cells were washed twice with Optimem before addition of the necessary transfection volume of Optimem. The Lipofectamine 2000 reagent-DNA-Optimem solution was then added to the target cells in a drop-wise fashion and mixed *via* gentle rocking. Cells were incubated at 37°C for 3 hours to allow transfer of DNA into the target cells after which time the transfection media was replaced with growth media. Cells were then allowed to proliferate for 24 hours at 37°C before the media was refreshed. After a further 24hrs at 37°C, the cells were harvested (Section 2.2.5).

2.2.13 Co-immunoprecipitation

2.2.13.1 Sepharose beads

Co-immunoprecipitation was performed using 40µl of 50% slurry (v/v) of Protein G Sepharose beads (Sigma). Prior to use, beads were washed twice in 1ml lysis buffer (50mM HEPES, pH 7.4, 120mM NaCl, 5mM EDTA, 10% (v/v) glycerol, 1% (v/v) Triton x-100, supplemented with phosphatase inhibitors 5mM NaF, 1mM Na₃VO₄, and protease inhibitors 10µg/ml benzamide, 0.1mM PMSF, 10µg/ml soybean trypsin inhibitor, 2% (w/v) EDTA-free complete protease inhibitor cocktail), which was completely removed using a Hamilton syringe following centrifugation at 300g for 30 seconds. Beads were resuspended in 100µl 2% (v/v) IgG free BSA as a blocking agent and incubated for 1-4 hours with rotation at 4°C. Soluble protein lysates prepared in lysis buffer were equalised to 1mg/ml and incubated with 40µl pre-equilibrated protein G beads at 4°C with rotation for one hour to remove non-specifically binding proteins. Recovered, pre-cleared lysate was added to 50µl of pre-equilibrated protein G Sepharose beads suspended in 100µl 2% (v/v) IgG free BSA plus an optimised volume of the relevant antibody and incubated overnight at 4°C with rotation. Beads were isolated following centrifugation at 300g for 30 seconds. Recovered beads, bound to antibody and protein, were washed three times using 1ml of lysis buffer, the final wash was removed using a Hamilton syringe. Protein complexes, from both pre-clear and antibody-bound beads, were eluted in 40µl of 12% (w/v) SDS sample buffer supplemented with DTT by incubating at 67°C for 30 minutes.

followed by a further 5 minutes at 95°C. Supernatant was collected using a Hamilton syringe following centrifugation at 300g for 30 seconds and prepared for western blot analysis.

2.2.13.2 Pre-conjugated anti-Flag M2-agarose beads

Co-immunoprecipitation was performed using 40µl of pre-conjugated anti-Flag M2-agarose beads (Sigma). The protocol shown in section 2.2.13.1 was repeated without pre-clearing of cell lysates.

2.2.14 Denatured immunoprecipitation of ubiquitinated proteins

To ensure precipitation of the ubiquitinome was unaffected by DUBs or uncontaminated by ubiquitin binding proteins or non-specifically bound proteins, a non-denaturing immunoprecipitation was performed on denatured cell lysates.

HEK293 cells were seeded on poly-D-lysine-treated dishes to achieve ~80% confluency the following day. Cells were transfected as previously described (Section 2.2.12) with cDNA constructs for Ub-HA and combinations of candidate SOCS3 substrates, SOCS3, and components the E3 ubiquitin ligase scaffold (cullin5, Rbx2, elonginB, and elonginC). Cells were treated with MG132 (6µM) for 2 hours prior to harvesting so to protect ubiquitinated proteins from degradation and then washed twice with ice cold PBS and scrapped into 0.1 ml of denaturing lysis buffer (50mM sodium HEPES, pH 7.5, 100mM sodium chloride, 1mM N-ethylmaleimide, 2% (w/v) SDS, 0.1mM PMSF, 10µg/ml soybean trypsin inhibitor, 10µg/1ml benzamidine, and 2% (w/v) EDTA-free complete protease inhibitor mix). The samples were then incubated at 95°C for 5 min before sonicating for three 10-second pulses, with a 10-second rest phase, at 40% amplitude with a 2mm diameter stepped micro-tip (150µl-1ml). To prevent denaturing the precipitating antibody, the denaturing lysis buffer was diluted with 0.9 ml lysis buffer containing sufficient Triton X-100 and sodium deoxycholate to give final concentrations of 1% (w/v) and 0.5% (w/v) respectively. Insoluble material was removed by centrifugation at 21000g for 5 minutes at 4°C and soluble fractions (~990µl) equalised for protein content volume prior to incubation for overnight at 4°C with rotation with 30µl of 50% slurry (v/v) monoclonal (HA-7) anti-HA agarose beads or 50µl of 50% slurry (v/v) protein G Sepharose plus 4µl (200ug)

anti-PTRF antibody. As negative controls, immunoprecipitation was also performed using either 30µl of 50% (v/v) slurry of pre-conjugated Flag M2 agarose beads or 40µl of 50% (v/v) slurry of protein G Sepharose beads and 4µl of MYPT1. Recovered proteins were isolated following centrifugation at 1000g for 1 minute at 4°C and washed three times with 1ml non-denaturing lysis buffer (50mM sodium HEPES, pH 7.5, 100mM sodium chloride, 1.1% (v/v) Triton X-100, 0.6% (w/v) sodium deoxycholate, 1mM N-ethylmaleimide, 0.1mM PMSF, 10µg/ml soybean trypsin inhibitor, 10µg/ml benzamidine, and 2% (w/v) EDTA-free complete protease inhibitor mix) prior to elution in 40µl of 12% (w/v) SDS sample buffer at 67°C for 30 minutes. Samples were then fractionated by SDS-PAGE and recovery of proteins visualised *via* immunoblotting.

2.2.15 Peptide array

2.2.15.1 CelluSpot synthesis of peptide array and overlay

It is predicted that the SOCS3-substrate interaction and subsequent ubiquitination of the substrate is dependent on the SOCS3-SH2 domain. As such, SOCS3 substrates are expected to be tyrosine-phosphorylated. Known tyrosine-phosphorylated peptides from potential SOCS3 substrates, identified from the proteomics screen (Section 5), were extracted using <http://www.phosphosite.org> (last accessed: 1-10-12). A Peptide array was produced using phosphorylated forms of these peptides (Table 2.3) *via* the CelluSpot™ system.

Peptide arrays were produced by Dr George Baillie (University of Glasgow, Institute of Cardiovascular and Medical Sciences) as described (195). Briefly, using an automated system, cellulose-conjugated peptides are synthesised and spotted onto a coated microscope slide producing a 3-dimensional layer of peptides. This system increases binding capacity as compared with monolayer peptide arrays (Section 2.2.15.2) and improves detection of weak interactions by providing a greater number of peptides in a given area.

Interactions between SOCS3 and tyrosine-phosphorylated peptides were identified by overlaying the peptide array with SOCS3-Flag, in its native state. SOCS3-Flag was detected using a Flag-specific antibody followed by an IR-tagged

secondary antibody. Any interaction between SOCS3 and a peptide was visualised using a LI-COR Odyssey Sa system. Briefly, before overlaying with SOCS3-Flag, the peptide arrays were moistened using TBST (50mM Tris pH 7.5, 150mM NaCl, 0.1% Tween 20) and blocked, to prevent non-specific interactions, in 3ml of TBST containing 5% (w/v) BSA for 4 hours at room temperature. CelluSpot™ peptide arrays are sensitive to mechanical stress and so to address this limitation and to reduce volumes of solutions used, all incubations were performed in 4-well dishes (Thermo-Scientific). Peptide arrays were overlaid with cell lysates (500µg/ml) diluted in a total volume of 2.5ml with TBST containing 0.5% (w/v) BSA and protease inhibitors (10µg/ml benzamidine, 0.1mM PMSF, 10µg/ml soybean trypsin inhibitor, 2% (w/v) EDTA-free complete protease inhibitor cocktail). Following three, ten minute washes in TBST with rocking, the peptide array was incubated with the primary, anti-FLAG (mouse), antibody diluted in TBST containing 1% (w/v) BSA overnight at 4°C with rocking. The peptide arrays were then washed three times for five minutes in TBST before incubating with the secondary, anti-mouse 800-IRDye (donkey) antibody diluted in TBST containing 1% (w/v) BSA for 45 minutes at RT. Due to the sensitivity of IR-tagged antibodies, this incubation period was performed in the dark. The SOCS3-peptide interactions were visualised using a LI-COR Odyssey Sa system. As a control, the same procedure was replicated in parallel using GFP-containing cell lysates.

2.2.15.2 SPOT synthesis of peptide array and overlay

It is predicted that the SOCS3-substrate interaction and subsequent ubiquitination of the substrate is dependent on the SOCS3-SH2 domain. As such, SOCS3 substrates are expected to be tyrosine-phosphorylated. Using peptides from candidate SOCS3 substrates previously found to interact significantly ($p < 0.05$, one-tailed, paired *t*-test) with SOCS3, a peptide array was produced using phosphorylated or non-phosphorylated forms of these peptides (Table 2.4). Candidate SOCS3 substrate peptides were produced by automatic SPOT synthesis on Whatman 50 cellulose membranes by the Baillie laboratory as described (196).

The array was first overlaid with an anti-SOCS3 antibody as a control to assess background before being stripped and overlaid with purified SOCS3 protein. Interactions between SOCS3 and peptides were identified by overlaying the peptide array with purified Trx-polyhis-tagged SOCS3 (Sino Biological Inc.) in its native state. Trx-polyhis-SOCS3 was detected using a SOCS3-specific antibody followed by an IR-tagged secondary antibody. Any interaction between SOCS3 and a peptide was visualised using a LI-COR Odyssey Sa system.

The array was first bathed in pure ethanol before washing in TBST (50mM Tris pH 7.5, 150mM NaCl, 0.1% Tween 20) for 5 minutes and then blocked, to prevent non-specific interactions, in 3ml of TBST containing 5% (w/v) BSA for 4 hours at RT. Blocking and overlaying was performed in sealed bags. The array was washed briefly in TBST before incubating with the primary, anti-SOCS3 antibody diluted in TBST containing 1% (w/v) BSA overnight at 4°C with rocking. The peptide arrays were then washed three times for five minutes in TBST before incubating with the secondary, 680-IRDye antibody diluted in TBST containing 1% (w/v) BSA for 45 minutes at RT. Due to the sensitivity of IR-tagged antibodies, this incubation period was performed in the dark. The SOCS3-peptide interactions were visualised using a LI-COR Odyssey Sa system. The array was then stripped in stripping buffer (Tris-Cl 62mM pH6.8, DTT 20mM, SDS 2% (w/v)) at 70°C for 30 minutes before washing three times for ten minutes in TBST. The array was then bathed in pure ethanol, washed in TBST and blocked as before prior to overlaying O/N with purified Trx-polyhis-tagged SOCS3 (10µg/ml) diluted in a total volume of 2.5ml with TBST containing 0.5% (w/v) BSA and protease inhibitors (10µg/ml benzamidine, 0.1mM PMSF, 10µg/ml soybean trypsin inhibitor, 2% (w/v) EDTA-free complete protease inhibitor cocktail). Following three, ten minute washes in TBST with rocking, the peptide array was incubated with the primary, anti-SOCS3, antibody diluted in TBST containing 1% (w/v) BSA overnight at 4°C with rocking. The peptide arrays were then washed three times for five minutes in TBST before incubating with the secondary, 680-IRDye antibody diluted in TBST containing 1% (w/v) BSA for 45 minutes at RT. Due to the sensitivity of IR-tagged antibodies, this incubation period was performed in the dark. The SOCS3-peptide interactions were visualised using a LI-COR Odyssey Sa system.

Table 2.3: Peptide array of tyrosine-phosphorylated peptide from candidate SOCS3 substrates

Peptide(s) of candidate proteins are listed in tabular form while the layout of peptides spotted in duplicate onto the CelluSpot array are presented below. Controls are highlighted in **bold**.

Protein (Peptide)	Sequence	Peptide	Sequence
1 Eps15L (1)	V-D-P-A-pY-T-G-R-V-G-A	36 Hsc73(1)	L-G-T-T-pY-S-C-V-G-V-F
2 Eps15L (2)	K-Q-G-F-pY-V-A-L-R-L-V	37 Hsc73(2)	T-T-P-S-pY-V-A-F-T-D-T
3 Eps15L (3)	S-L-E-Q-pY-D-Q-V-P-D-G	38 Hsc73(3)	V-Q-V-E-pY-K-G-E-T-K-S
4 Ube1 (1)	D-E-G-L-pY-S-R-Q-L-Y-V	39 Hsc73(4)	T-K-S-F-pY-P-E-E-V-S-S
5 Ube (2)	S-R-Q-L-pY-V-L-G-H-E-A	40 Hsc73 (5)	I-A-E-A-pY-L-G-K-T-V-T
6 Ube1 (3)	R-R-C-V-pY-Y-R-K-P-L-L	41 Tubb5 (1)	K-N-S-S-pY-F-V-E-W-I-P
7 Ube1 (4)	V-L-G-P-pY-T-F-S-I-C-D	42 Tubb5 (2)	P-T-G-T-pY-H-G-D-S-D-L
8 Ube1 (5)	N-F-S-D-pY-I-R-G-G-I-V	43 Tubb5 (3)	N-E-A-L-pY-D-I-C-F-R-T
9 Cavin-1 (1)	K-V-M-I-pY-Q-D-E-V-K-L	44 Usp5 (1)	L-S-G-E-pY-S-K-P-V-P-E
10 Cavin-1 (2)	D-H-V-V-pY-A-R-S-K-T-A	45 Usp5 (2)	E-L-L-E-pY-E-E-K-K-R-Q
11 Sqstm1 (1)	V-C-P-D-pY-D-L-C-S-V-C	46 FAK (1)	A-A-A-pY-L-D-P-N-L-N
12 Sqstm1 (2)	D-T-I-Q-pY-S-K-H-P-P-P	47 FAK (2)	L-N-F-F-pY-Q-Q-V-K-S-D
13 Impdh2	A-P-G-E-pY-F-F-S-D-G-I	48 FAK (3)	V-K-S-D-pY-M-L-E-I-A-D
14 Histone 3.1 (1)	K-P-H-R-pY-R-P-G-T-V-A	49 FAK (3)	K-K-S-N-pY-E-V-L-E-K-D
15 Histone 3.1 (2)	E-I-R-R-pY-Q-K-S-T-E-L	50 FAK (4)	L-I-D-G-pY-C-R-L-V-N-G
16 Histone 3.1 (3)	A-C-E-A-pY-L-V-G-L-F-E	51 FAK (5)	E-T-D-D-pY-A-E-I-I-D-E
17 Abi2 (1)	V-P-N-D-pY-V-P-S-P-T-R	52 FAK (6)	E-E-D-T-pY-T-M-P-S-T-R
18 Abi2 (2)	A-I-Y-D-pY-T-K-D-K-E-D	53 FAK (7)	H-Q-G-I-pY-M-S-P-E-N-P
19 Abi2 (3)	L-F-D-S-pY-T-N-L-E-R-V	54 FAK (8)	G-L-S-R-pY-M-E-D-S-T-Y
20 Abi2 (4)	R-V-A-D-pY-C-E-N-N-Y-I	55 FAK (9)	E-D-S-T-pY-Y-K-A-S-K-G
21 Abi2 (5)	R-H-S-P-pY-R-T-L-E-P-V	56 FAK (10)	D-S-T-Y-pY-K-A-S-K-G-K
22 Abi2 (6)	G-S-L-P-pY-R-R-P-P-S-I	57 FAK (11)	S-R-P-G-pY-P-S-P-R-S-S
23 Abi2 (7)	V-V-A-I-pY-D-Y-T-K-D-K	58 FAK (12)	N-Q-H-I-pY-Q-P-V-G-K-P
24 PsmA6 (1)	D-P-A-G-pY-Y-C-G-F-K-A	59 FAK (13)	P-A-D-S-pY-N-E-G-V-K-L
25 PsmA6 (2)	P-A-G-Y-pY-C-G-F-K-A-T	60 FAK (14)	N-D-K-V-pY-E-N-V-T-G-L
26 PsmA6 (3)	E-G-R-L-pY-Q-V-E-Y-A-F	61 FAK (15)	L-A-Q-Q-pY-V-M-T-S-L-Q
27 Rps3 (1)	D-P-V-N-pY-Y-V-D-T-A-V	62 Krt18 (1)	F-S-T-N-pY-R-S-L-G-S-V
28 Rps3 (2)	E-S-L-R-pY-K-L-L-G-G-L	63 Krt18 (2)	Q-A-P-S-pY-G-A-R-P-V-S
29 Actn4 (1)	M-V-D-pY-H-A-A-N-Q-S	64 Krt18 (3)	A-A-S-V-pY-A-G-A-G-G-S
30 Actn4 (2)	S-M-G-D-pY-M-A-Q-E-D-D	65 Krt18 (4)	R-L-A-S-pY-L-D-R-V-R-S
31 Actn4 (3)	V-S-S-F-pY-H-A-F-S-G-A	66 Krt18 (5)	D-W-S-H-pY-F-K-I-I-E-D
32 Actn (4)	V-A-E-K-pY-L-D-I-P-K-M	67 Krt18 (6)	V-E-A-R-pY-A-L-Q-M-E-Q
33 Actn (5)	E-L-I-E-pY-D-K-L-R-K-D	68 pY759gp130	S-T-V-Q-pY-S-T-V-V-H-S
34 Eps15 (1)	N-F-S-A-pY-P-S-E-E-D-M	69 Y759gp130	S-T-V-Q-Y-S-T-V-V-H-S
35 Eps15 (2)	Q-I-S-T-pY-E-E-E-L-A-K		

Table 2.4: Peptide array of tyrosine-/non-phosphorylated peptides from candidate SOCS3 substrates

Peptides from candidate SOCS3 substrates previously found to interact significantly ($p < 0.05$, one-tailed, paired t -test) were produced by automatic SPOT synthesis on Whatman 50 cellulose membranes. Peptide(s) of candidate proteins are listed in tabular form. Controls are highlighted in **bold**.

Protein (Peptide)	Sequence	Protein (Peptide)	Sequence
1 pY759gp130(+)	S-T-V-Q-pY-S-T-V-V-H-S	26 Hsc73(1)(-)	L-G-T-T-Y-S-C-V-G-V-F
2 pY759gp130(-)	S-T-V-Q-Y-S-T-V-V-H-S	27 Hsc73(2)(+)	T-T-P-S-pY-V-A-F-T-D-T
3 Eps15L (2) (+)	K-Q-G-F-pY-V-A-L-R-L-V	28 Hsc73(2)(-)	T-T-P-S-Y-V-A-F-T-D-T
4 Eps15L (2) (-)	K-Q-G-F-Y-V-A-L-R-L-V	29 Hsc73 (5)(+)	I-A-E-A-pY-L-G-K-T-V-T
5 Ube (2)(+)	S-R-Q-L-pY-V-L-G-H-E-A	30 Hsc73 (5)(-)	I-A-E-A-Y-L-G-K-T-V-T
6 Ube (2)(-)	S-R-Q-L-Y-V-L-G-H-E-A	31 Tubb5 (1)(+)	K-N-S-S-pY-F-V-E-W-I-P
7 Ube1 (4)(+)	V-L-G-P-pY-T-F-S-I-C-D	32 Tubb5 (1)(-)	K-N-S-S-Y-F-V-E-W-I-P
8 Ube1 (4)(-)	V-L-G-P-Y-T-F-S-I-C-D	33 Tubb5 (3)(+)	N-E-A-L-pY-D-I-C-F-R-T
9 Impdh2(+)	A-P-G-E-pY-F-F-S-D-G-I	34 Tubb5 (3)(-)	N-E-A-L-Y-D-I-C-F-R-T
10 Impdh2(-)	A-P-G-E-Y-F-F-S-D-G-I	35 pY759gp130(-)	S-T-V-Q-Y-S-T-V-V-H-S
11 Histone 3.1 (3)(+)	A-C-E-A-pY-L-V-G-L-F-E	36 pY759gp130(+)	S-T-V-Q-pY-S-T-V-V-H-S
12 Histone 3.1 (3)(-)	A-C-E-A-Y-L-V-G-L-F-E	37 FAK (2)(+)	L-N-F-F-pY-Q-Q-V-K-S-D
13 Abi2 (3)(+)	L-F-D-S-pY-T-N-L-E-R-V	38 FAK (2)(-)	L-N-F-F-Y-Q-Q-V-K-S-D
14 Abi2 (3)(-)	L-F-D-S-Y-T-N-L-E-R-V	39 FAK (4)(+)	L-I-D-G-pY-C-R-L-V-N-G
15 Abi2 (4)(+)	R-V-A-D-pY-C-E-N-N-Y-I	40 FAK (4)(-)	L-I-D-G-Y-C-R-L-V-N-G
16 Abi2 (4)(-)	R-V-A-D-Y-C-E-N-N-Y-I	41 FAK (5)(+)	E-T-D-D-pY-A-E-I-I-D-E
17 Psm6 (1)(+)	D-P-A-G-pY-Y-C-G-F-K-A	42 FAK (5)(-)	E-T-D-D-Y-A-E-I-I-D-E
18 Psm6 (1)(-)	D-P-A-G-Y-Y-C-G-F-K-A	43 FAK (8)(+)	G-L-S-R-pY-M-E-D-S-T-Y
19 Psm6 (2)(+)	P-A-G-Y-pY-C-G-F-K-A-T	44 FAK (8)(-)	G-L-S-R-Y-M-E-D-S-T-Y
20 Psm6 (2)(-)	P-A-G-Y-Y-C-G-F-K-A-T	45 FAK (9)(+)	E-D-S-T-pY-Y-K-A-S-K-G
21 Psm6 (3)(+)	E-G-R-L-pY-Q-V-E-Y-A-F	46 FAK (9)(-)	E-D-S-T-Y-Y-K-A-S-K-G
22 Psm6 (3)(-)	E-G-R-L-Y-Q-V-E-Y-A-F	47 Krt18 (5)(+)	D-W-S-H-pY-F-K-I-I-E-D
23 Rps3 (2)(+)	E-S-L-R-pY-K-L-L-G-G-L	48 Krt18 (5)(-)	D-W-S-H-Y-F-K-I-I-E-D
24 Rps3 (2)(-)	E-S-L-R-Y-K-L-L-G-G-L	49 pY759gp130(+)	S-T-V-Q-pY-S-T-V-V-H-S

2.2.16 Substrate degradation assay

The stability of candidate SOCS3 substrates is expected to be reduced in the presence of SOCS3. Inhibition of protein synthesis will enable the time-dependent degradation of SOCS3 targets to be detected. Emetine, an irreversible inhibitor of protein synthesis, which acts by binding to and blocking the translocation of the 40S ribosomal unit (197,198), will be used for this purpose.

HEK293 cells were seeded at 36×10^5 cells in poly-D-lysine-treated 10cm dishes for ~80% confluency the following day. Cells were then transfected as described (Section 2.2.12) with cavin-1 (24 μ g) cDNA plasmid. After 24 hours cells were split equally into 6 well plates and allowed to proliferate for a further 24 hours. Cells were then treated with emetine (100 μ M) with or without MG132 (6 μ M) or chloroquine (100mM) for 0-10 hours prior to harvesting using the co-immunoprecipitation protocol (section 2.2.5.4). Samples were then equalised for protein concentration prior to fractionation by SDS-PAGE and degradation assessed *via* immunoblotting.

2.3 External services

Biomers, DM:

www.biomers.net Primer synthesis

DNaseq, UK:

www.dnaseq.co.uk DNA sequencing

3.0 Characterisation of experimental cell lines

3.1 Introduction

Inflammation is a protective yet potentially damaging process that requires tight regulation. Dysregulation can lead to several disorders that are initiated by a state of low-grade chronic inflammation including atherosclerosis and rheumatoid arthritis (26,130). The concomitant occurrence of inflammatory diseases with obesity is thought to result from the chronically elevated secretion of adipocytokines such as IL6 from adipose tissue (5,199).

IL6 exerts its effect *via* the activation of the JAK/STAT and ERK pathways *via* its cognate receptor, gp130 (Figure 1.2). Cytokine-receptor ligation initiates STAT-driven gene transcription of several IL6-dependent genes including SOCS3. SOCS3, which is present at low basal levels, is rapidly induced following IL6 stimulation and negatively regulates IL6 signalling *via* several mechanisms. STAT1/3 activation is prevented by the direct binding of SOCS3 to the catalytic domain of JAKs *via* the N-terminal KIR, SH2, and ESS domains (123). ERK activation is dependent on the activation of pY⁷⁵⁹-gp130-bound SHP2. As such, ERK signalling is inhibited by competition from SOCS3 that also binds pY⁷⁵⁹ (55,200). SOCS1 similarly regulates JAK/STAT signalling in response to IFN γ and has also been shown to direct proteasomal degradation of tyrosine-phosphorylated JAK2 (87). JAK2 is mono-ubiquitinated in unstimulated cells but becomes polyubiquitinated and degraded following tyrosine phosphorylation (Y¹⁰⁰⁷) and subsequent association with SOCS1 (87). It is also possible that SOCS3 might similarly regulate JAK1 (73) but this has yet to be demonstrated directly. The study found that in response to LIF, pJAK1 accumulated to greater levels in SOCS3 SOCS-box knockout (SOCS3 ^{Δ SB/ Δ SB}) embryonic stem cells compared to WT. Turnover of JAK1 was not assessed.

Similar to SOCS1, SOCS3 regulates the polyubiquitin-dependent proteasomal degradation of signalling intermediates by acting as the specificity factor within an ECS-type E3 ubiquitin ligase (86). SOCS3 has been shown to regulate the ubiquitin-dependent proteasomal degradation of focal adhesion kinase (FAK)-1 (10), insulin receptor substrate (IRS)-1/2 (9), sialic-acid-binding immunoglobulin-

like lectin (SIGLEC)-7 (12), and CD33 (11). Furthermore, SOCS3 has also been shown to regulate lysosomal routing of the G-CSF receptor *via* ubiquitination of the juxtamembrane residue K⁶³² (8,201). However, the full spectrum of SOCS3-dependently ubiquitinated targets is currently unknown.

SOCS3 is also induced by elevated cAMP levels mediated by EPAC (70) and PKA-independent ERK activation (118). SOCS3 is currently one of two cAMP-inducible E3 ubiquitin ligases to be identified (202). It is hypothesised that since SOCS3 is inducible *via* several routes including the JAK/STAT pathway (55,55,70), toll-like receptors (51), and cAMP(70), the pool of SOCS3-ubiquitinated targets may vary depending on the route of SOCS3 induction. Cyclic AMP has long been recognised an important inhibitor of inflammatory signalling (115). Thus, uncovering new targets of cAMP/EPAC1's effects might provide potential therapeutic approaches for treating multiple inflammatory disorders.

The aim of this study was to compare ubiquitinomes from WT and SOCS3^{-/-}MEFs. By this approach, it should be possible to identify substrates ubiquitinated by SOCS3 following its cAMP-dependent induction in WT but not SOCS3^{-/-} MEFs. To capture the ubiquitinome, an N-terminally-(His)₆+biotin-tagged form of ubiquitin (HBUb) (168,175,203) was expressed in both cell lines. This tag enables tandem affinity purification of the ubiquitinome under highly denaturing conditions (8M urea). This environment will contribute to the protection of the ubiquitinome from DUBs, which cleave polyubiquitin chains to monomers for recycling. Furthermore, the strong interaction between the HBUb tag and streptavidin beads ($K_D=10^{-15}M$) allows stringent wash conditions to produce a sample minimally contaminated by non-specifically bound proteins. Such characteristics make the HBUb tag ideal for analysis of the ubiquitinome *via* mass spectrometry.

3.2 Experimental cell lines and strategy

MEFs were chosen as an experimental model due to their tractability and robustness with regards to retroviral transduction. Furthermore, their longevity and ability to grow quickly in large numbers supports their use for this study. Moreover, although not physiologically relevant, it was thought that these cells would allow identification of specific targets of SOCS3 with minimal effort.

Isolation of the ubiquitinome was facilitated by HBUb-tagged ubiquitin. Cell lines that stably express the HBUb transgene (WT HBUb, SOCS3^{-/-} HBUb) were produced *via* retroviral transduction of a HBUb-expressing plasmid (168) (donated by Prof. Peter Kaiser, University of California at Irvine). A control puromycin resistant cell line that stably expresses the puromycin-resistance plasmid vector pBabe-puro was also produced *via* the same method (Section 2.2.2).

To evaluate the suitability of control MEFs (WT and SOCS3^{-/-}) and HBUb-expressing MEFs (WT HBUb and SOCS3^{-/-} HBUb) as experimental models, the cells were fully characterised. Control and experimental MEFs need to fulfil several key requirements before qualifying as suitable experimental models. First, to prevent a toxic reaction to transgene expression, HBUb expression was assessed by its effect on cell viability (Section 3.3.1). Second, for accurate relative quantification, reduced data processing, and simplified data analysis following MS analysis, the HBUb transgene should be expressed at equivalent levels in WT HBUb and SOCS3^{-/-} HBUb MEFs. Furthermore, it is expected that, for normal cell function, endogenous ubiquitin is also expressed at equivalent levels in all cell lines (Section 3.3.2). Third, HBUb, which is co-expressed with endogenous ubiquitin, should not impact K48-linked polyubiquitination or formation of other well-characterised polyubiquitin chains such as K63-linked chains. To do so would potentially generate aberrant results. Therefore, HBUb transgene expression should not interfere with common ubiquitin-dependent signalling pathways such as the NFκB pathway (Section 3.3.3). Fourth, SOCS3 induction should not be affected by transgene expression thus WT and WT HBUb MEFs should express SOCS3 at equivalent levels while SOCS3^{-/-} HBUb MEFs and SOCS3^{-/-} control MEFs should not express SOCS3 (Section 3.3.4).

In addition, the sensitivity of detection of ubiquitylated, tyrosine-phosphorylated SOCS3 substrates will be enhanced *via* the used of the protein tyrosine phosphatase inhibitors sodium orthovanadate and hydrogen peroxide. Since these chemicals can be toxic, optimum concentration and incubation periods were assessed (Section 3.3.5).

In summary, I aimed to examine the possibility of potential adverse effects as a consequence of permanent or temporary cellular alterations i.e. SOCS3 knockout, transgene expression, or treatments. Presented here are the strategy, procedure, and results of those characterisation experiments.

3.3 Results and discussion

3.3.1 HBUb expression does not impact cell viability

The impact of HBUb expression on cell viability was assessed *via* an 3-(4,5-dimethylthiazol-2-yl)-2,5-diphenyltetrazolium bromide (MTT) assay (Section 2.2.4) (191). Cell density is estimated from the reduction of MTT to formazan that has a maximum absorbance at 590nm. MTT reduction can only occur in the mitochondria of live cells and so absorbance is directly proportional to live cell density and thus cell proliferation. The concentration of MTT (100 μ M) had previously been optimised by colleagues. Proliferation of each cell line was compared to controls consisting of a dish containing no cells (blank) and cells pre-killed with 50% (v/v) DMSO for one hour. Optimum DMSO incubation time had been previously assessed *via* a time course (data not shown) where cells were treated with 50% DMSO from 0 to 4 hours. The effectiveness of DMSO to promote cell death was confirmed by viewing rounded-up cells under a light microscope and *via* an MTT assay (results not shown).

The MTT assay was performed as described (Section 2.2.4). No significant difference was observed ($p>0.05$, t -test) in proliferation between the WT and WT HBUb (Figure 3.1) or between SOCS3^{-/-} and SOCS3^{-/-} HBUb MEFs. Furthermore, there was no significant difference ($p>0.05$, t -test) in proliferation between WT HBUb and SOCS3^{-/-} HBUb MEFs (Figure 3.1). These data suggested that overexpression of the HBUb transgene and/or SOCS3 knockout had no significant negative effect on cell viability.

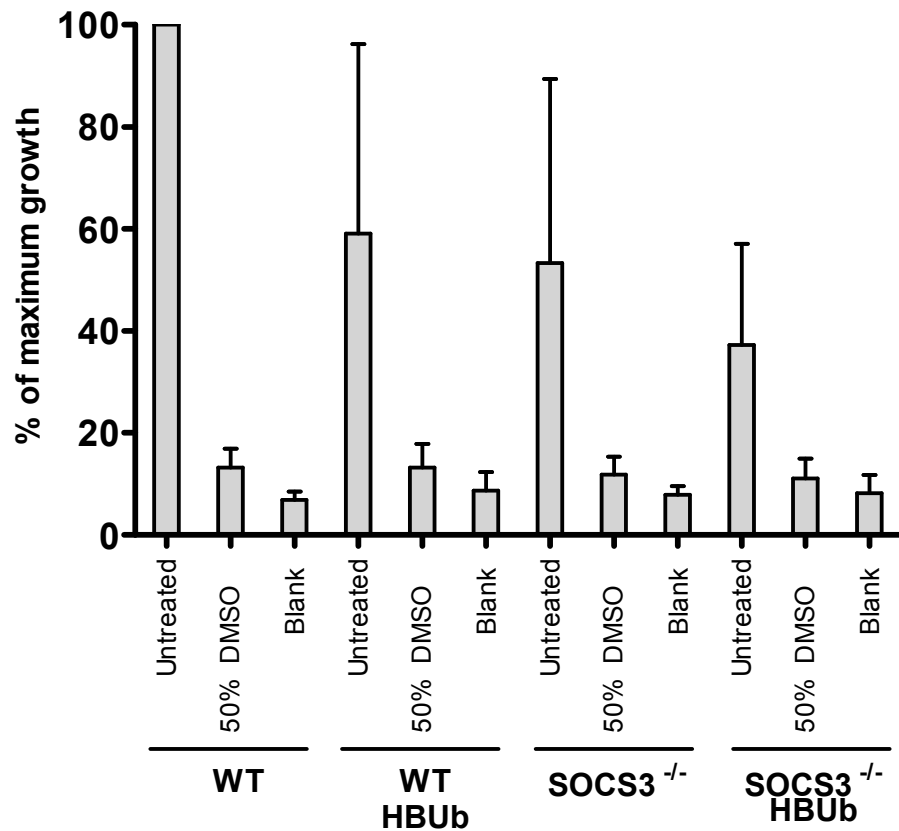


Figure 3.1: Impact of HBUb expression on cell viability

Cells were seeded at a density of 5×10^4 cells/well in 12 well plates and allowed to proliferate. After 24 hours incubation at 37°C, the media was refreshed before MTT (3-(4,5-Dimethylthiazol-2-yl)-2,5-diphenyltetrazolium bromide) reagent (100µM) was directly added to cells followed by a further incubation period of 3 hours. Negative controls included a dish containing no cells (blank) and cells pre-killed with 50% (v/v) DMSO for one hour. Media was removed and cells lysed with 500µl of DMSO which also solubilises the formazan crystals. Proliferation was assessed by measuring the absorbance of 200µl aliquots of DMSO-solubilised formazan crystals at 590nm. An averaged result from three experiments is shown. Results are presented as mean values \pm SEM for $n=3$ experiments.

3.3.2 HBUb transgene and endogenous ubiquitin are expressed at comparable levels in control and experimental cell lines

Isolation of the ubiquitinome is aided by HB-tagged ubiquitin which enables purification under highly denaturing conditions (175). Under this condition, the recovered sample will be minimally contaminated by ubiquitin binding proteins and non-specifically bead-bound proteins. Importantly, the ubiquitinome will be preserved due to the inactivation of DUBs. For accurate relative quantification of HBUb-modified proteins and to reduce the likelihood of producing false-positives in subsequent SILAC analysis, cell lines should express the HBUb transgene at equivalent levels. This requirement is not completely essential since variations in expression can be taken into account and the data sets manipulated accordingly. However, data manipulation might increase data processing time and potentially add further error into the data set if performed incorrectly. Therefore, to ensure comparable expression levels, several WT and *SOCS3*^{-/-} HBUb-expressing clones were compared. Furthermore, all cell lines should express endogenous ubiquitin at equivalent levels.

Cells grown to confluency in 10cm dishes were treated with 6 μ M MG132 for 2 hours to preserve the ubiquitinome from proteasomal degradation. Cell lysates were prepared and equalised prior to fractionation by SDS-PAGE and expression levels of ubiquitin and HBUb assessed *via* immunoblotting using either an anti-ubiquitin antibody for detection of total ubiquitin levels or an anti-polyhistidine antibody, which detects the hexahistidine domain within the HB-tagged ubiquitin (Figure 3.2). Glyceraldehyde-3-phosphate dehydrogenase (GAPDH), a housekeeping gene, was used as a loading control and detected using an anti-GAPDH antibody.

The ubiquitinome is the subset of the proteome that is mono-, multi-, or polyubiquitinated with chains of various lengths. As such, a range of mass shifts would be expected for each ubiquitinated protein generating a smear pattern following visualisation *via* immunoblotting (175). Consistent with this, smears were detected along with high molecular weight ubiquitin signals suggesting a functional ubiquitin and HBUb tag (Figure 3.2). Ubiquitin expression was found

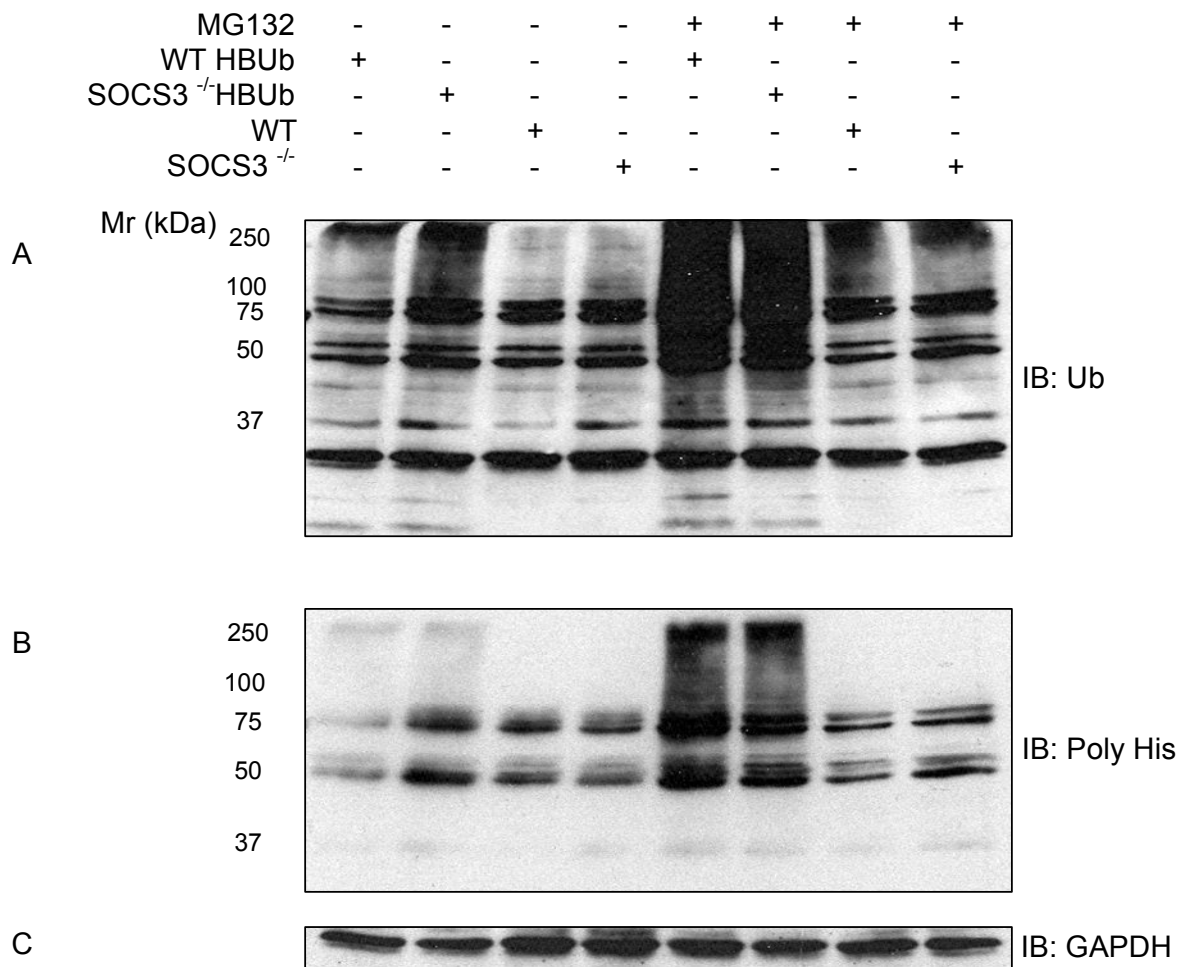


Figure 3.2: HBUb transgene and endogenous ubiquitin are expressed at comparable levels in control and experimental cell lines

WT HBUb, SOCS3^{-/-} HBUb, WT, and SOCS3^{-/-} MEFs were grown to confluency after which the media was refreshed before treating with vehicle (DMSO, 1:1000) or MG132 (6 μ M), to enrich for ubiquitinated proteins, for 2 hours prior to harvesting. Soluble protein lysates were equalised to 40 μ g before SDS-PAGE fractionation. Expression of total ubiquitin or HBUb was assessed by immunoblotting with specific anti-Ub (Panel A) or anti-polyhistidine antibody (Panel B) respectively. GAPDH antibody was used as a loading control (Panel C).

to be comparable between WT and SOCS3^{-/-} MEFs and also between WT HBUb and SOCS3^{-/-} HBUb MEFs (Figure 3.2, panel A). Only the experimental cell lines expressed HB-tagged ubiquitin and did so at approximately equivalent levels (Figure 3.2, panel B). Detection of ubiquitin and HBUb was enhanced following MG132 treatment suggesting that both moieties were being incorporated into K48-linked polyubiquitin chains and contributing to ubiquitin-dependent proteasomal degradation. Furthermore, GAPDH was detected at equivalent levels for all samples thereby confirming equivalent gel loading (Figure 3.2, panel C). This data suggests that it will be possible to make direct comparisons between the ubiquitinomes isolated from experimental (WT HBUb and SOCS3^{-/-} HBUb) or control lines (WT and SOCS3^{-/-} MEFs) enabling accurate relative quantification without the need for additional data manipulation.

3.3.3 HBUb transgene expression does not impair polyubiquitin chain formation and function

Ubiquitin is a 76 amino-acid protein, which is thought to be involved in the regulation of most cellular events. Covalent attachment of mono-, multi-, or polyubiquitin chains provides a diverse set of signals from which signalling pathways can be fine-tuned. Polyubiquitination involves the formation of an isopeptide bond between the ϵ -amino-group-lysine on target proteins and the C-terminal glycine residue (G⁷⁶) of ubiquitin by the individual actions of E1 activating, E2 conjugating, and E3 ligase proteins (Section 1.4, figure 1.6). Ubiquitin has seven lysine residues K6, K11, K27, K29, K33, K48, and K63 (98) and all can be used to form polyubiquitin chains although most is known about the K48- and K63-linked moieties. K48-linked chains are the most understood and direct proteasomal degradation (98) whereas K63-linked chains can function as scaffolds and activators of ubiquitin-interacting domain-bound complexes (16). However, recent studies suggest that all non-K63-polyubiquitin chains might have a role in targeting proteins to the proteasome (138).

While the HBUb tag has been used several times to successfully isolate polyubiquitinated proteins (168,175,203), it is approximately 18kDa, which is a substantial increase in size over endogenous ubiquitin (8kDa). As such, it may potentially disrupt certain ubiquitin-mediated events. The N-terminal attachment of the HB tag to ubiquitin suggests that mono-/multi-ubiquitination

would be unaffected although the tag could still disrupt the interaction with the components of the ubiquitin cascade or ubiquitin binding proteins. Polyubiquitination could be similarly affected. Furthermore, co-expression of the HBUb transgene and endogenous ubiquitin would be expected to produce polyubiquitin chains incorporating both moieties. As such, steric hindrance, as a consequence of the HB tag, could potentially disrupt the activation/association of ubiquitin binding proteins.

SOCS3 is known to regulate proteasomal degradation of several substrates (9-12) and so detection of these SOCS3 targets depends on their K48-linked polyubiquitination. However, due to the potentially multifunctional role of SOCS3 (8), the involvement of other forms of ubiquitin conjugation cannot be completely ruled-out. As such, expression of the HBUb transgene should not impact K48-linked polyubiquitination or other forms of ubiquitin conjugation.

The NF κ B pathway relies on both K48- and K63-linked polyubiquitin chains for full activation (16) (Section 1.4, figure 1.7) and as such was deemed a suitable model for assessing the impact of HBUb transgene expression on polyubiquitin chain formation and function. In response to pro-inflammatory cytokines (TNF α) or as a result of bacterial infection (LPS), NF κ B-dependent gene transcription is initiated to regulate cell survival and apoptosis (16). Under basal conditions, NF κ B is prevented from entering the nucleus by NF κ B inhibitor α (I κ B α) which binds NF κ B. NF κ B is released by I κ B α following a complex cascade of phosphorylation and ubiquitination eventually leading to the proteasomal degradation of I κ B α and translocation of NF κ B to the nucleus. Different stimulus initiates distinct sequences of events that eventually activate NF κ B, although in each case many ubiquitin mediated events such as protein localisation/activation and proteasomal degradation are common (16). Given the importance of ubiquitin regulated events, disruption by the HBUb tag could impair several signalling pathways resulting in the generation of spurious results. As such, the NF κ B pathway, specifically I κ B α degradation, will be employed to assess the impact of HBUb expression on this well-defined ubiquitin-dependent pathway.

To assess the impact of HBUb transgene expression on the formation of functional polyubiquitin chains, the effects of LPS on I κ B α levels and phosphorylation were investigated. WT, WT HBUb, SOCS3^{-/-}, and SOCS3^{-/-} HBUb MEFs grown to confluency in 6-well plates were treated with 1 μ g/ml of LPS for 0-90 minutes to activate the NF κ B pathway. Cells were then lysed and I κ B α phosphorylation and degradation assessed using phospho-specific anti-I κ B α and specific anti-I κ B α antibodies respectively (Figure 3.3).

Treatment with LPS led to an accumulation of pI κ B α Ser32 that peaked after 15 minutes. Subsequently, I κ B α levels decreased to a minimum level after 30 minutes (Figure 3.3). Consistent with I κ B α being a gene target of NF κ B, total I κ B α was seen to increase after this time. For all cell lines, phosphorylation preceded degradation, which peaked at 15 and 30 minutes respectively. Moreover, the same pattern of shifts in I κ B α phosphorylation and degradation was observed for each cell line over three experiments (Figure 3.4). These results suggest that I κ B α regulation by LPS is fully functional.

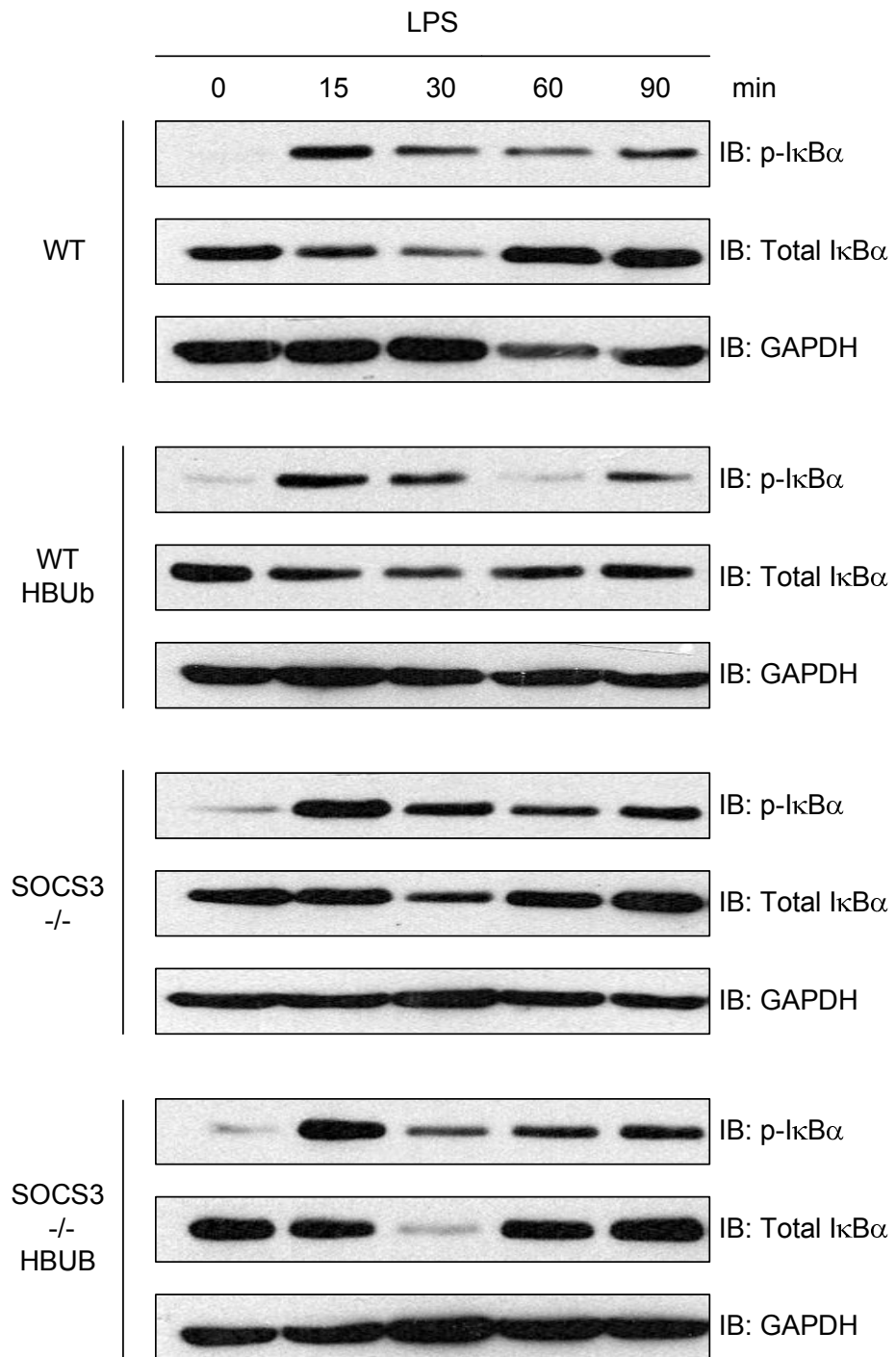


Figure 3.3: The K48- and K63-polyubiquitin-dependent NFκB pathway is not affected by HBUb transgene expression

WT, WT HBUb, SOCS3^{-/-}, and SOCS3^{-/-} HBUb MEFs were grown to confluency in 6-well plates after which the media was refreshed before treating with LPS (1μg/ml) for the indicated time intervals prior to harvesting. Soluble protein lysates were equalised to 40μg before SDS-PAGE fractionation. Phosphorylation and degradation of IκBα was assessed by immunoblotting with specific anti-pIκBα or anti-IκBα antibody respectively. GAPDH was used as a loading control. Results representative of *n*=3 experiments.

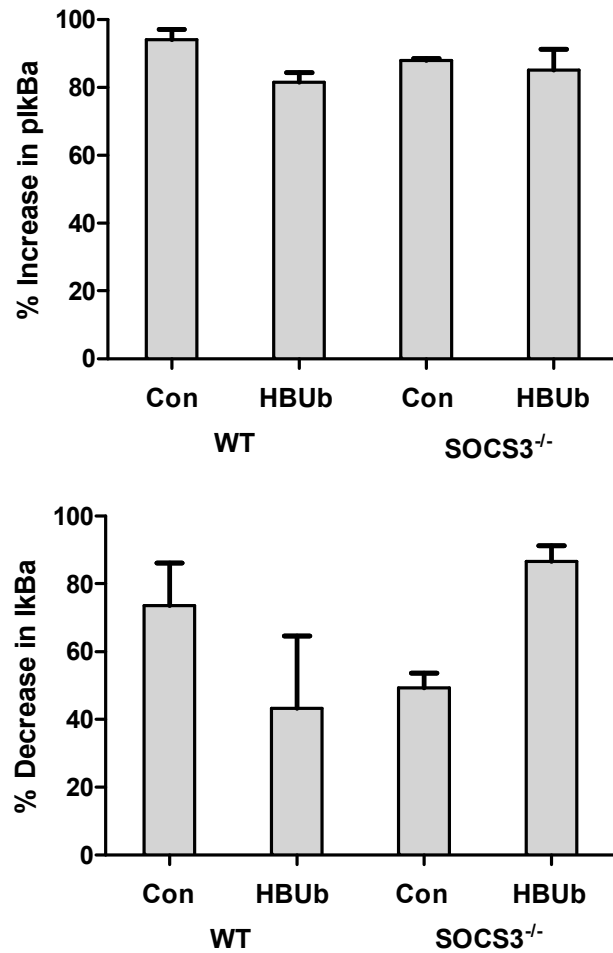


Figure 3.4 LPS-dependent activation of the NFκB pathway results in significant phosphorylation and degradation of IκBa

Basal pIκBa Ser32 or IκBa levels (untreated cells, time = 0) were compared with pIκBa or IκBa levels at a time period corresponding to either maximum phosphorylation (15 minutes) or degradation (30 minutes) respectively. Phosphorylation was measured as a percentage of maximum whereas degradation was measured as a percentage of unstimulated levels. Results are presented as mean values \pm SEM for $n=3$ experiments.

3.3.4 SOCS3 can be induced in WT but not SOCS3^{-/-} MEFs by forskolin, LPS and IL6/IL6R

SOCS3 is present in cells at low basal levels, due to its removal *via* proteasomal degradation, but levels are quickly elevated following its induction. SOCS3 is inducible *via* several different routes including, but not limited to, cytokines (IL1, IL6, LIF, OSM, IFN γ , TNF, EPO, and prolactin), chemo-attractants (IL8, N-formyl-Met-Leu-Phe), bacterial components (LPS, unmethylated CpG DNA), and the intracellular second-messenger cAMP. Since this study is concerned with understanding specific cAMP/EPAC1 effects of SOCS3, forskolin was used as the primary stimulus. *Via* distinct, cAMP-independent mechanisms, the pro-inflammatory cytokine IL6 and the Gram-negative bacteria cell membrane component and endotoxin, LPS, were used as controls because of their availability and ability to strongly induce SOCS3 (70,158). All three stimuli induce SOCS3 through distinct routes; forskolin elevates cAMP *via* direct activation of adenylyl cyclase, while IL6 induces the dimerisation of the receptor gp130 leading to STAT-mediated gene transcription (Section 1.2). LPS induces SOCS3 *via* NF κ B-dependent gene transcription (Section 1.4).

This study relies on cAMP-induced SOCS3 to tag proteins with K48-linked HBUb chains, thus enabling SOCS3-dependently HBUb-modified proteins to be detectable in WT but not SOCS3^{-/-} MEFs. It is therefore important that prior manipulation of the cells e.g. retroviral transformation, should not influence SOCS3 induction. As such, SOCS3 induction should be comparable between both WT and WT HBUb MEFs in response to all stimuli. Conversely, SOCS3^{-/-} and SOCS3^{-/-} HBUb MEFs should not express SOCS3. All cell lines were grown to confluency in 10cm dishes after which the media was refreshed and treated for two hours with forskolin (50 μ M), IL6/IL6R (5ng/ml, 25ng/ml) or LPS (1 μ g/ml) with or without the proteasome inhibitor MG132 (6 μ M) to prevent SOCS3 degradation. Soluble protein lysates were equalised before SDS-PAGE fractionation and immunoblotting.

SOCS3 was observed to be inducible to comparable levels with each stimulus in WT and WT HBUb MEFs (Figure 3.5). Moreover, for each WT cell line, forskolin was observed to be the strongest inducer of SOCS3 followed by IL6 and LPS

(Figure 3.6). Furthermore, consistent with the fact that SOCS3 is regulated *via* proteasomal degradation, SOCS3 could only be detected upon treatment with the proteasome inhibitor MG132. SOCS3 was not inducible in either SOCS3^{-/-} or SOCS3^{-/-} HBUb MEFs following the same treatments as compared with the WT control (Figures 3.5). In conclusion, this data suggests that prior manipulation of cells did not impact three distinct routes of SOCS3 induction in WT or WT HBUb MEFs. Furthermore, MG132 treatment is necessary to maximise SOCS3 accumulation. The use of MG132 will also be necessary to prevent SOCS3-dependent substrate degradation and thus enable isolation of sufficient protein for mass spectromeric analysis. Moreover, since the SOCS3^{-/-} cell lines are unable to express SOCS3, SOCS3-dependent ubiquitination of substrates should only occur in WT HBUb and SOCS3^{-/-} HBUb MEFs.

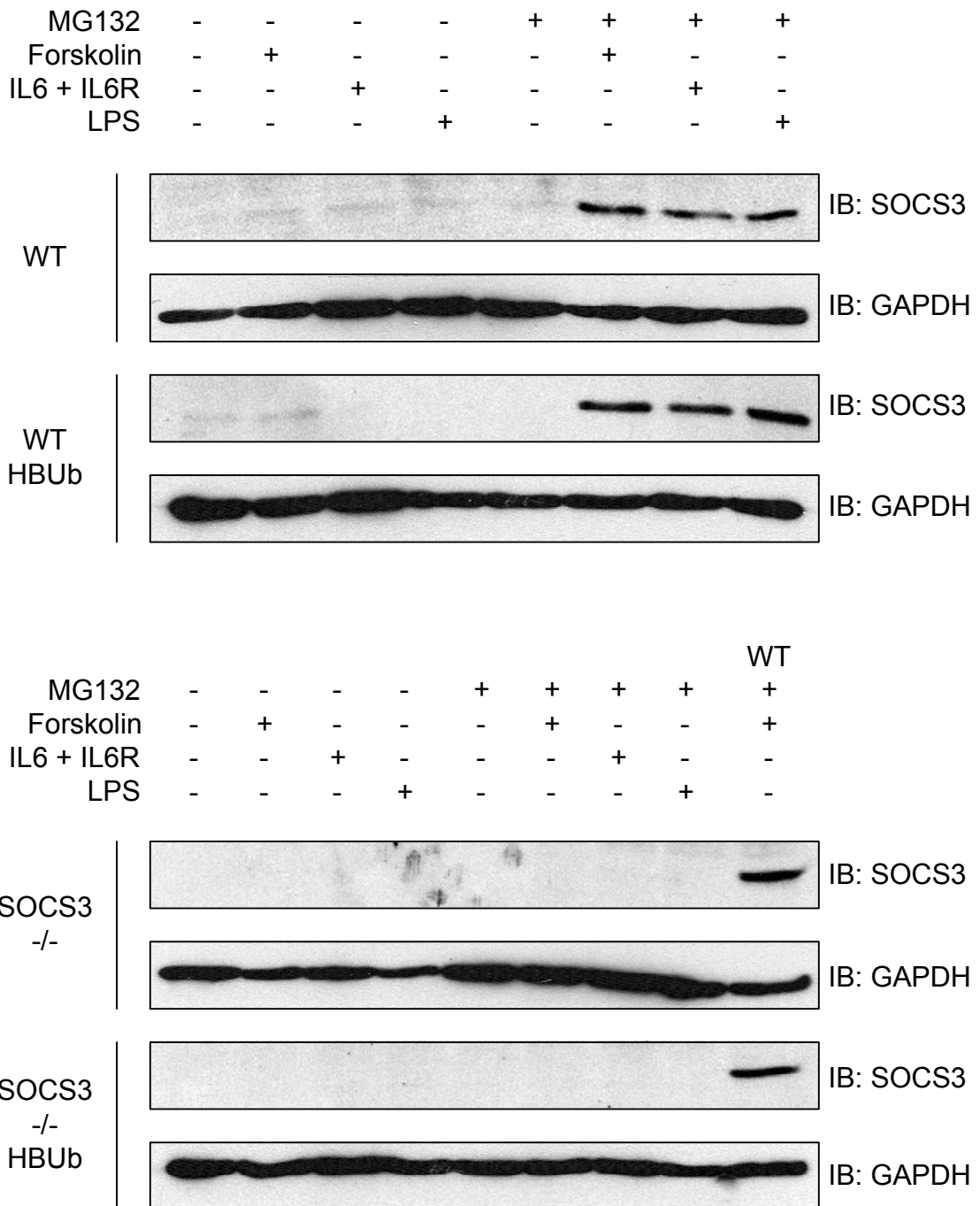


Figure 3.5: SOCS3 is induced to similar levels by forskolin, LPS or IL6/IL6R in WT but not SOCS3^{-/-} MEFs

WT, WT HBUb, SOCS3^{-/-}, and SOCS3^{-/-} HBUb MEFs were grown to confluency before treating with either forskolin (50µM), IL6/IL6R (5ng/ml, 25ng/ml) or LPS (1µg/ml) with or without MG132 (6µM) along with the relevant vehicle control (ethanol, 1:100; DMSO 1:1000) for two hours prior to harvesting. Soluble protein lysates were equalised to 40µg before SDS-PAGE fractionation. SOCS3 induction was assessed by immunoblotting with specific anti-SOCS3 antibody. GAPDH was used as a loading control.

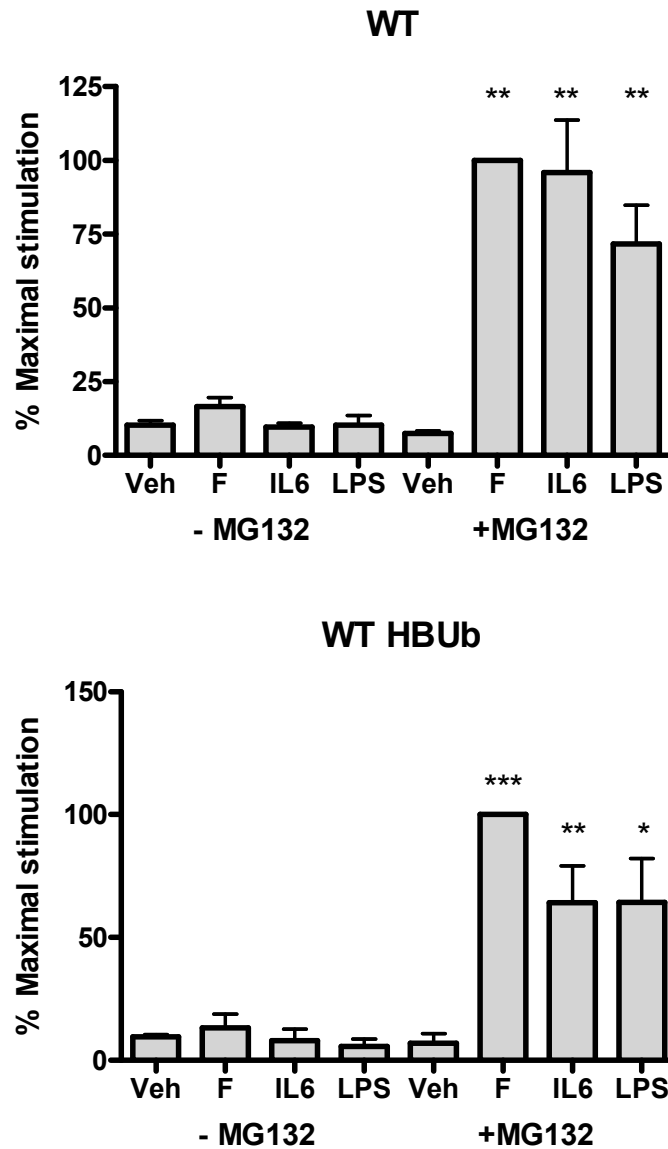


Figure 3.6: SOCS3 is significantly induced to comparable levels by forskolin, LPS or IL6/IL6R in WT but not SOCS3^{-/-} MEFs

WT, WT HBUb, SOCS3^{-/-}, and SOCS3^{-/-} HBUb MEFs were grown to confluency before treating with either forskolin (50µM), IL6/IL6R (5ng/ml, 25ng/ml) or LPS (1µg/ml) with or without MG132 (6µM) along with the relevant vehicle control (Ethanol, 1:100; DMSO 1:1000) for two hours prior to harvesting. Soluble protein lysates were equalised before SDS-PAGE fractionation. SOCS3 induction was assessed by immunoblotting with anti-SOCS3 antibody. GAPDH was used as a loading control. Immunoblots from three independent experiments were analysed using Total Lab v.2009 software. SOCS3 induction was measured as a percentage of maximal stimulation. SOCS3 induction was normalised to GAPDH loading control. Results are presented as mean values ±SEM for *n*=3 experiments. *** = *p*<0.001, ** = *p*<0.01, * = *p*<0.05 with respect to vehicle (One-way ANOVA with Bonferroni post test) .

3.3.5 Impact of hydrogen peroxide and sodium orthovanadate on global tyrosine phosphorylation, K48-specific ubiquitination, and SOCS3 induction.

Cellular tyrosine-phosphorylated proteins, which are expected to include potential SOCS3 substrates, are kept at very low basal levels due to the action of protein tyrosine phosphatases (PTPs) (204). Sodium orthovanadate (Na_3VO_4), a tyrosine phosphatase inhibitor, enables the accumulation of tyrosine-phosphorylated proteins. It does so by acting as a reversible competitive inhibitor that binds to the active site of PTPs *via* its negatively charged tetrahedral Na_3VO_4 (VO_4^{3-}) region. Thus, Na_3VO_4 treatment will potentially enable accumulation of tyrosine-phosphorylated SOCS3 substrates and extend the period of time over which SOCS3 substrates are marked for interaction and subsequent ubiquitination by SOCS3. It is hoped that increasing the abundance of SOCS3-ubiquitinated proteins *via* this route will increase the chance of their detection *via* LC-MS/MS.

It has been demonstrated that in combination with hydrogen peroxide (H_2O_2), the effects of Na_3VO_4 can be amplified 6-10 fold (204) in a cell-specific and time-dependent manner. H_2O_2 increases cellular uptake of vanadate by the oxidation of orthovanadate to its more cell permeable form pervanadate. The H_2O_2 , Na_3VO_4 combination was initially tested on rat hepatoma Fao, HL-60, BC3H-1 myoblasts and myocytes (204), others (205) and more recently with HeLa cells to elucidate the regulation of EGFR by PTPs (206). Its effects on MEFs, specifically its effects on SOCS3 induction and the ubiquitin pathway, are unknown. It was speculated that since H_2O_2 has multiple non-specific effects such as being an insulin mimetic (204) as well as a PTP inhibitor, it might also adversely affect these pathways. Na_3VO_4 in combination with H_2O_2 was therefore tested on MEFs to see if a similar increase in tyrosine-phosphorylated proteins could be achieved without impacting either SOCS3 induction or the ubiquitin pathway. Due to the cellular toxicity of H_2O_2 , concentration and incubation periods were optimised for increased global tyrosine phosphorylation but without loss of cells through apoptosis and disruption to K48-specific ubiquitination.

WT MEFs were grown to confluency before treating and harvesting cell lysates. To assess optimum H_2O_2 concentration, cells were treated with increasing,

indicated concentrations of H₂O₂ for 2 hours at fixed concentrations of Na₃VO₄ (1mM) and MG132 (6μM) (Figure 3.7, panel A). To assess optimum H₂O₂ incubation period, cells were treated with H₂O₂ (0.2mM), Na₃VO₄ (1mM), and MG132 (6μM) for 0 to 120 minutes prior to harvesting (Figure 3.8, panel B). Soluble protein lysates prepared in 8M urea buffer were then equalised and fractionated by SDS-PAGE. Global tyrosine phosphorylation and K48-specific ubiquitination was assessed using specific anti-phosphotyrosine antibody (4G10) and anti-K48-Ub antibodies respectively.

Increasing concentrations of H₂O₂ in combination with Na₃VO₄ had a dramatic yet equivalent effect on global tyrosine phosphorylation compared to vehicle or MG132 alone (Figure 3.7, panel A). Furthermore, a concentration of H₂O₂ greater than 1.5mM resulted in a reduction in K48-specific ubiquitination. Similarly, no difference was detected in global tyrosine phosphorylation over the increasing incubation periods (Figure 3.7, panel B). Reduced K48-specific ubiquitination was also seen following longer incubation periods with H₂O₂. Moreover, H₂O₂ concentrations above 0.2mM and incubation periods longer than 60 minutes resulted in excessive cell death (data not shown). As such, the lower concentration and incubation period of 0.2mM and 30 minutes respectively were used in subsequent experiments. Since MEFs are to be treated for 2 hours with forskolin, MG132, and Na₃VO₄, H₂O₂ treatment was performed for the final 30 minutes of this 2-hour period.

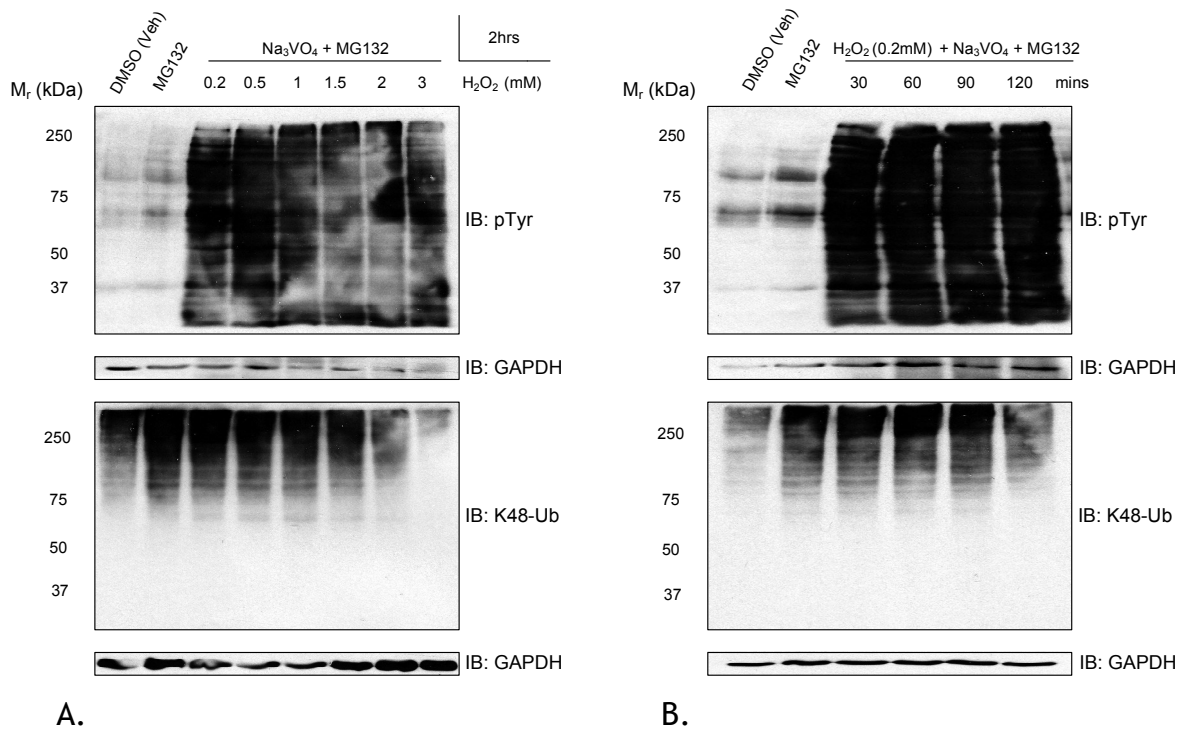


Figure 3.7: Impact of H₂O₂ concentration or treatment period on global tyrosine phosphorylation and K48-specific ubiquitination

WT MEFs were seeded at a density of 5×10^5 cells/10cm dish and grown to confluency before enriching for ubiquitinated proteins with MG132 ($6 \mu\text{M}$) and tyrosine-phosphorylated proteins with sodium orthovanadate (Na_3VO_4) and hydrogen peroxide (H_2O_2) for the indicated times and concentrations prior to harvesting. **A.** Cells were treated for two hours with increasing, indicated concentrations of H_2O_2 with fixed concentrations of Na_3VO_4 (1mM) and MG132 ($6 \mu\text{M}$). **B.** Cells were treated with H_2O_2 (0.2mM), Na_3VO_4 (1mM), and MG132 ($6 \mu\text{M}$) for increasing, indicated periods of time prior to harvesting. Soluble protein lysates prepared in 8M urea buffer were equalised to $50 \mu\text{g}$ and SDS-PAGE fractionated in an equal volume of 12% (w/v) SDS sample buffer. Global tyrosine phosphorylation and K48-specific ubiquitination was assessed using specific anti-K48-Ub antibody and anti-phospho-tyrosine antibody (4G10). GAPDH was used as a loading control.

Using the optimised conditions for H₂O₂, the impact on SOCS3 induction was assessed (Figure 3.8). WT MEFs were grown to confluency before treating with the indicated drug combinations to enrich for ubiquitinated proteins (MG132, 6µM), phosphorylated proteins (Na₃VO₄, 1mM), and to induce SOCS3 (Forskolin, 50µM) for two hours prior to harvesting. The cells were also treated with or without H₂O₂ (0.2mM) for the final 30 minutes of this two-hour period. Soluble protein lysates prepared in 8M urea buffer were equalised and fractionated by SDS-PAGE. Global tyrosine phosphorylation, K48-specific ubiquitination and SOCS3 induction was assessed using specific anti-K48-Ub antibody, anti-phosphotyrosine antibody (4G10), and anti-SOCS3 antibody.

A combination of Na₃VO₄ and H₂O₂ produced a detectable increase in global tyrosine phosphorylation compared to Na₃VO₄ alone (Figure 3.8, panel A, lane 4 vs. lane 5). Consistent with being a proteasome inhibitor and thus protecting ubiquitinated substrates from degradation, an increase in K48-specific ubiquitination (Figure 3.8, panel B, lane 1-2 vs. lanes 3-8) and SOCS3 (Figure 3.8, panel C, lane 1-2 vs. lanes 3) were observed. K48-specific ubiquitination was unaffected by Na₃VO₄ and H₂O₂. Treatment with Na₃VO₄ and H₂O₂ or Na₃VO₄ alone, resulted in a 35% reduction in forskolin-induced SOCS3 expression. Given the significant enrichment of tyrosine-phosphorylated proteins, it was thought that this trade-off was acceptable. These data suggest that neither formation of K48-linked polyubiquitin chains nor the induction of SOCS3 is adversely effected by Na₃VO₄ and H₂O₂ treatment.

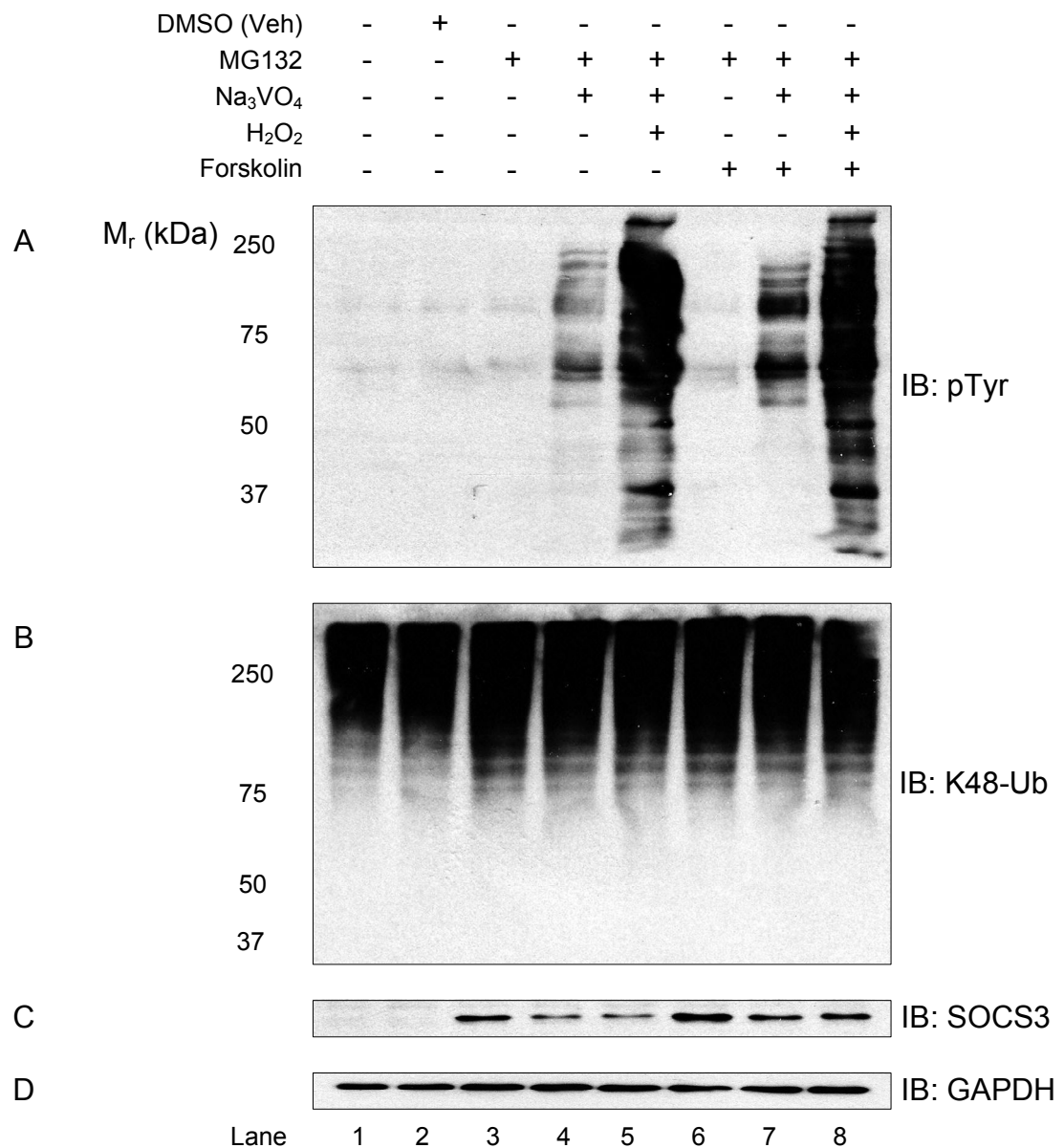


Figure 3.8: Impact of H₂O₂ concentration or treatment period on global tyrosine phosphorylation and K48-specific ubiquitination

WT MEFs were seeded at a density of 5×10^5 cells/10cm dish and grown to confluency before treating with the indicated drug combinations to enrich for ubiquitinated proteins with MG132 ($6 \mu\text{M}$), tyrosine-phosphorylated proteins with sodium orthovanadate (Na_3VO_4) (1mM), and SOCS3 induction with forskolin ($50 \mu\text{M}$) for two-hours prior to harvesting. The cells were also treated with or without hydrogen peroxide (H_2O_2) (0.2mM) for the final 30 minutes. Soluble protein lysates prepared in 8M urea buffer were equalised to $50 \mu\text{g}$ and fractionated by SDS-PAGE. Global tyrosine phosphorylation, K48-specific ubiquitination and SOCS3 induction was assessed using specific anti-K48-Ub antibody, anti-phosphotyrosine antibody (4G10), and anti-SOCS3 antibody. GAPDH was used as a loading control.

3.4 Conclusions

Here, I aimed to characterise the experimental cell lines and assess any adverse effects imparted by the expression of the HBUb transgene, SOCS3 knockout, or planned treatments. It was demonstrated that cell viability was not compromised by expression of the HBUb transgene (Section 3.3.1). HBUb transgene expression was also unable to affect the NF κ B pathway, specifically I κ B α degradation and Ser32 phosphorylation, in response to LPS (Section 3.3.3). The reliance of this pathway on both K48- and K63-linked polyubiquitination (16), suggests that polyubiquitin chain formation and function are unaffected. Ubiquitin has seven lysine residues K6, K11, K27, K29, K33, K48, and K63 (98) and all can be used to form polyubiquitin chains. Although not tested, this result may also be applicable to less understood polyubiquitin chain formats. Furthermore, SOCS3 was induced to comparable levels by three distinct stimuli in WT but not SOCS3^{-/-} cell lines (Section 3.3.4). These data increases confidence in the likelihood that the cell lines are unaffected by retroviral transduction and transgene expression. Moreover, the inability of SOCS3^{-/-} MEFs to respond to three SOCS3-inducing stimuli confirmed that these cells are true SOCS3 knockouts.

Besides transgene expression, treatments with known toxic and off-target effects such as H₂O₂ could adversely affect cell lines. H₂O₂ was shown to impact K48-specific polyubiquitination and induce apoptosis at high concentrations or when used for extended periods of time (Section 3.3.5). Following optimisation experiments a concentration (0.2mM) and incubation period (30 minutes) were identified that resulted in maximum enrichment of tyrosine-phosphorylated proteins without affecting cell viability, K48-specific polyubiquitination, or induction of SOCS3. All other treatments had been previously optimised within the laboratory and all cell lines responded as expected.

To simplify data analysis following mass spectrometric processing of the isolated ubiquitinome, the HBUb transgene was required to be expressed at equivalent levels. This was subsequently demonstrated for WT HBUb and SOCS3^{-/-} MEFs (Section 3.3.2). In addition, endogenous ubiquitin was also expressed at

comparable levels supporting previous data suggesting that cells are unaffected by prior manipulation.

To summarise, where expected, all cells lines respond identically to all treatments. In addition, where not already optimised, treatments were modified for maximum effectiveness. Furthermore, differences as a consequence of genetic manipulation i.e. HBUb-transgene expression and SOCS3 knockout produced predicable results and did not adversely affect key cellular functions. In conclusion, these cells lines are suitable experimental models for this project.

4.0 Experimental strategy

4.1 Introduction

SOCS3 regulates several pathways in part by acting as a specificity factor for an ECS-type E3 ubiquitin ligase complex (9-12). E3 ligases do not recognise a consensus ubiquitylated sequence. Furthermore, SOCS3 does not ubiquitinate all its binding partners (162). Therefore, analysis of SOCS3 protein-protein interactions *via* microarray, immunoprecipitation, or GST pull-down is insufficient for identification of SOCS3-dependently ubiquitinated substrates. Direct analysis of the ubiquitinome is necessary. Differentially SILAC-labelled, tandem affinity purified ubiquitinomes of WT MEFs and SOCS3^{-/-} MEFs each expressing epitope-tagged forms of ubiquitin were compared using mass spectrometry following cAMP-mediated SOCS3 induction (Section 1.5, figure 1.11). Using this approach, proteins modified by SOCS3 with the epitope-tagged form of ubiquitin should be enriched in WT MEFs but not SOCS3^{-/-} MEFs. The details of this methodology was previously discussed (Section 1.5). Here, the aim is to validate and optimise the proposed experimental strategy. The finalised strategy should achieve the following:

- Full SILAC labelling of the proteome.
- Specific isolation of the HBUb-modified ubiquitinome *via* TAP.
- Discrimination of WT HBUb and SOCS3^{-/-} HBUb-isolated ubiquitinomes following SILAC.
- An enriched ubiquitinome of sufficient purity and quantity for subsequent mass spectromeric analysis.

Doing so should allow the strategy to be exploited for the identification of SOCS3-dependently ubiquitinated substrates.

4.2 Optimisation of experimental strategy

This study employs a three-step experimental strategy of SILAC, TAP, and mass spectrometry. Each step was separately assessed and optimised to ensure complete labelling of the proteome, isolation of the ubiquitinome, and capture of sufficient material for downstream MS analysis.

Several groups have successfully applied a similar experimental strategy as proposed here. Thus, each TAP stage was optimised using a published protocol e.g. (168) as a starting point. First, maximum incorporation of SILAC isotopes depends on incubation period and purity of the SILAC media. Complete incorporation has been reported over five cell doublings (163) however, this is dependent on the use of dialysed serum to avoid contamination from the natural isotope. Given that dialysed serum may affect cell proliferation (163), complete isotope incorporation was assessed along with the impact of dialysed serum-supplemented SILAC media on MEFs (Section 4.3.2). Second, volumes of beads for both Ni²⁺ and streptavidin affinity chromatography were optimised for maximum and specific recovery of HBUb-modified proteins with minimal loss over the two-step process (Section 4.3.1.1-3, 4.3.1.6-9). Importantly, because of the interaction with SOCS3, SOCS3-dependently ubiquitinated proteins were expected to be tagged with K48-linked polyubiquitin chains and as such, specific enrichment of this ubiquitin moiety is essential. Furthermore, a potential problem identified by Tagwerker et al (175,203) was failure of streptavidin affinity chromatography due to reduced availability of cellular/active biotin (D-biotin) in HeLa cells. However, supplementation of growth media with biotin prevented the saturation of *in vivo* biotinylation by excessive HBUb-tag expression. The necessity for biotin supplementation in MEFs and its potential impact on prior stages of TAP was therefore examined (Section 4.3.1.4-5). Third, while optimisation of TAP can be performed on a small scale, isolation of sufficient material for MS analysis requires scaling-up of the experimental strategy. As such, the optimum amount of starting material was assessed that enabled enrichment of sufficient HBUb-modified proteins prior to MS. Finally, individually optimised, scaled-up procedures were combined to demonstrate specificity and compatibility with the requirements of mass spectrometric analysis (Section 4.4.0).

4.3 Results and discussion

4.3.1 Optimisation of tandem affinity purification

4.3.1.1 Optimisation of Ni²⁺ bead volume to maximise recovery of HBUb-modified proteins

Tandem affinity purification first employs nickel affinity chromatography to isolate HBUb-modified proteins *via* the interaction of Ni²⁺ with the hexahistidine tag. To estimate the minimum bead volume necessary to maximise recovery of HBUb-modified proteins, a titration of the Ni²⁺-NTA-Sepharose beads was performed.

WT HBUb MEFs were grown to confluency before enriching for ubiquitinated proteins with MG132 (6µM) for two hours prior to harvesting. Soluble protein lysates prepared in 8M urea buffer were equalised to 1mg/ml. Ubiquitinated proteins were isolated with 20, 30, 40, or 50µl of 50% (v/v) Ni²⁺-NTA-Sepharose bead slurry and the recovery of HBUb-modified proteins assessed *via* immunoblotting using anti-ubiquitin and anti-polyhistidine antibodies.

A volume of 30µl of 50% (v/v) Ni²⁺-NTA-Sepharose bead slurry was found to be sufficient for optimal purification of HBUb-modified proteins with no improvement detected upon increase in bead volume (Figure 4.0). However, only a weak signal was obtained using the anti-polyhistidine antibody (Figure 4.0, panel B). While this might suggest that the HBUb-tag was not being incorporated into polyubiquitin chains, it was later attributed to lack of antibody specificity; the use of a more specific streptavidin-HRP antibody produced a similar smear to the total anti-ubiquitin antibody (Figure 4.2, panel B). Specificity of purification is highlighted by the absence of GAPDH in the eluate. GAPDH (Figure 4.0, panel C), which has not been reported to be ubiquitinated (207), was present in lysates and subsequently lost in the flow-through and wash stages.

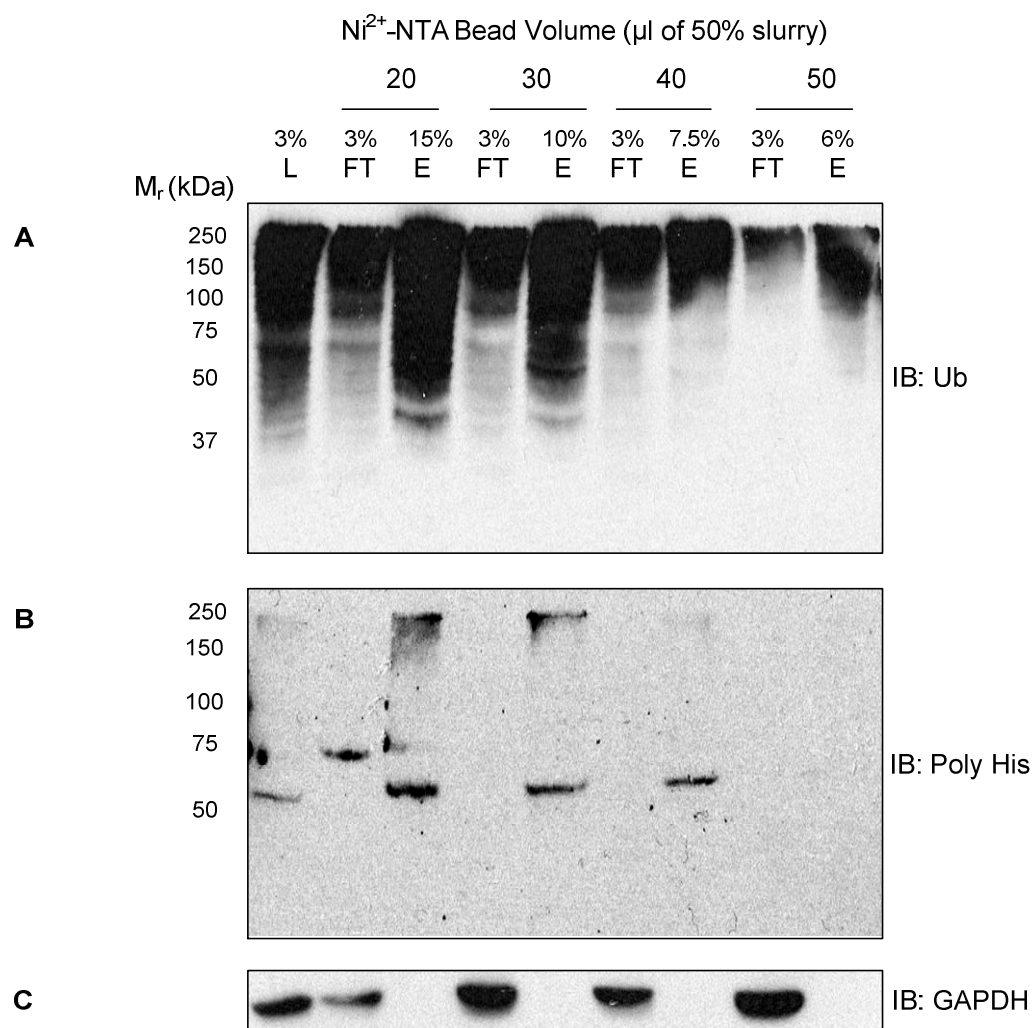


Figure 4.0: Optimisation of Ni²⁺ bead volume to maximise recovery of HBUb-modified proteins

WT HBUb MEFs were grown to confluency before enriching for ubiquitinated proteins with MG132 (6μM) for two hours prior to harvesting. Soluble protein lysates prepared in 8M urea buffer were equalised to 1mg/ml before nickel affinity chromatography using the indicated volumes of 50% (v/v) slurry of Ni²⁺-NTA-Sepharose beads. Purified HBUb-modified proteins were fractionated by SDS-PAGE using the indicated percentages of lysate/input (L), flow-through (FT), and eluate (E). Recovery of HBUb-modified proteins was assessed by immunoblotting with anti-ubiquitin (panel A) and anti-polyhistidine antibody (Panel B). GAPDH was used as a loading control (Panel C).

4.3.1.2 Biotin supplementation is essential for detection of HBUb-modified proteins and does not impact Ni²⁺ affinity chromatography.

The HBUb-tag has a 75 amino acid biotinylation signal peptide (BIO) which can be covalently linked *via* Lys41 to the carboxyl group of biotin by endogenous biotin ligases (175). Tagwerker et al (175,203) reported a failure of streptavidin affinity chromatography due to reduced availability of cellular biotin in HeLa cells following excessive HBUb expression. This problem was resolved following supplementation of growth media with biotin (1 μ M). D-biotin, the active isomer, is an essential co-factor for several carboxylases involved in fatty acid synthesis as well as amino acid and energy metabolism (208). Tagwerker et al reported no impact on cell viability and likewise, HBUb expression did not affect cell viability in this study (Section 3.3.1). As such, the effect of biotin supplementation on cell viability was not pursued. The necessity for biotin supplementation for the biotinylation, isolation, and detection of HBUb-modified proteins was assessed *via* a biotin titration experiment.

WT HBUb MEFs were grown to confluency in media supplemented with biotin (0, 0.25, 0.5, 1, and 2 μ M) before enriching for ubiquitinated proteins with MG132 (6 μ M) for two hours prior to harvesting cells. HBUb-modified proteins were then isolated using 30 μ l of 50% (v/v) Ni²⁺-NTA-Sepharose bead slurry and biotinylation assessed by probing blots with streptavidin-HRP.

While equivalent levels of ubiquitinated proteins were detected in all lysates (Figure 4.1, panel A), significant levels of biotinylated proteins could only be detected in biotin-supplemented lysates (Figure 4.1, panel B, lane 1 vs. lanes 2-5). This confirms that biotin supplementation is essential for detection and thus biotin-dependent capture of HBUb-modified proteins. Furthermore, increasing the biotin concentration did not improve the detection of biotinylated proteins. Given that no optimum concentration could be identified, the same biotin concentration (1 μ M) as suggested by Tagwerker et al (175) was used throughout.

To ensure Ni²⁺ affinity chromatography was unaffected by biotin supplementation, using optimised conditions, Ni²⁺ affinity chromatography was repeated in the presence or absence of biotin. While ubiquitinated/HBUb-

modified proteins were eluted in each case (Figure 4.2, panel A), biotinylated proteins could only be detected in the presence of biotin (Figure 4.2, panel B). Variations in the eluate of ubiquitinated proteins (Figure 4.2, panel A) are assumed to be a consequence of inaccurate preparation of initial protein lysates. This is supported by levels of the GAPDH loading control. As before, the specificity of purification was highlighted by the absence of GAPDH in the eluate. This data suggests that biotinylation does not negatively affect Ni²⁺ affinity chromatography and that biotin supplementation will be essential for streptavidin affinity chromatography.

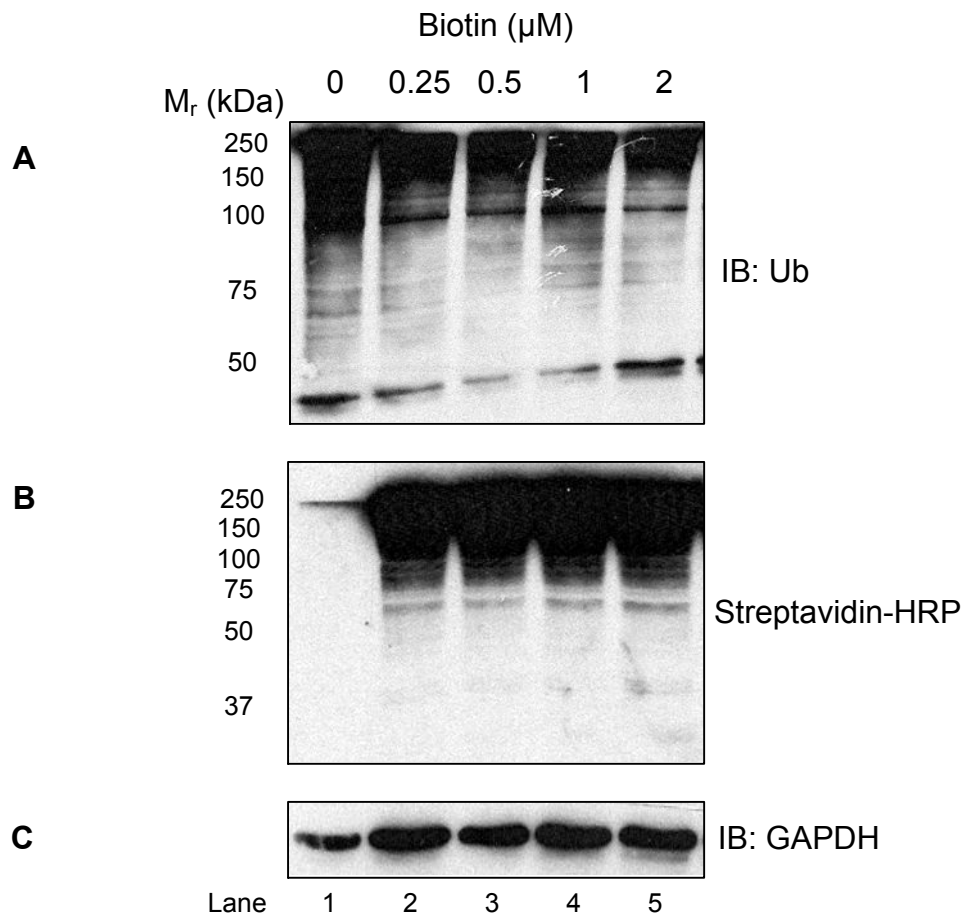


Figure 4.1: Biotin supplementation is essential for biotin-dependent detection of HBUb-modified proteins

WT HBUb MEFs were grown to confluency in biotin-supplemented media of the indicated concentrations before enriching for ubiquitinated proteins with MG132 ($6\mu\text{M}$) for two hours prior to harvesting in an 8M urea buffer. Soluble protein lysates were fractionation by SDS-PAGE and the abundance of ubiquitinated and HBUb-modified proteins assessed by immunoblotting with anti-ubiquitin antibody (Panel A) and streptavidin-HRP respectively (Panel B). GAPDH was used as a loading control (Panel C).

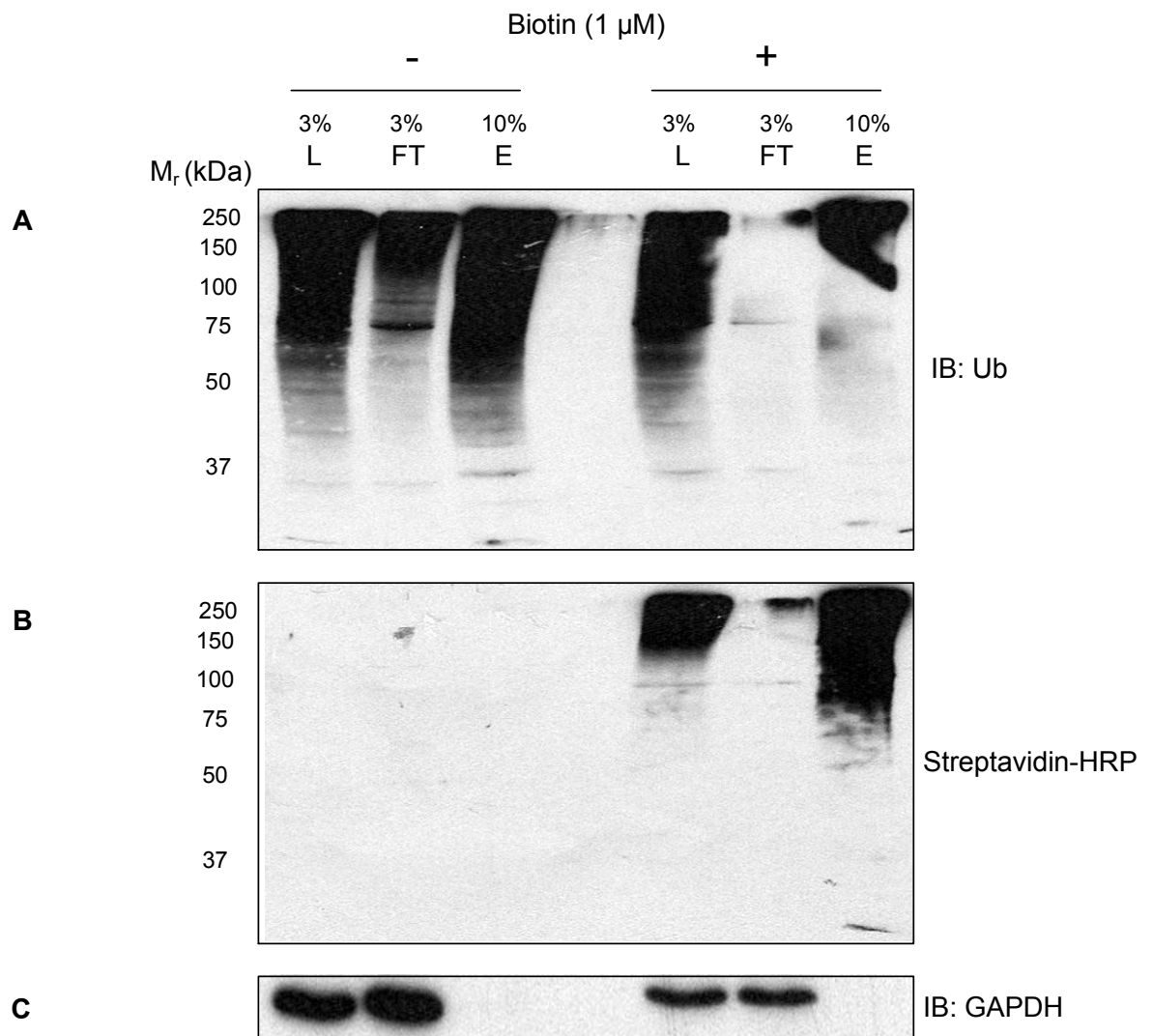


Figure 4.2: Biotin supplementation does not impact nickel affinity chromatography

WT HBUb MEFs were grown to confluency in biotin-supplemented media (1 μ M) before enriching for ubiquitinated proteins with MG132 (6 μ M) for two hours prior to harvesting. Soluble protein lysates prepared in 8M urea buffer were equalised to 1mg/ml before nickel affinity chromatography using 30 μ l of 50% (v/v) slurry of Ni²⁺-NTA-Sepharose beads. Recovered HBUb-modified proteins were fractionated by SDS-PAGE using indicated percentages of lysate/input (L), flow-through (FT), and eluate (E). Recovery of biotinylated, HBUb-modified proteins was assessed by immunoblotting using anti-ubiquitin antibody (Panel A) and streptavidin-HRP (Panel B). GAPDH was used as a loading control (Panel C).

4.3.1.3 Nickel affinity chromatography specifically recovers HBUb-modified proteins

Nickel affinity chromatography relies on the strong (μM) interaction between Ni^{2+} and the hexahistidine tag. Given that this epitope is uncommon in nature, specific recovery HBUb-modified protein is expected. As such, HBUb-modified proteins should only be recovered from WT HBUb and $\text{SOCS3}^{-/-}$ HBUb MEFs but not WT or $\text{SOCS3}^{-/-}$ MEFs. Furthermore, loss of HBUb-modified proteins should be minimised over several wash stages.

To evaluate binding and loss of target protein, Ni^{2+} affinity chromatography was repeated as in section 4.3.1.2 with the inclusion of samples taken from all pre-elution wash steps. Following incubation with Ni^{2+} -NTA-Sepharose beads, there was minimal loss of HBUb-modified protein detected in flow-through and wash stages (Figure 4.3, panel B). This suggests that the Ni^{2+} beads were saturated with HBUb-modified proteins and that the Ni^{2+} -hexahistidine interaction was not disrupted by washing. Interestingly, a large amount of ubiquitinated protein was lost in the flow-through (Figure 4.3, panel A). This suggests that the HBUb-tag is not being completely incorporated into polyubiquitin chains i.e. incomplete labelling of the ubiquitinome. This result might be a consequence of preferential incorporation of WT ubiquitin or reduced availability of the HBUb tag. Given that WT HBUb and $\text{SOCS3}^{-/-}$ HBUb MEFs should express and incorporate the HBUb-tag similarly, this result should have minimal impact.

To evaluate specific recovery of HBUb-modified proteins, Ni^{2+} affinity chromatography was performed using both experimental and control MEFs. While HBUb-modified proteins were isolated from WT HBUb and $\text{SOCS3}^{-/-}$ HBUb MEFs, no HBUb-modified proteins were recovered from WT or $\text{SOCS3}^{-/-}$ MEFs (Figure 4.4, panel B/E). WT HBUb and $\text{SOCS3}^{-/-}$ HBUb MEFs were not assessed for equal expression of the HBUb tag prior to this experiment. As such, the difference in isolation of HBUb-modified proteins is expected to be a consequence of a variation in HBUb expression. Furthermore, a similar loss of ubiquitinated proteins was detected (Figure 4.4, panel A/D, flow-through (FT)) as discussed above while only minimal loss of HBUb-modified protein was detected (Figure

4.4, panel B/E, flow-through (FT)). These results suggest that nickel affinity chromatography is specific for the recovery of HBUb-modified proteins.

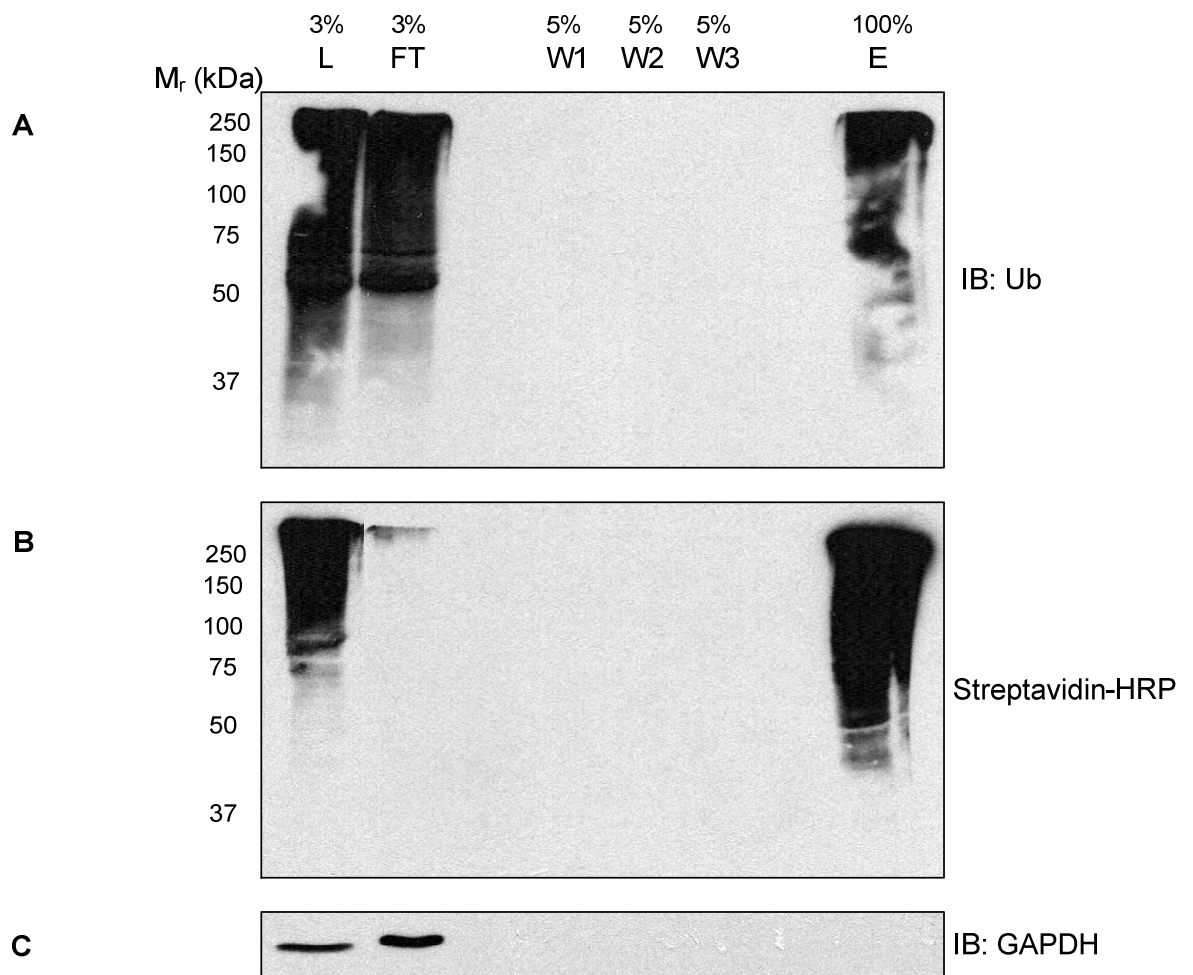


Figure 4.3: Nickel affinity chromatography specifically recovers HBUb-modified proteins

WT HBUb MEFs were grown to confluency in biotin-supplemented media ($1\mu\text{M}$) before enriching for ubiquitinated proteins with MG132 ($6\mu\text{M}$) for two hours prior to harvesting. Soluble protein lysates prepared in an 8M urea buffer were equalised to 1mg/ml before nickel affinity chromatography using 30 μl of 50% (v/v) slurry of Ni^{2+} -NTA-Sepharose beads. Purified HBUb-modified proteins were fractionated by SDS-PAGE along with the indicated percentages of lysate/input (L), flow-through (FT), wash stage (W1, W2, W3), and eluate (E). Recovery of ubiquitinated and HBUb-modified proteins was assessed by immunoblotting using anti-ubiquitin antibody (Panel A) and streptavidin-HRP (Panel B) respectively. GAPDH was used as a loading control (Panel C).

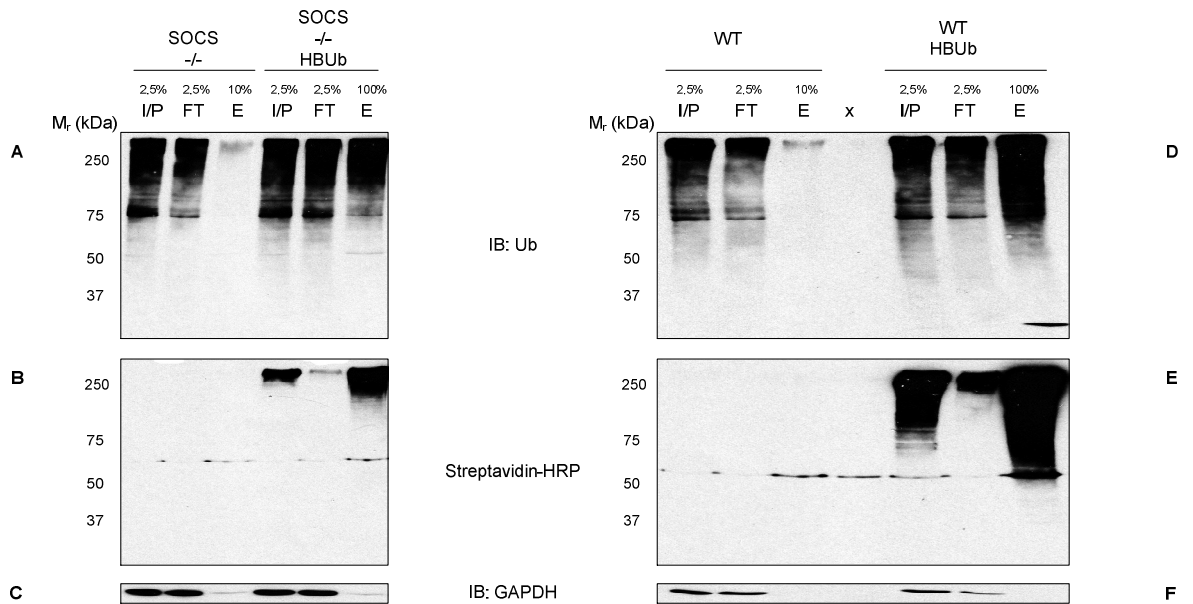


Figure 4.4: Nickel affinity chromatography specifically recovers HBUb-modified proteins

SOCS3^{-/-} and SOCS3^{-/-} HBUb (Left panel) and WT HBUb and WT MEFs (Right panel) were grown to confluency in biotin supplemented media (1 μ M) before enriching for ubiquitinated proteins with MG132 (6 μ M) for two hours prior to harvesting. Soluble protein lysates prepared in 8M urea buffer were equalised to 1mg/ml before incubating with 30 μ l (50% (v/v) slurry) of Ni²⁺-NTA-Sepharose beads overnight at 4°C with rotation. HBUb-modified proteins, recovered in 12% (v/v) SDS buffer following heating treatment at 95°C for 5 minutes, were fractionated by SDS-PAGE. Gels were loaded with input (I/P), flow-through (FT) and eluate (E) with the indicated percentages. Recovery of HBUb-modified proteins was assessed by immunoblotting with anti-ubiquitin antibody (Panel A/D) and streptavidin-HRP (Panel B/E). GAPDH was used as a loading control (Panel C/F).

4.3.1.4 Optimisation of streptavidin bead volume to maximise recovery of HBUb-modified proteins.

The final stage of tandem affinity purification strategy employs streptavidin affinity chromatography to isolate HBUb-modified proteins *via* the strong interaction ($K_d=10^{-15}M$) of streptavidin with the biotinylated signal peptide (BIO) of the HBUb-tag. To estimate the minimum bead volume necessary for the maximum recovery of HBUb-modified proteins, a titration was performed.

WT HBUb MEFs were grown to confluency before enriching for ubiquitinated proteins with MG132 (6 μ M) for two hours prior to harvesting. Soluble protein lysates prepared in 8M urea buffer were equalised to 1mg/ml. Ubiquitinated proteins were then purified with 5, 10, or 15 μ l of 50% (v/v) streptavidin-Sepharose bead slurry. Biotinylated proteins were eluted from the streptavidin-Sepharose beads by heat treatment at 95°C in 12% (w/v) SDS sample buffer for 5 minutes after which the recovery of HBUb-modified, biotinylated proteins was assessed following SDS-PAGE and immunoblotting with anti-ubiquitin antibody and streptavidin-HRP.

While the recovery of biotinylated protein increased with streptavidin-Sepharose bead volume, little improvement was noticed with a volume greater than 10 μ l (Figure 4.5). Furthermore, although ubiquitinated proteins were lost in the flow-through, no biotinylated protein could be detected. This suggests the specific isolation of biotinylated proteins. Furthermore, specificity of purification was highlighted by the absence of GAPDH in the eluate. GAPDH, which has not been reported to be biotinylated (207), was present in lysate and subsequently lost in the flow-through and wash stages. These results indicate that 10 μ l of 50% (v/v) streptavidin-Sepharose bead slurry is sufficient for maximum recovery of HBUb-modified proteins.

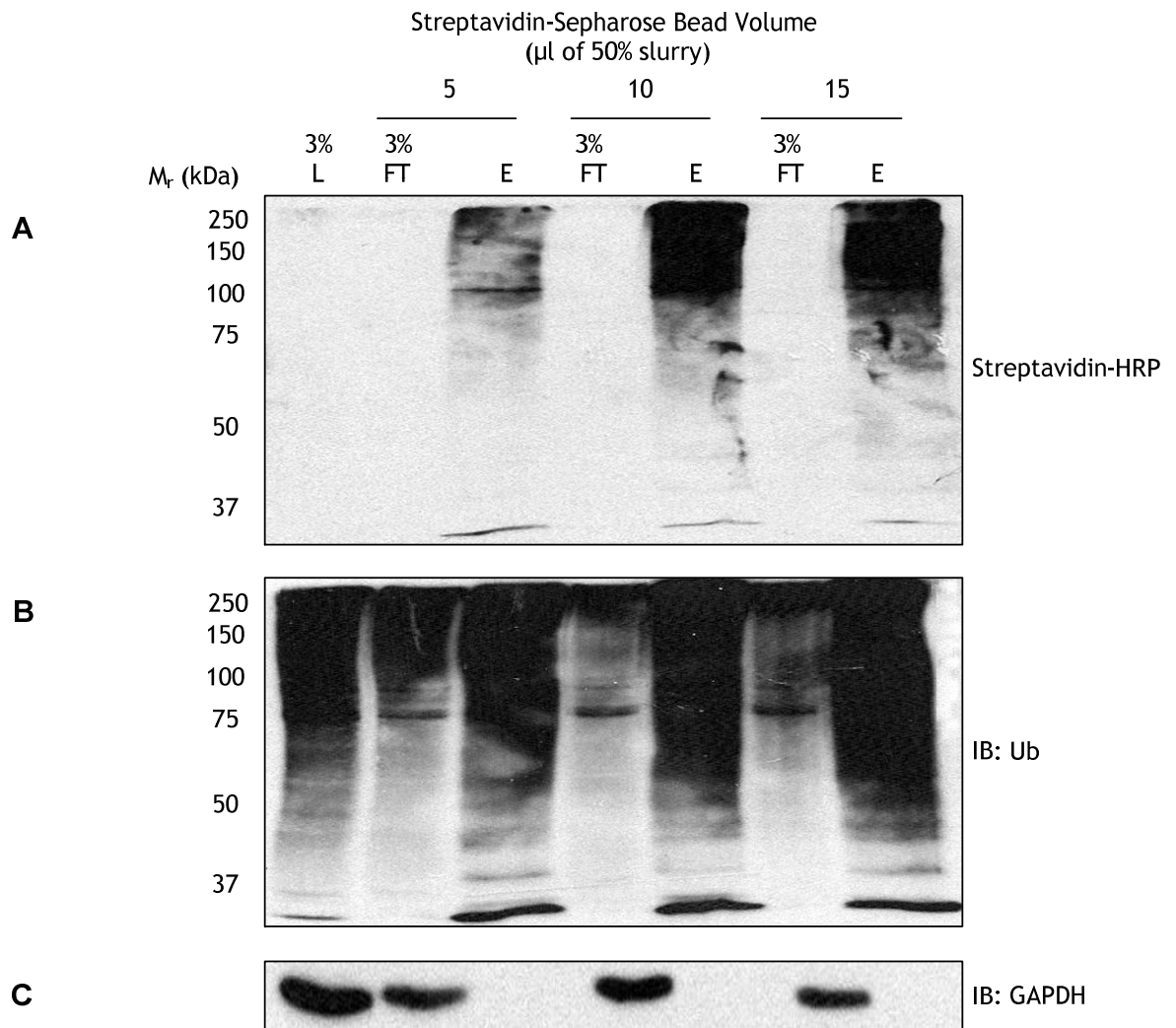


Figure 4.5: Streptavidin-Sepharose bead optimisation to maximise recovery of HBUb-modified proteins

WT HBUb MEFs were grown to confluency in biotin-supplemented media ($1\mu\text{M}$) before enriching for ubiquitinated proteins with MG132 ($6\mu\text{M}$) for two hours prior to harvesting. Soluble protein lysates prepared in an 8M urea buffer was equalised to 1mg/ml before streptavidin affinity chromatography using indicated volumes of 50% (v/v) slurry of streptavidin-Sepharose beads. Biotinylated proteins were eluted by heating the beads in 50 μ l of 12% (w/v) SDS sample buffer for 5 minutes at 95°C. Eluate (E) was isolated using a Hamilton syringe following centrifugation. Recovered biotinylated proteins were fractionated by SDS-PAGE using the indicated percentages of lysate/input (L) and flow-through (FT). Recovery of HBUb-modified, biotinylated proteins was assessed by immunoblotting using anti-ubiquitin antibody (Panel B) and streptavidin-linked-HRP (Panel A). GAPDH was used as a loading control (Panel C).

4.3.1.5 Streptavidin affinity chromatography specifically recovers HBUb-modified proteins

Streptavidin affinity chromatography relies on the strong interaction between streptavidin and biotin. As such, specific recovery HBUb-modified protein is expected with minimal loss over several wash stages. To evaluate binding, loss, and recovery of HBUb-modified proteins, streptavidin affinity chromatography was repeated as in section 4.3.1.4 under optimised conditions with the inclusion of samples taken from all pre-elution wash steps.

While ubiquitinated proteins are lost in the flow-through (Figure 4.6, panel A), minimal loss of HBUb-modified, biotinylated proteins are detected in the same fraction suggesting specific isolation of these proteins (Figure 4.6, panel B). Furthermore, HBUb-modified proteins are detected in eluate but not in the wash stages suggesting that the strong interaction between streptavidin and biotin prevents any disruption by washing. Seeing as nickel affinity chromatography was not performed beforehand, any biotinylated protein detected in the flow-through might be endogenously biotinylated protein or, if the streptavidin-Sepharose beads are completely saturated, HBUb-modified protein. Specificity of purification was highlighted by the absence of GAPDH in the eluate. GAPDH, which has not been reported to be biotinylated (207), is present in lysate by subsequently lost in the flow-through.

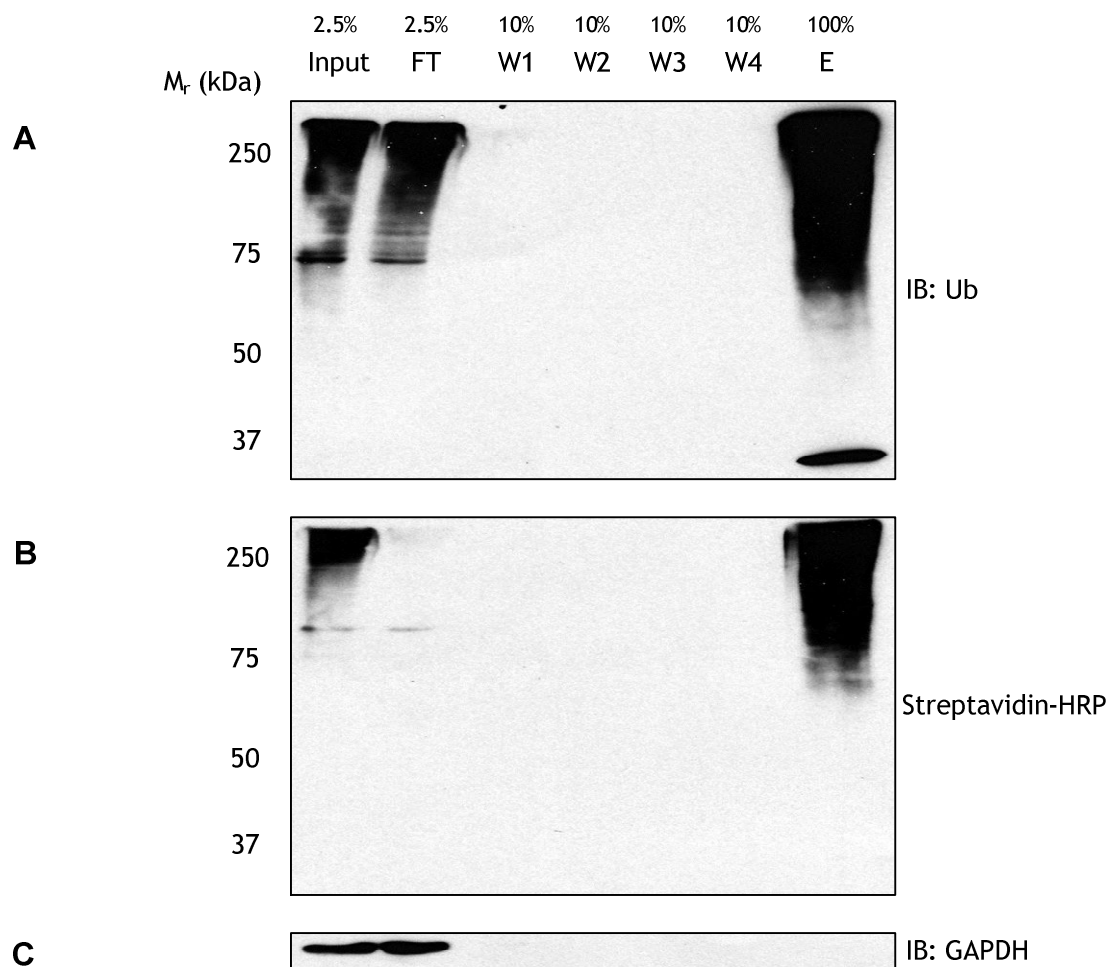


Figure 4.6: Streptavidin bead optimisation to maximise recovery of HBUb-modified proteins

WT HBUb MEFs were grown to confluency in biotin-supplemented media ($1\mu\text{M}$) before enriching for ubiquitinated proteins with MG132 ($6\mu\text{M}$) for two hours prior to harvesting. Soluble protein lysates prepared in an 8M urea buffer were equalised to 1mg/ml before streptavidin affinity chromatography using 10 μl (50% (v/v) slurry) of streptavidin-Sepharose beads. Biotinylated proteins were eluted by boiling the beads in 50 μl of 12% (w/v) SDS sample buffer for 5 minutes at 95°C. Recovered biotinylated proteins (E) were fractionated by SDS-PAGE along with the indicated percentages of input (I/P) and flow-through (FT). Recovery of HBUb-modified, biotinylated proteins was assessed by immunoblotting using an anti-ubiquitin antibody (Panel A), and streptavidin-linked-HRP (Panel B). GAPDH was used as a loading control (Panel C).

4.3.1.6 Specificity of TAP for the specific recovery of K48-linked poly-HBUb-modified proteins

SOCS3 regulates ubiquitin-mediated proteasomal degradation of several substrates (9,10,12). As such, detection of SOCS3 targets depends on their K48-linked polyubiquitination. Due to the complexity of the ubiquitin system, multiple polyubiquitin chain variants are expected to be isolated along with the target K48-linked polyubiquitin chains. It has been demonstrated separately (Section 4.3.1.3 and 4.3.1.5) that nickel and streptavidin affinity chromatography specifically isolate HBUb-modified proteins. However, the efficiency of HBUb isolation when both are performed in sequence has not been tested. Furthermore, the abundance of K48-linked polyubiquitin chains is unknown. To evaluate this, both stages of TAP were performed in sequence and the abundance of isolated K48-linked HBUb-modified proteins assessed following SDS-PAGE *via* immunoblotting using anti-K48-ubiquitin antibody.

WT HBUb MEFs were grown to confluency in biotin-supplemented media (1 μ M) before enriching for ubiquitinated proteins with MG132 (6 μ M) for two hours prior to harvesting. Soluble protein lysates prepared in 8M urea buffer were equalised to 1mg/ml before nickel affinity chromatography using 30 μ l (50% (v/v) slurry) of Ni²⁺-NTA-Sepharose beads followed by streptavidin affinity chromatography using 10 μ l (50% (v/v) slurry) of streptavidin-Sepharose beads. Recovery of K48-linked HBUb-modified proteins was assessed following SDS-PAGE by immunoblotting with anti-K48-linked ubiquitin antibody, anti-ubiquitin antibody, and streptavidin-HRP.

Over the course of the TAP procedure, endogenously biotinylated and non-HBUb modified proteins are lost in the flow-through (Figure 4.7, panel A/B) whereas biotinylated, HBUb-modified proteins are retained within the eluate (Figure 4.7, panel C). Furthermore, HBUb-modified proteins are highly enriched following the final stage of TAP. Specificity of purification was highlighted by the absence of GAPDH in the eluate. GAPDH, which has not been reported to be ubiquitinated or biotinylated (207), is present in the lysate but subsequently lost in the flow-through.

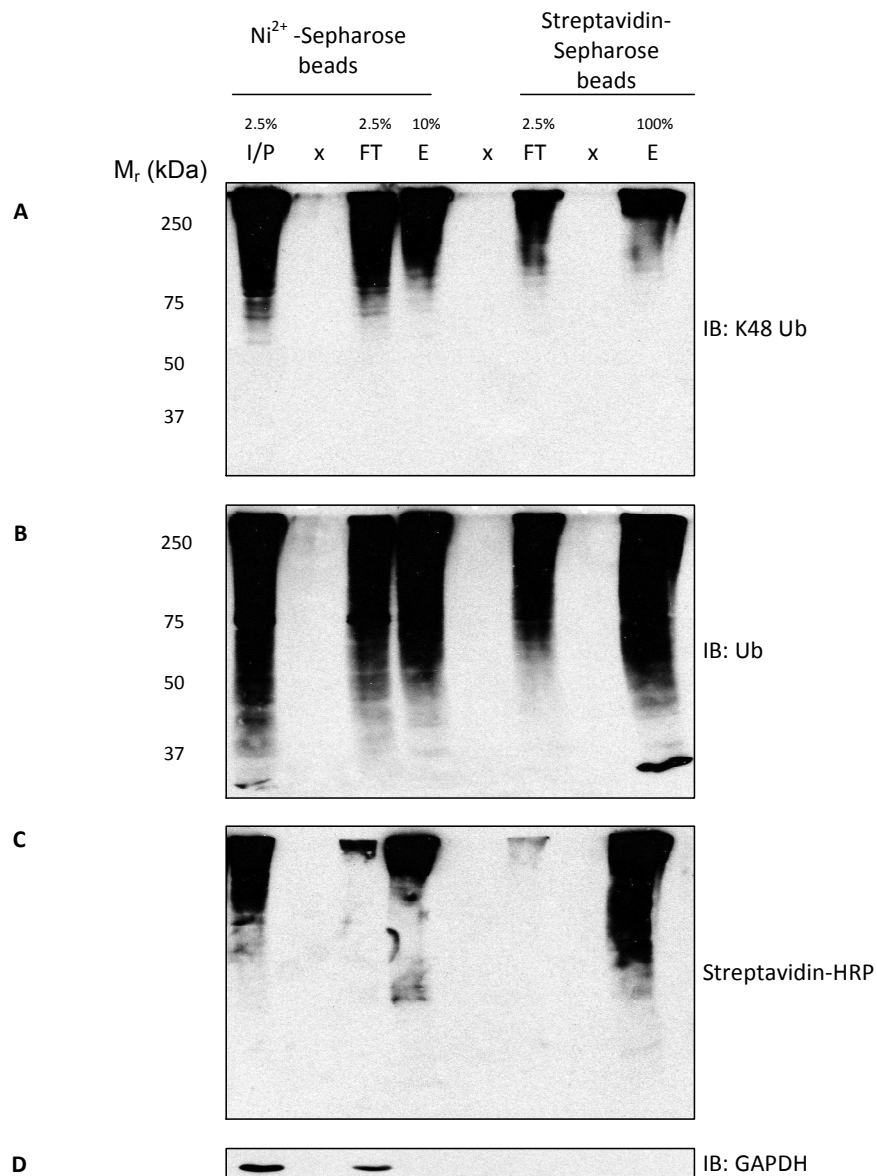


Figure 4.7: Tandem affinity purification recovers K48-linked poly-HBUb-modified proteins

WT HBUb MEFs were grown to confluency in biotin-supplemented media (1 μ M) before enriching for ubiquitinated proteins with MG132 (6 μ M) for two hours prior to harvesting. Soluble protein lysates prepared in 8M urea buffer were equalised to 1mg/ml before nickel affinity chromatography using 30 μ l (50% (v/v) slurry) of Ni²⁺-NTA-Sepharose beads followed by streptavidin affinity chromatography using 10 μ l (50% (v/v) slurry) of streptavidin-Sepharose beads. Purified proteins were fractionated by SDS-PAGE along with the indicated percentages of input (I/P), flow-through (FT), and eluate (E). Specific recovery of K48-linked HBUb-modified proteins was assessed by immunoblotting with anti-K48-linked ubiquitin antibody (Panel A), anti-ubiquitin antibody (Panel B), and streptavidin-HRP (Panel C). GAPDH was used as a loading control (Panel D).

Compared to total ubiquitin levels, a reduced level of K48-linked poly-HBUb-modified proteins was detected (>50%) (Figure 4.7, panel A). This might suggest reduced specificity of the K48-specific antibody or that multiple polyubiquitin chain variants are present. If the latter is true, no impact on relative quantitation and SOCS3 target identification is expected since WT HBUb and SOCS3^{-/-} HBUb MEFs would be equally affected.

4.3.1.7 Tandem affinity purification specifically recovers HBUb-modified proteins

TAP has previously been demonstrated to isolate HBUb-modified proteins (Section 4.3.1.6). However, if purification is specific then HBUb-modified proteins would be recovered from WT HBUb and SOCS3^{-/-} HBUb MEFs but not WT and SOCS3^{-/-} MEFs. To ensure this specificity, TAP was repeated using both experimental and control cell lines.

While biotinylated, HBUb-modified proteins were recovered from WT HBUb and SOCS3^{-/-} HBUb MEFs, no protein was recovered from WT or SOCS3^{-/-} MEFs (Figures 4.8 and 4.9, panel A vs. E in each case). This suggests that TAP is specific for the isolation of HBUb modified proteins. Following nickel affinity chromatography, high levels of ubiquitinated and/or biotinylated proteins were lost in the flow-through (Figures 4.8 and 4.9, panel B/C in each case). This was previously attributed to incomplete labelling of the ubiquitinome due to inadequate HBUb expression. This might also be applicable here, however the loss of HBUb-modified proteins in the flow-through (Figure 4.8 and 4.9, panel A in each case) suggests that the nickel beads are saturated. Moreover, this result might also be explained by loss of endogenously biotinylated proteins. However, a similar loss is not seen for the WT MEFs and given that biotinylated proteins are rare (~4-6 in eukaryotes), such an intense signal would not be expected. As such, this data supports the former explanation of bead saturation. As with previous findings (Figure 4.7), reduced levels of K48-linked poly-HBUb-modified proteins are detected compared with total levels of polyubiquitinated proteins suggesting that multiple polyubiquitin chain variants are present. Furthermore, in all cases, the specificity of the procedure is supported by the absence of GAPDH in the eluate. GAPDH, which has not been reported to be ubiquitinated or biotinylated

(207), is present in lysate by subsequently lost in the flow-through. These results indicate that TAP specifically isolates HBUb-modified proteins.

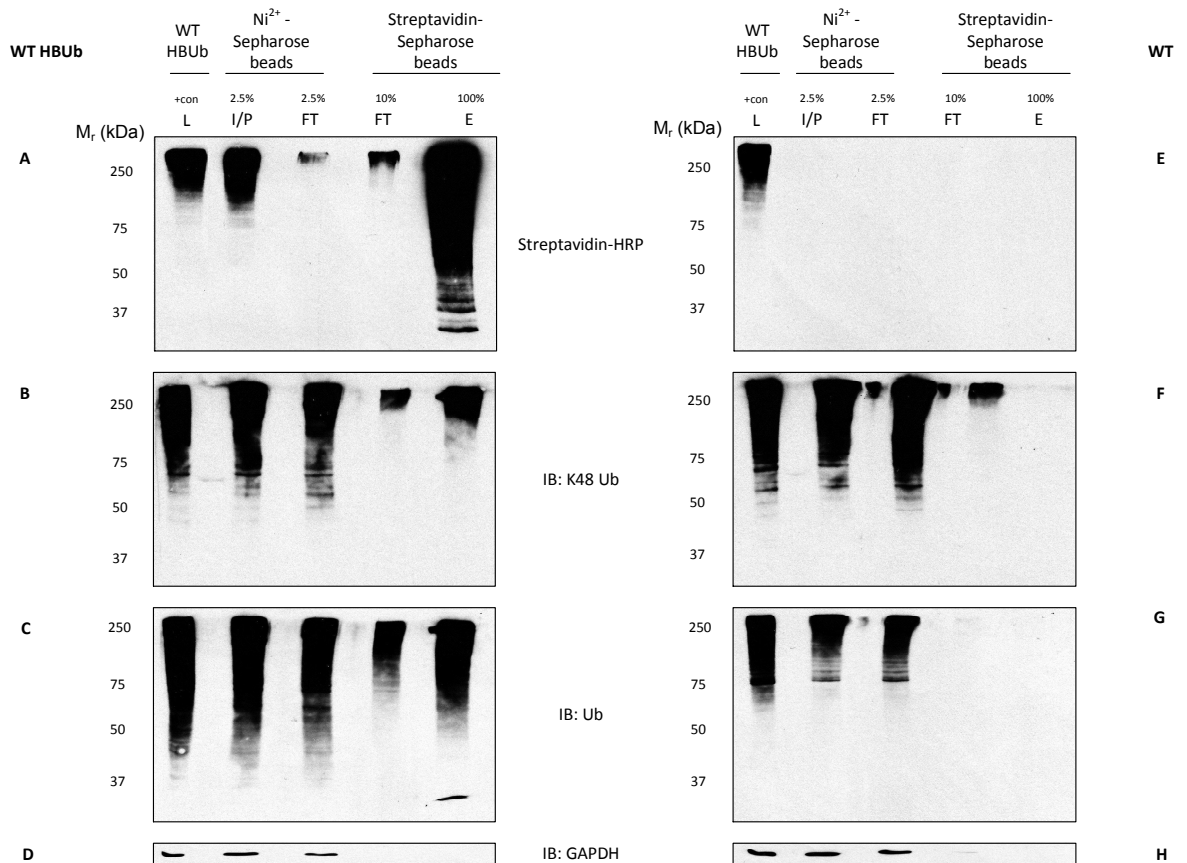


Figure 4.8: Specificity of TAP for the recovery of K48-linked poly-HBUb-modified proteins from WT or WT HBUb MEFs

Control (Right panel) or experimental (Left Panel) MEFs were grown to confluency in biotin-supplemented media ($1\mu\text{M}$) before enriching for ubiquitinated proteins with MG132 ($6\mu\text{M}$) for two hours prior to harvesting. Soluble protein lysates prepared in 8M urea buffer were equalised to 1mg/ml before nickel affinity chromatography using $30\mu\text{l}$ (50% (v/v) slurry) of Ni^{2+} -NTA-Sepharose beads followed by streptavidin affinity chromatography using $10\mu\text{l}$ (50% (v/v) slurry) of streptavidin-Sepharose beads. Purified proteins were fractionated *via* SDS-PAGE along with the indicated percentages of input (I/P), flow-through (FT), and eluate (E). Specific recovery of K48-linked HBUb-modified proteins was assessed by immunoblotting with anti-K48-linked-ubiquitin antibody (Panels B/F), anti-ubiquitin antibody (Panels C/G), and streptavidin-HRP (Panels A/E). GAPDH was used as a loading control (Panels D/H).

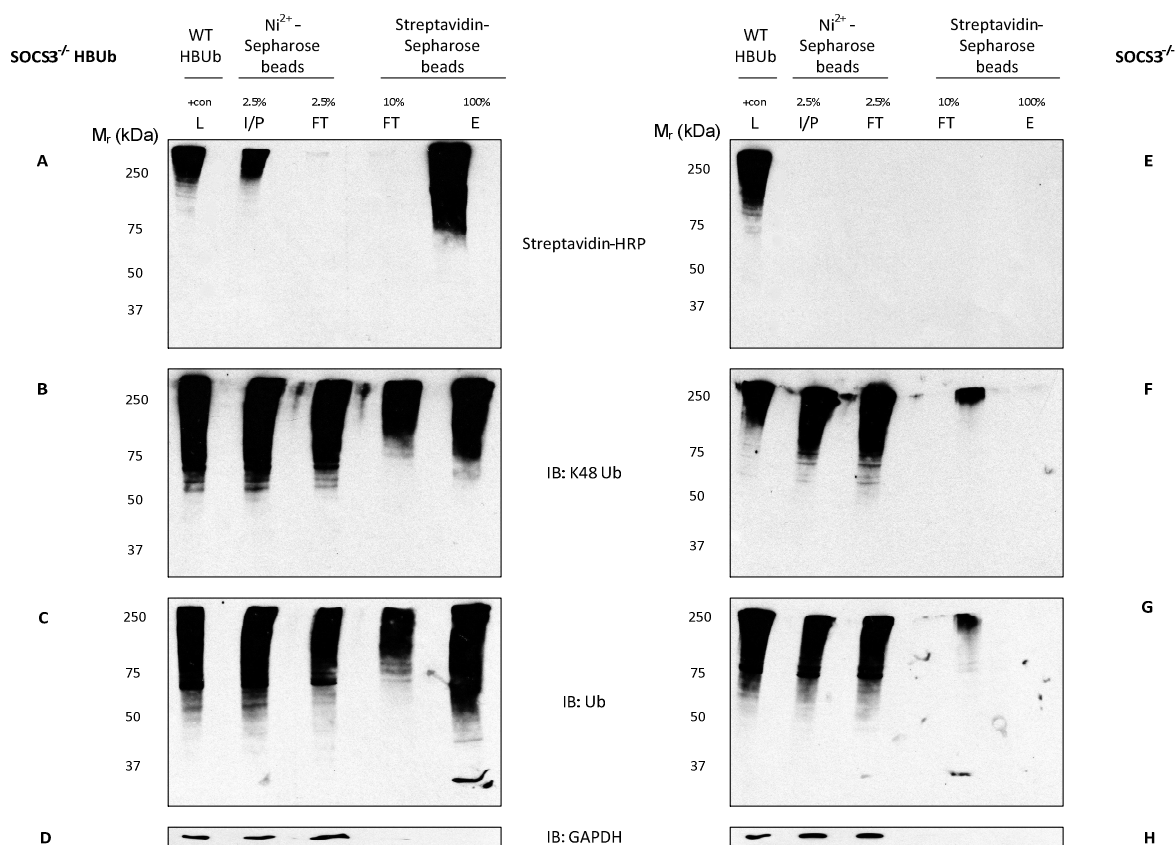


Figure 4.9: Specificity of TAP for the recovery of K48-linked poly-HBUb-modified proteins from SOCS3^{-/-} HBUb MEFs

Control (Right panel) or experimental (Left panel) MEFs were grown to confluency in biotin-supplemented media (1 μ M) before enriching for ubiquitinated proteins with MG132 (6 μ M) for two hours prior to harvesting. Soluble protein lysates prepared in 8M urea buffer were equalised to 1mg/ml before nickel affinity chromatography using 30 μ l (50% (v/v) slurry) of Ni²⁺-NTA-Sepharose beads followed by streptavidin affinity chromatography using 10 μ l (50% (v/v) slurry) of streptavidin-Sepharose beads. Purified proteins were fractionated *via* SDS-PAGE along with the indicated percentages of input (I/P), flow-through (FT), and eluate (E). Specific recovery of K48-linked HBUb-modified proteins was assessed by immunoblotting with anti-K48-linked-ubiquitin antibody (Panels B/F), anti-ubiquitin antibody (Panels C/G), and streptavidin-HRP (Panels A/E). GAPDH was used as a loading control (Panels D/H).

4.3.2 Optimisation of stable isotope labelling of amino acids in cell culture

4.3.2.1 SILAC media supplemented with dialysed serum does not affect cell viability

SILAC can achieve almost 100% incorporation of the labelled isotope. However, this is partly dependent on the purity of the SILAC media. As such, the use of dialysed serum is essential, although its use could potentially impact cell proliferation, adherence, and thus viability. This is not expected to be an issue since dialysed serum has been used with MEFs in other studies (209) although it must be considered as a potential obstacle and will need to be tested. The impact of dialysed serum on cell viability was assessed *via* an MTT assay (191).

WT MEFs were first expanded in either DMEM or SILAC control media and then seeded at 5×10^4 cells per well in 24-well plates and incubated overnight in either 1ml SILAC control ROKO media supplemented with 10% (v/v) dialysed foetal bovine serum, 100U/ml penicillin, 100 μ M streptomycin, and 4 μ g/ml puromycin or Dulbecco's modified Eagle's medium (DMEM) supplemented with 10% (v/v) foetal bovine serum, 100U/ml penicillin, 100 μ M streptomycin, 1mM L-glutamine, and 4 μ g/ml puromycin. The MTT assay was then performed as previously described (Section 2.2.4).

No significant difference in proliferation was detected between the two growth media suggesting that the WT MEFs can tolerate SILAC control media containing dialysed serum (Figure 4.10).

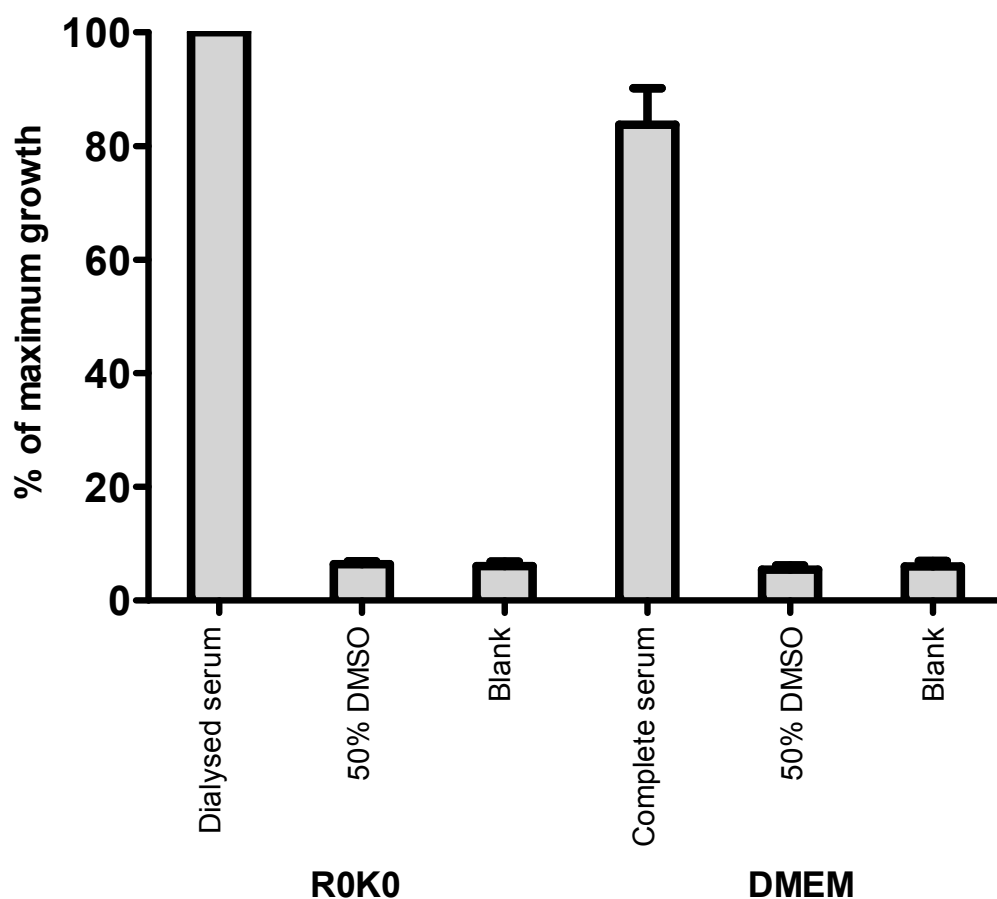


Figure 4.10: SILAC media supplemented with dialysed serum does not affect cell viability

WT MEFs were seeded at a density of 5×10^4 cells per well (24-well plates) and incubated overnight in either 1ml SILAC control R0K0 media supplemented with 10% (v/v) dialysed foetal bovine serum, 100U/ml penicillin, 100 μ M streptomycin, and 4 μ g/ml puromycin or Dulbecco's modified Eagle medium (DMEM) supplemented with 10% (v/v) foetal bovine serum, 100U/ml penicillin, 100 μ M streptomycin, 1mM L-glutamine, and 4 μ g/ml puromycin. The next day, control cells were treated with 50% (v/v) DMSO-media at 37°C for two hours. A blank well containing only culture media was included as a further control. MTT (100 μ M) was then directly added to each well and incubated at 37°C for three hours after which the media was removed and cells lysed with DMSO which also solubilises the formazan crystals. Proliferation was assessed by measuring the absorbance of 200 μ l aliquots of DMSO-solubilised crystals at 590nm. Results are presented as mean values \pm SEM for $n=3$ experiments (One-way ANOVA with Bonferroni post test).

4.3.2.2 SILAC can achieve full incorporation into MEF proteome over five days

SILAC essentially enables the production of two separate proteomes distinguishable by a mass shift imparted by a stable isotope of a suitable amino acid. Complete labelling of the proteome means that each natural amino acid i.e. $^{12}\text{C}_6$ -arginine and $^{12}\text{C}_6$ -lysine is replaced by its heavy isotope. Full incorporation is dependent on the purity of the SILAC media and incubation period. It has been demonstrated for HEK293 cells that five cell doublings equating to five days of cell proliferation is sufficient to achieve complete incorporation (163). Furthermore, the metabolism of arginine to proline, which complicates relative quantitation of peptide abundance, can be prevented by supplementation media with proline (200mg/L) (169). To determine if full incorporation could be accomplished in MEFs over the same time period and without conversion of $^{13}\text{C}_6$ -arginine to $^{13}\text{C}_5$ -proline, a time course was performed. WT MEFs were seeded appropriately so that they would achieve confluency after 2 or 5 days. During this time, cells were grown in either SILAC media (R6K6, where 6 relates to the mass shift of 6Da) or control media (R0K0). Soluble protein lysates were equalised prior to SDS-PAGE fractionation and Coomassie staining. A single gel slice per time-point was extracted and submitted for in-gel trypsin digestion and LC-MS/MS. Proteins contained in each gel slice were identified from the subsequent raw data using the Mascot search engine as described (Section 2.2.10.1). Incorporation was assessed using the returned Mascot data by manual inspection of the mass spectra using Analyst QS v.1.1, Applied Biosystems.

Peptides incorporating stable isotopes of arginine or lysine should produce monoisotopic peaks that are shifted, relative to the natural species, by 6Da. Due to the doubly charged nature of the selected peptide (AGFAGDDAPR, alpha-cardiac actin [Mus musculus]) this shift is reduced to 3Da (Figure 4.11). However, this shift is more than adequate to discriminate heavy and light peptides. Furthermore, peaks relating to the natural isotope are reduced to the level of background over five days and incorporation from this spectra is estimated to be 95% (Figure 4.11, panel C). Furthermore, due to the natural abundance (1.1%) of the heavy isotope of ^{12}C , ^{13}C , two further peaks are

produced relating to the presence of 1 or 2 ^{13}C that have replaced the natural species. These peaks are similarly affected by the charge status of the peptide and are therefore staggered by multiples of 0.5Da to the right of the monoisotopic peak.

In cases where ^{13}C arginine has been converted into ^{13}C proline, peptides that contain proline will have an additional mass shift of 5Da, 2.5Da for a doubly charged peptide, for each proline residue present. As such, a monoisotopic peak would be expected at $m/z=494.3\text{Da}$. This peak is not seen (Figure 4.11, panel C) suggesting that arginine to proline conversion is undetectable. Furthermore, contamination of ^{13}C -labelled amino acids with ^{12}C would produce minor peaks shifted by 1Da (0.5Da) to the left of the monoisotopic peak. A weak peak is seen in both labelled and unlabelled spectra suggesting that this is background.

A second example (Figure 4.12) shows the same result. However, in this case, due to a missed cleavage, the peptide is doubly labelled with a C-terminal arginine and lysine. Such an artefact is common and is taken into account by MaxQuant which can manage up to three labelled amino-acids per peptide (170). Furthermore, miscleavages can also occur in the presence of an N-terminal proline which prevent trypsin digestion thus producing similar artefact (167). Peaks at around 456.3Da (Figure 4.12, panel B/C) probably relate to a partially labelled peptide and as such would be left unmatched to a light peptide. Such an artefact might lead to the SILAC ratio being underestimated. However, this can be overcome by incubating cells in SILAC media for a longer time period. In this case labelling was estimated to be 77% with the reduction attributable to partial labelling.

This data suggests that the over five days, SILAC achieves a high level of incorporation that enables discrimination of differentially labelled peptides. However, an extended period of SILAC labelling would be recommended. Furthermore, although the estimation of isotope incorporation is understandably inaccurate, 95% coverage would be sufficient to determine the significance of variations in peptide abundance.

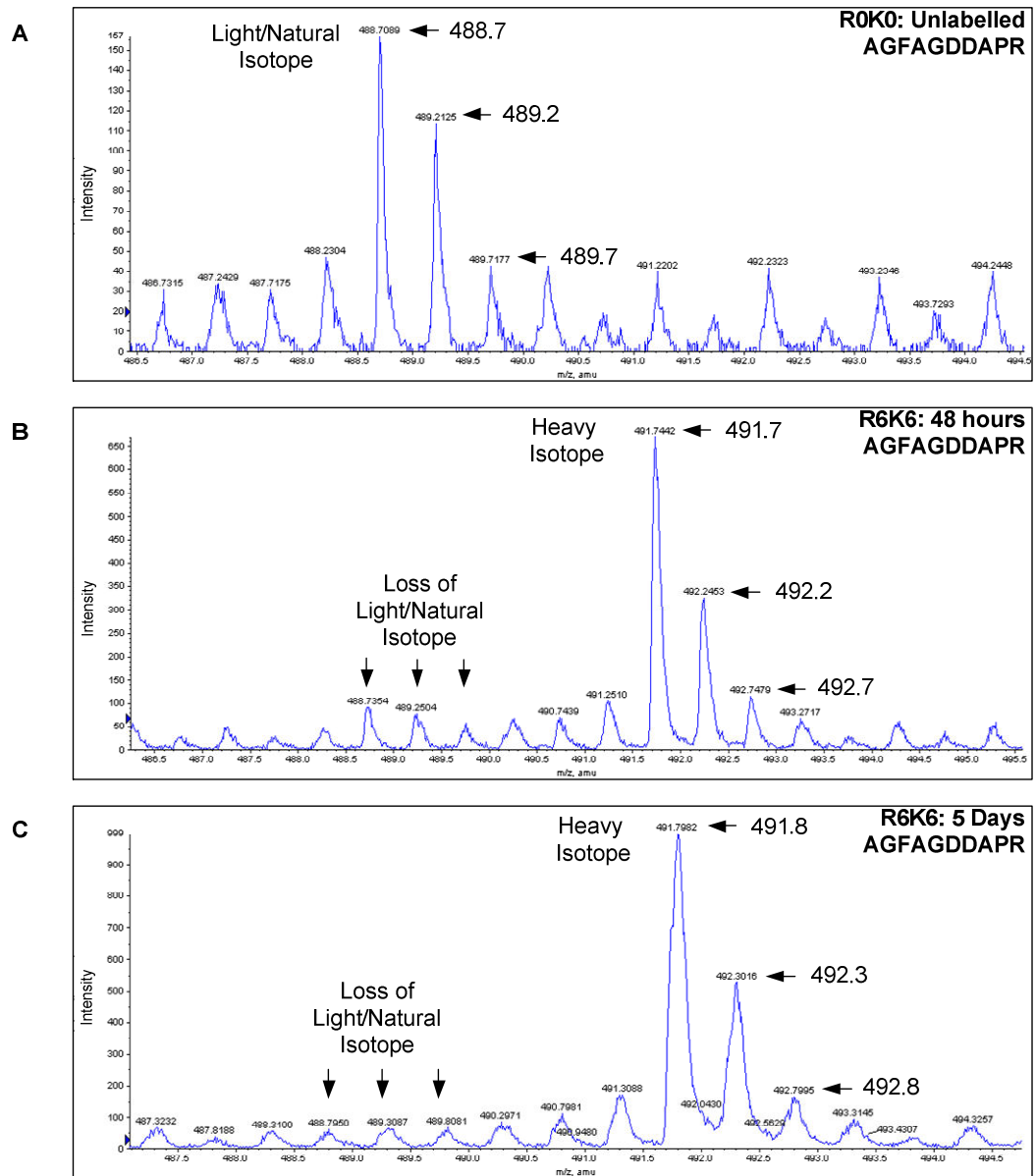


Figure 4.11: Incorporation of SILAC isotope $^{13}\text{C}_6\text{-Arg}$

WT HBUb MEFs were seeded at various densities to allow proliferation to confluency after 2 or 5 days. Control (R0K0) (Panel A) or SILAC (R6K6) (Panels B/C) media was introduced to MEFs previously adapted to control media at the initial time point and allowed to proliferate. Soluble protein lysates were prepared using an 8M urea-based lysis buffer after the indicated time points. Following SDS-PAGE fractionation, gel slices were prepared and submitted for in-gel trypsin digestion and LC-MS/MS. The peaks shown are the doubly charged peaks of the peptide AGFAGDDAPR, assigned to the protein alpha-cardiac actin [*Mus musculus*] by the Mascot search engine as described (Section 2.2.10.1). This peptide, which contains a single C-terminal arginine, has an observed mass of 488.2756kDa, an experimental mass of 974.5367kDa, and a calculated mass of 975.4410kDa. Panel C shows the complete incorporation of $^{13}\text{C}_6\text{-Arg}$ in the peptide at day 5.

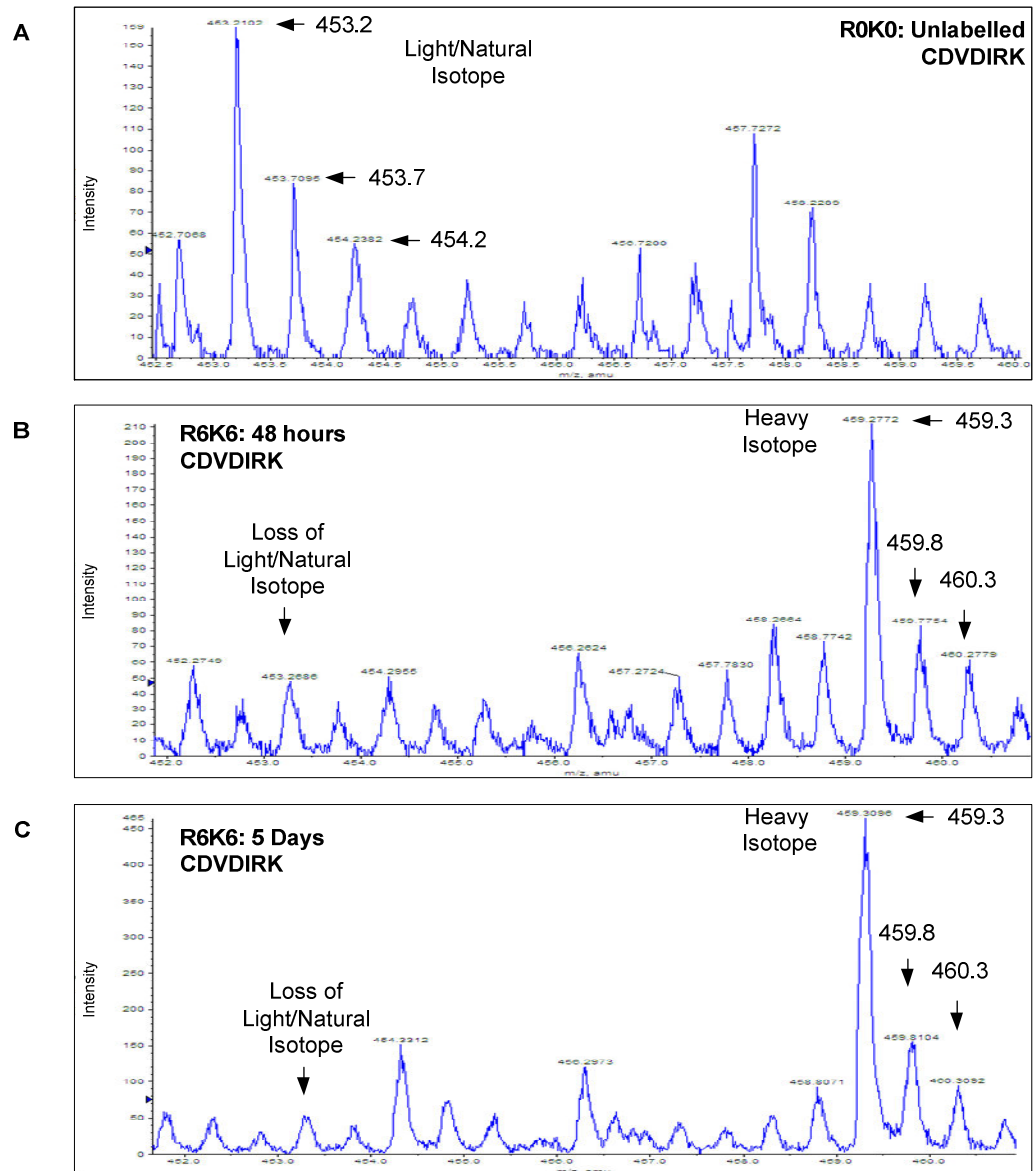


Figure 4.12: Incorporation of SILAC isotope $^{13}\text{C6}$ -Arg/Lys

WT HBUb MEFs were seeded at various densities to allow proliferation to confluency after 2 or 5 days. Control (ROK0) (Panel A) or SILAC (R6K6) (Panels B/C) media was introduced to MEFs previously adapted to control media at the initial time point and allowed to proliferate. Soluble protein lysates were prepared using an 8M urea-based lysis buffer after the indicated time points. Following SDS-PAGE fractionation, gel slices were prepared and submitted for in-gel trypsin digestion and LC-MS/MS. The peaks shown are the triply charged peaks of the peptide CDVDIRK, assigned to the protein alpha-cardiac actin [Mus musculus] by the Mascot search engine as described (Section 2.2.10.1). This peptide, which contains a double labelled C-terminal arginine and lysine, has an observed mass of 453.2102kDa, an experimental mass of 904.4058kDa, and a calculated mass of 904.4436kDa. Panel C shows the complete incorporation of $^{13}\text{C6}$ -Arg/Lys in the peptide at day 5.

4.3.3 Optimisation of sample preparation required for detection LC-MS/MS

4.3.3.1 Optimisation of preparation of raw material for LC-MS/MS

The complexity of the proteome is reduced by TAP and so less protein will be available for subsequent analysis. Furthermore, smaller proteins are generally more abundant and thus produce more peptides while large proteins are less abundant and produce fewer peptides. These limitations are important considerations for performing confident protein identification, which recommends the assignment of at least two unique peptides. However, where peptides are in low abundance and difficult to analyse i.e. phosphopeptides, a single peptide often suffices (179). Evidently, the isolation and identification of low abundance proteins is improved with higher quantities of proteins i.e. μg amounts. As such, the initial raw material used should be scaled-up so that a sufficient quantity of protein can be isolated following TAP. As a general rule, if proteins can be detected with Coomassie stain (R250), which is sensitive down to $0.1\mu\text{g}$ of protein, then this quantity is sufficient for MS analysis. To assess the quantity of initial raw material necessary to isolate sufficient HBUb-modified protein following TAP for MS analysis, a titration was performed.

WT HBUb MEFs were grown to confluency in biotin-supplemented media ($1\mu\text{M}$) on 5, 10, 15, or $20\times 10\text{cm}$ dishes before enriching for ubiquitinated proteins with MG132 ($6\mu\text{M}$) for two hours prior to harvesting. Soluble protein lysates prepared in 8M urea buffer were pooled and equalised to 1mg/ml before nickel affinity chromatography using $30\mu\text{l}$ (50% (v/v) slurry) of Ni^{2+} -NTA-Sepharose beads per milligram of initial protein. This was followed by streptavidin affinity chromatography using $10\mu\text{l}$ (50% (v/v) slurry) of streptavidin-Sepharose beads per milligram of initial protein. The final eluate was then fractionated by SDS-PAGE and recovered proteins visualised using Coomassie stain (R250).

The initial quantity of protein used for TAP ranged from 5 to 30mg. Subsequent isolation and detection of HBUb-modified protein increased with the number of 10cm dishes used (Figure 4.13). Furthermore, in each case, a smear pattern typical of polyubiquitinated protein was produced. The use of $20\times 10\text{cm}$ dishes produced the strongest signal where the majority of the proteins were present in the $2\text{-}4\mu\text{g}$ range although higher molecular weight proteins exceeded this range.

Strong bands detected around 150kDa and 25kDa are thought to be non-specifically purified proteins whereas bands below 20kDa might correspond to free HBUb, which has a predicted molecular mass of around 18kDa. These results suggest that the use of 20x10cm dishes enables sufficient material to be isolated following TAP. However, for improved confidence of detection of proteins across the full mass range, a greater amount is recommended.

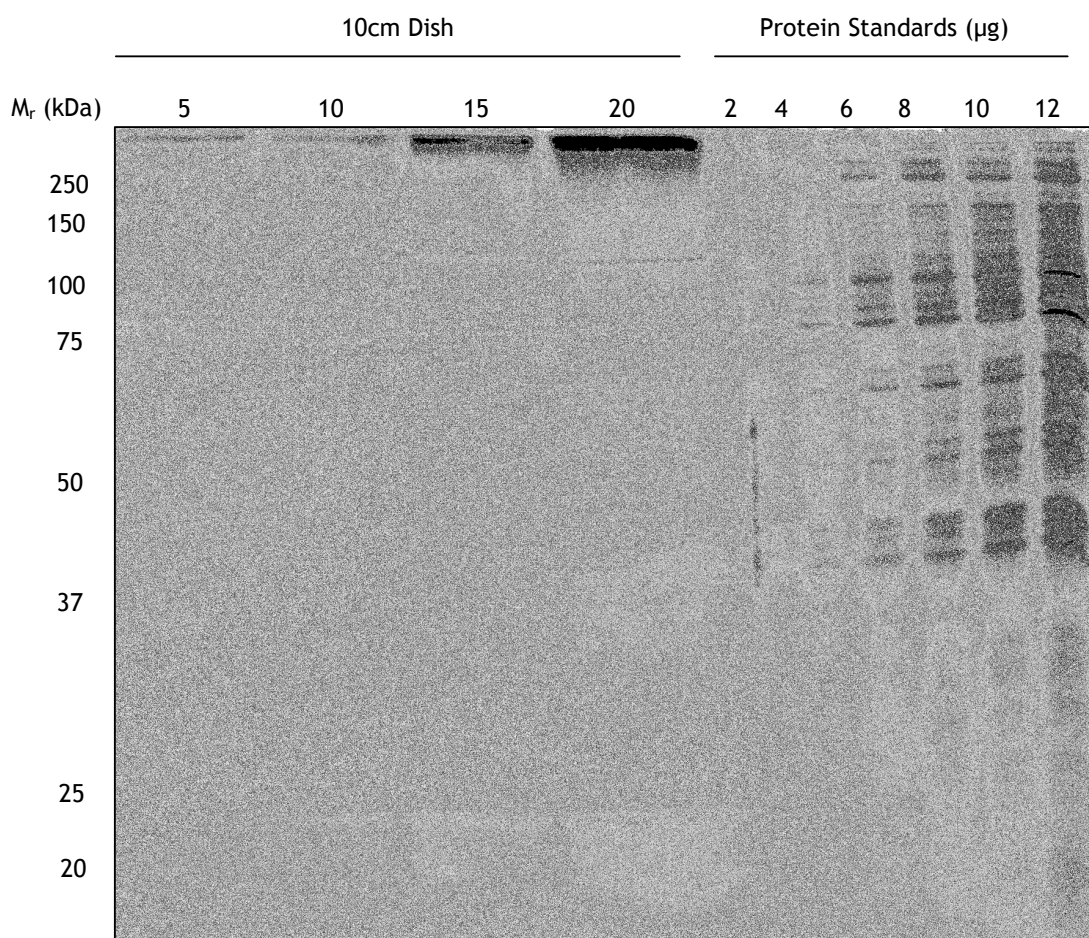


Figure 4.13: Optimisation of sample preparation required for detection LC-MS/MS

WT HBUb MEFs were grown to confluency in biotin-supplemented media (1 μ M) on 5, 10, 15, or 20x10cm dishes before enriching for ubiquitinated proteins with MG132 (6 μ M) for two hours prior to harvesting. Soluble protein lysates prepared in 8M urea buffer were pooled and equalised to 1mg/ml before nickel affinity chromatography using 30 μ l (50% (v/v) slurry) of Ni²⁺-NTA-Sepharose beads per milligram of initial protein. This was followed by streptavidin affinity chromatography using 10 μ l (50% (v/v) slurry) of streptavidin-Sepharose beads per milligram of initial protein. The eluate was then fractionated by SDS-PAGE and recovered proteins visualised using Coomassie stain (R250).

4.3.3.2 The streptavidin-biotin interaction can be disrupted with an aqueous biotin solution and elevated temperature

The biotin-streptavidin interaction is one of the strongest non-covalent interactions in nature ($K_d=10^{-15}M$). So far, optimisation of TAP has employed SDS buffer and elevated temperatures to elute HBUb-modified proteins from streptavidin beads. Furthermore, a large volume (>1ml) of eluate was isolated following TAP in the previous section (4.3.3.2). A result of this, a large 2mm, 18x16cm gel with merged wells was necessary to enable the loading of such a large volume. This is not ideal since the strength of the signal was weakened as it was spread over a large area. In-gel trypsin digestion is an optimised method of peptide generation for MS commonly performed at the University of Glasgow. Efficient in-gel trypsin digestion is achieved by reducing the volume of acrylamide to a minimum. As such, a small, thin (1mm) gel with narrow lanes (10-well) is recommended. Given that such gels (Invitrogen, NuPAGE 4-12% Bis-Tris Gel), have a capacity of around 30 μ l/well, the TAP eluate must be concentrated prior to SDS-PAGE fractionation. However, SDS-based sample buffer is not compatible with standard protein concentration spin columns. Therefore, a different elution strategy is necessary. Current literature offers several potential solutions including elution with excess free biotin (210), water (211), and low salt (211). Furthermore, other commercially available streptavidin bead providers advise other methods such as low (0.1%) SDS and glycine-HCL, pH 2.5. However, these conditions might be specific for the products for which they were designed. Here, these elution strategies are individually tested or combined with the aim to produce a high yielding elution buffer.

WT HBUb MEFs were grown to confluency in biotin-supplemented media (1 μ M) before enriching for ubiquitinated proteins with MG132 (6 μ M) for two hours prior to harvesting. Soluble protein lysate prepared in an 8M urea buffer was equalised to 1mg/ml before streptavidin affinity chromatography. Biotinylated proteins were eluted in one bead volume of 0.1% (w/v) SDS sample buffer or the indicated concentration of biotin diluted in either H₂O or a low salt buffer (LSB; 10mM HEPES, 1% (v/v) Igepal CA-630, 0.1% (w/v) SDS, 5mM EDTA) followed by incubation at 95°C for 5 minutes. Additionally, elution was performed using one

bead volume of glycine-HCL (0.1M, pH2.5) at RT for 5 minutes prior to isolation of supernatant. Captured biotinylated proteins were fractionated by SDS-PAGE and recovery assessed using streptavidin-linked-HRP.

While biotin-supplemented H₂O or low salt buffers (LSB) have comparable elution efficiency, both glycine-HCL and low SDS buffer failed to elute (Figure 4.14). As demonstrated by Holmberg et al (211) salt, even in low concentrations can stabilise the streptavidin-biotin interaction preventing release of biotinylated molecules. In this case, excess biotin is assumed to be the key disrupting agent. Elution from the streptavidin beads (300nmol biotin/ml binding capacity) was not affected by increasing concentrations of biotin over a 5-30mM range. This suggests that the minimum concentration (5mM) of biotin used combined with elevated temperature was sufficient to out-compete bound HBUB-modified proteins. These data suggest that an aqueous biotin solution combined with brief elevated temperature is sufficient to elute biotinylated proteins from streptavidin beads. Moreover, the chosen solution is compatible with commercially available protein concentration spin columns.

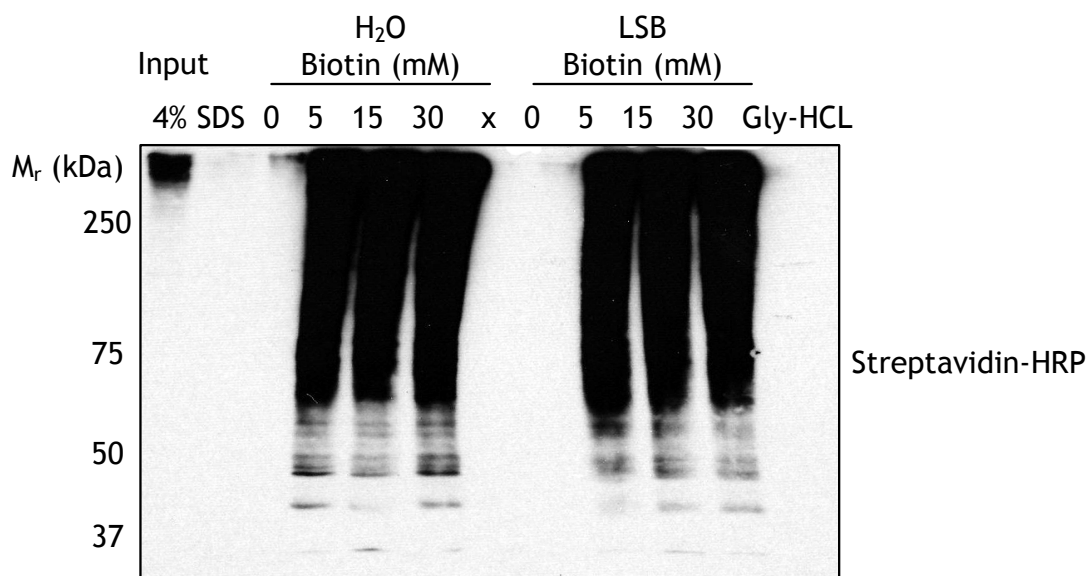


Figure 4.14: Optimisation of streptavidin bead elution strategy for the recovery of HBUb-modified proteins

WT HBUb MEFs were grown to confluency in biotin-supplemented media (1 μ M) before enriching for ubiquitinated proteins with MG132 (6 μ M) for two hours prior to harvesting. Soluble protein lysates prepared in an 8M urea buffer were equalised to 1mg/ml before streptavidin affinity chromatography using 10 μ l (50% (v/v) slurry) of streptavidin-Sepharose beads. Biotinylated proteins were eluted by heating the beads for 5 minutes at 95 $^{\circ}$ C in one bead volume of 0.1% (w/v) SDS sample buffer or the indicated concentration of biotin diluted in either H₂O or a low salt buffer (LSB; 10mM HEPES, 1% (v/v) Igepal CA-630, 0.1% (w/v) SDS, 5mM EDTA). Elution was also performed by incubating beads with glycine-HCL (0.1M, pH2.5) at RT for 5 minutes. Recovered biotinylated proteins were fractionated by SDS-PAGE along with the indicated percentage of input (I/P). Recovery of HBUb-modified, biotinylated proteins was assessed following transfer onto nitrocellulose membrane using streptavidin-HRP.

4.4 Scaled-up tandem affinity purification specifically enriches sufficient HBUb-modified protein for MS analysis.

The previous sections (4.3.1-4.3.3) have specified requirements for initial sample preparation, affinity chromatography, and pre-MS conditioning. When combined in to a single protocol, it is expected that not only are HBUb-modified proteins captured and recovered with high yield, but that this sample can then be concentrated and detected *via* Coomassie stain. This would confirm the effectiveness of the experimental strategy. Using these optimised conditions TAP, protein concentration and SDS-PAGE fractionation were performed in sequence. WT and WT HBUb MEFs were grown to confluency in biotin-supplemented media (1 μ M) on 20x10cm dishes before enriching for ubiquitinated proteins with MG132 (6 μ M) for two hours prior to harvesting. Soluble protein lysates prepared in 8M urea buffer were pooled and equalised to 1mg/ml before nickel and streptavidin affinity chromatography using optimised conditions. Eluted proteins were concentrated using Amicon, Ultra-2 centrifugal filter device (Molecular weight cut-off (MWCO)=10kDa) after which the recovered sample was fractionated *via* SDS-PAGE and recovered proteins visualised using Coomassie stain or streptavidin-HRP.

While proteins were isolated from WT HBUb MEFs, none could be detected using WT MEFs (Figure 4.15). Furthermore, a smear showing an enrichment of high molecular mass proteins is detected which is typical of polyubiquitinated proteins. The yield of HBUb-modified proteins is comparable to that seen previously (Section 4.3.3.1, figure 4.13, panel A) however, use of a gradient gel with narrow lanes has improved fractionation and signal strength. The bands of lowest molecular mass (Figure 4.15, panel A, lanes 1 and 2) are thought to be non-specific since they appear in both WT and WT HBUb eluate whereas those found below 25kDa only in the WT HBUb lane are predicted to correspond to free HBUb or Ub-HBUb oligomers. Specificity of the procedure is supported by the streptavidin visualisation (Figure 4.15, panel B). While HBUb-proteins are highly enriched in WT HBUb MEFs (Figure 4.15, panel B, lane 1), only a weak non-specific band can be detected for WT MEFs (Figure 4.15, panel B, lane 2). These data confirm that using this procedure, a sufficient quantity of HBUb-modified protein can be isolated for MS-analysis.

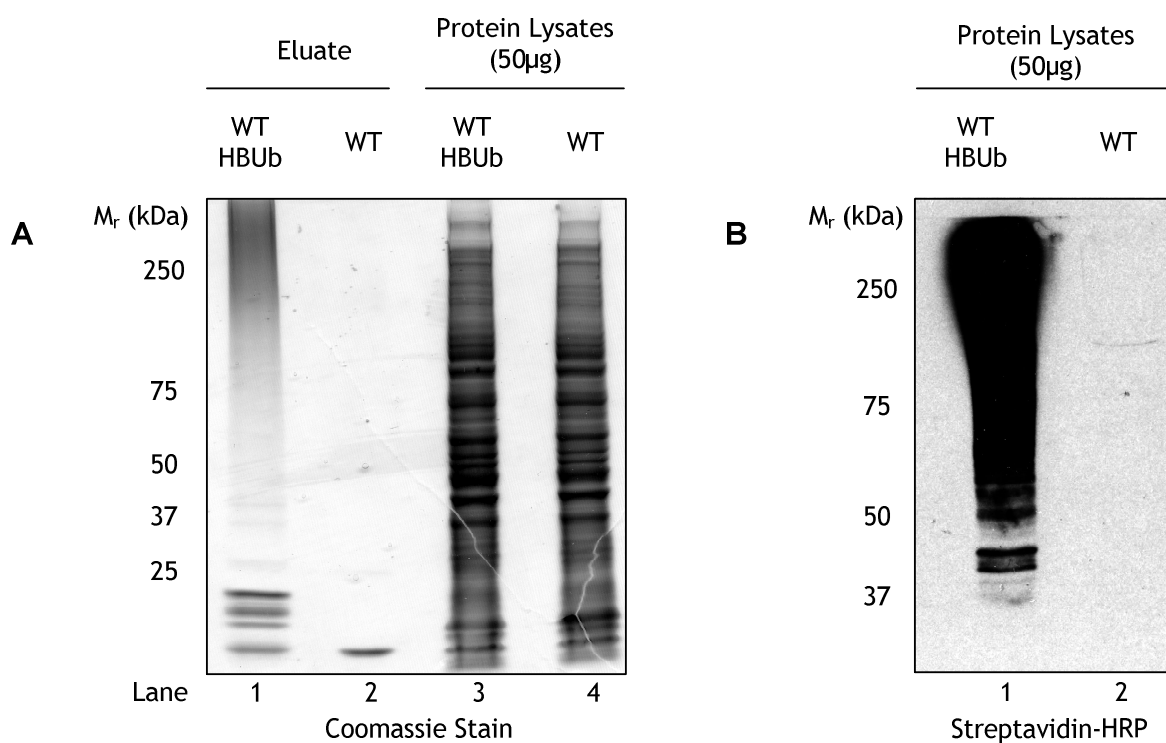


Figure 4.15: Scaled-up tandem affinity purification specifically enriches sufficient HBUb-modified protein for MS analysis

WT and WT HBUb MEFs were grown to confluency in biotin-supplemented media (1 μ M) on 20x10cm dishes before enriching for ubiquitinated proteins with MG132 (6 μ M) for two hours prior to harvesting. Soluble protein lysates prepared in 8M urea buffer were pooled and equalised to 1mg/ml before nickel affinity chromatography using 30 μ l (50% (v/v) slurry) per milligram of initial protein of Ni²⁺-NTA-Sepharose beads followed by streptavidin affinity chromatography using 10 μ l (50% (v/v) slurry) per milligram of initial protein of streptavidin-Sepharose beads. Eluted proteins were concentrated using Amicon, Ultra-2 centrifugal filter device after which the recovered sample was fractionated *via* SDS-PAGE and proteins visualised using Coomassie stain (R250) (Panel A) or streptavidin-HRP (Panel B).

4.5 Conclusions

Here, the aim was to assess and optimise the experimental strategy. It was shown that SILAC was able to label the proteome without adversely affecting cell viability (Section 4.3.2). The method used to assess incorporation was not ideal. Even though proteins with a long half-life were chosen, analysis of single peptides does not reflect the efficiency of SILAC to label the whole proteome. Moreover, I was able to perform a search for either labelled or unlabelled peptides, from cells SILAC-labelled for five days, using the Mascot search engine (data not shown). While labelled peptides were in abundance, no unlabelled peptides could be detected. This result suggested full incorporation of the stable isotope into the proteome. A more informative approach would be to assess the whole proteome. This can be achieved by a comparison of the proteomes extracted from single cell type, differentially labelled *via* SILAC. If full incorporation has been achieved then SILAC ratios for each peptide should equal $1 \pm$ error. This analysis requires software such as MaxQuant or Mascot Distiller however, only the former was available the time. Furthermore, samples were analysed using a QTOF MS, the output of which (.wiff) is not compatible with MaxQuant. Moreover, I was not able to convert this file to the required format. As such, an Orbitrap mass spectrometer, which is supported by MaxQuant, would be required. In addition, although the same analysis should be possible with MSQuant, the predecessor to MaxQuant, MSQuant requires data extracted from a now defunct web browser (IE6). As such, I was not able to analyse the data as I would have liked. Given that these samples should still be available, repeating the analysis on an Orbitrap could be performed belatedly.

Tandem affinity purification was shown to be specific and enriched HBUb-modified proteins giving a high yield that was sufficient for analysis by MS. Furthermore, it was found that biotin supplementation was essential for streptavidin affinity chromatography (Sections 4.3.1 and 4.33). It was interesting to find that, during nickel affinity chromatography and to a lesser extent, streptavidin affinity chromatography, a large amount of ubiquitinated protein was being lost in the flow-through (Section 4.3.1.7, figure 4.8). Importantly, this also included loss of K48-linked ubiquitin. This was in contrast to that of HBUb-modified protein, which was highly enriched, in the final eluate

while only a minimal amount was lost in the previous steps. This was surprising since the bead volume had been previously optimised. This might suggest that bead volume was insufficient or that expression of the HBUb tag varied significantly between HBUb-expressing clones resulting in reduced availability of the HBUb tag i.e. incomplete labelling of the ubiquitinome. This would require optimisation be repeated for each clone used, which was not done due to time restrictions. Furthermore, the increase in size of HB-tagged ubiquitin (18kDa) over the endogenous moiety (8kDa) might make the HBUb-tag incompatible with a specific set of E3 ligases. This would result in preferential incorporation of endogenous ubiquitin and produce an endogenous ubiquitin-tagged subpopulation that would be lost during affinity chromatography. Although WT and SOCS3^{-/-} cell lines would be affected equally, this limitation might potentially reduce the probability of detecting low abundant SOCS3-dependently ubiquitinated targets.

To maximise the isolation of K48-linked polyubiquitin chains, a potential solution might be to express a K48-only mutant form of HBUb. This might reduce the recovery of polyubiquitin chain variants and potentially improve detection of SOCS3 targets. K48-only ubiquitin mutants have been used previously to identify the specificity of E3 ligases (212). However, stable overexpression of a K48-only mutant might have adverse effects that impact cell function and thus the use of ubiquitin mutants was not pursued.

Important for MS-analysis is the scaling-up of raw materials and reagents. Comparable results were obtained using scaled-up conditions as compared to initial small-scale reactions (Section 4.4). Furthermore, 20x10cm dishes were shown to enable TAP isolation of a sufficient quantity of HBUb-modified protein for MS analysis. However, detection/identification of proteins can be improved following analysis of more peptides. Moreover, given the loss of ubiquitinated protein seen during affinity chromatography it was decided to use 20x15cm dishes.

The choice to use in-gel trypsin digestion required the development of an elution strategy that would be compatible with standard protein concentration methods. It was found that an aqueous biotin solution combined with a period of elevated

temperature was sufficient to disrupt the streptavidin-biotin interaction (Section 4.3.3). The use of heat is concerning due to the sensitivity of urea to heat. With heat and time, urea decomposes to isocyanate which carbamylates the N-terminus of proteins or side chains of basic amino acids lysine and arginine. Carbamylation of protein side chains increases their mass and thus the mass of the protein/peptide. Although this modification can be accounted for during post-MS analysis, it might reduce the number of proteins identifiable and also increase database search time. However, both issues can be overcome by using fresh urea buffers and keeping the temperature below 37°C. Since the chosen elution method still relies on elevated temperatures, streptavidin beads should be washed with a non-urea based wash buffer several times and excess buffer removed prior to elution. With hindsight, elution efficiency should have been assessed for a range of temperatures and as such further reduce the risk of disrupting peptide modifications. Another possible strategy would be to use avidin beads which have a lower affinity ($K_d = 10^{-8}M$) for biotin than streptavidin and would therefore require milder elution conditions (2mM D-biotin in PBS at room temperature). However, this might result in a reduced yield and limit the ability to capture low abundant proteins. Furthermore, wash conditions would need to be less stringent which would increase background.

In conclusion, while not without its limitations, the optimised experimental strategy enables the almost complete labelling of the proteome and the specific enrichment of HBUb-modified proteins with a high yield. Importantly, for the detection of proteasome-degraded proteins, a large proportion of isolated ubiquitin chains are K48-linked. The data generated in this section suggests that using this strategy, it should be possible to capture sufficient quantity of HBUb-modified proteins and identify potential SOCS3-dependently ubiquitinated substrates *via* mass spectrometric analysis.

5.0 Identification of SOCS3-dependently ubiquitinated substrates

5.1 Introduction

Optimisation of the experimental strategy confirmed the specific enrichment of a differentially-labelled, HBUb-modified ubiquitinome (Section 4.0). Once performed under optimised conditions, the samples produced were processed for LC-MS/MS analysis. This involved tryptic digestion of proteins and fractionation by reverse-phase liquid chromatography, after which co-eluting peptides were ionised and their abundance and m/z analysed by mass spectrometry. The most abundant peptides (top ten) from this first scan are selected for fragmentation and sequencing *via* a second round of MS to produce an MS/MS spectra. Following the analysis of this raw data by proteomics software packages e.g. MaxQuant and Mascot, proteins were identified from the MS-sequenced peptides. MaxQuant, the primary software package used in this study, is designed specifically for SILAC-labelling experiments. As such, it quantifies SILAC ratios of the identified proteins from assigned peptides. Using this strategy, I aimed to identify SOCS3-dependently ubiquitinated proteins enriched in WT but not in SOCS3^{-/-} MEFs.

MS is a very sensitive technique and thus vulnerable to variations such as electronic noise, miss-calibration or calibration drift. These variations can drastically alter the output over multiple samples or experimental repeats. In combination with sample variations, unbiased comparisons of experimental data can be compromised (213). To ensure confidence in data acquisition, several biological and technical repeats are recommended. Unfortunately, cost constraints make this unfeasible. As such, only two biological repeats were performed with reverse SILAC labelling being performed on the repeat experiment to account for any impact of SILAC. Post-MS data analysis was performed using the free quantitative proteomics software MaxQuant (Section 2.2.10.2) (170).

5.1.1 Strategy to identify potential SOCS3-dependently ubiquitinated substrates

In order to identify potential SOCS3-dependently ubiquitinated substrates a differentially SILAC-labelled, TAP-isolated ubiquitinome was captured using the previously optimised experimental strategy (Section 4.0). Samples generated *via* this process were submitted for in-gel trypsin digestion (Section 2.2.9.3) and LC-MS/MS (Section 2.2.10). While automated data analysis is a typically black-box procedure, increased confidence in returned results can be achieved by using multiple analysis software packages or search engines (180,214). Raw MS data was therefore assessed using both MaxQuant/Andromeda (170,180,193) and Mascot (180) search engines. While Mascot simply returns a list of identified proteins based on analysis of peptide sequences, MaxQuant can return a list of proteins based not only on peptide sequence analysis but also on quantitative analysis of their SILAC ratios. As such, using Mascot, I aimed to identify proteins present in WT but not SOCS3^{-/-} MEFs, whereas using MaxQuant, I aimed to identify proteins that are *enriched* in WT but not in the SOCS3^{-/-} MEFs. A protein which is significantly enriched ($\log_2(\text{normalised H/L}) > 1$ or $\log_2(\text{normalised L/H}) > 1$ for reverse labelling experiment) would signify a potential SOCS3 substrate.

Additionally, based on user-defined parameters, both programs can consider PTMs, thus ubiquitination (GlyGly, trypsin remnants) and tyrosine phosphorylation sites may be identified. Such evidence may support the protein as a SOCS3 target and would also facilitate further studies e.g. mutational analysis. However, since PTMs are sometimes difficult to detect due to the low abundance or loss during sequence fragmentation (179), this data might not be retrievable.

5.2 Results and discussion

5.2.1 Selection of HBUb-expressing MEF clones

As previously discussed (Section 3.0), the HBUb transgene should be expressed at comparable levels to simplify quantitation of MS data. As such, prior to further investigation, several WT and SOCS3^{-/-} HBUb-expressing clones were assessed for comparable HBUb expression. Doing so would ensure that any changes in expression occurring during the experimental process could be monitored and accounted for.

Lysates of MEF clones were prepared as described (Section 2.2.5.3), equalised prior to SDS-PAGE fractionation and expression of the HBUb transgene and SOCS3 analysed by immunoblotting (Figure 5.0).

Expression of the HBUb transgene varied among the MEF clones (Figure 5.0, panel A). However, SOCS3^{-/-} HBUb clone 8 and WT HBUb clone 17 expressed the HBUb transgene at comparable levels (Figure 5.0, panel A, small arrows). Furthermore, SOCS3 was expressed in WT but not SOCS3^{-/-} MEFs confirming that the clones were correctly assigned (Panel B, large arrow). Moreover, WT HBUb clone 17 showed the highest SOCS3 expression. As such, SOCS3^{-/-} HBUb clone 8 and WT HBUb clone 17 were selected for further experimentation.

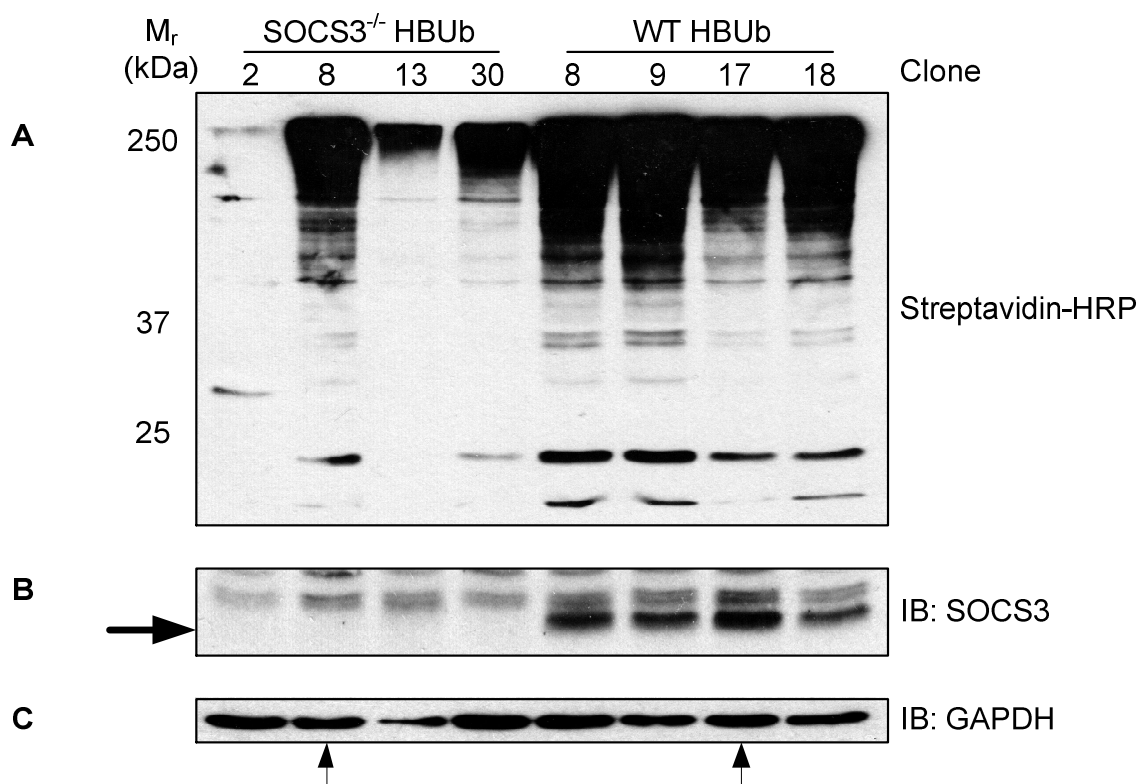


Figure 5.0: Selection of HBUb expressing clones

WT HBUb and SOCS3^{-/-} MEFs were grown in biotin-supplemented media (1 μ M) before enriching for ubiquitinated proteins with MG132 (6 μ M) for two hours prior to harvesting as described (Section 2.2.5.3). Soluble protein lysates were equalised and fractionated by SDS-PAGE. Expression of the HBUb-transgene and SOCS3 was assessed using streptavidin-HRP (Panel A) and anti-SOCS3 antibody (Panel B). GAPDH was used as a loading control (Panel C). A large arrow indicates SOCS3 while small arrows indicate WT and SOCS^{-/-} MEF clones used for further experimentation.

5.2.2 Preparation of differentially SILAC-labelled, TAP-isolated ubiquitinome for mass spectrometry

Using SOCS3^{-/-} HBUb clone 8 and WT HBUb clone 17, the previously optimised experimental strategy (Section 1.5, figure 1.11) was performed. In addition, small adjustments were made to improve SILAC labelling and the recovery of the ubiquitinome. This involved a period of pre-SILAC labelling during cell expansion and the use of 20x15cm tissue culture dishes. It was previously demonstrated that SILAC media supplemented with dialysed serum does not affect cell viability (Section 4.3.2.1) and so longer incubation periods were not expected to be an issue. Briefly, prior to seeding cells into dishes, cells were adapted to dialysed serum-supplemented control (R0K0) media while being expanded in T150 flasks as before. After reaching ~80% confluency, cells that were to be heavy labelled were passaged into SILAC media (R6K6) while unlabelled cells were passaged into control (R0K0) media. Cells were then allowed to expand to ~80% confluency (5-7 days) after which time they were seeded into 20x15cm dishes at a density (1:5) sufficient to achieved confluency over 5 days. As such, SILAC labelling was performed for double the time previously assessed during optimisation and should therefore achieve greater incorporation of the SILAC isotope. To reduce workload, forward (WT HBUb=R6K6/heavy media, SOCS3^{-/-} HBUb=R0K0/light control media) and reverse (WT HBUb=R0K0/light control media, SOCS3^{-/-} HBUb=R6K6/heavy media) labelling experiments were performed separately. Furthermore, for the same reason, treatment (MG132 (6µM), Na₃VO₄ (1mM), forskolin (50µM) for two hours plus H₂O₂ (0.2mM) for the final 30 minutes) and harvesting (Section 2.2.5.3) of the WT HBUb and SOCS3^{-/-} HBUb cells were also performed separately. Harvested cells were then flash-frozen using dry ice and methanol before storing at -80°C prior to further processing.

Using this approach, the forward labelling experiment produced a total of 170mg (From WT HBUb=86.4mg; SOCS3^{-/-} HBUb=135mg) of protein following equalisation and mixing. The reverse labelling experiment produced a total of 400mg (From WT HBUb = 340.6mg; SOCS3^{-/-} HBUb=237.4 mg) of protein following equalisation and mixing.

Prior to mixing cell lysates and further processing, expression of the HBUb transgene was re-evaluated. Cell lysates were equalised prior to fractionation by SDS-PAGE and expression of the HBUb transgene and SOCS3 induction were analysed by immunoblotting (Figure 5.1). The HBUb transgene was expressed to comparable levels in cell lysates from forward and reverse labelling experiments (Figure 5.1, panel A). Furthermore, SOCS3 was induced in WT HBUb but not SOCS3^{-/-} HBUb MEFS (Figure 5.1, panel B, arrow).

After equalisation and mixing of cell lysates, tandem affinity purification (Section 2.2.7) and protein concentration (Section 2.2.9.1) was performed. The generated TAP eluate was fractionated by SDS-PAGE (Section 2.2.9.2) prior to preparing gel slices (Section 2.2.9.2) for in-gel trypsin digestion (Section 2.2.9.3). Following Coomassie staining of the TAP eluate from forward and reverse labelling experiments, a high molecular weight smear typical of ubiquitinated proteins was detected (Figure 5.2). This suggests that sufficient material was recovered for mass spectrometric analysis. Additionally, unmixed cell lysates from the same experiments showed comparable Coomassie staining suggesting that cell lysates were correctly equalised prior to mixing and TAP. This is important since incorrect equalisation could adversely affect data by the generation of false-positives during quantitation.

Finally, in-gel trypsin-digested (Section 2.2.9.3) samples were submitted for LC-MS/MS using an Orbitrap Velos Fourier transform mass spectrometry (FTMS), operated by William Mullen (University of Glasgow, Proteomics Biomarkers and Systems Medicine). Retrieved spectrometric data was then automatically analysed using Mascot and MaxQuant. Using the generated information, raw mass spectra was also manually assessed using the Orbitrap control and monitoring software Xcalibur v2.1 (Thermo Scientific).

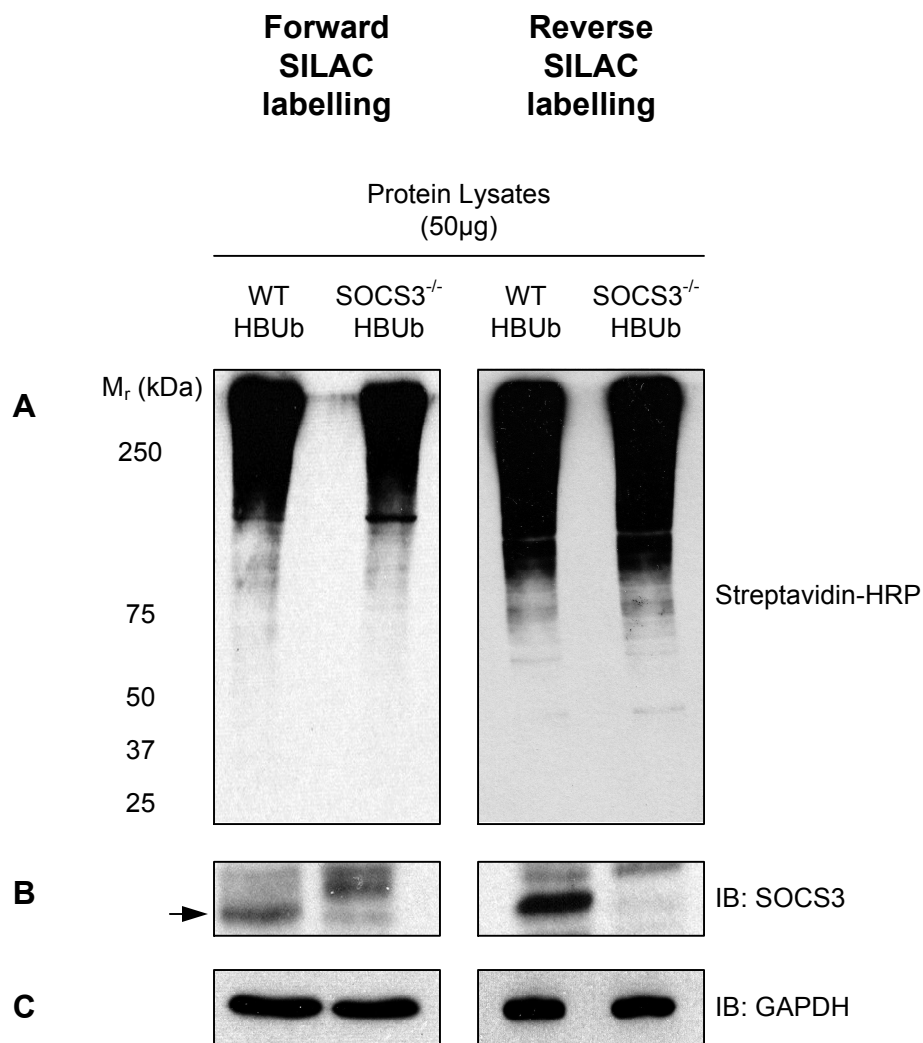


Figure 5.1: Evaluation of HBUb transgene expression and SOCS3 induction prior to TAP and MS

WT HBUb and SOCS3^{-/-} HBUb MEFs were SILAC-labelled as described (Section 5.2.2). Prior to harvesting (Section 2.2.5.3), MEFs were treated with MG132 (6µM), Na₃VO₄ (1mM), and forskolin (50µM) for two hours. Cells were treated with H₂O₂ (0.2mM) for the final 30 minutes. Soluble protein lysates were then equalised and fractionated by SDS-PAGE. HBUb-transgene and SOCS3 expression were assessed using streptavidin-HRP (Panel A) and anti-SOCS3 antibody (Panel B) respectively. GAPDH was used as the loading control (Panel C). Arrow indicates SOCS3.

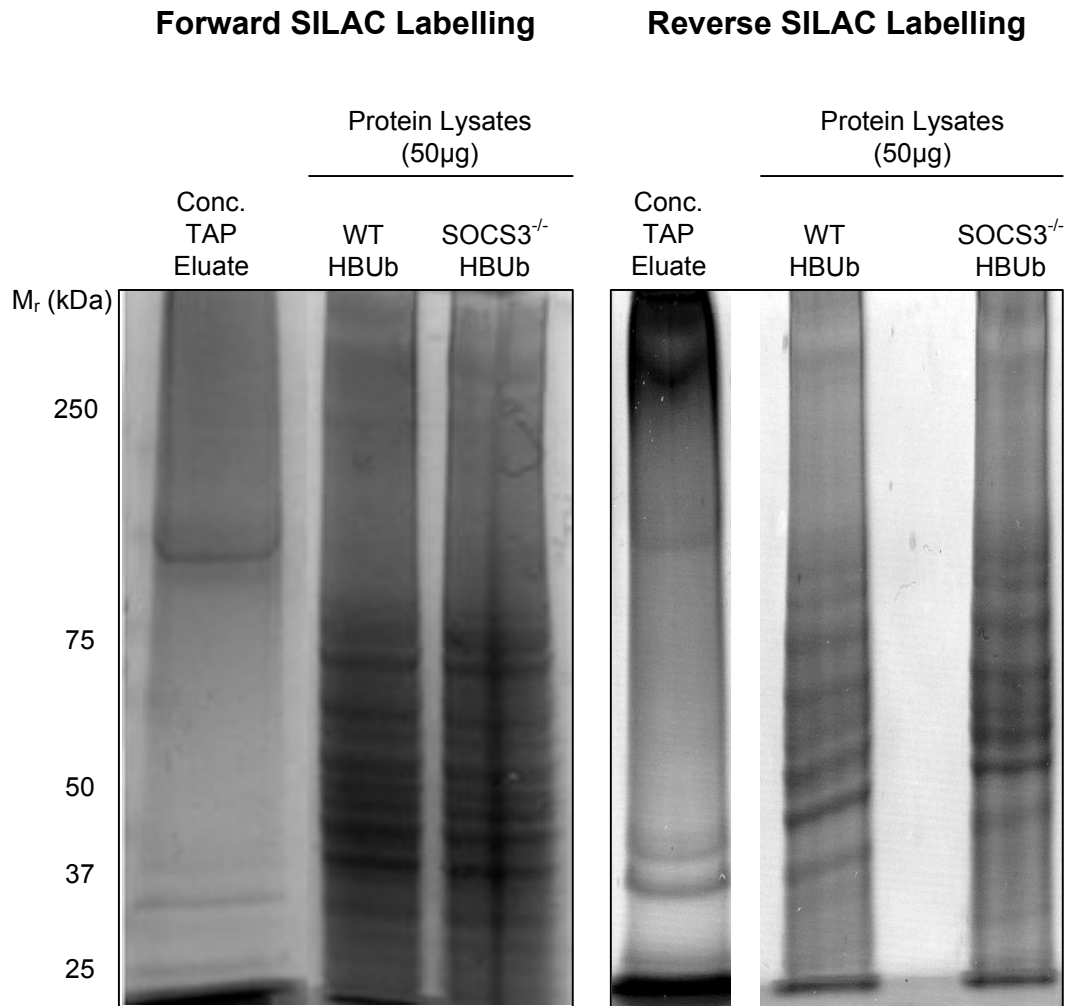


Figure 5.2: Fractionation of concentrated SILAC-labelled, TAP-isolated HBUb-modified proteins prior to MS

WT HBUb and SOCS3^{-/-} HBUb MEFs were SILAC-labelled as described (Section 5.2.2). Prior to harvesting (Section 2.2.5.3), MEFs were treated with MG132 (6µM), Na₃VO₄ (1mM), and forskolin (50µM) for two hours and with H₂O₂ (0.2mM) for the final 30 minutes. After equalisation and mixing of cell lysates, tandem affinity purification (Section 2.2.7) and protein concentration (Section 2.2.9.1) was performed and the generated sample fractionated by SDS PAGE (Section 2.2.9.2). Recovery of HBUb-modified proteins was assessed *via* Coomassie staining. The concentrated TAP eluate from forward labelled (Left panel) and reverse labelled (Right panel) experiments are compared with equalised, unmixed cell lysates from the sample experiment.

5.2.3 Data analysis

5.2.3.1 Mascot-based protein identification and mass spectra analysis of raw MS data

Potential SOCS3-dependently ubiquitinated targets are expected to be enriched in WT HBUb MEFs but not SOCS3^{-/-} HBUb MEFs. To identify the presence of these proteins, raw MS data from the forward SILAC-labelled experiment was searched using the Mascot search engine as described (Section 2.2.10.1). Prior to MS, the SDS-PAGE-fractionated TAP eluate was sectioned into several manageable gel slices and then processed and analysed separately (Section 2.2.9.2). As such, the Mascot search engine returned several lists of identified proteins with each set corresponding to a specific gel slice/mass range. Furthermore, separate searches were performed for proteins containing only labelled or unlabelled peptides. Peptides detectable in heavy-labelled WT HBUb MEFs but not light-labelled SOCS3^{-/-} HBUb MEFs were extracted from the returned results (Table 5.0). A total of 73 proteins were identified to be exclusively from heavy labelled WT HBUb MEFs. Several of these proteins were identified in multiple mass ranges, a characteristic typical of polyubiquitinated species (Table 5.0, dark grey boxes). Supporting this observation, many of these proteins had an expected mass much lower than the mass range from which they were extracted e.g. cavin-1 (PTRF, O54724) a protein with a predicted mass of ~44kDa was detected in gel slice corresponding to a mass range of 75-100kDa (Table 5.0, protein 47, light grey box). Importantly, a known SOCS3-dependently ubiquitinated substrate FAK1 was identified (Table 5.0, protein 43, bold, light grey box). Furthermore, a component of the SOCS3-E3 complex, cullin5 (Table 5.0, protein 52, bold, light grey box) was also identified.

Using returned Mascot search data, mass spectra from selected peptides were manually assessed. Selected peptides included a protein detected in WT HBUb MEFs and SOCS3^{-/-} HBUb MEFs, pyruvate kinase i.e. a probable non-SOCS3 substrate (Figure 5.3), the known SOCS3 substrate FAK1 (Figure 5.4), and a potential SOCS3 substrate, cavin-1 (Figure 5.5). Spectra were assessed for the presence of peaks relating to heavy or light-labelled species. Doing so would confirm that proteins have been identified as being exclusively from the heavy-labelled WT HBUb MEFs i.e. they do not have a light-labelled peptide equivalent.

Furthermore, the conversion of $^{13}\text{C}_6$ -arginine to $^{13}\text{C}_6$ -proline was assessed which if present, is expected to produce satellite peaks shifted by 5Da from the mono-isotopic peak.

Analysis of the spectra for pyruvate kinase (Figure 5.3, panel A, arrows indicate monoisotopic peaks), detected two sets of peaks relating to doubly charged peptides with a C-terminal arginine (Figure 5.3, panel B1/2). The nature of the charge meant that the observed mass was half that of the expected mass. The ladder peaks to the right of the monoisotopic peaks related to the incorporation of naturally present ^{13}C (~1.1% of total). The observed monoisotopic peaks were separated by 3Da suggesting that this shift is due to the SILAC isotope. Furthermore, these peaks were of similar intensity i.e. a SILAC ratio ~1. Additionally, the conversion of $^{13}\text{C}_6$ -arginine to $^{13}\text{C}_5$ -proline could not be detected since no significant peaks were visible at the expected location of 779.8Da i.e. 2.5Da to the right of the heavy-labelled monoisotopic peak. These data confirmed that the protein was present in both differentially labelled cells and is therefore not expected to be a substrate of SOCS3. Furthermore, this data did not seem to be affected by $^{13}\text{C}_5$ -proline contamination suggesting that SILAC ratios can be accurately calculated from the monoisotopic peaks.

In contrast to pyruvate kinase, the spectra of the known SOCS3 substrate FAK1 (10) (Figure 5.4, panel A, arrows indicate monoisotopic peaks), detected a single doubly charged monoisotopic peak. This protein was identified *via* a search using the SILAC label as a fixed modification and is therefore expected to be a heavy-labelled peptide. No peak corresponding to a doubly-charged light-labelled peptide was detected at the predicted location of 578.3Da i.e. 3Da to the left of the heavy-labelled monoisotopic peak. As such, the SILAC ratio could not be estimated. This data confirmed that the protein was correctly identified as being present in only heavy-labelled cells. However, in contrast to pyruvate kinase which was identified from several high-scoring peptides (data not shown), FAK1 was identified from a single peptide with a low score. This resulted in a protein score of 866/595 for pyruvate kinase (Figure 5.3, panel B1/2) as opposed to 26 for FAK1 (Figure 5.4, panel B), although this result is still above the limit of 19 set by the significance threshold ($p < 0.05$). As such, while being exclusively found in WT HBUb MEFs, the peptide might still be incorrectly assigned.

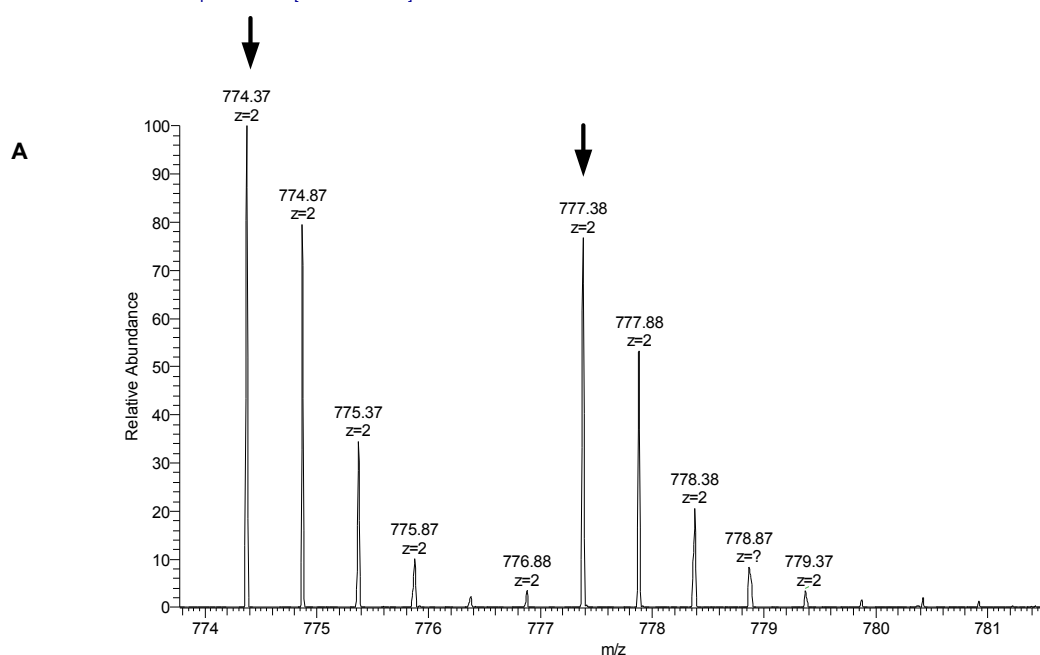
Cavin-1 was identified from several low-scoring peptides (Figure 5.5, panel B, full peptide list not shown) with a protein score of 21. An intense peak at 449.11Da prevented clear analysis of the spectra (Figure 5.5, panel A). However, a single doubly charged monoisotopic peak was identified (Figure 5.5, panel A, arrows indicate monoisotopic peaks). This protein was identified by a search using the SILAC label as a fixed modification and is therefore expected to be a heavy labelled peptide. However, no peak corresponding to a doubly-charged light-labelled peptide was detected at the predicted location of 448.74Da i.e. 3Da to the left of the heavy-labelled monoisotopic peak. As such, the SILAC ratio could not be estimated. This data confirmed that the protein was correctly identified as being present in only heavy-labelled cells and as such might be a potential SOCS3 substrate.

The Mascot search engine performed peptide assignment while considering modifications due to phosphorylation and ubiquitination. However, for the data presented, no modifications were identified. Furthermore, analysis of mass spectra allowed checks to be made with regards to peptide assignment and proline contamination. Moreover, from the peak intensities of SILAC-paired peaks of individual peptides, a SILAC ratio can be estimated. For example, pyruvate kinase had a SILAC ratio of ~1 whereas FAK1 and PTRF/cavin-1 would have had a much higher/significant SILAC ratio if the corresponding light peaks were visible. However, this project aims to identify specifically enriched proteins from calculated SILAC ratios. Such analysis must consider all peptides of a single protein simultaneously. The Mascot search engine cannot perform this analysis. As such, protein identified by Mascot might not be detected as being significantly enriched when all peptides are considered. For these reasons, MaxQuant data analysis was used as the primary tool for identifying potential SOCS3 substrates. Furthermore, this approach might be able to account for SILAC-paired peaks where the light peak is of low intensity such as in the case of FAK1 and cavin-1.

Table 5.0: Mascot analysis of the forward SILAC-labelling experiment

Using the Mascot Daemon server (v2.2), raw MS data from the forward SILAC-labelled experiment was searched using Mascot search engine as described (Section 2.2.10.1). Separate searches were performed for labelled and unlabelled peptides. Protein identifications with a significant score ($p < 0.05$) were accepted. Peptides detectable only in heavy-labelled WT HBUb MEFs were extracted from the returned results. Dark grey boxes indicate proteins found in several mass ranges. Light grey boxes indicate proteins of interest.

	Gel slice/ Mass range (kDa)	Gene Name	Uniprot accession number	Expected Size (kDa)		Gel slice/ Mass range	Gene Name	Uniprot accession number	Expected Size (kDa)
1	1 >>250	Trim27	Q62158	58.5	39	5 75 - 100	Psmc1	P62192	49.2
2		Sfi1	Q3UZY0	144.0	40		Impdh1	P50096	55.3
3		Lats2	Q7TSJ6	115.5	41		Aarsd1	Q3THG9	45.0
4		Ywhah	P68510	28.2	42		Ttll12	Q3UDE2	74.0
5		Actr1a	P61164	42.6	43		Ptk2/FAK1	P34152	23-123
6		Actr2	P61161	44.8	44		Tbc1d15	Q9CXF4	76.5
7		Trap1	Q9CQN1	80.2	45		Tubb2a	Q7TMM9	49.9
8		Fasn	P19096	272.4	46		Plod3	Q9R0E1	84.9
9	2 > 250	Tert	O70372	128.0	47	Ptrf/Cavin-1	O54724	44.0	
10		Fads2	Q9Z0R9	52.4	48	Exosc3	Q7TQK4	29.5	
11		Derl2	Q8BNI4	27.6	49	Fam132a	Q8R2Z0	33.3	
12		Maged1	Q9QYH6	85.7	50	Ssbp1	Q9CYR0	17.3	
13		Kel	Q9EQF2	81	51	Zc3hav1	Q3UPF5	88-107	
14		Radil	Q69Z89	52-121	52	Cul5	Q9D5V5	91.0	
15		Peo1	Q8CIW5	33-77	53	Anxa1	P10107	38.7	
16		Polr1a	O35134	194.1	54	Prkaa1	Q5EG47	63.9	
17	6 ~60 - 75	Cd2ap	Q9JLQ0	70	55	Ccdc50	Q810U5	30-35	
18		Mllt10	O54826	113.0	56	Wbp2	P97765	28.0	
19	3 150 - 250	Tubb2a	Q7TMM9	49.9	57	Stxbp1	O08599	68.0	
20		Maged1	Q9QYH6	85.7	58	Ube2n	P61089	17.1	
21	4 100 - 150	Rrp1	P56183	50.0	59	Psm6	Q9QUM9	27.4	
22		Usp5	P56399	95.8	60	Tert	O70372	128.0	
23		Fam63b	Q6PDI6	39-66	61	Actr1a	P61164	42.6	
24		Krt18	P05784	47.5	62	Actr2	P61161	44.8	
25		Eps15	P42567	64-98	63	Mllt10	O54826	113.0	
26		Mbtps1	Q9WTZ2	117.5	64	Eral1	Q9CZU4	48.2	
27		Tubb2a	Q7TMM9	49.9	65	Peo1	Q8CIW5	33-77	
28		Eps15l1	Q60902	75-99	66	Kel	Q9EQF2	81	
29	Tert	O70372	128.0	67	Radil	Q69Z89	52-121		
30	Rps3	P62908	26.7	68	Polr1a	O35134	194.1		
31	Psm2	Q8VDM4	100.2	69	Cd2ap	Q9JLQ0	70.4		
32	Trap1	Q9CQN1	80.2	70	Derl2	Q8BNI4	27.6		
33	Cep135	Q6P5D4	133.3	71	Krt18	P05784	47.5		
34	Mllt10	O54826	113.0	72	8 30 - 40	N4bp2l2	Q8JZS6	54-66	
35	Hgs	Q99LI8	86.0	73		Rps4x	P62702	29.6	
36	5 75 - 100	Tuba1b	P05213	50.2					
37		Nsfl1c	Q9CZ44	29-40					
38		Rabgef1	Q9JM13	56.9					



B1

PYC MOUSE	Mass: 130344	Score: 866	Queries matched: 121	emPAI: 1.05		
Pyruvate carboxylase, mitochondrial OS=Mus musculus GN=Pc PE=1 SV=1						
Query Observed	Mr(expt)	Mr(calc)	ppm	Miss Score	Expect Rank	Peptide
3792	<u>774.3696</u>	1546.7246	1546.7263	-1.07	0	86 1.5e-08 1 R.AEAEQAQEELSFPR.S

B2

PYC MOUSE	Mass: 130765	Score: 595	Queries matched: 94	emPAI: 0.90		
Pyruvate carboxylase, mitochondrial OS=Mus musculus GN=Pc PE=1 SV=1						
Query Observed	Mr(expt)	Mr(calc)	ppm	Miss Score	Expect Rank	Peptide
3798	<u>777.3800</u>	1552.7454	1552.7464	-0.64	0	61 5.1e-06 1 R.AEAEQAQEELSFPR.S

Figure 5.3: Spectra of pyruvate carboxylase, a protein detectable in differentially labelled WT HBUb and SOCS3^{-/-} HBUb MEFs

Using the Mascot Daemon server (v2.2), raw MS data from the forward SILAC-labelled experiment was searched using Mascot search engine as described (Section 2.2.10.1). Separate searches were performed for labelled and unlabelled peptides. Proteins containing peptides detectable in heavy-labelled WT HBUb and light-labelled SOCS3^{-/-} MEFs were extracted from the returned results. Spectra of peptides from identified proteins were manually analysed using Xcalibur 2.1 (Thermo Scientific). **A.** Mass spectra of pyruvate carboxylase. **B.** Selected data returned by the Mascot search engine. B1. Unlabelled peptide search. B2. Labelled peptide search. Arrows indicate locations of monoisotopic peaks of heavy or light-labelled peptides. Ions score is $-10 \cdot \log(P)$, where P is the probability that the observed match is a random event. Individual ions scores > 19 indicate identity or extensive homology ($p < 0.05$).

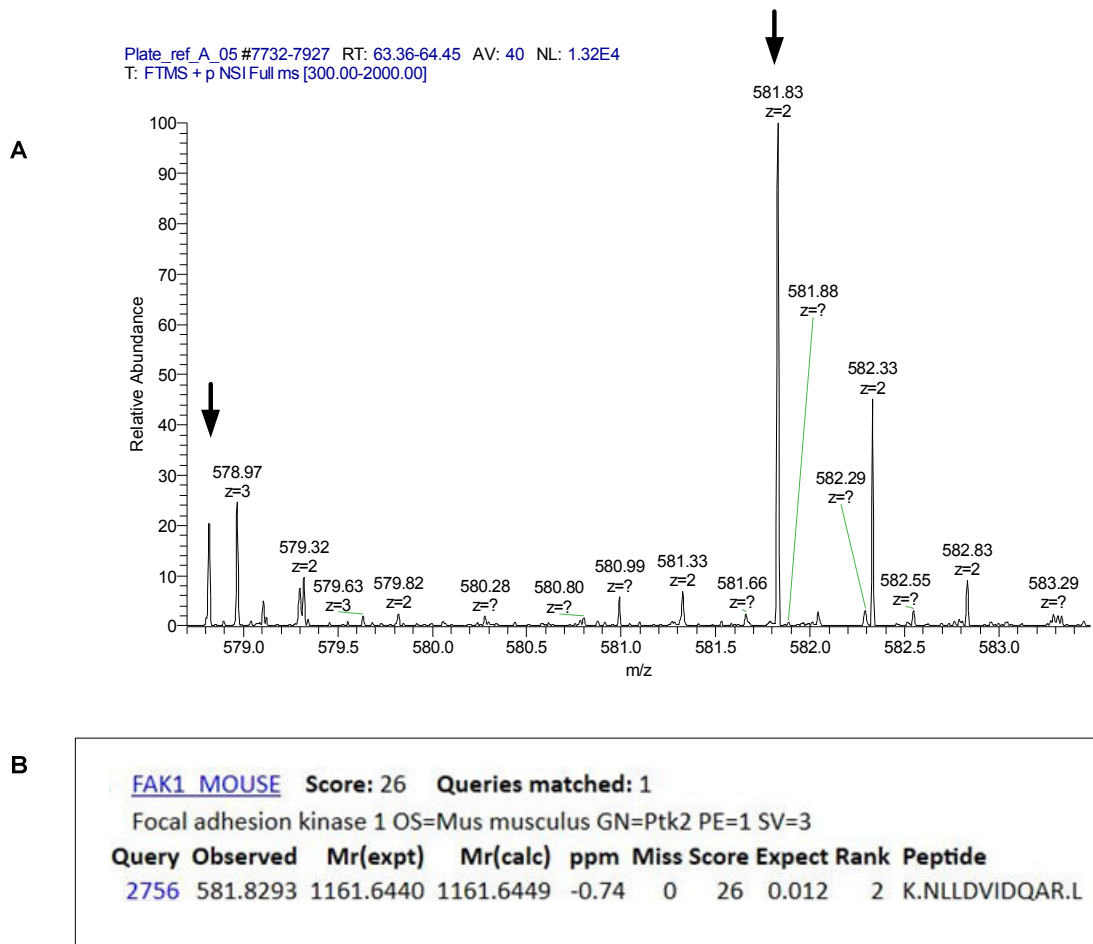
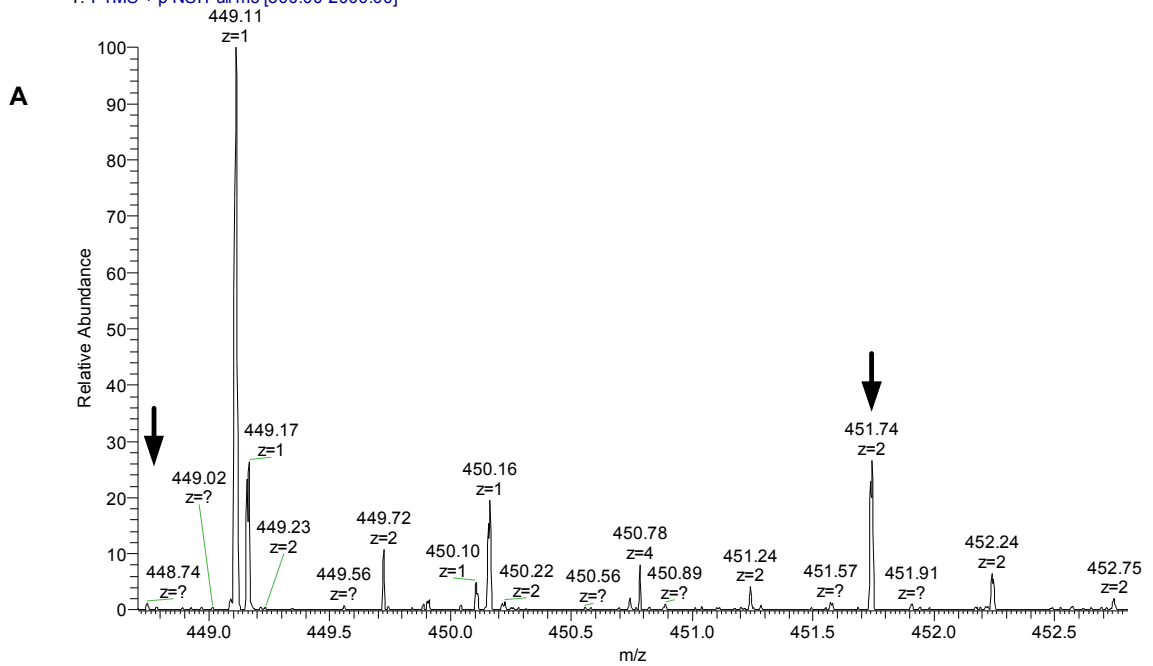


Figure 5.4: Spectra of a known SOCS3-dependently ubiquitinated substrate, FAK-1, detectable in heavy-labelled WT but not light-labelled SOCS3^{-/-} MEFs

Using the Mascot Daemon server (v2.2), raw MS data from the forward SILAC-labelled experiment was searched using Mascot search engine as described (Section 2.2.10.1). Separate searches were performed for labelled and unlabelled peptides. Proteins containing peptides detectable only in heavy-labelled WT HBUb MEFs were extracted from the returned results. Spectra of peptides from proteins identified by this search were manually analysed using Xcalibur 2.1 (Thermo Scientific). **A.** Mass spectra of FAK1. **B.** Selected data returned by the Mascot search engine. Arrows indicate locations/expected locations of monoisotopic peaks of heavy or light labelled peptides respectively. Ions score is $-10 \cdot \log(P)$, where P is the probability that the observed match is a random event. Individual ions scores > 19 indicate identity or extensive homology ($p < 0.05$).



B

PTRF MOUSE	Mass: 44102	Score: 21	Queries matched: 4	emPAI: 0.07					
Polymerase I and transcript release factor OS=Mus musculus GN=Ptrf PE=1 SV=1									
Query	Observed	Mr(expt)	Mr(calc)	ppm	Miss	Score	Expect	Rank	Peptide
1000	451.7447	901.4748	901.4756	-0.89	0	21	0.044	1	R.EGEVEVLK.A

Figure 5.5: Spectra of a potential SOCS3-dependently ubiquitinated substrate, PTRF (cavin-1) detectable in heavy-labelled WT but not light-labelled SOCS3^{-/-} MEFs

Using the Mascot Daemon server (v2.2), raw MS data from the forward SILAC-labelled experiment was searched using Mascot search engine as described (Section 2.2.10.1). Separate searches were performed for labelled and unlabelled peptides. Proteins containing peptides detectable only in heavy-labelled WT HBUb MEFs were extracted from the returned results. Spectra of peptides from proteins identified by this search were manually analysed using Xcalibur 2.1 (Thermo Scientific). **A.** Mass spectra of PTRF/cavin-1. **B.** Selected data returned by the Mascot search engine. Arrows indicate locations/expected locations of monoisotopic peaks of heavy or light-labelled peptides respectively. Ions score is $-10 \cdot \log(P)$, where P is the probability that the observed match is a random event. Individual ions scores > 19 indicate identity or extensive homology ($p < 0.05$).

5.2.3.2 MaxQuant: identification of potential SOCS3 substrates using SILAC ratios calculated using raw MS data

Raw MS data from both forward and reverse SILAC-labelling experiments were analysed using MaxQuant as described (Section 2.2.10.2 and Table 2.2). The subsequent ProteinGroups.txt results table generated by MaxQuant was manually assessed. Detected contaminants were removed and proteins arranged by their \log_2 -transformed, normalised SILAC ratios (Figure 5.6, Tables 5.1 and 5.2). SILAC ratio is taken as H/L for the forward-labelling experiment (WT HBUB=heavy, SOCS3^{-/-} HBUB=light) and L/H for the reverse (WT HBUB=light, SOCS3^{-/-} HBUB=heavy).

Analysis of both forward and reverse experiments produced a similar pattern of SILAC ratio distributions (Figure 5.6). However, while several proteins were found significantly enriched (\log_2 (normalised SILAC ratio) > 1 i.e. a two fold increase) in the forward experiment, only one was found in the reverse experiment. Most proteins had an unvarying SILAC ratio ($-1 > \log_2$ (normalised SILAC ratio) < 1) suggesting that they were detectable in WT HBUB and SOCS3^{-/-} HBUB MEFs. Several proteins were found enriched in SOCS3^{-/-} HBUB MEFs (\log_2 (normalised SILAC ratio) < -1) and as such might be a consequence of the deletion of SOCS3. For example, if there is a case where SOCS3 ubiquitinates another E3 ligase, then substrates of this E3 might be enriched in the differentially-labelled SOCS3^{-/-} MEFs. These extra data may contribute to the identification of further SOCS3 substrates. While these proteins might be of interest in the future, they were not considered here.

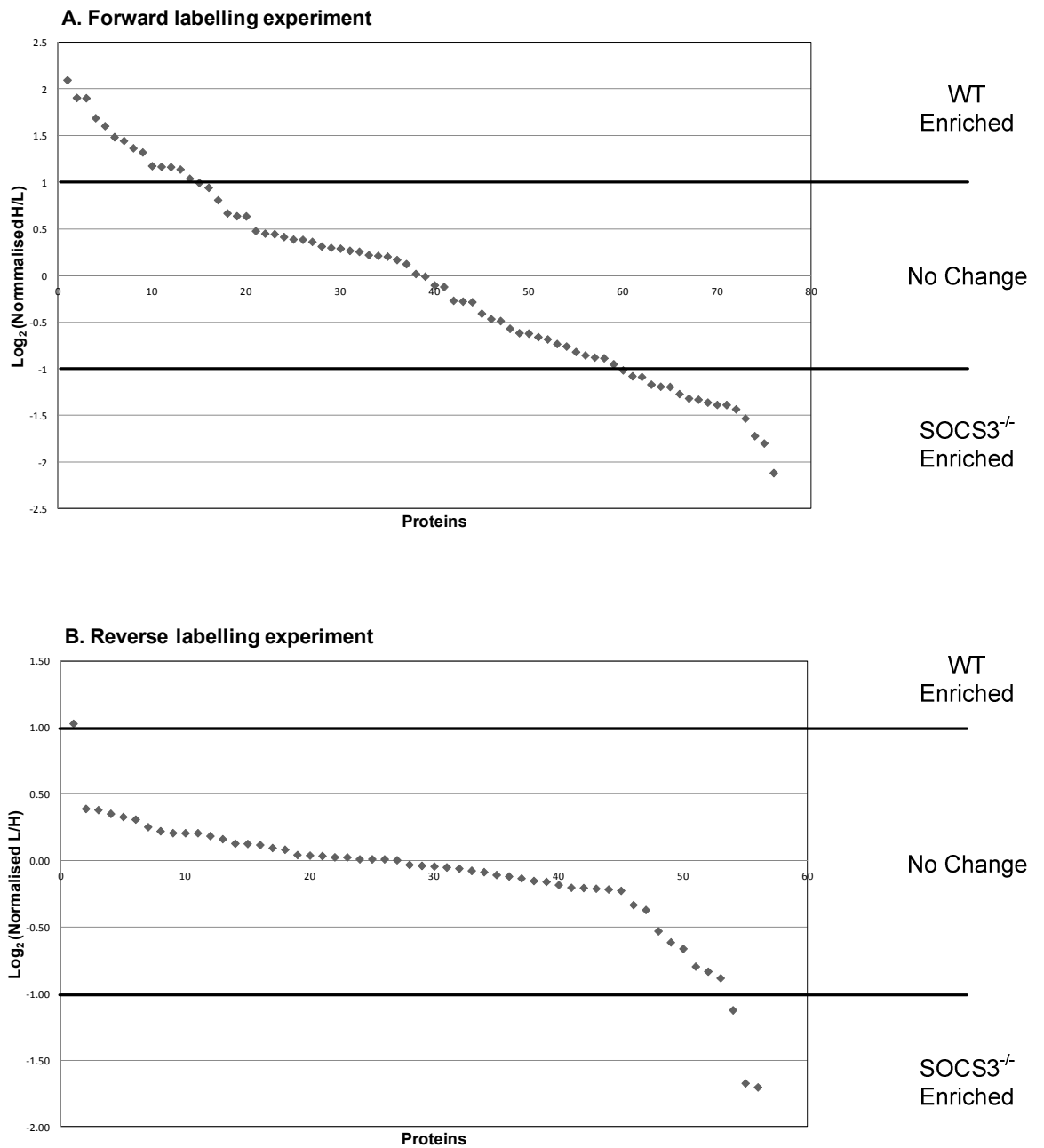


Figure 5.6: Value-ordered plots of log₂-transformed normalised SILAC ratios from forward and reverse SILAC-labelled experiments

Raw MS data was analysed using MaxQuant as described (Section 2.2.10.2 and Table 2.2). Detected contaminants were removed and proteins arranged by their log₂-transformed, normalised SILAC ratios. **A.** Forward-labelling experiment. **B.** Reverse labelling experiment. Proteins with a log₂ SILAC ratio greater than 1 i.e. a two fold increase, is considered significant.

Selections of identified proteins with the highest SILAC ratios from forward and reverse experiments are presented in Table 5.1 and 5.2. Seventy-six proteins were identified overall in the forward-labelling experiment, and using normalised SILAC ratios, 15 were found to be significantly enriched (Table 5.1, double line indicates cut-off). Most of these proteins were identified from multiple unique peptides, with a high sequence coverage and a low PEP score (FDR<1%). Furthermore, multiple SILAC-paired peaks were used to calculate the SILAC ratio (Ratio H/L count). As such, these characteristics increased confidence in protein assignment. Interestingly, several proteins found using Mascot were also identified using MaxQuant e.g. cavin-1. However, a known SOCS3-dependently ubiquitinated substrate FAK1 or the SOCS3 E3 component cullin5 were not detected. This might be a consequence of the mode of SOCS3 induction i.e. forskolin and being a non-SOCS3 substrate respectively. In contrast, in the reverse experiment, while having slightly improved peptide identification characteristics, only 56 proteins were identified with only a single protein identified as being significantly enriched in the WT HBUb MEFs (Table 5.2, Maged1, protein 1). Furthermore, Maged1 was previously identified (Table 5.1, protein 17) as an unvarying protein. As such, Maged1 was not considered as a potential SOCS3 substrate. Additionally, while a few ubiquitinated lysine residues were identified in both experiments, no phosphorylated residues could be found.

While the SILAC ratios are disappointing, many proteins were identified in both forward and reverse experiments. Out of 76 proteins found in the forward labelling experiment, 44 (out of 56) were found in the reverse experiment (Tables 5.1 and 5.2, **bold**, full list not shown). Ten of these 48 proteins were found to be significantly enriched in the forward labelling experiment. Over these two experiments, while similar arrays of proteins were identified, the SILAC ratios were not replicated. This is indicative of experimental error although the source of this error is not apparent. A comparison of the total ion chromatograms (TIC, the summed ion intensities of each mass spectrum plotted against time) of both experiments showed a more intense signal was produced for the reverse experiment as indicated by the normalised level (NL) (Figure 5.7, lower panel vs. upper panel). Furthermore, extracted spectra contained more

complex/improved peak information (data not shown). This is supported by the improved sequence coverage and ratio H/L count (Table 5.2 vs. Table 5.1).

Ubiquitin was detected in both forward (Table 5.1, dark grey box, protein 34) and reverse experiments (Table 5.2, dark grey box, protein 34). This allowed the quality of the data to be assessed. For the forward-labelled experiment, ubiquitin was identified using 16 unique peptides and an 88% sequence coverage whereas the reverse used 10 unique peptides and 85.6% sequence coverage. Furthermore, MaxQuant was able to identify six out of seven ubiquitinated lysine residues in the forward experiment whereas only two were identified in the reverse. Importantly, for both cases, the \log_2 -transformed normalised SILAC ratios were approximately zero indicating that ubiquitin/HBUb was expressed to comparable levels in WT HBUb and SOCS3^{-/-} HBUb MEFs. Furthermore, it also suggests the complete incorporation of the SILAC label. As such, it can be concluded that the data from both experiments is of similar quality.

Table 5.1: MaxQuant analysis of forward labelling experiment

MS data was analysed using MaxQuant as described (Section 2.2.10.2). Proteins were arranged by their log₂-transformed, normalised SILAC ratio. Proteins in **bold** were also found in the reverse-labelling experiment. Light grey/dotted boxes indicate proteins investigated further (Section 6.0). Dark grey box indicates ubiquitin.

	Gene Names	Uniprot Accession Number	Peptides/Unique		Unique Sequence Coverage [%]	PEP	Ratio H/L / Normalised H/L		Log ₂ Normalised H/L ratio	Ratio H/L Count	GlyGly (K) Site
1	Usp5	P56399	4	4	5.6	1.52E-09	2.66	4.28	2.10	5	
2	Eps15l1	Q60902-1	1	1	1.2	9.62E-11	2.37	3.75	1.91	1	
3	Uchl1	Q3TCH2	1	1	8	0.00263	2.69	3.74	1.90	1	
4	Ube1	Q02053	9	9	10.9	3.43E-44	1.96	3.22	1.69	8	
5	Ccdc113	Q8C5T8	1	1	3.4	0.107	1.86	3.04	1.60	2	145
6	Psmc2	Q8VDM4	3	3	4.2	4.68E-14	1.90	2.80	1.49	9	
7	Smt3h1	Q9Z172-1	1	1	10.9	7.99E-06	3.41	2.72	1.45	3	
8	Cavin-1	O54724	5	5	15.8	1.26E-48	4.05	2.58	1.37	6	
9	Sqstm1	Q64337-1	8	8	32.6	4.29E-85	3.62	2.50	1.32	14	
10	Impdh	P24547	4	4	8.1	9.22E-14	3.49	2.26	1.18	4	
11	Abi2	Q6AXD2	1	1	3.3	0.001494	3.11	2.25	1.17	1	
12	H3.3a	P84244	3	3	12.7	7.62E-05	3.28	2.24	1.16	7	
13	Hgs	Q99L18	2	2	2.6	0.001888	1.38	2.20	1.14	1	
14	Rps3	P62908	2	2	10.3	2.97E-08	1.29	2.06	1.04	2	
15	Fam63b	Q6PDI6-1	1	1	2.5	0.000195	1.48	1.99	1.00	1	
16	Vcp	Q01853	11	11	16.7	2.17E-36	1.16	1.92	0.94	11	
17	Maged1	Q571N9	1	1	1.4	2.74E-06	2.74	1.75	0.81	2	
18	Hsc70	P63017	19	19	37.8	3.47E-123	1.92	1.59	0.67	46	
19	Hist1h2bp	Q8CGP2-2	2	2	13	0.008093	2.28	1.56	0.64	2	
20	Ube2n	P61089	1	1	5.4	8.59E-10	2.69	1.56	0.64	1	
21	Vim	P20152	8	8	17.8	8.42E-20	1.81	1.39	0.48	15	
22	Eps15	P42567-1	2	2	3	2.34E-15	0.86	1.37	0.45	2	
23	Ttn	A2ASS6-1	1	1	0	0.16482	1.89	1.36	0.45	1	4963
24	Psmc1	P62192	2	2	9.3	0.001057	2.12	1.33	0.42	2	
25	Rad23b	P54728	3	3	5.3	0.000183	1.99	1.31	0.39	11	
26	H2a.x	P27661	3	1	13.3	8.77E-20	2.69	1.31	0.39	8	
27	Ccdc50	Q810U5-1	1	1	3.9	3.28E-09	1.44	1.29	0.36	1	
28	Rabgef1	Q9JM13	4	4	8.1	5.96E-08	1.52	1.24	0.31	3	
29	Hsp90aa1	P07901	10	3	5.2	3.66E-54	1.02	1.23	0.30	5	
30	Tbc1D15	Q9CXF4	3	3	4.9	1.89E-08	1.57	1.22	0.29	3	
31	Hsp90ab1	Q71LX8	11	1	1.5	2.53E-57	1.29	1.20	0.27	28	
32	Nsf1c	Q9CZ44-3	6	6	20.2	3.32E-32	2.01	1.19	0.26	6	
33	Hsp90ab1	P11499	11	1	1.4	5.73E-53	1.34	1.17	0.22	4	
34	Ubc	P0CG50	16	16	88	4.02E-176	1.92	1.16	0.21	561	6;11;29;33;48;63
35	Anxa1	Q3US43	1	1	3.1	0.007636	1.26	1.15	0.21	1	
36	Rps10	P63325	5	5	30.9	4.74E-20	1.76	1.12	0.17	8	
37	Pcna	Q9CZD6	3	3	9.9	1.80E-08	1.29	1.09	0.13	3	
38	Stam	P70297	1	1	1.8	0.006177	1.22	1.01	0.02	1	
39	Pgam1	Q9DBJ1	3	3	14.6	0.000212	1.30	0.99	-0.01	3	5
40	Psmc4	O35226-2	1	1	4.5	1.60E-20	1.55	0.93	-0.10	1	

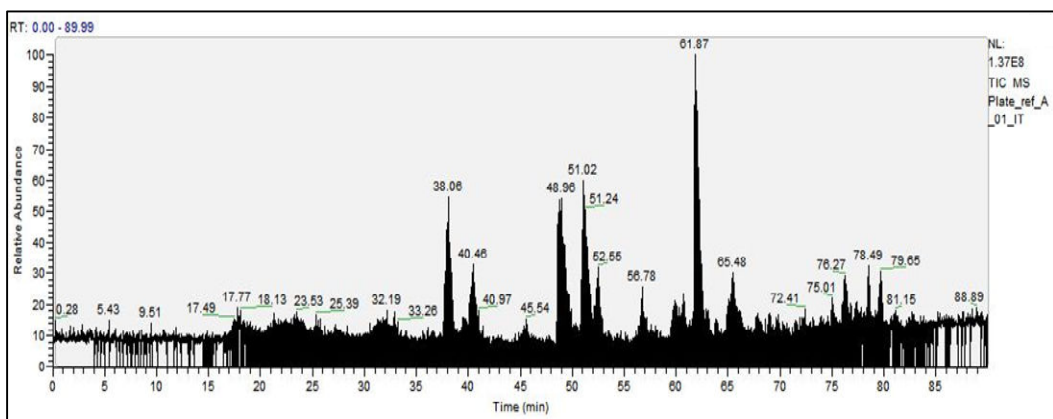
Table 5.2: MaxQuant analysis of reverse labelling experiment

MS data was analysed using MaxQuant as described (Section 2.2.10.2). Proteins were arranged by their log₂-transformed, normalised SILAC ratio. Proteins in **bold** were also found in the forward-labelling experiment. Light grey/dotted boxes indicate proteins investigated further (Section 6.0). Dark grey box indicates ubiquitin.

	Gene Names	Uniprot Accession Number	Peptides/ Unique		Unique Sequence Coverage [%]	PEP	Ratio H/L / Normalised H/L		Log2 Normalised L/H ratio	Ratio H/L Count	GlyGly (K) Site
1	Maged1	Q9QYH6	3	3	4.4	2.07E-06	0.48	0.49	1.03	8	
2	Rps3	P62908	3	3	14	5.29E-06	0.72	0.76	0.39	7	
3	Actg1	Q9QZ83	8	1	5.3	5.55E-37	0.78	0.77	0.38	6	
4	Psm�4	O35226-2	2	2	7.1	0.0001434	0.79	0.78	0.35	5	
5	Hsp90ab1	P11499	10	8	14.8	1.94E-25	0.78	0.80	0.33	51	
6	Impdh	P24547	7	7	16.2	1.08E-10	0.80	0.81	0.31	15	
7	Hsc70	P63017	15	15	27.7	3.12E-78	0.84	0.84	0.25	53	
8	Pcx	Q3T9S7	46	46	50.6	0	0.85	0.86	0.22	334	
9	Usp5	P56399	7	7	11.9	2.57E-12	0.78	0.87	0.21	13	
10	Acta	P68134	8	1	4.2	9.40E-38	0.90	0.87	0.21	11	
11	Rpl18	P35980	2	2	11.7	0.0008755	0.88	0.87	0.21	8	
12	Pcna	P17918	3	3	11.1	0.0007213	0.91	0.88	0.19	5	
13	Smt3h1	Q9Z172-1	1	1	10.9	2.83E-08	0.89	0.89	0.16	5	
14	Hist1h2bp	Q8CGP02	1	1	9.7	0.017583	0.90	0.91	0.13	3	
15	Pk3	P52480-1	3	3	6.6	3.49E-05	0.93	0.92	0.13	15	
16	Rps20	P60867	1	1	9.2	0.0064067	0.91	0.92	0.12	4	
17	Rad23b	P54728	2	2	4.3	0.0009927	0.86	0.93	0.10	5	
18	Rps7	D3YWP6	3	3	14.9	0.0002335	0.95	0.94	0.08	7	
19	Psmc2	P46471	1	1	2.3	0.001442	0.98	0.97	0.04	1	
20	Nsf1c	Q9CZ44-3	4	4	14.8	5.59E-09	0.99	0.97	0.04	8	
21	Lamr1	P14206	2	2	7.1	0.0033983	0.97	0.97	0.04	2	
22	Ldh1	Q3TCI7	2	2	7.5	2.93E-05	0.99	0.98	0.03	7	
23	Eps15	P42567-1	5	5	7.4	6.83E-38	0.96	0.98	0.03	5	
24	Psm�2	Q8VDM4	4	4	6.9	3.86E-10	0.96	0.99	0.01	14	
25	Eef1a	P10126	5	5	11.5	1.13E-15	1.00	0.99	0.01	40	
26	Cct8	P42932	2	2	3.6	0.0004716	0.98	0.99	0.01	5	
27	H2a.x	Q3THW5	3	3	20.2	9.91E-06	0.94	1.00	0.01	8	
28	Rps10	P63325	3	3	23	2.28E-09	1.02	1.02	-0.03	13	
29	Nono	Q99K48-1	3	3	5.3	2.90E-06	1.02	1.03	-0.04	7	
30	Rpl3	D3YZ47	2	2	5	0.0022049	1.04	1.03	-0.04	4	
31	Ccng2	O08918	1	1	2.3	0.01304	1.09	1.03	-0.05	3	262
32	Sqstm1	Q64337-1	4	4	15.2	7.49E-33	1.06	1.04	-0.06	14	
33	Mcca	Q99MR8	14	14	24.1	1.04E-27	1.07	1.05	-0.07	19	
34	Ubc	P0CG50	10	10	85.6	8.29E-124	1.08	1.06	-0.08	392	11;48
35	H3.3a	P84244	2	2	8.8	0.0021028	1.06	1.08	-0.11	8	
36	Pcca	Q91ZA3	11	11	19.3	1.36E-34	1.11	1.08	-0.12	29	
37	Rpl7	P14148	1	1	3.9	0.0058481	1.16	1.10	-0.13	1	
38	Vcp	Q01853	17	17	28.8	1.40E-70	1.02	1.11	-0.15	28	
39	Ddx2b	P10630-2	2	2	5.4	0.0015976	1.11	1.11	-0.16	5	
40	Ube1	Q02053	9	9	11.8	6.56E-22	1.09	1.13	-0.18	21	
41	Cavin-1	O54724	5	5	15.1	2.45E-08	1.18	1.15	-0.20	11	

Forward-labelling experiment

Normalised Level (NL):1.37E8



Reverse-labelling experiment

Normalised Level (NL):1.26E9

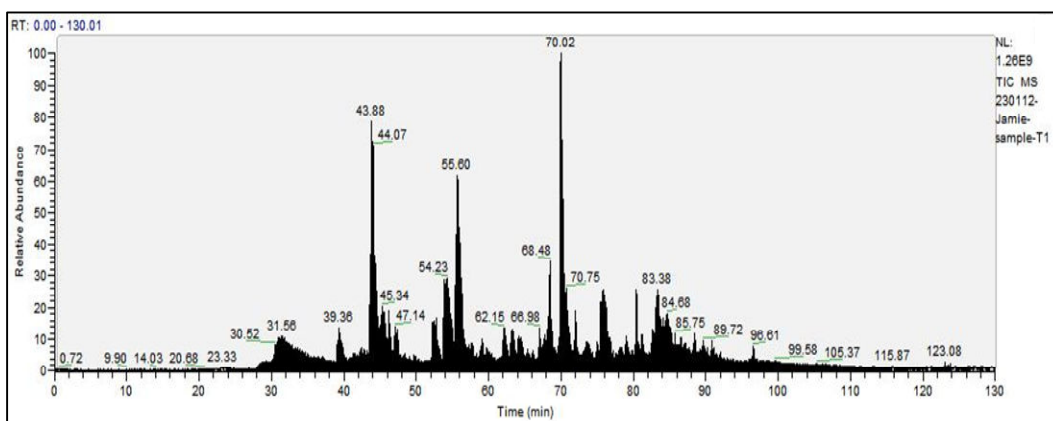


Figure 5.7: Total ion chromatogram from forward and reverse-labelled experiments

Representative total ion chromatograms (TIC), the summed ion intensities of each mass spectrum plotted against time, of forward (Upper panel) and reverse (Lower panel) labelled experiments using Xcalibur v2.1 (Thermo Scientific). Data was obtained under the same conditions using an Orbitrap Velos Fourier Transform Mass Spectrometer (FTMS), operated by William Mullen (University of Glasgow, Proteomics Biomarkers and Systems Medicine).

5.3 Conclusions

Using Mascot and MaxQuant I aimed to identify protein specifically enriched in the WT HBUb but not SOCS3^{-/-} HBUb MEFs. In doing so, I might be able to identify SOCS3-dependently ubiquitinated substrates. Using Mascot, it was possible to identify proteins present in only WT HBUb MEFs or in WT HBUb and SOCS3^{-/-} HBUb MEFs. The repeated identification of several proteins in different gel slices/mass ranges suggested that these proteins were ubiquitinated with several different lengths of polyubiquitin-chain. Furthermore, using the approach, a known SOCS3-dependently ubiquitinated substrate, FAK1, was identified. However, it was not detected in the subsequent MaxQuant analysis suggesting that it was not sufficiently enriched, perhaps due to the mode of SOCS3 induction or incorrectly assigned by Mascot due to the method of identification i.e. single low scoring peptide. In contrast, other proteins such as cavin-1 were found using MaxQuant.

Using the data returned by Mascot I was also able to manually assess the raw mass spectra of pyruvate kinase, which was detected in WT HBUb and SOCS3^{-/-} HBUb MEFs i.e. a probable non-SOCS3 substrate, FAK1, and a potential SOCS3 substrate, cavin-1. It was shown that these proteins were correctly assigned from the presence of heavy and/or light peaks and from an estimation of the SILAC ratio. Additionally, analysis of mass spectra found that there was no detectable contamination from ¹³C₆-arginine to ¹³C₆-proline conversion.

The aim of the project was to analyse the enrichment of proteins in a specific cell type facilitated by SILAC. This was not possible using Mascot. MaxQuant was designed specifically for SILAC studies and so it was used as the primary tool for identifying potential SOCS3 substrates. Seventy-six proteins were found in the forward-labelled experiment whereas only 56 were found in the reverse. Furthermore, a large proportion (44 proteins) of these proteins was detected in both experiments. However, only 15 proteins were found to be significantly enriched ($\log_2(\text{normalised H/L})$) in the WT HBUb MEFs.

Interestingly, SOCS3 itself was not identified using either Mascot or MaxQuant. This might be considered surprising given that SOCS3 has been shown to be

degraded concomitantly with its substrates, suggesting autoubiquitination (11,12). As such, SOCS3 might have been expected to be isolated during TAP of the ubiquitinome. It may be possible that the experimental context prevented autoubiquitination i.e. cAMP-dependent SOCS3 induction and/or phosphorylation-dependent inhibition following $\text{Na}_3\text{VO}_4/\text{H}_2\text{O}_2$ treatment. If this is the case then this too would have contributed to the low numbers of proteins detected. Alternatively, MaxQuant and/or its quantitation parameters might also be responsible. For quantification purposes, a single SILAC ratio was required (Table 2.2, minimum ratio count= 1). Since SOCS3 was absent in the SOCS3^{-/-} MEFs, no SILAC-paired peaks (clearly visible for pyruvate kinase, figure 5.3) would have been detected and thus not reported by MaxQuant. As such, this too would have contribute to the low number of proteins detected since SOCS3-ubiquitinated substrates would only be detected in one cell type, no SILAC-paired peaks detected and so no SILAC ratio would be calculated or protein reported. This might explain why FAK1 was detected using Mascot but not MaxQuant i.e. undetectable SILAC pair. However, this is not the case here, at least in the forward experiment, since several proteins were enriched in the presence but not absence of SOCS3 while others such as ubiquitin had the expected character. The detection of these proteins might be a consequence of using the MaxQuant “re-quantify” option, which forces MaxQuant to look for peaks pairs. If peaks are found then they are used to quantify the missing peptide pair. However, this often this results in the quantification of the background, which should be very low. In this way, a SILAC ratio is returned which should be a good estimation of the different amounts of the protein in the heavy and light samples (Sara Zanivan, personal communication). Supporting this, if MaxQuant was presenting a reduced list of proteins, due to undetectable SILAC-paired peaks, since the Mascot search did not rely on SILAC-paired peaks, a larger protein list would have been expected to have been generated by Mascot. This was not the case. However, a better approach might have been to assess the down-regulation of the proteins in cell lysates in the presence or absence of SOCS3 (215). In contrast, this project analysed the enhancement of ubiquitination in the presence of SOCS3.

The selection of the stable isotopes used for SILAC might have contributed to the small number of proteins detected. Here, both arginine and lysine imparted the

same mass shift of 6Da, which would make differentially-labelled, unique peptides with similar mass indistinguishable. However, such a scenario can be accounted for using MaxQuant. To increase the amount of information gained from MS, SILAC isotopes with different masses could have been used e.g. $^{13}\text{C}_6^{15}\text{N}_2$ -lysine (K8) and $^{13}\text{C}_6^{15}\text{N}_4$ -arginine (R10). In addition to the use of different SILAC isotopes, it would also have been preferable to have performed both experiments at the same time. Since this was not the case, the concentrated TAP eluates (Figure 5.2) were run on separate gels and a different number of gel slices/samples were prepared for each experiment. In doing so I was not able to use additional functionality provided by MaxQuant, “match between runs” (216). This allows peptide identities to be combined from each run and increase the number of proteins identified. However, to do so with non-equivalent gel slices would result in the increased generation of false positives.

Through analysis of ubiquitin, forward and reverse-labelled experiments seemed to be of similar quality. This was because in both cases ubiquitin was identified with a similar number of unique peptides with high sequence coverage and low PEP values. Furthermore, \log_2 -transformed normalised SILAC ratios were both approximately zero which likely suggests that ubiquitin/HBUb tag was expressed at comparable levels and that incorporation of the SILAC label was near complete. However, more ubiquitin-modified lysine residues of ubiquitin were identified in the forward compared to the reverse-labelling experiment. This might be a consequence of less unique peptides of ubiquitin being analysed (10 vs.16, Ubc, Table 5.1 vs. Table 5.2) in the reverse experiment and that PTMs can be lost during MS/MS fragmentation and sequencing (179).

The precise identification of ubiquitin is not surprising since it is highly expressed in both cell types in the form of the HBUb-transgene. In fact, overexpression of the HBUb-transgene might also be responsible for the small number of proteins identified. During MS analysis, the top most abundant peptides are selected for MS/MS sequencing (William Mullen, personal communication). As such, low abundant peptides might be lost due to the over abundant ubiquitin peptides. MS analysis does account for this in that upon detection of a peptide, it is ignored for a period of ten seconds before it is accepted again. During this period, less abundant peptides would be analysed.

However, where peptides are overabundant or where contamination is an issue, samples can be re-analysed using exclusion tables listing these unwanted peptides/ions. Doing so enables low abundant peptides to be assessed thus increasing the data set. This type of MS run could be performed here but it was found to be financially unfeasible.

Even so, while similar arrays of proteins were identified, the full range of proteins and their SILAC ratios were much lower in the reverse compared to the forward-labelling experiments. The detection of fewer proteins was not expected given that significantly more protein was used in the reverse experiment (400mg) compared to the forward (170mg). Furthermore, this translated to an enhanced total ion chromatogram (TIC, the summed ion intensities of each mass spectrum plotted against time) being produced for the reverse experiment as indicated by the normalised level (NL) (Figure 5.7, lower panel vs. upper panel). Moreover, extracted spectra from this TIC contained more complex/improved peak information (data not shown). As such, increased numbers of peptides and SILAC-paired peaks were available for protein identification and calculation of the SILAC ratio (Table 5.2 vs. Table 5.1). This suggests that the data generated by MaxQuant, following the reverse experiment, was more accurate. However, in some cases, small improvements were seen to dramatically affect the SILAC ratio. This is indicative of experimental error although the source of this error is not apparent. Reverse SILAC was performed to assess its impact on results. However, following analysis of ubiquitin, this is not thought to be the issue. Alternatively, a reduced protein list might have been generated due to the way MaxQuant identifies proteins. Peptides are assigned to all proteins in which they are found but are accepted to belong to proteins with the most identified peptides (Razor peptides). The use of these peptides for quantitation might have adversely affected the SILAC ratio. While quantitation was performed using unique and razor peptides, using only unique peptide might have lead to an improved result. Additionally, urea can decompose over time and when heated to produce isocyanate which carbamylates (H_2NCO) the N-terminus of proteins or side chains of basic amino acids lysine and arginine. As such, fresh buffers were used and TAP beads washed with non-urea buffer prior to elution to avoid additional protein modifications. However, such a modification might still have taken place. Since

MaxQuant was did not consider the extra mass shift (43Da), a reduced list of proteins might have been generated.

In conclusion, it was decided that while the reverse SILAC experiments seemed more accurate, they were also un-useable being of limited information. As such, only data from the forward-labelled experiments were further pursued. From this experiment, only proteins significantly elevated in the WT HBUB MEFs were selected for further validation (Table 5.1). This included cavin-1, which was identified by both Mascot (Table 5.0) and MaxQuant (Table 5.1) searches.

6.0 *In vitro* verification of candidate SOCS3 substrates

6.1 Introduction

In its role as a regulator of intracellular cell signalling, SOCS3 acts in part as a specificity factor for an E3 ubiquitin ligase. The main body of the E3 consists of the scaffold protein cullin5 that binds to the adaptor protein complex of elonginB and elonginC *via* its N-terminus and to the RING finger-containing protein Rbx2 *via* its C-terminus (86,194). Rbx2 binds a ubiquitin-charged E2 conjugation protein that facilitates the transfer of ubiquitin to the substrate. SOCS3 binds to this larger complex *via* its C-terminal SOCS-box motif that interacts with the elonginBC heterodimer. The SOCS3-dependent E3 is thought to bind tyrosine-phosphorylated substrates *via* a centrally located SH2 domain. In support of this, known substrates of SOCS3 are tyrosine-phosphorylated prior ubiquitination (9-12). However, SOCS3 has three defined N-terminal domains, the KIR, ESS, and SH2 domains that cannot be ruled-out as potential sites of interaction. The main function of the E3 complex seems to be to regulate proteasomal degradation of substrates *via* K48-linked polyubiquitination. However, SOCS3 has also been implicated in the ubiquitin-mediated lysosomal routing and degradation of the G-CSF receptors (8,201). As such, potentially wider roles for SOCS3 likely exist.

Global proteomics screening for SOCS3-dependently ubiquitinated targets was previously carried out (Section 5.0). However, due to limitations of all screening methodologies, a proportion a false-positives is expected and as a result, verification of individual substrates must be performed. Basic validation can be performed by demonstrating a protein-protein interaction. This can be achieved *via* several methods, including but not limited to, yeast-2-hybrid, fluorescence resonance energy transfer (FRET), co-immunoprecipitation, GST-pull-down, protein-microarray, and peptide array. Furthermore, these techniques can be elaborated *via* the addition of mutations, PTMs, and by varying conditions to improve stringency and selectivity. Ultimately, protein interactions result in functional outcomes and investigations require function-dependent assays. In the case of SOCS3, substrates are expected to be degraded in a polyubiquitin-dependent fashion *via* the 26S proteasome (9-12). As such, SOCS3 substrates

would be affected by a mass-shift detectable *via* immunoblotting, as well as a reduced half-life in the presence but not absence of SOCS3. Furthermore, the impact of SOCS3 should be investigated using well-characterised substrate-dependent effects (see below). Finally, interdependency can be further investigated by using small molecule and peptide inhibitors as well as siRNA knockdown or gene knockout and rescue experiments.

6.1.1 Cavin-1: a potential SOCS3-dependently ubiquitinated substrate

Cavin-1 (Polymerase 1 and transcript release factor, PTRF) (217) is one of a family of four proteins cavin-1-4 (218). While cavin-1-3 are expressed at high levels in endothelial cells, adipocytes, fibroblasts, and epithelial cells, cavin-4 is restricted to cardiac and skeletal muscle (219,220). While a three-dimensional structure for any of the cavins has yet to be solved, common features include leucine-zipper motifs, PEST domains, and phospho-regulatory sites (219,221). Prototypical member cavin-1 is 392 amino acids in length, giving a predicted mass of 43kDa. However, following SDS-PAGE fractionation it is commonly detected at 50-60kDa (219), such a shift is characteristic of multiple PTMs. Furthermore, five truncated isoforms of 47, 43, 30, 25, and 15 kDa are commonly detected (219,222). Aboulaich et al (222) showed that while cavin-1 contains three PEST sites, these domains could only be detected in the full-length but not truncated forms of cavin-1 suggesting that the latter are the consequence of proteolytic-mediated degradation. While cavin-1 has previously been shown to function within the nucleus as a polymerase I transcript release factor (223), it is also abundant on the cytosolic face of the plasma membrane where it functions as an adaptor protein involved in the formation of caveolae, flask shaped invaginations within the plasma membrane. Cavin-1 aggregates into large oligomeric complexes along with other family members (219). It is thought that this complex makes several weak interactions with phosphatidylserine (PS) thus strengthening its association with the components of caveolae at the plasma membrane. As such, altering the lipid environment might regulate the association of the cavin complex with the PM. Caveolae are involved in endocytosis, cholesterol homeostasis, and sequestration of cell signalling mediators for efficient signalling but also for signal ablation, as reviewed in (224). Interestingly, caveolae sequester several PEST domain-containing proteins, including cavin-1 and all its truncated forms (222).

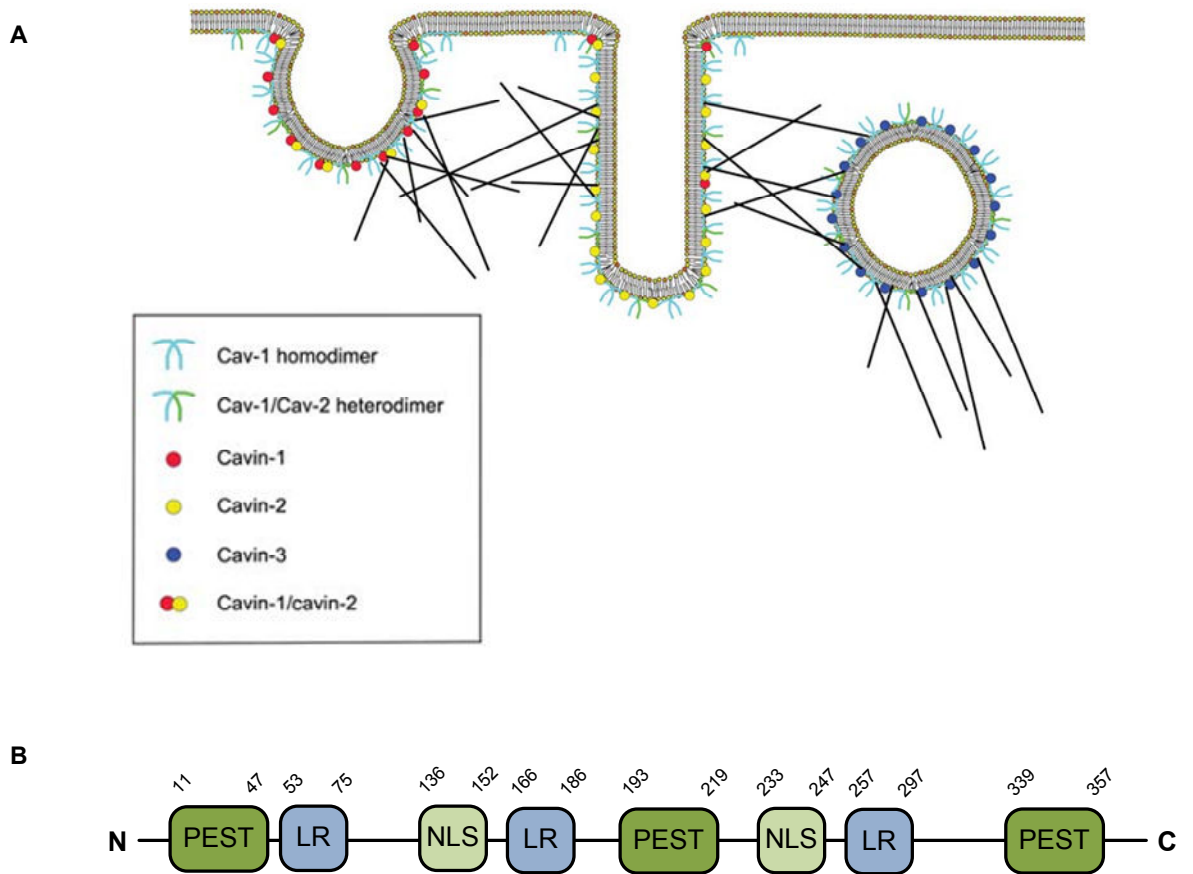


Figure 6.0: Cavin-1, caveolin-1, and the formation of caveolae

A. Caveolae are 50-100nm flask shaped invaginations within the plasma membrane (PM). Adapted with permission from (218). Caveolin-1 (Cav-1), an integral membrane protein that forms the main structural component of caveolae, is sequestered into caveolae by cavin-1, a peripheral membrane protein located on the cytoplasmic face of the PM. Caveolin-2, which is dependent on caveolin-1 for PM-localisation, forms a heterodimer with caveolin-1 and supports the structural and scaffold role of caveolin-1. Cavin-2 is thought to sequester cavin-1 to the plasma membrane and modulate caveolae structure since overexpression of cavin-2 results in the formation of elongated caveolae (225). Cavin-3 drives vesicle formation and is involved intracellular microtubule trafficking (225). **B.** Domain structure of cavin-1. PEST, Pro-Glu-Ser-Thr-rich regions; LR, Leu rich region; NLS, nuclear localisation sequence. Adapted with permission from (219).

However, the truncated forms are not detected in the nucleus or cytosol suggesting that proteolysis may occur *in situ*.

Caveolins are a family of three proteins (caveolin-1-3) which serve as the main structural components of caveolae. As such, ectopic expression of caveolin-1 or caveolin-3 is usually sufficient to form caveolae (226). Whereas caveolin-1 and 2 are widely expressed, caveolin-3 is limited to striated muscle (224). Cavin-1 is thought to sequester caveolin-1 to caveolae and regulates location and stability of caveolin-1 by preventing lateral motion and lysosomal degradation (227). Expression of cavin-1 and caveolin-1 are tightly linked such that overexpression of cavin-1 results in a concomitant increase in caveolin-1. Genetic deletion of cavin-1 in mice leads to impaired caveolae formation and loss of stability of all three caveolins (226). As such, it could be hypothesised that any effect on cavin-1 expression might similarly affect caveolin-1.

Caveolin-1 is critical in regulating inflammatory signalling (218), regulates vascular permeability *via* sequestration and inhibition of eNOS and its dysregulation has been linked to enhanced AKT and ERK1/2 signalling resulting in several cardiovascular phenotypes (228-230). For example, while caveolin-1 KO mice models are viable, they develop pulmonary hypertension and cardiac hypertrophy (225). However, it is not known if the same is true for cavin-1 KO mice, which have a lipodystrophic phenotype i.e. high circulating triglyceride levels, reduced adipose tissue mass, glucose intolerance, and hyperinsulinaemia (226). This phenotype is believed to stem from the impaired triglyceride uptake and storage by adipocytes due to the lack of caveolae (226). Caveolin-1 also enhances COX-2 degradation and controls integrin signalling (231-233). Interestingly, caveolin-1 has been described as a novel regulator of cytokine signalling due to its ability to inhibit prolactin-induced STAT5 signalling *via* a conserved pseudo-kinase domain (234) similar to that of SOCS1/3. Caveolin-1 has also been shown to regulate innate immunity by being protective against infection by maintaining a balance between host response and cytokine-dependent tissue damage (235). It was found that compared to WT mice, caveolin-1 knockout mice infected with the respiratory pathogen *Pseudomonas aeruginosa* had elevated levels of inflammatory cytokines (IL6, TNF α) as a result of sustained JAK/STAT and NF κ B signalling within lung tissue (235). Furthermore,

increased ROS production was noted along with decreased survival and phagocytic ability of alveolar macrophages (235). Additionally, in adipocytes, caveolin-1-binding is thought necessary for full activation of the insulin receptor β while tyrosine phosphorylation of caveolin-1 results in endocytosis of the activated insulin receptor (236). In contrast to its protective effects, caveolin-1/caveolae are thought to regulate the transcytosis of LDL in blood vessels resulting in the accumulation of pro-atherogenic lipids in the sub-endothelial space, which is important for lesion formation (Section 1.13) (237). As such, loss of caveolin-1 has been suggested to be protective against atherosclerosis (237). Recently, cavin-1 has been found to be downregulated, due to epigenetic silencing, in breast cancer (238). Since cavin-1 is crucial for caveolae formation, it is thought that it might function as a tumour suppressor by attenuating downstream signalling events (238). Furthermore, cavin-1 has also been found to be downregulated in both adenocarcinoma and squamous cell carcinoma compared to healthy tissue (239). The same has previously been found in prostate cancer cell lines PC3 and LNCaP (240). Moreover, expression of cavin-1 has been demonstrated to inhibit cell migration in PC3, DU145, and NIH-3T3 cells and that loss of cavin-1 leads to increased migration and matrix metalloprotease-9 production (241). This suggests that cavin-1 might be important in the development and progression of several forms of cancer.

Caveolin-1 and presumably cavin-1 might therefore be critical in cardiovascular disease, diabetes, breast cancer, and inflammation. Furthermore, cAMP-induced SOCS3 might serve to negatively regulate several pro-inflammatory signalling pathways. As such, cavin-1 is an ideal candidate for SOCS3-dependent regulation. However, SOCS3 is up-regulated in several chronic inflammatory disorders and obesity (159). In such a case, it might be hypothesised that levels of cavin-1 and caveolin-1 would be reduced, resulting in an up-regulation of eNOS and loss of insulin signalling and as such, contribute to a metabolic syndrome. However, loss of caveolin-1 might be protective. Effectively targeting SOCS3 levels might therefore be therapeutically beneficial.

6.1.2 Hsc70: a potential SOCS3-dependently ubiquitinated substrate

Heat shock proteins (HSPs) are well-defined protein chaperones that upon induction e.g. by heat, ischemia, or oxidative stress, bind unfolded proteins to

improve stability or mark them for degradation *via* the ubiquitin-proteasome pathway or autophagy. Furthermore, HSPs are also involved in protein synthesis and trafficking (242) and other roles are increasingly being found.

Hsc70, a member of the largest heat shock protein family Hsp70, is constitutively and ubiquitously expressed and has been linked to EC health and homeostasis. Hsc70 knockout is embryonic lethal and Shiota et al (243) showed that siRNA-mediated knock-down results in ~40% EC cell death over 48 hours. Shiota et al also demonstrated the importance of Hsc70 as a regulator of angiogenesis *via* its action upon the PI3K/Akt signalling pathway. Inhibition (non-specific) or siRNA-mediated knockdown of Hsc70 was able to block VEGF-mediated HUVEC cell migration by inhibition of PI3K transcription, which blocked phosphorylation of Akt and its downstream effector eNOS. Furthermore, siRNA silencing of Hsc70 blocked EC migration and tube formation *in vitro* (243). As such, Hsc70 might be important in recovery from vascular insufficiency (ischaemia) and tumourigenesis. A further role for Hsc70 in tumourigenesis was described in a study by Ding et al (244) where it was found that Hsc70 regulates agonist-induced (CXCL12) endocytosis of the chemokine receptor CXCR4 in HEK293 cells. Furthermore, siRNA knockdown of Hsc70 reduced endocytosis of endogenous CXCR4 and inhibited CXCL12-induced chemotaxis in U87 glioma cells. Thus, Hsc70 may similarly regulate other receptors (244,245). If Hsc70 is a potential SOCS3-dependently ubiquitinated target, then overexpression of SOCS3 might prevent metastasis of these neural tumour cells. In some cancers, loss of SOCS3 due to promoter hypermethylation can lead to uncontrolled IL6 signalling which can support tumourigenesis due the proliferative and anti-apoptotic effects of IL6 (246). Regulation of Hsc70 by SOCS3 might therefore be a novel mechanism by which a loss of SOCS3 contributes to tumourigenesis.

6.1.3 Experimental strategy

SOCS3 has been demonstrated to regulate the polyubiquitination and subsequent degradation of several proteins (9-12). As such, proteins identified in this study *via* a proteomics screen are also hypothesised to be similarly regulated. A prerequisite for substrate polyubiquitination is an interaction with SOCS3. Co-immunoprecipitation was used as the preliminary assay to assess protein-protein interactions.

Prior to SOCS3-substrate interaction, substrates are expected to be tyrosine-phosphorylated (9-12). While the role of tyrosine-phosphorylation can be investigated during co-immunoprecipitation experiments, peptide arrays enable the identification of important residues and protein domains. Furthermore, peptides can be fabricated with or without PTMs and thus interactions are unaffected by either basal phosphorylation or unanticipated modifications. SOCS3 binds tyrosine-phosphorylated substrates *via* a well-defined SH2-domain with the consensus binding sequence (S/A/V/Y/F) - Φ - (V/I/L) - Φ - (H/V/I/Y), where Φ is a hydrophobic residue (78). Furthermore, tyrosine-phosphorylated residues of potential substrates are available online at protein databases such as phosphosite.org. While these sites might not be comprehensive, they do act as a starting point. Furthermore, the dependency on other protein domains can be investigated using full-length peptide arrays of both SOCS3 and any candidate substrate. Peptide arrays are commonly fabricated on-site by the Baillie laboratory. As such, they offer an efficient and cost effective technique to assess SOCS3-substrate interactions *in vitro*.

Until recently, proteasome-mediated degradation was thought to be a K48-polyubiquitin-dependent process (137). However, evidence now suggests that all non-K63 polyubiquitin chains might contribute to proteasomal degradation (138,247). Nevertheless, K48-polyubiquitin chains are the most abundant form of polyubiquitin-chain linkage in mammals (247) and so might serve as the major signal that drives proteasomal degradation. As such, isolation of polyubiquitinated candidate substrates in the presence but not absence of SOCS3 would support the substrate as a target of SOCS3. This could be achieved *via in vitro* ubiquitination assays using purified proteins. Using this technique, results would be unaffected by non-SOCS3-dependent E3 ligases or other modifying proteins. Others (11) have successfully performed ubiquitination reactions *in situ* following transfection and overexpression of the necessary components. In both cases, isolation of the substrate or ubiquitinome can be performed *via* immunoprecipitation. Given the availability of cDNA constructs, the latter technique was preferred.

While immunoprecipitation might detect enhanced ubiquitination in the presence of SOCS3, polyubiquitin-chain specificity directs functional outcome. In

this case, SOCS3 substrates are predicted to be degraded. The presence of K48-linked ubiquitination can be assessed using polyubiquitin-chain-specific antibodies. However, the definitive test is to show degradation of the substrate in the presence but not absence of SOCS3. I decided to perform this assay *in situ* following transfection of the relevant components into WT HEK293 cells. Rescuing degradation *via* inhibition of the proteasome would add further supporting evidence to the hypothesis.

Using these techniques, I aimed to show that potential substrates not only interacted with SOCS3 but also identify which protein domains and/or residues were important. Furthermore, I aimed to show that following interaction, substrates were subsequently ubiquitinated in a SOCS3-dependent manner. Additionally, the availability of cDNA constructs meant that only a proportion of the potential SOCS3 substrates were assessed (Table 5.1, light grey/dotted boxes). However, only a selection is presented here including cavin-1 and Hsc70 (Table 5.1, light grey boxes).

6.2 Results and discussion

6.2.1 Optimisation of experimental conditions

6.2.1.1 Optimisation of co-immunoprecipitation assay

SOCS3 substrate verification was initially performed using a co-immunoprecipitation assay. If potential SOCS3 substrates interact with SOCS3, then SOCS3 is expected to specifically isolate the substrate from a complex mixture of proteins present in cell lysates. Antibody-antigen complexes can have strong binding affinities although the range of affinities can be wide ($K_d=10^{-5}$ to 10^{-12} M). However, due to the transient nature of many intracellular protein-protein interactions, their binding affinities might be lower. As such, experimental conditions must be optimised to support the detection of these protein interactions. Given that SOCS3-substrate interactions are the only interactions being investigated, repeated manipulation of co-immunoprecipitation conditions is not expected, a single condition should be sufficient. To assess selection of co-immunoprecipitation conditions, the SOCS3-dependent interaction between SOCS3 and the elonginBC-cullin5 scaffold

($K_d=10^{-7}M$) (86) was used as a model system. Furthermore, specificity of this interaction was tested using a SOCS3-L189A SOCS-box mutant that cannot bind components of the E3 ligase (194). Importantly, SOCS3 is expected to interact with SOCS3-dependently ubiquitinated substrates *via* its SH2 domain (9-12). As a more stringent examination of reaction conditions, the interaction between SOCS3 and FAK1 (10), a known SOCS3-dependently ubiquitinated substrate was assessed. It was thought that if SOCS3 could precipitate all proteins under a single experimental condition then it should similarly precipitate candidate substrates.

HEK293 cells were transfected as described (Section 2.2.12) with SOCS3-Flag, cullin5, elonginB-myc, and elonginC cDNA constructs in the indicated combinations (Figure 6.1). To evaluate the impact of tyrosine phosphorylation on protein-protein interactions, cells were treated with or without Na_3VO_4 (1mM) for 2 hours and H_2O_2 (0.2mM) for the final 15 minutes prior to harvesting. Soluble protein lysates were prepared and co-immunoprecipitation performed as described (Section 2.2.13) using pre-conjugated Flag M2 agarose beads. Recovered protein complexes were fractionated by SDS-PAGE and analysed by immunoblotting.

ElonginB and cullin5 were precipitated in the presence but not absence of SOCS3 (Figure 6.1, panel F/G lane 2 vs. 3 and 5 vs. 6) thus confirming the suitability of the conditions for this interaction. The interaction of SOCS3 with E3 ligase components has been reported to be disrupted by JAK2-mediated tyrosine phosphorylation at Y²⁰⁴ and Y²²¹ within the SOCS-box and the subsequent disruption was found to have a destabilising effect on SOCS3 (100). Importantly, cullin5 and elonginB were precipitated at comparable levels before and after PTP inhibition suggesting that elevating global levels of tyrosine-phosphorylation in this manner does not affect formation of the E3 ligase complex. Furthermore, no impact on SOCS3 expression levels was detected. Interestingly, levels of SOCS3 are reduced when not co-expressed with the E3 components suggesting that this interaction is stabilising (Figure 6.1, panel B/E lane 1 vs. 3 and 4 vs. 6).

To demonstrate the specificity of the SOCS3-elonginB-cullin5 interaction, the previous experiment was then repeated using the SOCS3-L189A SOCS-box

mutant, which has been shown to be defective in binding E3 scaffold proteins (194). PTP inhibitors were not used here due to the previous experiment showing them to be redundant. SOCS3 but not SOCS3-L189A precipitated elonginB and cullin5 indicating the specificity of the SOCS3-E3 interaction (Figure 6.2, panel D/E, lane 4 vs. 5). Furthermore, this data confirmed that conditions used for co-immunoprecipitation were adequate to preserve interactions between these proteins. Although cullin5 was detected in immunoprecipitates, expression in cell lysates was masked by non-specific bands and was therefore not presented here.

Co-immunoprecipitation conditions were more stringently tested by repeating the previous experiments using FAK1, a known SOCS3-dependently ubiquitinated substrate(10). FAK1 was precipitated to high levels in the presence but not absence of SOCS3 (Figure 6.3, panel E, lane 1 vs. 3). Although the cells were not treated with PTP inhibitors, probing with anti-pY antibody detected a strong band with the same mass as that predicted for FAK1 (115kDa) (Figure 6.3, panel A) suggesting that basal levels of tyrosine phosphorylation are sufficient for the interaction. Furthermore, the absence of this band in the singly transfected cells suggests that interaction with SOCS3 might preserve tyrosine phosphorylation and prolong the FAK1-SOCS3 interaction.

These data confirm that co-immunoprecipitation conditions are sufficient to preserve the protein-protein interactions tested. These conditions were then used to demonstrate an interaction between SOCS3 and its candidate substrates.

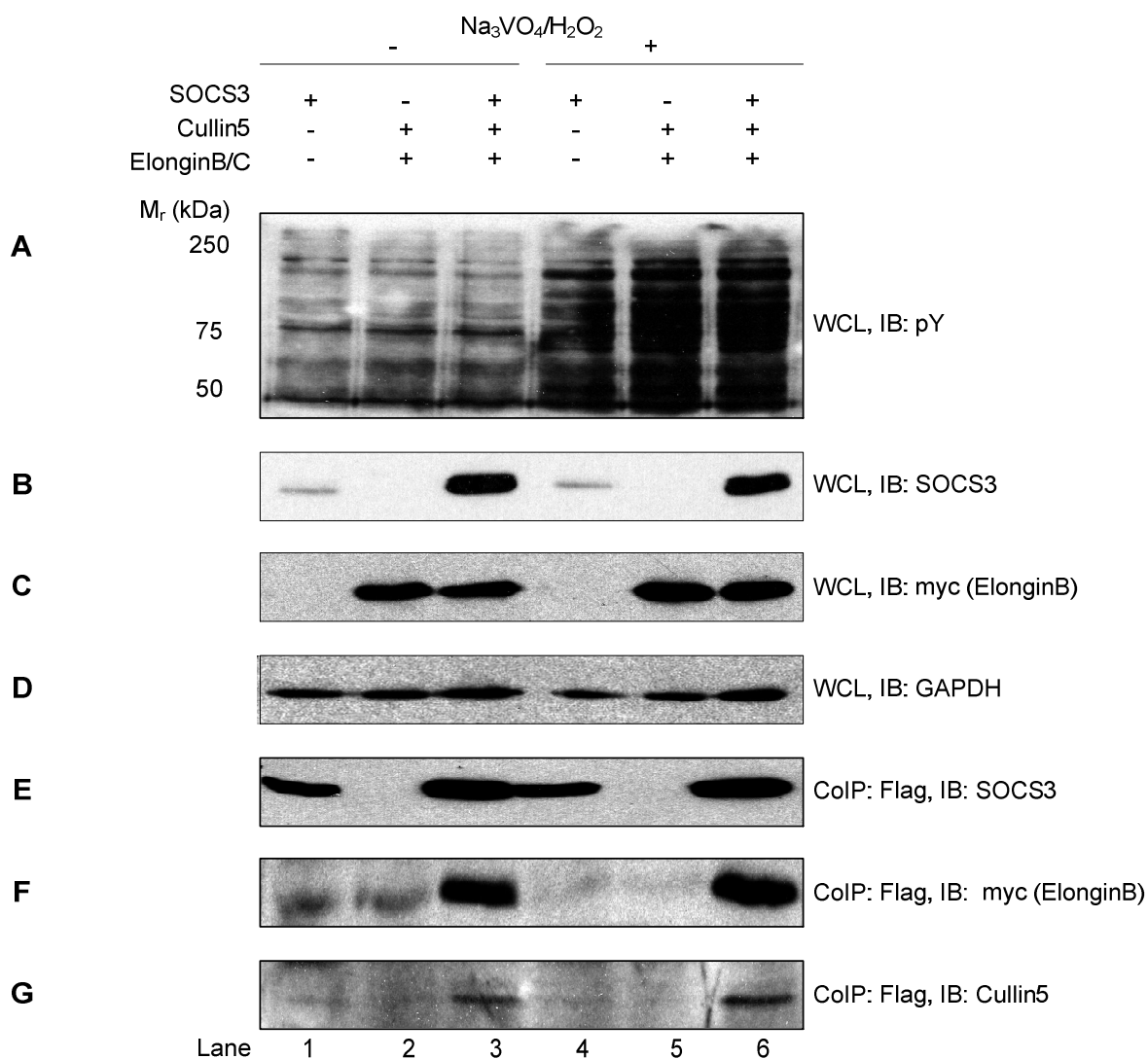


Figure 6.1: The impact on tyrosine phosphorylation on the interaction between SOCS3 and the E3 scaffold proteins elonginB and cullin5

HEK293 cells were transfected as described (Section 2.2.12) with SOCS3-Flag, cullin5, elonginB-myc, and elonginC cDNA constructs in the indicated combinations. Soluble protein lysates were prepared and co-immunoprecipitation performed as described (Section 2.2.13) using 30µl of 50% (v/v) slurry of pre-conjugated Flag M2 agarose beads. Recovered protein complexes were fractionated by SDS-PAGE and analysed by immunoblotting using anti-SOCS3 (Panel B/E), anti-cullin5 (Panel G), and anti-myc antibody (Panel C/F). Global tyrosine phosphorylation was assessed using anti-phosphotyrosine antibody (4G10) (Panel A) while GAPDH was used as a loading control (Panel D).

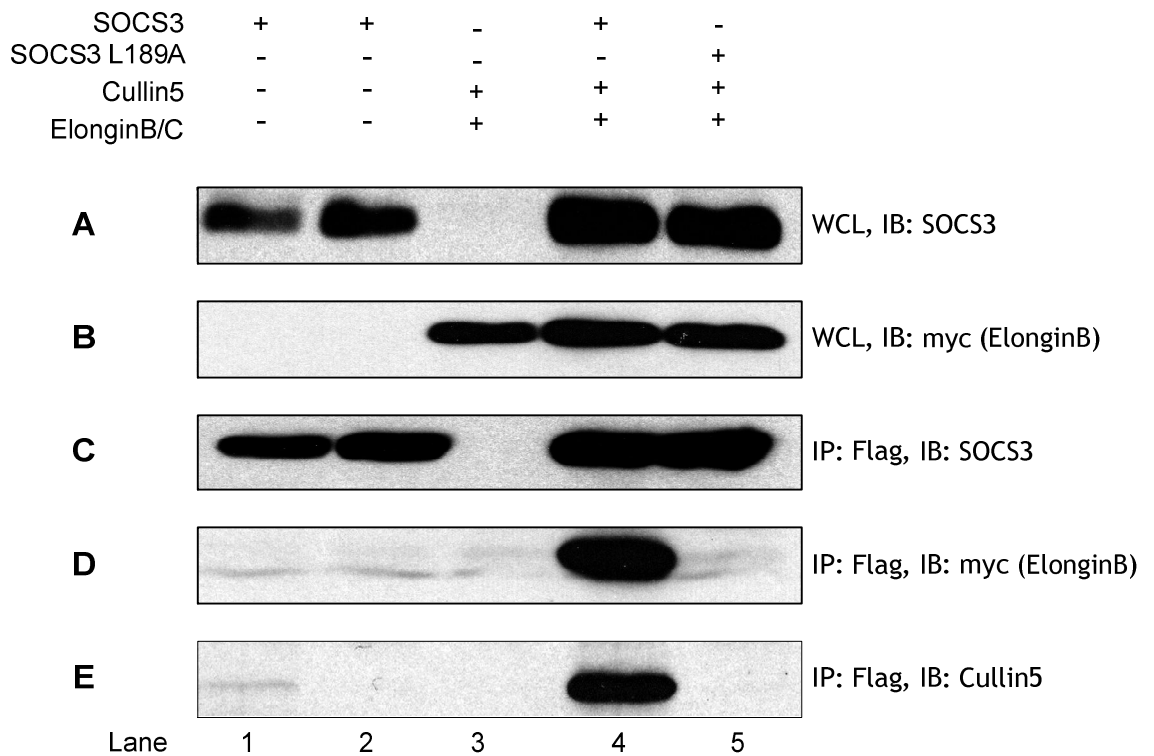


Figure 6.2: The impact of the SOCS3-L189A SOCS-box mutation on its interaction with the E3 ligase components elonginB and cullin5

HEK293 cells were transfected as described (Section 2.2.12) with SOCS3-Flag, SOCS3-L189A-Flag, cullin5, elonginB-myc, and elonginC cDNA constructs in the indicated combinations. Soluble protein lysates were prepared and co-immunoprecipitation performed as described (Section 2.2.13) using 30µl of 50% (v/v) slurry of pre-conjugated Flag M2 agarose beads. Recovered protein complexes were fractionated by SDS-PAGE and analysed by immunoblotting using anti-SOCS3 (Panel A/C), anti-cullin5 (Panel E), and anti-myc antibody (Panel B/D).

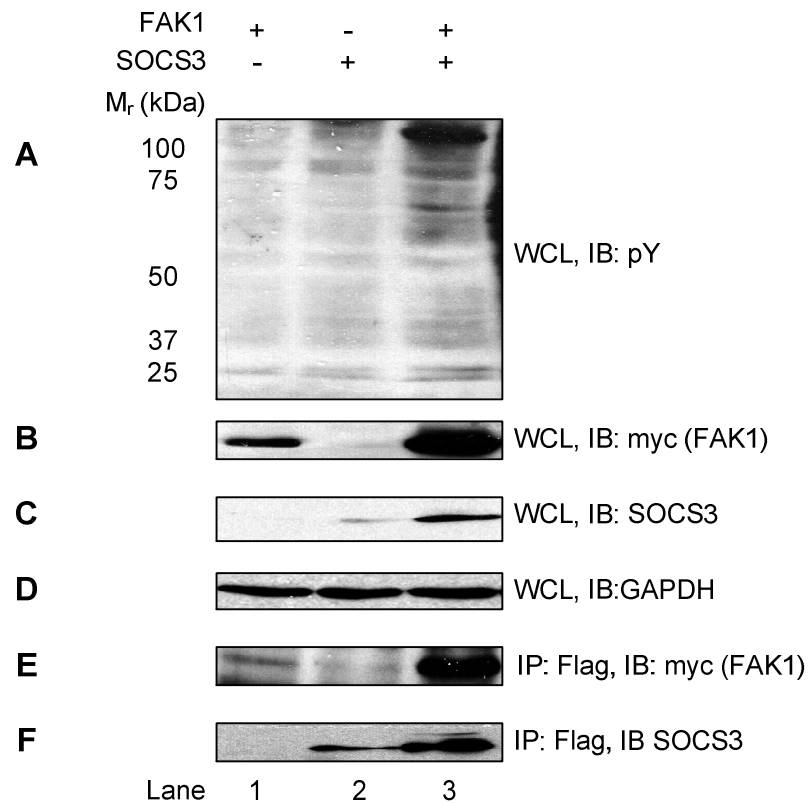


Figure 6.3: SOCS3 precipitates known SOCS3-dependently ubiquitinated substrate FAK1

HEK293 cells were transfected as described (Section 2.2.12) with SOCS3-Flag and FAK1-myc cDNA constructs in the indicated combinations. Soluble protein lysates were prepared and co-immunoprecipitation performed as described (Section 2.2.13) using 30µl of 50% (v/v) slurry of pre-conjugated Flag M2 agarose beads. Recovered protein complexes were fractionated by SDS-PAGE and analysed by immunoblotting using anti-SOCS3 (Panel C/F) and anti-myc antibody (Panel B/E). Global tyrosine phosphorylation was assessed using anti-phosphotyrosine antibody (4G10) (Panel A) while GAPDH was used as a loading control (Panel D).

6.2.1.2 Optimisation of denatured immunoprecipitation assay

SOCS3 is expected to ubiquitinate its candidate substrates. Therefore, an enhanced ubiquitin signal is expected in the presence but not absence of SOCS3 following isolation of the ubiquitinome or candidate substrate *via* immunoprecipitation. To reduce background from ubiquitin-interacting proteins, candidate-binding proteins, and preserve ubiquitin chains from DUBs, immunoprecipitation will be performed on denatured cell lysates. Furthermore, isolation of the ubiquitinome will be facilitated by the use of HA-tagged ubiquitin (Ub-HA) and pre-conjugated anti-HA agarose beads. Prior to experimentation, the expression of Ub-HA was assessed. Furthermore, the volume of anti-HA agarose beads were optimised for maximum recovery of Ub-HA-modified protein.

HEK293 cells were transfected as described (Section 2.2.12) with Ub-HA or GFP cDNA constructs using the indicated concentrations (Figure 6.4). Soluble protein lysates were then either directly fractionated by SDS-PAGE (Figure 6.4, left panel) or denatured immunoprecipitation was performed as described (Section 2.2.14) (Figure 6.4, right panel). Captured proteins were fractionated by SDS-PAGE and recovery or expression of ubiquitinated proteins analysed by immunoblotting.

Ub-HA was highly expressed in a dose-dependent manner with 4 μ g per 6cm diameter dish giving the strongest signal (Figure 6.4, panel A). However, Ub-HA was significantly expressed compared to the control using a lower concentration of 2 μ g. Recovery of Ub-HA using anti-HA agarose beads increased in a dose-dependent manner with no improvement gained above 30 μ l (50% (v/v) slurry) (Figure 6.4, Panel C). These data suggest that 2-4 μ g per 6cm diameter dish of cDNA construct is sufficient to express detectable Ub-HA and that 30 μ l (50% (v/v) anti-HA agarose beads is optimal for recovery of Ub-UA-tagged proteins.

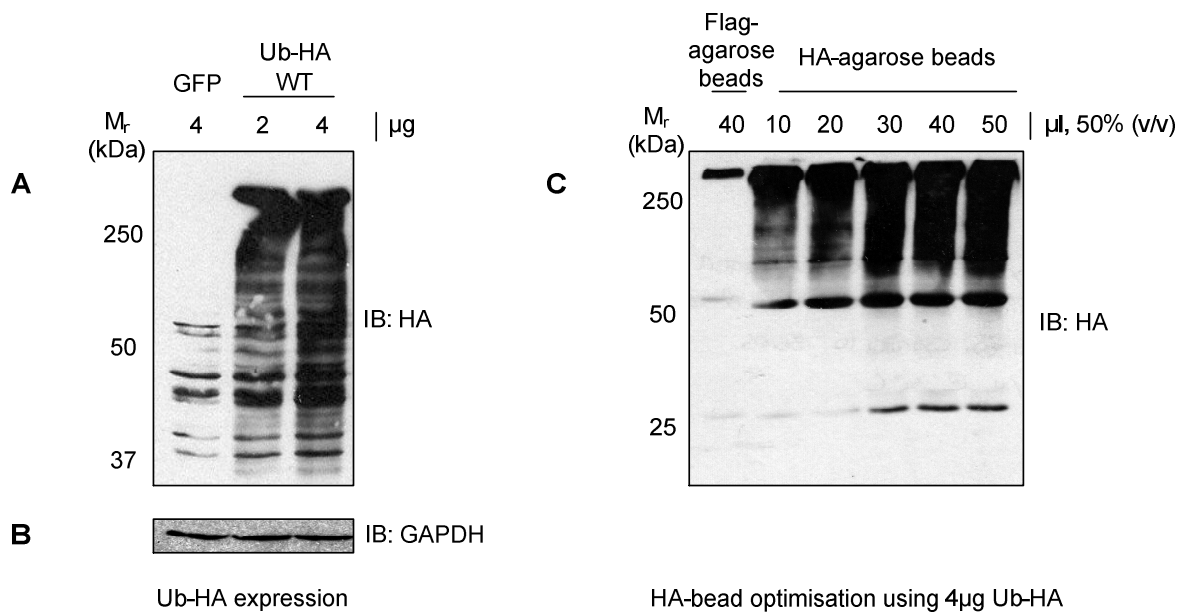


Figure 6.4: Expression of Ub-HA and optimisation of denaturing co-immunoprecipitation

HEK293 cells were transfected as described (Section 2.2.12) using the indicated amounts of Ub-HA or GFP cDNA constructs per dish. The ubiquitinome was preserved by treating with MG132 for 2 hours prior to harvesting. Samples were equalised before fractionated by SDS-PAGE and expression of the tagged moieties assessed by immunoblotting using an anti-HA antibody (Panel A). GAPDH was used as a loading control (Panel B). Additionally, denatured immunoprecipitation was performed as described (Section 2.2.14) using 30 μl of 50% slurry (v/v) monoclonal (HA-7) anti-HA agarose beads or as a control, 30 μl of 50% (v/v) slurry of pre-conjugated Flag M2 agarose beads. Captured ubiquitinated proteins were fractionated by SDS-PAGE and recovery assessed by immunoblotting using anti-HA antibody (Panel C).

6.2.2 A SOCS3-Hsc70 interaction could not be confirmed *via* co-immunoprecipitation

Hsc70 (Section 6.1.2) was identified in the proteomics screen (Section 5.0) with a \log_2 normalised SILAC ratio of 0.67 (Table 5.1). Although not significant, a miscommunication led it being verified here. Optimised experimental conditions for co-immunoprecipitation (Section 6.2.1.1) were used to assess an interaction between Hsc70 and SOCS3. If Hsc70 is a substrate of SOCS3, then Hsc70 is expected to be precipitated in the presence but not absence of SOCS3.

HEK293 cells were transfected as previously described (Section 2.2.12) with SOCS3-Flag, Hsc70-myc, Hsc70-GFP, and FAK1-myc cDNA constructs in the indicated combinations (Figure 6.5). Tyrosine phosphorylation was preserved by treating cells with Na_3VO_4 (1mM) for 2 hours and H_2O_2 (0.2mM) for the final 15 minutes prior to harvesting. Soluble protein lysates were prepared and co-immunoprecipitation performed as described (Section 2.2.13) using 40 μl of 50% (v/v) slurry of protein G Sepharose beads and 10 μl of anti-SOCS3 antibody. Recovered protein complexes were fractionated by SDS-PAGE and analysed by immunoblotting.

While Hsc70 was precipitated in the presence of SOCS3, it was also precipitated in its absence (Figure 6.5, H/I lanes 5 vs. 6 and 7 vs. 8). This result was replicated using an anti-Flag antibody (data not shown). This suggests the isolation of Hsc70 was not due to cross-reactivity of the precipitating antibody but because of Hsc70 binding non-specifically to the protein G Sepharose beads. As such, performing the reciprocal experiment i.e. using GFP, myc, or Hsc70-specific precipitating antibodies would also be vulnerable to the same effect. It was decided that a peptide array might provide a more definitive result (Section 6.2.5). As such, no further co-immunoprecipitation experiments were performed using Hsc70.

Figure 6.5: A SOCS3-Hsc70 interaction could not be confirmed *via* co-immunoprecipitation

HEK293 cells were transfected as described (Section 2.2.12) with SOCS3-Flag, Hsc70-myc, Hsc70-GFP, and FAK1 cDNA constructs in the indicated combinations. Tyrosine phosphorylation was preserved by treating cells with Na_3VO_4 (1mM) for 2 hours and H_2O_2 (0.2mM) for the final 15 minutes prior to harvesting. Soluble protein lysates were prepared and co-immunoprecipitation performed as described (Section 2.2.13) using 40 μl of 50% (v/v) slurry of protein G Sepharose beads and 10 μl of anti-SOCS3 antibody. Recovered protein complexes were fractionated by SDS-PAGE and precipitation analysed by immunoblotting using anti-GFP (Panel C/I), anti-myc (Panel B/D/G/H), and anti-Flag antibody (Panel J). GAPDH was used as a loading control (Panel F).

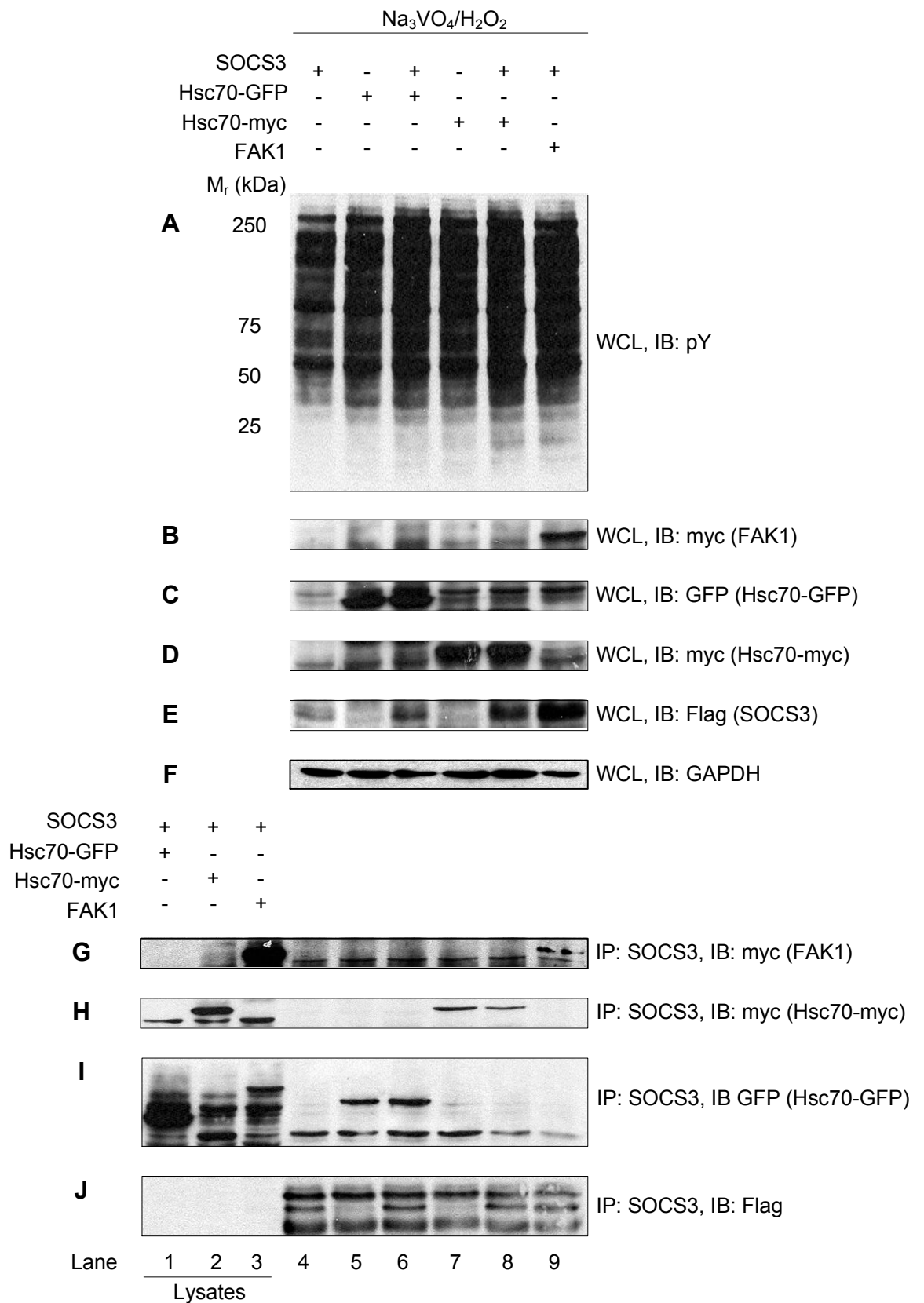


Figure 6.5: A SOCS3-Hsc70 interaction could not be confirmed *via* co-immunoprecipitation

6.2.3 SOCS3 can precipitate cavin-1 but not Abi2

Cavin-1 (Section 6.1.1) and Abi2 were identified in the proteomics screen (Section 5.0) with significant \log_2 normalised SILAC ratios of 1.37 and 1.17 respectively (Table 5.1). Optimised experimental conditions for co-immunoprecipitation (Section 6.2.1.1) were used to assess an interaction between cavin-1 or Abi2 and SOCS3.

HEK293 cells transfected as previously described (Section 2.2.12) with SOCS3-Flag, Abi2-GFP, cavin-1-GFP cDNA constructs in the indicated combinations (Figure 6.6). To evaluate the impact of tyrosine phosphorylation on protein-protein interactions, cells were treated with or without Na_3VO_4 (1mM) for 2 hours and H_2O_2 (0.2mM) for the final 15 minutes prior to harvesting. Soluble protein lysates were prepared and co-immunoprecipitation performed as described (Section 2.2.13) using 40 μl of 50% (v/v) slurry of protein G Sepharose beads and 10 μl of anti-SOCS3 antibody. Recovered protein complexes were fractionated by SDS-PAGE and assessed by immunoblotting.

Cavin-1 was precipitated in the presence but not absence of SOCS3 (Figure 6.6, panel E, lane 7 vs. 8) whereas Abi2 could not be precipitated (Figure 6.6, panel E, lane 5 vs. 6). While a weak signal for cavin-1 was detected in the absence of SOCS3, this signal is significantly enhanced in its presence. Furthermore, this enhancement is not due to variations in cavin-1 expression (Figure 6.6, panel B, lane 7 vs. 8). This data suggest that cavin-1 specifically interacts with SOCS3. Interestingly, cavin-1 is detected as three separate bands (Figure 6.6, panel E, lane 2) but only the top bands seems to be precipitated. The lower bands might be proteolysed fragments that have been previously detected in caveolae by other groups (219,222) suggesting that only full-length cavin-1 interacts with SOCS3.

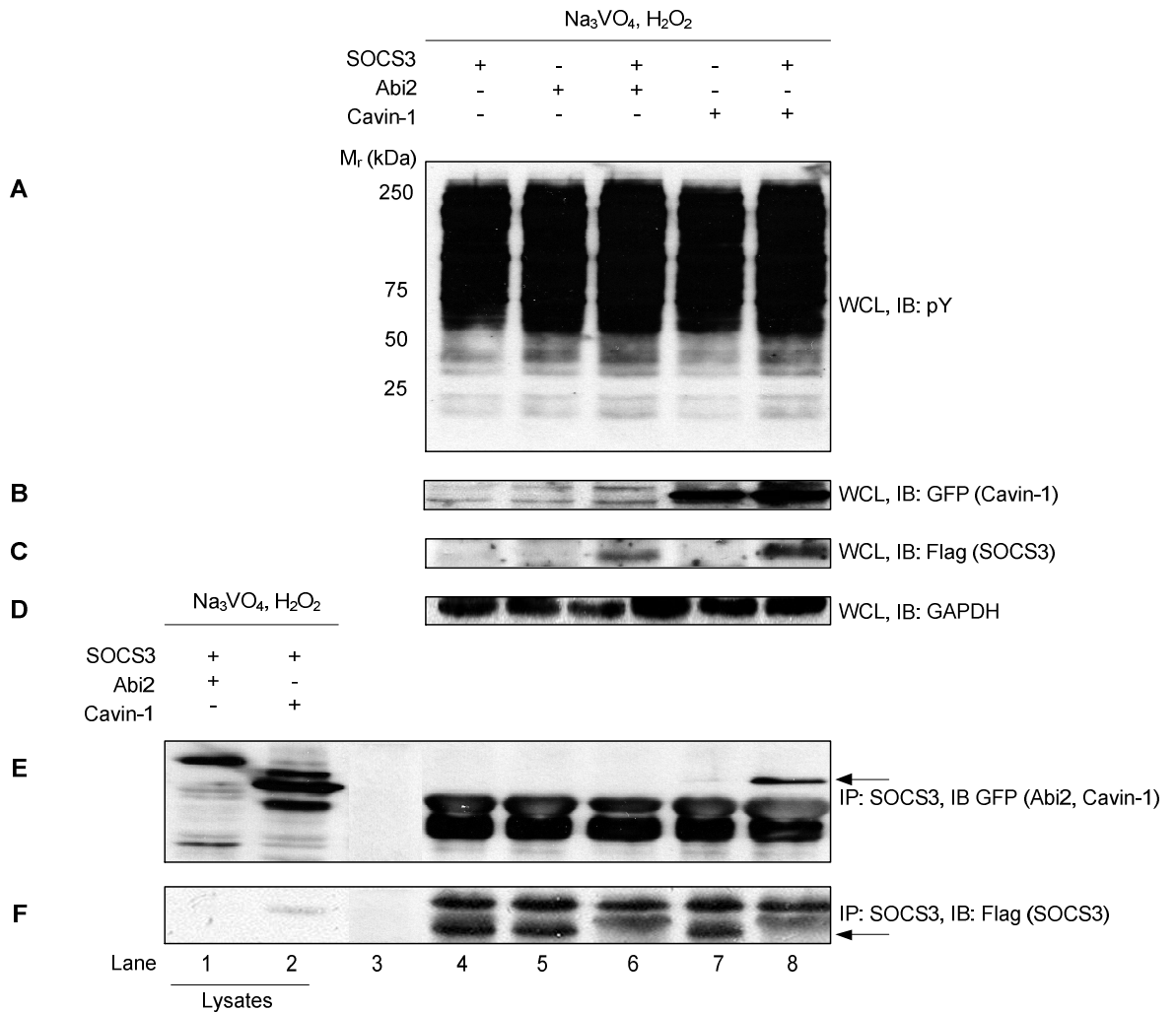


Figure 6.6:SOCS3 precipitates potential substrate cavin-1 but not Abi2

HEK293 cells were transfected as described (Section 2.2.12) with SOCS3-Flag, Abi2-GFP, cavin-1-GFP cDNA constructs in the indicated combinations. Tyrosine phosphorylation was preserved by treating cells with Na₃VO₄ (1mM) for 2 hours and H₂O₂ (0.2mM) for the final 15 minutes prior to harvesting. Soluble protein lysates were prepared and co-immunoprecipitation performed as described (Section 2.2.13) using 40µl of 50% (v/v) slurry of protein G Sepharose beads and 10µl of anti-SOCS3 antibody. Recovered protein complexes were fractionated by SDS-PAGE and precipitation analysed by immunoblotting using anti-GFP (Panel B/E, arrow indicates cavin-1) and anti-Flag antibody (Panel C/F, arrow indicates SOCS3). Global tyrosine phosphorylation was assessed using anti-phosphotyrosine antibody (4G10) (Panel A) while GAPDH was used as a loading control (Panel D).

SOCS3 substrates are predicted to be tyrosine-phosphorylated prior to interacting with the SOCS3-SH2 domain. To further explore the dependence on the SOCS3-cavin-1 interaction on tyrosine-phosphorylation, the previous experiment was repeated by reducing basal levels of tyrosine-phosphorylation by incubating in cells in serum free medium overnight prior to treating with or without PTP inhibitors (Figure 6.7).

Although cavin-1 was precipitated in the presence and absence of PTP inhibitors (Figure 6.7, panel E, lane 5 vs. 7), a much weaker signal was detected following treatment with PTP inhibitors. Although Na_3VO_4 specifically targets PTPs, H_2O_2 also has off-target effects such as acting as an insulin mimetic (204). In this role it has been shown to increase phosphorylation of serine residues (248). However, since its effects have not been fully characterised, its effects on global phosphorylation cannot be predicted. As such, it is possible that serine, threonine, or tyrosine-phosphorylation of either SOCS3 or cavin-1 may be responsible for disrupting the interaction. Interestingly, these same disrupting conditions were used to isolate cavin-1 during the proteomics screen (Section 5.0). In this case, a weak signal might have been compensated for by ubiquitination and stabilisation of cavin-1 following MG132-mediated proteasome inhibition.

All known SOCS3-dependently ubiquitinated substrates are tyrosine-phosphorylated prior to interacting and being ubiquitinated by SOCS3 (9-12). As such, the SOCS3-SH2 domain was predicted to be involved in binding cavn-1. However, it might bind at other locations such as the KIR, ESS, SOCS-box, or at a novel uncharacterised site. The SOCS3 SOCS-box is an unstructured domain that becomes organised following binding, *via* a mainly hydrophobic interaction, to the E3 components elonginB and elonginC (77). As such, this trimer must be formed prior to binding cullin5 (77). SOCS3-L189A carries a mutation within the most conserved domain within the SOCS family, the B/C-box. It is thought that if SOCS3-L189A cannot bind elonginBC then the region will remain unstructured and should be unable to interact with other proteins including cavin-1. Due to the availability of the SOCS3-L189A mutant, it was used to assess whether the SOCS-box had a role in the SOCS3-cavin-1 interaction (Figure 6.8). Thus, the

previous co-immunoprecipitation experiment was repeated to compare precipitation of cavin-1 in the presence of WT or the SOCS-box mutant.

Cavin-1 was precipitated equivalently with both WT and SOCS3-L189A mutant suggesting that the SOCS-box might not be involved in binding cavin-1 (Figure 6.8). However, this does not completely rule-out this domain since the mutant has only been characterised in relation to the elonginBC interaction.

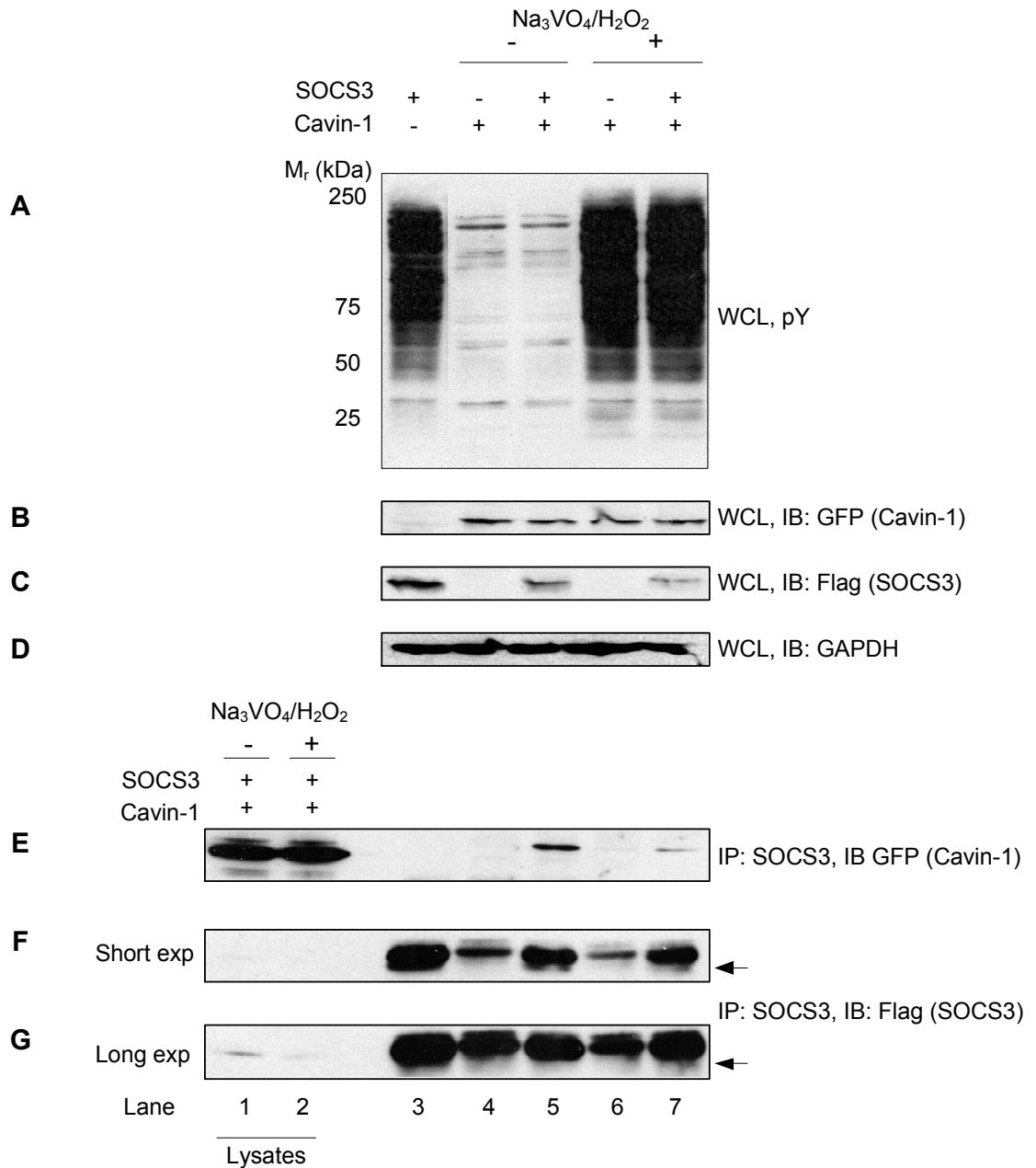


Figure 6.7: Tyrosine-phosphorylation inhibits the cavin-1-SOCS3 interaction

HEK293 cells were transfected as described (Section 2.2.12) with SOCS3-Flag, cavin-1-GFP cDNA constructs in the indicated combinations. Cells were treated with or without Na₃VO₄ (1mM) for 2 hours and H₂O₂ (0.2mM) for the final 15 minutes prior to harvesting. Soluble protein lysates were prepared and co-immunoprecipitation performed as described (Section 2.2.13) using 40µl of 50% (v/v) slurry of protein G Sepharose beads and 10µl of anti-SOCS3 antibody. Recovered protein complexes were fractionated by SDS-PAGE and precipitation assessed by immunoblotting using anti-GFP (Panel B/E) and anti-Flag antibody (Panel C/F/G, arrow indicates SOCS3). Global tyrosine phosphorylation was assessed using anti-phosphotyrosine antibody (4G10) (Panel A) while GAPDH was used as a loading control (Panel D).

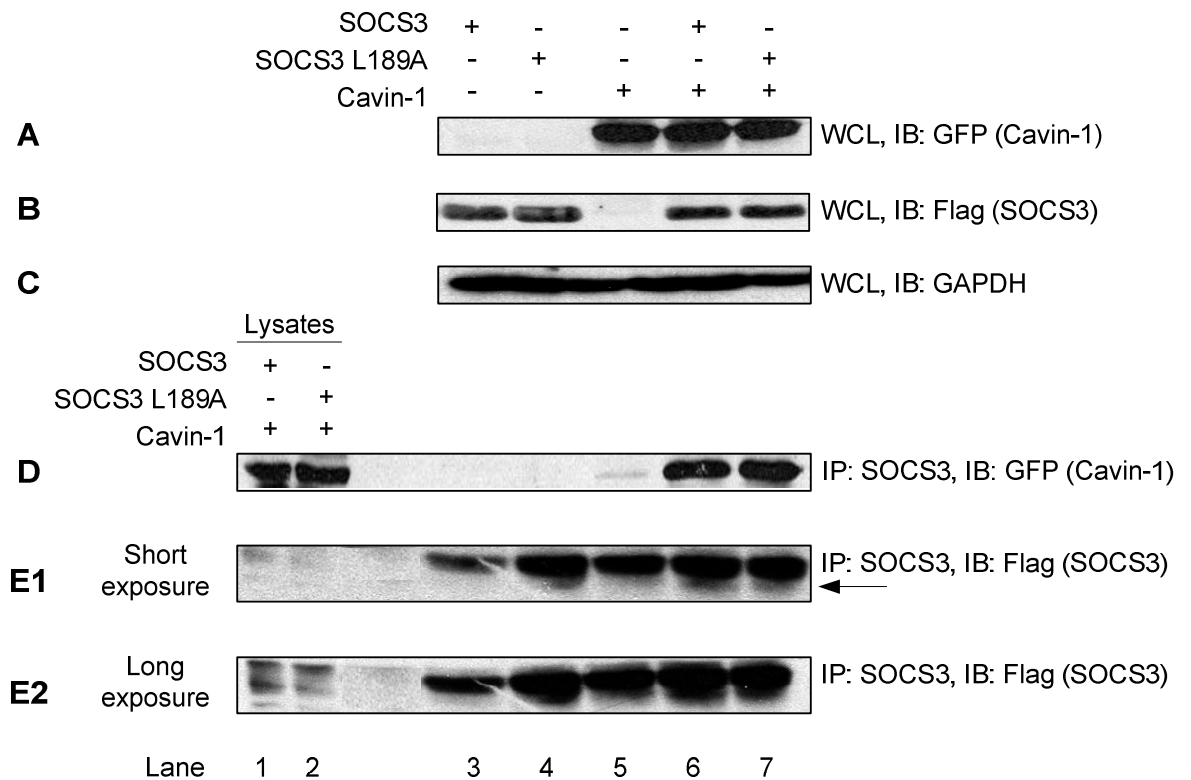


Figure 6.8: SOCS3 and the SOCS3 L189A SOCS-Box mutant precipitates cavin-1

HEK293 cells were transfected as described (Section 2.2.12) with SOCS3-Flag, SOCS3-L189A-Flag, and cavin-1-GFP cDNA constructs in the indicated combinations. Soluble protein lysates were prepared and co-immunoprecipitation performed as described (Section 2.2.13) using 40 μ l of 50% (v/v) slurry of protein G Sepharose beads and 10 μ l of anti-SOCS3 antibody. Recovered protein complexes were fractionated by SDS-PAGE and precipitation assessed by immunoblotting using anti-GFP (Panel A/D) and anti-Flag antibody (Panel B/E1/2, arrow indicates SOCS3). GAPDH was used as a loading control (Panel C).

6.2.4 Cavin-1 ubiquitination is enriched in the presence of SOCS3

SOCS3 is predicted to attach K48-linked polyubiquitin chains to its substrates. As such, an increased ubiquitin signal is expected in the presence but not absence of SOCS3 following the isolation of the ubiquitinome or candidate substrate by immunoprecipitation. To reduce background and preserve polyubiquitin chains immunoprecipitation was performed under denatured conditions.

HEK293 cells were transfected as described (Section 2.2.12) with the relevant cDNA constructs in the indicated combinations (Figures 6.9-6.13). Soluble protein lysates were prepared and denatured immunoprecipitation performed as described (Section 2.2.14) (Figures 6.9-6.13). Captured proteins were fractionated by SDS-PAGE analysed by immunoblotting.

Following isolation of the ubiquitinome, cavin-1 appears to be highly enriched in the presence but not absence of SOCS3 and components of the E3 ligase (Figure 6.9, panel A/B, lane 6 vs.8, and arrow). Previous data (Figure 6.6, panel E, lane 2 and 8) showed that cavin-1 was detected as three bands while only the top band was precipitated. However, in this case the signal relating to the bottom band is enhanced while other bands are similarly precipitated. As such, this new data suggests that SOCS3 can bind full-length and fragmented cavin-1. However, there seems to be little difference between these lanes in the levels of high molecular weight ubiquitin signal expected of polyubiquitination (small differences are indicated by brackets 1 and 3). This suggests that cavin-1 might be mono-ubiquitinated by SOCS3 and polyubiquitinated *via* another route. Alternatively, since cavin-1 is not greatly enriched, the ubiquitin signal might be too weak to produce a visible difference. The band (~75kDa) present in the control (Figure 6.9, panel A/B, lane 7) is assumed to be non-specific since an anti-Flag antibody was used during precipitation. While this antibody would have precipitated SOCS3-Flag, the use of denaturing conditions would have prevented the isolation of SOCS3-bound proteins.

The same enhancement of cavin-1 was seen with the reciprocal co-immunoprecipitation experiment (Figure 6.10, panel A/B, lane 5 vs. 7, arrows). However, in this case an enhanced polyubiquitin signal was detected in the high

molecular fraction (Figure 6.10, lane 5 vs. lane 7, bracket 1) in the cavin-1-only transfected cells. Interestingly, in the presence of the SOCS3-E3 complex, an enhanced polyubiquitin signal was detected around 75kDa i.e. the expected mass of cavin-1 (Figure 6.10, lane 5 vs. lane 7, bracket 2). The same variation in the ubiquitin smear was seen to a lesser extent previously (Figure 6.9, panel A/B, lanes 6 vs. 8, brackets 1-4). It therefore seems that in the presence of SOCS3, the ubiquitin smear relating to cavin-1 is shifted to a lower molecular fraction. This suggests that SOCS3 might somehow inhibit or negatively regulate polyubiquitination of cavin-1, possibly by out-competing other E3 ligases. Given that only low molecular weight ubiquitination is enhanced in the presence of the SOCS3-E3, cavin-1 might be mono-/multi-ubiquitinated. SOCS3 might therefore protect or preferentially ubiquitinate cavin-1 leading to this switch in the ubiquitin smear. As a negative control, the impact of the SOCS3-L189A SOCS-box mutant on cavin-1 ubiquitination was assessed. However, no difference was seen in the ubiquitination of cavin-1 compared to the WT (Figure 6.10, panel A/B, lanes 7 and 8). As such, this result supports the role of SOCS3 in protecting a certain ubiquitinated form of cavin-1.

The strong smear detected in the control (Figure 6.10, panel A, lane 6) is due to the use of an anti-Flag antibody as the control, which resulted in the precipitation of ubiquitinated SOCS3-Flag. The same result should also have been expected in the previous experiment (Figure 6.9, panel A, lane 7). However, given the varying efficiencies of antibodies to precipitate their target (anti-cavin-1 being less efficient than anti-HA), different exposure times were necessary which resulted in the overexposure of the control (Figure 6.10, panel A, lane 6). To avoid precipitation of SOCS3, all future experiments employed an unrelated antibody, myosin phosphatase-targeting subunit 1 (MYPT1) as the control.

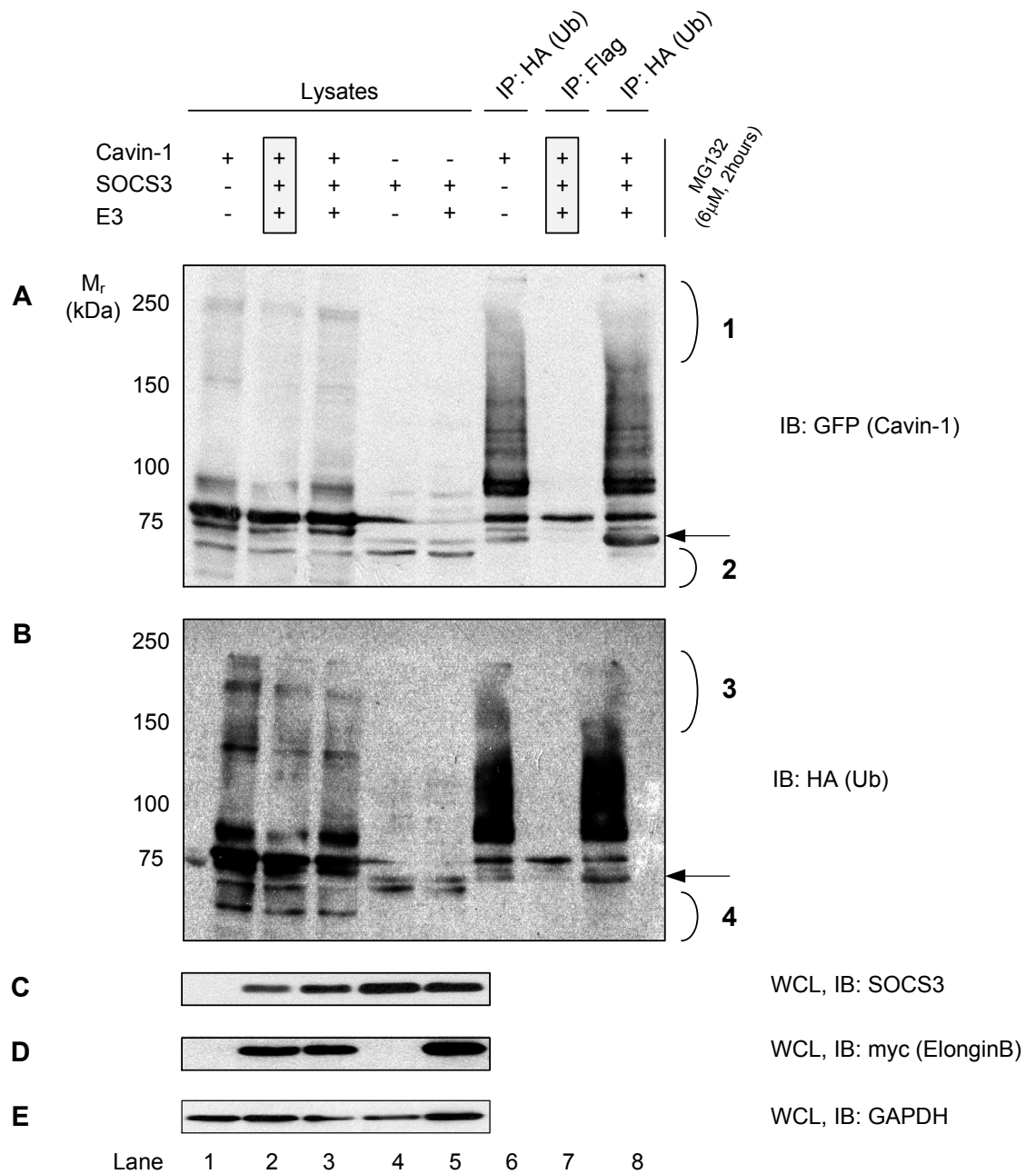


Figure 6.9: Cavin-1 ubiquitination is enriched in the presence of SOCS3

HEK293 cells were transfected as described (Section 2.2.12) with Ub-HA plus SOCS3-Flag, cavin-1-GFP, and E3 ligase components cullin5, elonginB-myc, elonginC, and Rbx1-myc cDNA constructs in the indicated combinations. Soluble protein lysates were prepared and denatured immunoprecipitation performed as described (Section 2.2.14). Captured ubiquitinated proteins were fractionated by SDS-PAGE and recovery assessed by immunoblotting using anti-GFP (Panel A) and anti-HA antibody (Panel B). Where possible, protein expression was assessed using anti-SOCS3 (Panel C) and anti-myc antibody (Panel D). GAPDH was used as a loading control (Panel E). The greyed-out box indicates which lysates were used for the control immunoprecipitation. Arrows indicate cavin-1 while brackets indicate variations in the ubiquitin smear.

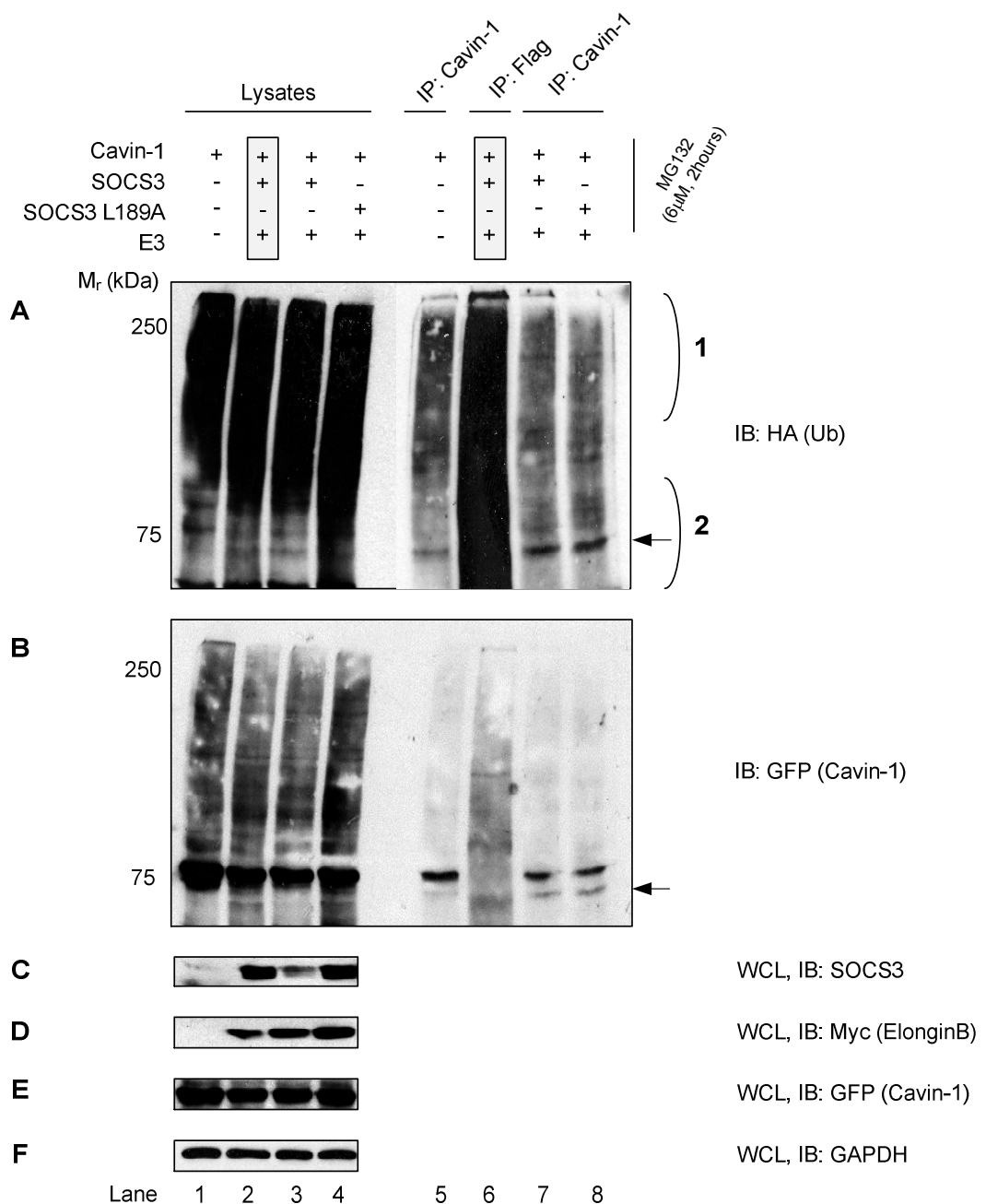


Figure 6.10: Cavin-1 ubiquitination is enriched in the presence of SOCS3

HEK293 cells were transfected as described (Section 2.2.12) with Ub-HA plus SOCS3-Flag, SOCS3-L189A-Flag, cavin-1-GFP, and E3 ligase components cullin5, elonginB-myc, elonginC, and Rbx1-myc cDNA constructs in the indicated combinations. Soluble protein lysates were prepared and denatured immunoprecipitation performed as described (Section 2.2.14). Captured proteins were fractionated by SDS-PAGE and recovery assessed by immunoblotting using anti-HA (Panel A) and anti-GFP antibody (Panel B). Where possible, protein expression was assessed using anti-SOCS3 (Panel C), anti-GFP (Panel E), and anti-myc antibody (Panel D). GAPDH was used as a loading control (Panel F). The greyed-out box indicates which lysates were used for the control immunoprecipitation. Arrows indicate cavin-1 while brackets indicate variations in the ubiquitin smear.

As controls for the previous experiments (Figure 6.9 and 6.10), ubiquitination of SOCS3 was assessed in the presence and absence of components of the E3 ligase. SOCS3 was found to be highly ubiquitinated in the absence but not the presence of the E3 scaffold (Figure 6.11, panel A, lane 3 vs. 4). Furthermore, levels of SOCS3 were lower in the presence of the E3 components. However, treatment with MG132 is expected to preserve SOCS3 suggesting that loss of SOCS3 might be occurring *via* an alternative route, possibly *via* a PEST-domain mediated route. Ubiquitination of SOCS3 in the absence of the E3 scaffold might suggest that ubiquitination occurs due to the presence of endogenous E3 proteins i.e. cullin5, elonginBC, and Rbx2 or alternatively by a completely different E3 ligase. The lack of ubiquitination in the presence of the E3 complex is perhaps a consequence of the unequal expression of its individual components. Since these components are required in a 1:1 stoichiometry, varying expression levels might result in the formation of several variations of an incomplete complex. As such, a reduced ubiquitination signal would be expected. Although the same μg -amount of cDNA construct was used in each case, expression levels of each component was not checked, in part, due to the lack of specific antibodies. Plasmids for E3 ligase scaffolds optimised for expression are now commercially available and could be an option in the future. It might also be beneficial to perform an *in vitro* ubiquitination assay, using a purified E3 complex, since it would be unaffected by alternative routes of ubiquitination.

The reciprocal control immunoprecipitation produced the same result (Figure 6.12). In this case, the SOCS3-L189A mutant was also included and was seen to be ubiquitinated to a higher degree than the WT in the absence of the E3 scaffold. This suggests that SOCS3 is being ubiquitinated by different E3 ligase since, as it was previously shown (Figure 6.2, panel D/E, lanes 4 vs. 5), that SOCS3-L189A cannot bind elonginB or cullin5.

This control data suggests that the ubiquitinated cavin-1 is enriched in the presence of SOCS3. However, SOCS3 is present at reduced levels when expressed with components of the E3 ligase. As such, ubiquitinated cavin-1 might be expected to be enriched to greater levels in the presence of SOCS3 alone. Of course, this would rely on the presence of endogenous E3 ligase components for SOCS3-dependent ubiquitination.

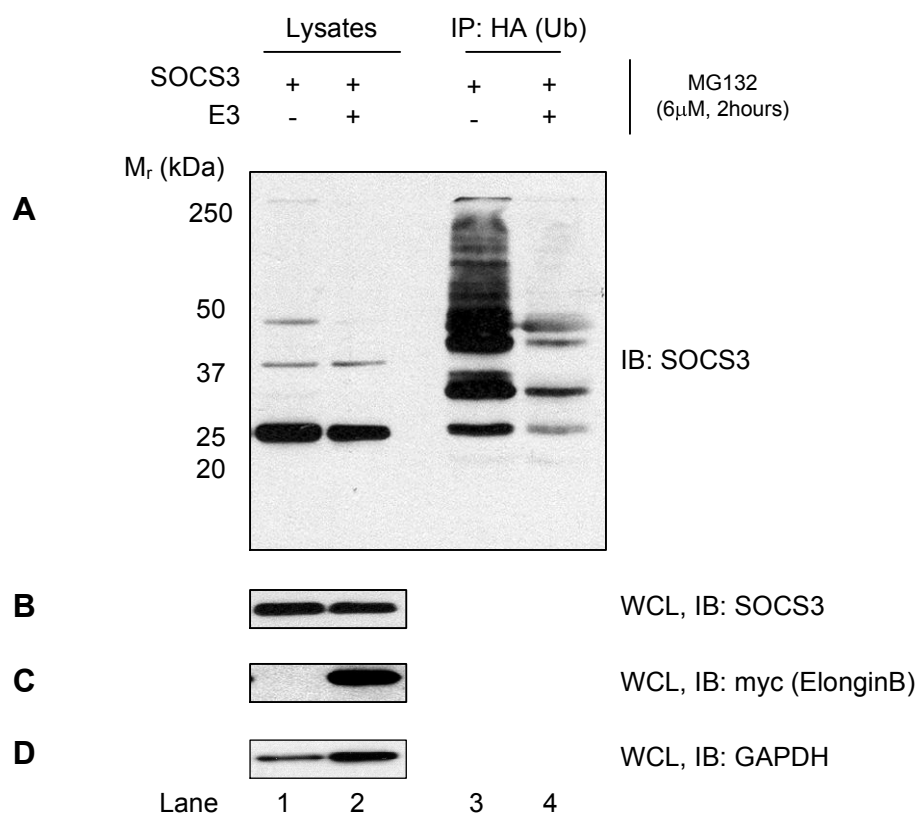


Figure 6.11: SOCS3 ubiquitination is enriched in the absence of components of the E3 ligase

HEK293 cells were transfected as described (Section 2.2.12) with Ub-HA plus SOCS3-Flag, and E3 ligase components cullin5, elonginB-myc, elonginC, and Rbx1-myc cDNA constructs in the indicated combinations. Soluble protein lysates were prepared and denatured immunoprecipitation performed as described (Section 2.2.14). Captured proteins were fractionated by SDS-PAGE and recovery assessed by immunoblotting using anti-SOCS3 (Panel A). Where possible, protein expression was assessed using anti-SOCS3 (Panel B), and anti-myc antibody (Panel C). GAPDH was used as a loading control (Panel D).

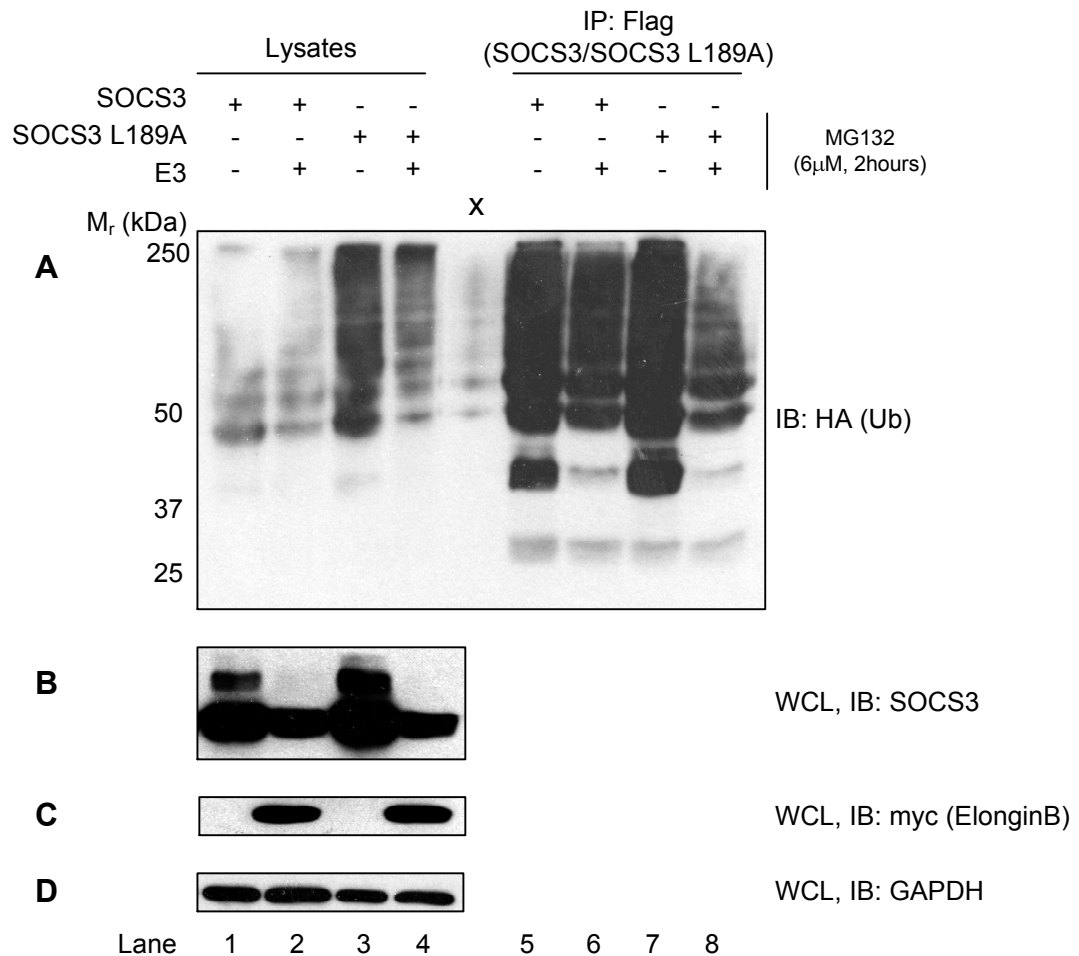


Figure 6.12: SOCS3 ubiquitination is enriched in the absence of components of the E3 ligase

HEK293 cells were transfected as described (Section 2.2.12) with Ub-HA plus SOCS3-Flag, SOCS3-L189A-Flag, and E3 ligase components cullin5, elonginB-myc, elonginC, and Rbx1-myc cDNA constructs in the indicated combinations. Soluble protein lysates were prepared and denatured immunoprecipitation performed as described (Section 2.2.14). Captured proteins were fractionated by SDS-PAGE and recovery assessed by immunoblotting using anti-HA antibody (Panel A). Where possible, protein expression was assessed using anti-SOCS3 (Panel B), and anti-myc antibody (Panel C). GAPDH was used as a loading control (Panel D).

So far, it has been demonstrated that low molecular weight ubiquitination of cavin-1 is enriched in the presence but not absence of SOCS3. If SOCS3 was to mediate proteasomal degradation of cavin-1 then an enrichment of K48-specific polyubiquitination should be detected. Furthermore, control experiments suggest that SOCS3 levels can be enhanced in the absence of the E3 complex. As such, cavin-1 immunoprecipitation experiments were performed as before in the presence or absence of SOCS3 or SOCS3-L189A. Enrichment of K48-polyubiquitination was assessed *via* immunoblotting with K48-polyubiquitin chain-specific antibody.

Cavin-1 was again detected to be enriched in the presence but not absence of SOCS3 (Figure 6.13, panel B/C1, lane 5 vs. 7/8, and arrows). Furthermore, as discussed previously, a switch in the ubiquitin smear is seen. While a high molecular weight polyubiquitination signal is detected in the absence of SOCS3 (Figure 6.13, lane 5 vs. 7, brackets 2 and 4), in its presence, an enhanced signal is detected around the expected mass of cavin-1 (Figure 6.13, lane 5 vs. 7/8, brackets 3 and 5). The low molecular weight fraction (Figure 6.13, lane 5 vs. 7/8, brackets 3 and 5) might be attributable to ubiquitinated forms of full-length cavin-1 and cavin-1 fragments. Interestingly, K48-specific polyubiquitination is also enhanced in the presence of SOCS3 within this same region (Figure 6.13, lane 5 vs. 7/8, bracket 1). However, since SOCS3-L189A produces the same effect, it suggests that K48-polyubiquitination is *via* a non-SOCS3 mechanism. However, it may support SOCS3 as functioning to protect cavin-1 K48-polyubiquitination.

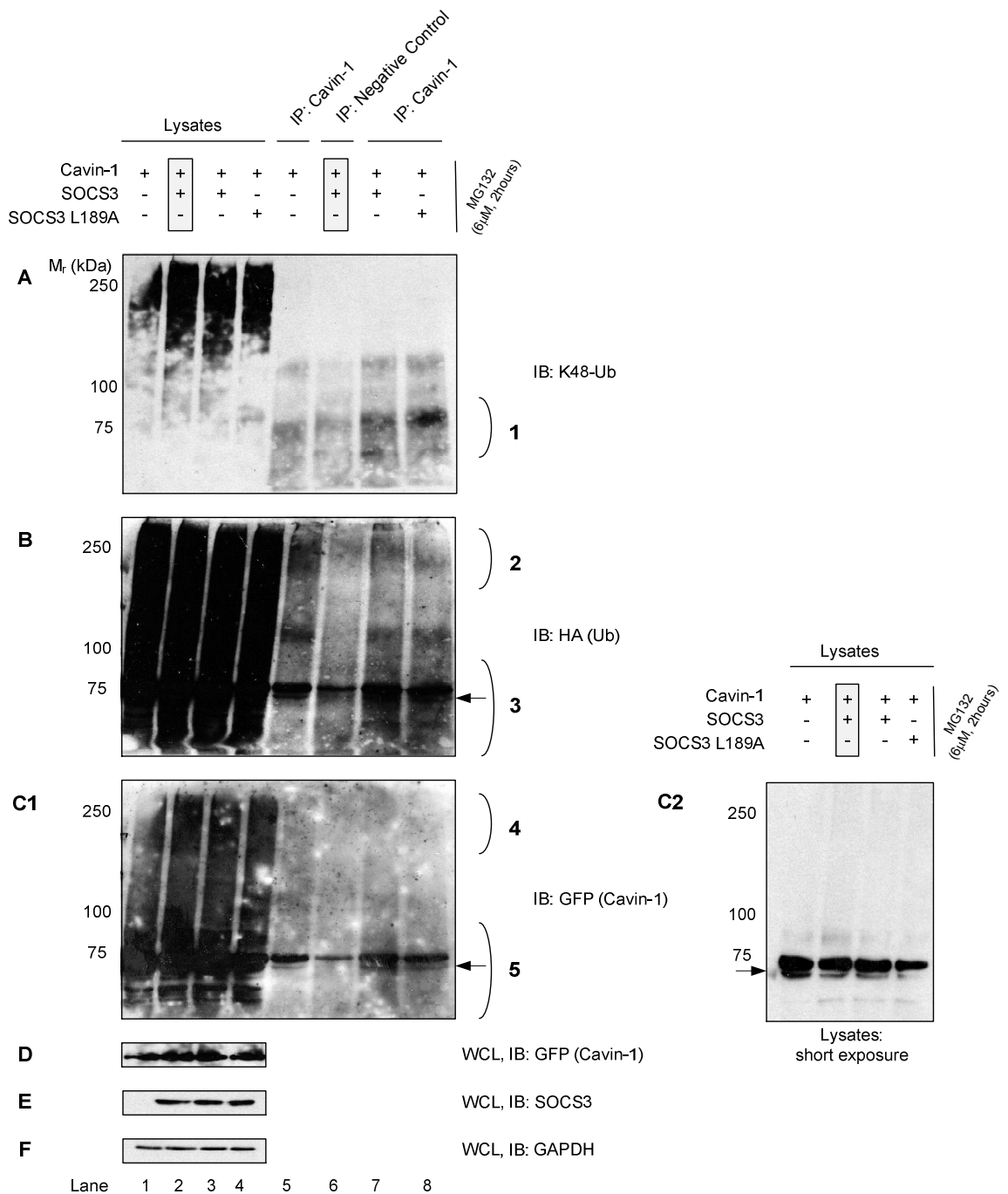


Figure 6.13: Cavin-1 ubiquitination is enriched in the presence of SOCS3

HEK293 cells were transfected as described (Section 2.2.12) with Ub-HA plus SOCS3-Flag, SOCS3-L189A-Flag, and cavin-1-GFP cDNA constructs in the indicated combinations. Soluble protein lysates were prepared and denatured immunoprecipitation performed as described (Section 2.2.14). Captured proteins were fractionated by SDS-PAGE and recovery assessed by immunoblotting using anti-K48-Ub (Panel A), anti-HA (Panel B) and anti-GFP (Panel C1 (long exposure), C2 (short exposure)) antibody. Where possible, protein expression was assessed using anti-GFP (Panel D), anti-SOCS3 antibody (Panel E). GAPDH was used as a loading control (Panel F). The greyed-out box indicates which lysates were used for the control immunoprecipitation.

6.2.5 Peptide array of tyrosine-phosphorylated peptides from SOCS3 candidates supports an interaction between SOCS3 and Hsp70 but not cavin-1

SOCS3 is predicted to interact with and ubiquitinate, tyrosine-phosphorylated substrates (9-12). Online databases such as phosphosite.org provide access to proteins and the identity of their known tyrosine-phosphorylated peptides. To assess the interaction of SOCS3 with candidate substrates identified *via* a proteomics screen (Section 5.0), peptide arrays were fabricated using known tyrosine-phosphorylated peptides from these candidates (Section 2.2.15, Table 2.3). Proteins were selected for peptide array analysis based on their SILAC ratio ($\log_2(\text{normalised H/L}) > 1$) and the presence of known tyrosine-phosphorylated residues. While purified GST-fusion proteins are typically used for peptide array overlays, a quicker approach would be to use cell lysates from cells over-expressing the protein of interest (249).

HEK293 cells were transfected with SOCS3-Flag, SOCS3-L189A-Flag, or GFP cDNA constructs as described (Section 2.2.12). Soluble protein lysates were then prepared and the peptide array overlaid and visualised as described (Section 2.2.15.1).

SOCS3 was found to interact with several tyrosine-phosphorylated peptides (Figure 6.14, panel A vs. panel C). Proteins that significantly ($p < 0.05$, paired one-tailed *t*-test) interact with SOCS3 are presented in Table 6.0. Importantly, SH2-interacting positive control peptides pY-FAK1 and pY-gp130, but not gp130, significantly interacted with SOCS3. Three peptides from Hsc70 significantly interacted with SOCS3. Furthermore, the interaction with peptide Hsc70 (1) produced the strongest signal over all peptide interactions (Figure 6.14, panel A vs. panel C, dashed oval) thus appeared to be specific as other peptides from Hsc70 (Figure 6.14, panel A vs. panel C, solid oval) did not interact as strongly. Interestingly, SOCS3 did not interact significantly with known tyrosine-phosphorylated peptides from cavin-1 (Figure 6.14, panel A vs. panel C, solid rectangle) supporting previous data suggesting that tyrosine phosphorylation inhibits the cavin-1-SOCS interaction (Figure 6.7).

Several SOCS3-peptide interactions were preserved when the peptide arrays were overlaid with the C-terminal domain SOCS-box mutant, SOCS3-L189A (Figure 6.14, panel B vs. panel A) (Table 6.0). Importantly this included several peptides from Hsc70. This suggested that these interactions were specific and potentially SOCS-box independent. However, since the impact of the L189A mutation on non-elonginBC interactions is unknown, it still cannot be completely ruled-out. A SOCS-box deletion mutant would give a more informative result. As before, SH2-interacting control peptides pY-FAK1 and pY-gp130, but not gp130, still significantly interacted with SOCS3-L189A.

So far, SOCS3 has been shown interact with several tyrosine-phosphorylated candidate peptides. However, if these interactions are specific and the SOCS3-substrate interaction is dependent on tyrosine phosphorylation then these interactions would be expected to be lost if the PTM was removed. A further peptide array was fabricated using peptides that significantly interacted with SOCS3, with or without tyrosine phosphorylation. Due to the unavailability of the CelluSpot system, the peptide array was fabricated using a different technique (Section 2.2.15.2). Furthermore, only a single peptide array was fabricated meaning that the array had to be overlaid with the control and then stripped before overlaying with SOCS3.

Overlaying the peptide array with the control showed some non-specific background, however, the control peptides pY-FAK1, pY-gp130, and gp130 were unaffected (Data not shown). Specific interactions were detected when the peptide array was overlaid with purified SOCS3. Unfortunately, variations in size and intensity were detected between duplicate spots that may be a consequence of a non-uniform fabrication process and/or membrane stripping. As such, quantitation was not attempted. Repeating the experiment with separate arrays for control and SOCS3 overlay and thus avoiding membrane stripping might produce more clear results. However, this was not possible due to time constraints.

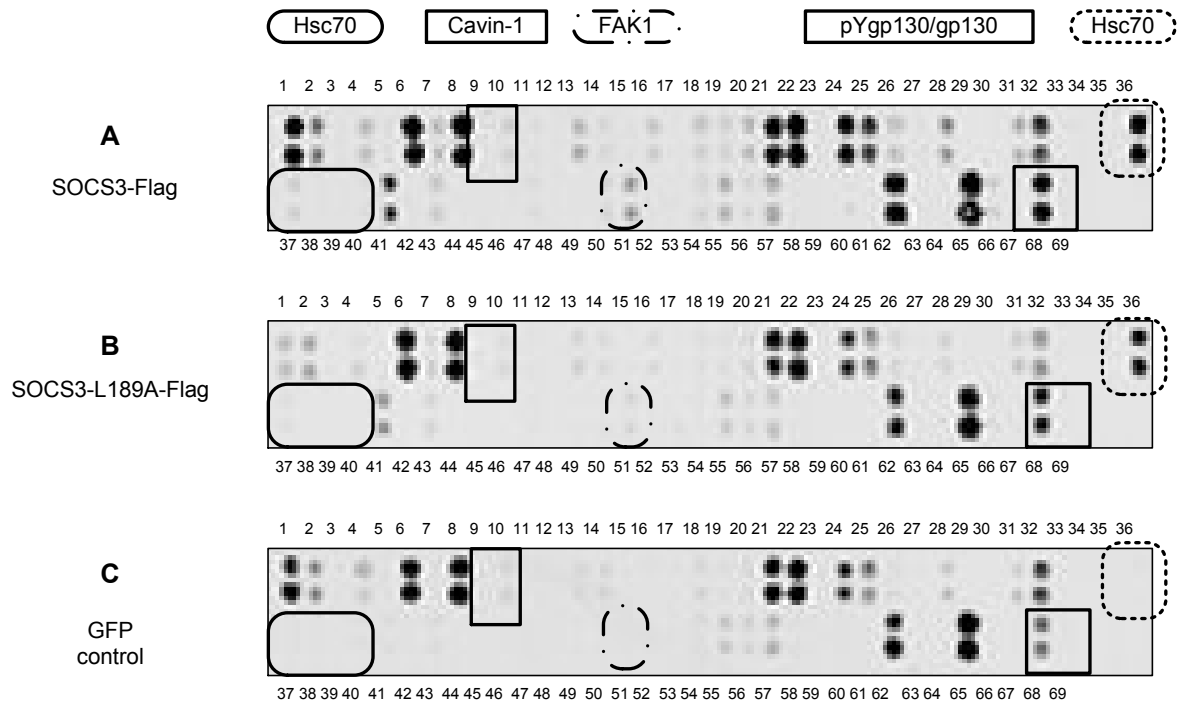


Figure 6.14: SOCS3 interacts with several known tyrosine-phosphorylated peptides from candidate proteins

HEK293 cells were transfected as described (Section 2.2.12) with SOCS3-Flag, SOCS3-L189A-Flag, or GFP cDNA constructs. Soluble protein lysates were then prepared and the peptide array overlaid as described (Section 2.2.15.1) with SOCS3-Flag (Panel A), SOCS3-L189A-Flag (Panel B), or GFP-containing cell lysates (Panel C). SOCS3-peptide interactions were assessed using anti-Flag primary antibody and an 800-IRDye secondary antibody. Interactions were visualized using a LI-COR Odyssey system Sa.

Table 6.0: SOCS3 interacts with several known tyrosine-phosphorylated peptides from candidate proteins

Peptide arrays spotted with known tyrosine-phosphorylated peptides of candidate proteins (Figure 6.14) (Table 2.3) were overlaid with SOCS3, SOCS3-L189A, or GFP control. Candidate peptides (Table 2.3) that significantly ($p < 0.05$, paired one-tailed t -test) interacted with SOCS3 compared to the GFP control and are presented here. Moreover, of these interactions, several were preserved following overlaying the array with the SOCS3 SOCS-box mutant SOCS3-L189A. Positive controls are highlighted in **bold** while greyed out boxes signify interactions lost following SOCS3-L189A overlay.

Array Spot	Peptide Sequence	SOCS3-FLAG	SOCS3-L189A-FLAG
		Protein (Peptide)	
1	V-D-P-A-pY-T-G-R-V-G-A	Eps15L (1)	
5	S-R-Q-L-pY-V-L-G-H-E-A	Ube (2)	
7	V-L-G-P-pY-T-F-S-I-C-D	Ube1 (4)	
13	A-P-G-E-pY-F-F-S-D-G-I	Impdh2	
16	A-C-E-A-pY-L-V-G-L-F-E	Histone 3.1 (3)	Histone 3.1 (3)
19	L-F-D-S-pY-T-N-L-E-R-V	Abi2 (3)	Abi2 (3)
20	R-V-A-D-pY-C-E-N-N-Y-I	Abi2 (4)	
24	D-P-A-G-pY-Y-C-G-F-K-A	Psm6 (1)	
25	P-A-G-Y-pY-C-G-F-K-A-T	Psm6 (2)	
26	E-G-R-L-pY-Q-V-E-Y-A-F	Psm6 (3)	Psm6 (3)
28	E-S-L-R-pY-K-L-L-G-G-L	Rps3 (2)	
36	L-G-T-T-pY-S-C-V-G-V-F	Hsc73(1)	Hsc73(1)
37	T-T-P-S-pY-V-A-F-T-D-T	Hsc73(2)	Hsc73(2)
40	I-A-E-A-pY-L-G-K-T-V-T	Hsc73 (5)	Hsc73 (5)
41	K-N-S-S-pY-F-V-E-W-I-P	Tubb5 (1)	Tubb5 (1)
43	N-E-A-L-pY-D-I-C-F-R-T	Tubb5 (3)	Tubb5 (3)
47	L-N-F-F-pY-Q-Q-V-K-S-D	FAK (2)	
50	L-I-D-G-pY-C-R-L-V-N-G	FAK (4)	
51	E-T-D-D-pY-A-E-I-I-D-E	FAK (5)	FAK (5)
54	G-L-S-R-pY-M-E-D-S-T-Y	FAK (8)	
55	E-D-S-T-pY-Y-K-A-S-K-G	FAK (9)	
66	D-W-S-H-pY-F-K-I-I-E-D	Krt18 (5)	
68	S-T-V-Q-pY-S-T-V-V-H-S	pY759gp130	pY759gp130

6.2.6 SOCS3 specifically interacts with several domains of cavin-1

While immunoprecipitation has demonstrated an interaction between SOCS3 and cavin-1, protein domains or residues necessary for this interaction are unknown. Furthermore, apart from protein-sequence-predicted motifs, no further structural information about cavin-1 is available. Due to its availability, a peptide array was decided to be the most efficient technique to begin investigating the interaction. The array was spotted with 25mer, 5 residue overlapping peptides of the 392 amino-acid-long cavin-1 (*Mus musculus*, UniProtKB accession number: O54724). SOCS3 would be expected to interact with some but not all peptide spots if the SOCS3-cavin-1 interaction was specific.

HEK293 cells were transfected with SOCS3-Flag or GFP cDNA constructs as described (Section 2.2.12). Soluble protein lysates were then prepared and the peptide array overlaid and visualised as described (Section 2.2.15.2).

The LI-COR Odyssey is an efficient method of visualisation since it has a wider linear range of detection than chemiluminescence techniques allowing weak and strong signals to be detected on the same membrane. As opposed to enzymatic techniques where signal intensity depends on exposure times, the LI-COR system allows the signal to be boosted using an intensity setting. A low intensity dampens the signal and a high intensity boosts the signal. Since I was unable to predict the high intensity of the SOCS3 overlay, the control and SOCS3 overlay were visualised at different intensities. While SOCS3 was visualised with intensity=5, the control was visualised with intensity=7. As such, spots detected by the control are stronger (x4) than they should be and thus undervalues the intensity of the SOCS3 overlay. However, this error has not affected the result (Table 6.1).

Table 6.1: SOCS3 specifically interacts with several domains of cavin-1

The peptide array was spotted with 25mer-long, 5 residue overlapping peptides from murine cavin-1. Background was detected by probing with an anti-SOCS3 antibody (control). SOCS3-peptide interactions were assessed using purified SOCS3. Background and specific interactions were visualised using the LI-COR 800-IRDye LI-COR Odyssey Sa system. (see text for details)

Array			N	Peptide Sequence	C	Cavin-1 putative domains (residues)
Peptide	SOCS3	Control				
1			1	M-E-D-V-T-L-H-I-V-E-R-P-Y-S-G-F-P-D-A-S-S-E-G-P-E	25	PEST Domain (11-47)
2			6	L-H-I-V-E-R-P-Y-S-G-F-P-D-A-S-S-E-G-P-E-P-T-Q-G-E	30	
3			11	R-P-Y-S-G-F-P-D-A-S-S-E-G-P-E-P-T-Q-G-E-A-R-A-T-E	35	
4			16	F-P-D-A-S-S-E-G-P-E-P-T-Q-G-E-A-R-A-T-E-E-P-S-G-T	40	
5			21	S-E-G-P-E-P-T-Q-G-E-A-R-A-T-E-E-P-S-G-T-G-S-D-E-L	45	
6			26	P-T-Q-G-E-A-R-A-T-E-E-P-S-G-T-G-S-D-E-L-I-K-S-D-Q	50	
7			31	A-R-A-T-E-E-P-S-G-T-G-S-D-E-L-I-K-S-D-Q-V-N-G-V-L	55	
8	●		36	E-P-S-G-T-G-S-D-E-L-I-K-S-D-Q-V-N-G-V-L-V-L-S-L-L	60	
9	●		41	G-S-D-E-L-I-K-S-D-Q-V-N-G-V-L-V-L-S-L-L-D-K-I-I-G	65	
10	●		46	I-K-S-D-Q-V-N-G-V-L-V-L-S-L-L-D-K-I-I-G-A-V-D-Q-I	70	
11	●		51	V-N-G-V-L-V-L-S-L-L-D-K-I-I-G-A-V-D-Q-I-Q-L-T-Q-A	75	
12			56	V-L-S-L-L-D-K-I-I-G-A-V-D-Q-I-Q-L-T-Q-A-Q-L-E-E-R	80	
13			61	D-K-I-I-G-A-V-D-Q-I-Q-L-T-Q-A-Q-L-E-E-R-Q-A-E-M-E	85	
14			66	A-V-D-Q-I-Q-L-T-Q-A-Q-L-E-E-R-Q-A-E-M-E-G-A-V-Q-S	90	
15			71	Q-L-T-Q-A-Q-L-E-E-R-Q-A-E-M-E-G-A-V-Q-S-I-Q-G-E-L	95	
16	●		76	Q-L-E-E-R-Q-A-E-M-E-G-A-V-Q-S-I-Q-G-E-L-S-K-L-G-K	100	
17	●		81	Q-A-E-M-E-G-A-V-Q-S-I-Q-G-E-L-S-K-L-G-K-A-H-A-T-T	105	
18	●		86	G-A-V-Q-S-I-Q-G-E-L-S-K-L-G-K-A-H-A-T-T-S-N-T-V-S	110	
19	●		91	I-Q-G-E-L-S-K-L-G-K-A-H-A-T-T-S-N-T-V-S-K-L-L-E-K	115	
20	●		96	S-K-L-G-K-A-H-A-T-T-S-N-T-V-S-K-L-L-E-K-V-R-K-V-S	120	
21	●		101	A-H-A-T-T-S-N-T-V-S-K-L-L-E-K-V-R-K-V-S-V-N-V-K-T	125	Conserved Coiled-Coil domain (46-167)
22	●		106	S-N-T-V-S-K-L-L-E-K-V-R-K-V-S-V-N-V-K-T-V-R-G-S-L	130	
23	●		111	K-L-L-E-K-V-R-K-V-S-V-N-V-K-T-V-R-G-S-L-E-R-Q-A-G	135	
24	●		116	V-R-K-V-S-V-N-V-K-T-V-R-G-S-L-E-R-Q-A-G-Q-I-K-K-L	140	
25	●		121	V-N-V-K-T-V-R-G-S-L-E-R-Q-A-G-Q-I- <u>K-K-L-E-V-N-E-A</u>	145	
26	●		126	V-R-G-S-L-E-R-Q-A-G-Q-I- <u>K-K-L-E-V-N-E-A-E-L-L-R-R</u>	150	
27	●		131	E-R-Q-A-G-Q-I- <u>K-K-L-E-V-N-E-A-E-L-L-R-R-R-N-F-K</u> -V	155	
28	●		136	Q-I- <u>K-K-L-E-V-N-E-A-E-L-L-R-R-R-N-F-K</u> -V-M-I-Y-Q-D	160	
29	●		141	<u>E-V-N-E-A-E-L-L-R-R-R-N-F-K</u> -V-M-I-Y-Q-D-E-V-K-L-P	165	
30	●		146	<u>E-L-L-R-R-R-N-F-K</u> -V-M-I-Y-Q-D-E-V-K-L-P-A-K-L-S-V	170	
31	●		151	<u>R-N-F-K</u> -V-M-I-Y-Q-D-E-V-K-L-P-A-K-L-S-V-S-K-S-L-K	175	LRR (166-186)
32	●		156	M-I-Y-Q-D-E-V-K-L-P-A-K-L-S-V-S-K-S-L-K-E-S-E-A-L	180	
33	●		161	E-V-K-L-P-A-K-L-S-V-S-K-S-L-K-E-S-E-A-L-P-E-K-E-G	185	

Array		N	Peptide Sequence	C	Cavin-1 putative domains (residues)	
Peptide	SOCS3				Control	
34		166	A-K-L-S-V-S-K-S-L-K-E-S-E-A-L-P-E-K-E-G-D-E-L-G-E	190		
35		171	S-K-S-L-K-E-S-E-A-L-P-E-K-E-G-D-E-L-G-E-G-E-R-P-E	195		
36		176	E-S-E-A-L-P-E-K-E-G-D-E-L-G-E-G-E-R-P-E-D-D-T-A-A	200		
37		181	P-E-K-E-G-D-E-L-G-E-G-E-R-P-E-D-D-T-A-A-I-E-L-S-S	205		
38		186	D-E-L-G-E-G-E-R-P-E-D-D-T-A-A-I-E-L-S-S-D-E-A-V-E	210	PEST Domain (193-219)	
39		191	G-E-R-P-E-D-D-T-A-A-I-E-L-S-S-D-E-A-V-E-V-E-E-V-I	215		
40		196	D-D-T-A-A-I-E-L-S-S-D-E-A-V-E-V-E-E-V-I-E-E-S-R-A	220		
41		201	I-E-L-S-S-D-E-A-V-E-V-E-E-V-I-E-E-S-R-A-E-R-I-K-R	225		
42		206	D-E-A-V-E-V-E-E-V-I-E-E-S-R-A-E-R-I-K-R-S-G-L-R-R	230	NLS (233-249)	
43		211	V-E-E-V-I-E-E-S-R-A-E-R-I-K-R-S-G-L-R-R-V-D-D-F-K	235		
44		216	E-E-S-R-A-E-R-I-K-R-S-G-L-R-R-V-D-D-F- K-K-A-F-S-K	240	LRR (257-297)	Conserved Basic regions (220-298)
45		221	E-R-I-K-R-S-G-L-R-R-V-D-D-F- K-K-A-F-S-K-E-K-M-E-K	245		
46		226	S-G-L-R-R-V-D-D-F- K-K-A-F-S-K-E-K-M-E-K-T-K-V-R-T	250		
47		231	V-D-D-F- K-K-A-F-S-K-E-K-M-E-K-T-K-V-R-T-R -E-N-L-E	255		
48		236	K-A-F-S-K-E-K-M-E-K-T-K-V-R-T-R -E-N-L-E-K-T-R-L-K	260		
49		241	E-K-M-E-K-T-K-V-R-T-R -E-N-L-E-K-T-R-L-K-T-K-E-N-L	265		
50		246	T-K-V-R-T-R -E-N-L-E-K-T-R-L-K-T-K-E-N-L-E-K-T-R-H	270		
51		251	R-E-N-L-E-K-T-R-L-K-T-K-E-N-L-E-K-T-R-H-T-L-E-K-R	275		
52		256	K-T-R-L-K-T-K-E-N-L-E-K-T-R-H-T-L-E-K-R-M-N-K-L-G	280		
53		261	T-K-E-N-L-E-K-T-R-H-T-L-E-K-R-M-N-K-L-G-T-R-L-V-P	285		
54		266	E-K-T-R-H-T-L-E-K-R-M-N-K-L-G-T-R-L-V-P-V-E-R-R-E	290		
55		271	T-L-E-K-R-M-N-K-L-G-T-R-L-V-P-V-E-R-R-E-K-L-K-T-S	295		
56		276	M-N-K-L-G-T-R-L-V-P-V-E-R-R-E-K-L-K-T-S-R-D-K-L-R	300		
57		281	T-R-L-V-P-V-E-R-R-E-K-L-K-T-S-R-D-K-L-R-K-S-F-T-P	305		
58		286	V-E-R-R-E-K-L-K-T-S-R-D-K-L-R-K-S-F-T-P-D-H-V-V-Y	310		
59		291	K-L-K-T-S-R-D-K-L-R-K-S-F-T-P-D-H-V-V-Y-A-R-S-K-T	315		
60		296	R-D-K-L-R-K-S-F-T-P-D-H-V-V-Y-A-R-S-K-T-A-V-Y-K-V	320		
61		301	K-S-F-T-P-D-H-V-V-Y-A-R-S-K-T-A-V-Y-K-V-P-P-F-T-F	325		
62		306	D-H-V-V-Y-A-R-S-K-T-A-V-Y-K-V-P-P-F-T-F-H-V-K-K-I	330		
63		311	A-R-S-K-T-A-V-Y-K-V-P-P-F-T-F-H-V-K-K-I-R-E-G-E-V	335		
64		316	A-V-Y-K-V-P-P-F-T-F-H-V-K-K-I-R-E-G-E-V-E-V-L-K-A	340	PEST Domain (339 - 375)	
65		321	P-P-F-T-F-H-V-K-K-I-R-E-G-E-V-E-V-L-K-A-T-E-M-V-E	345		
66		326	H-V-K-K-I-R-E-G-E-V-E-V-L-K-A-T-E-M-V-E-V-G-P-E-D	350		
67		331	R-E-G-E-V-E-V-L-K-A-T-E-M-V-E-V-G-P-E-D-D-E-V-G-A	355		
68		336	E-V-L-K-A-T-E-M-V-E-V-G-P-E-D-D-E-V-G-A-E-R-G-E-A	360		
69		341	T-E-M-V-E-V-G-P-E-D-D-E-V-G-A-E-R-G-E-A-T-D-L-L-R	365		
70		346	V-G-P-E-D-D-E-V-G-A-E-R-G-E-A-T-D-L-L-R-G-S-S-P-D	370		
71		351	D-E-V-G-A-E-R-G-E-A-T-D-L-L-R-G-S-S-P-D-V-H-T-L-L	375		
72		356	E-R-G-E-A-T-D-L-L-R-G-S-S-P-D-V-H-T-L-L-E-I-T-E-E	380		
73		361	T-D-L-L-R-G-S-S-P-D-V-H-T-L-L-E-I-T-E-E-S-D-A-V-L	385		
74		366	G-S-S-P-D-V-H-T-L-L-E-I-T-E-E-S-D-A-V-L-V-D-K-S-D	390		
75		368	S-P-D-V-H-T-L-L-E-I-T-E-E-S-D-A-V-L-V-D-K-S-D-S-D	392		

SOCS3 interacts with cavin-1 at several regions but most intensely at peptides 16-24 and two seemingly repeating regions at peptides 42-46 and 52-56. Putative domain assignment has been previously established by Aboulaich et al (222), Bastiani et al (219), and Hansen et al (221). As such, cavin-1 is predicted to have three disordered PEST domains associated with proteolysis, two nuclear localisation signals (NLS) and three leucine rich repeats (LRR) which might be important for protein-protein interactions and impart structural characteristics. SOCS3 seems to interact strongly at an N-terminal region predicted to form a coiled-coil/leucine zipper protein-interaction motif as well as with a C-terminal domain basic region that is also predicted to contain LRR and NLS motifs.

Ideally, the reciprocal experiment should be performed so that binding sites on SOCS3 can also be assessed. Due to time restrictions this has not yet been performed. Furthermore, I would also have liked to fabricate several SOCS3/cavin-1 sequential and/or single residue mutants to further explore the interaction *via* this technique. These same mutants could also be used for *in vitro* analysis such as co-immunoprecipitation and functional studies.

6.2.7 Degradation of cavin-1 could not be detected following the inhibition of protein synthesis

The stability of SOCS3 substrates is expected to be reduced in the presence of but not absence SOCS3. Inhibition of protein synthesis will enable the time-dependent degradation of SOCS3 targets to be detected. Emetine, an irreversible inhibitor of protein synthesis that acts by binding to and blocking the translocation of the 40S ribosomal unit (197,198), was used for this purpose. Prior to performing the degradation experiments, the natural degradation of cavin-1, following inhibition of protein synthesis, was assessed *via* a time-course. Furthermore, the action of the proteasome inhibitor MG132 and lysosome inhibitor chloroquine was also assessed over the same time course with the aim of providing evidence of the route of cavin-1 degradation.

The degradation assay was performed as described (Section 2.2.16). Despite seven attempts, time-dependent degradation of cavin-1 could not be reproducibly detected (Figure 6.15, panel A). Bands assumed to be cavin-1 did vary although not as predicted. In the presence of only the protein synthesis

inhibitor (emetine, 100 μ M), no degradation was detected (Lanes 2-6) while degradation was observed in the presence of the inhibitor of proteasome (MG132, 6 μ M) (Lanes 7-10). However, correcting for GAPDH levels (Panel B, lanes 11-14), treatment with the lysosomal inhibitor (chloroquine, 100mM) appears to protect cavin-1. Given that the emetine-only positive control did not show any change in cavin-1, a conclusion cannot be made about its route of degradation using this data. Cavin-1 has been detected by other groups as several bands, possibly due to a susceptibility to proteolysis (219,222). As such, the several lower bands (70-40kDa) detected might relate to cavin-1 fragments. Alternatively, since bands were visualised using an anti-PTRF (cavin-1) antibody, these bands might equally be endogenous cavin-1. Given that these bands also vary unpredictably in intensity, they add extra variability that limits interpretation of the data. Cavin-1 has been suggested to have a long half-life (220) and performing a longer time-course might produce a more definitive result. However, treatment with emetine is toxic and even after 8 hours cell death was seen (data not shown). As such, it was decided not to pursue this experimental strategy further.

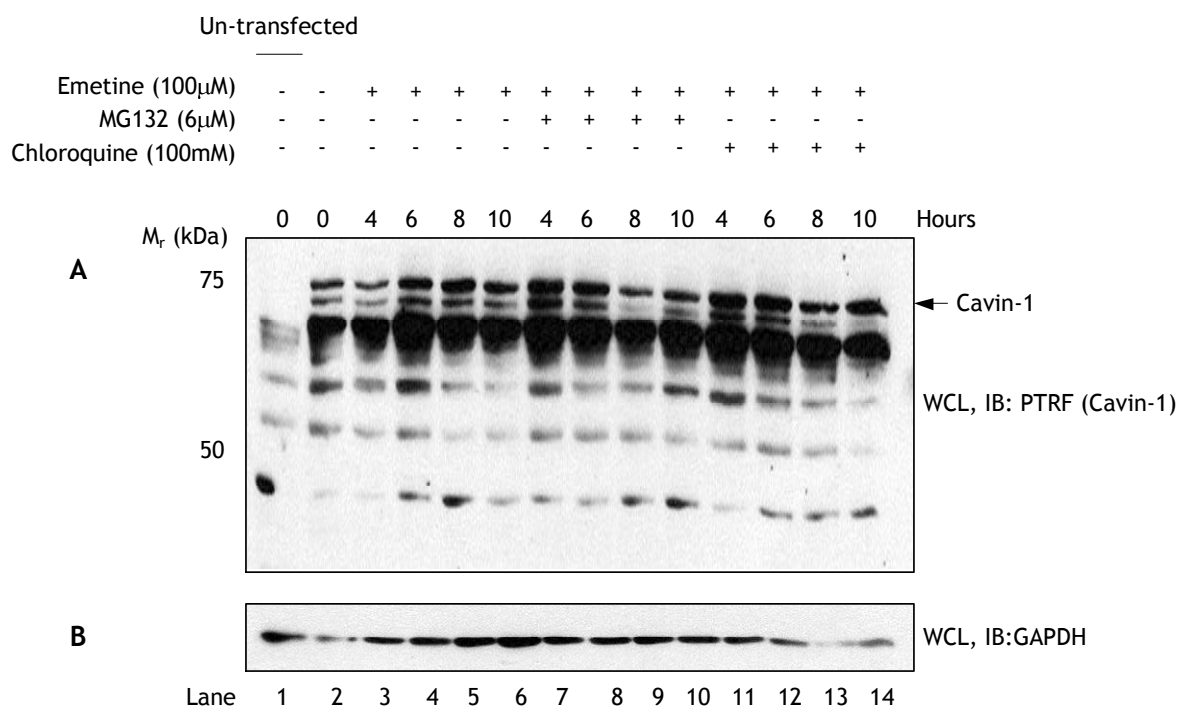


Figure 6.15: Degradation of cavin-1 could not be detected following inhibition of protein synthesis

The degradation assay was performed as described (Section 2.2.16). Samples were equalised for protein concentration prior to fractionation by SDS-PAGE and degradation assessed *via* immunoblotting with anti-PTRF(cavin-1) antibody (Panel A). GAPDH was used as a loading control (Panel B). One of seven experiments.

6.3 Conclusions

Numerous candidate SOCS3-dependently ubiquitinated substrates were identified *via* a proteomics screen (Section 5.0). Here, the aim was to validate substrates *via* co-immunoprecipitation, analysis of ubiquitination *in situ*, and peptide array analysis. Initial investigations used co-immunoprecipitation experiments to demonstrate an interaction between SOCS3 and the candidate substrates. While Hsc70 was precipitated, it also interacted non-specifically with the agarose beads (Figure 6.5). It was decided that other techniques such as peptide arrays and/or functional assays might be more informative. Cavin-1 was the only candidate substrate that was found to interact with SOCS3 *via* this route (Figure 6.6). Interestingly, this interaction seemed to be disrupted in the presence of PTPs inhibitors Na_3VO_4 and H_2O_2 (Figure 6.7). This was not expected since the SOCS3-dependent E3 is predicted to bind tyrosine-phosphorylated substrates. However, due to the off-target effects of H_2O_2 (204,248), it is possible that the interaction is being disrupted by hyper-phosphorylation of other residues. As such, the experiment should have been repeated in the absence of H_2O_2 . However, it is interesting to note that the condition demonstrated to inhibit the interaction was also used to enrich cavin-1 *via* a proteomics screen.

The interaction between cavin-1 and SOCS3 also seemed to be independent of the SOCS3 SOCS-box since WT and the SOCS3-L189A SOCS-box mutant both precipitated cavin-1 at comparable levels (Figure 6.8). This is important since SOCS3 is required to bind components of the E3 ligase *via* its SOCS-box motif. Any interaction between cavin-1 and the SOCS3 SOCS-box might rule out cavin-1 as a SOCS3-dependently ubiquitinated substrate. However, this does not completely rule-out this domain since the mutant has only been characterised in relation to the elonginBC interaction. A more informative approach would be to use a SOCS-box deletion mutant and also to use disrupting or deletion mutations of other domains to assess their involvement. Alternatively, this interaction could be further explored using full-length peptide arrays of both SOCS3 and cavin-1 to map the SOCS3-cavin-1 interacting sites. This may also enable the location of potentially disrupting phosphorylated residues. Furthermore, mutagenesis or peptide fabrication with or without phosphorylation would enable localisation of the individual disrupting residues.

It was disappointing to validate only a single candidate *via* these experiments however not all of the top candidates identified from the proteomics screen were tested due to the unavailability of cDNA constructs. Furthermore, while conditions for co-immunoprecipitation were tested (Section 6.2.1.1), these conditions might not be ideal for weakly interacting proteins and as such would require modifications of the experimental conditions to reduce stringency. This is a major limitation of this strategy and might have led to missed interactions. The use of *in vivo* techniques such as yeast-2-hybrid might be more successful. However, while protein tyrosine kinases have been identified in yeast, they are not as common as in multi-cellular organisms and so yeast might not convey the PTM to non-native proteins (250). Given that the candidate SOCS3 substrate protein tyrosine kinases are also unknown, analysis of tyrosine-phosphorylation-dependent protein-protein interactions *via* this assay is not possible at this time.

A peptide array spotted with tyrosine-phosphorylated peptides from candidate SOCS3 substrates (Figure 6.14) showed that Hsc70 seemed to specifically interact with SOCS3 at a specific tyrosine-phosphorylated peptide. Furthermore, the array also supported previous data suggesting that tyrosine phosphorylation inhibits the SOCS3-cavin-1 interaction. Here, tyrosine-phosphorylated peptides from cavin-1 were shown not to significantly interact with SOCS3. A SOCS3-cavin-1 interaction was however supported by a full-length peptide array, which demonstrated that SOCS3 specifically interacts with several peptides of cavin-1 (Table 6.1). SOCS3 seems to interact strongly at an N-terminal region predicted to form a coiled-coil/leucine zipper protein-interaction motif as well as with a C-terminal domain basic region that is also predicted to contain LRR and NLS motifs. Such an interaction might lead to disruption of the cavin-complex and/or sequestration to the cytoplasm/plasma membrane. SOCS3 can be induced by insulin (160) but it is disputed whether cavin-1 translocates from the plasma membrane to the nucleus upon insulin signalling (251,252). Binding of SOCS3 to the NLS might act to prevent nuclear translocation and sequester cavin-1 to the plasma membrane/cytosol. Furthermore, while association with basic regions might be predicted to be phosphorylation dependent, the use of *E.coli* as the expression host for the purified SOCS3 suggests that this might not be the case. Association at this site might therefore be a consequence of the charge profile of SOCS3. Cavin-1-3, and potentially cavin-4, binds phosphatidylserine (PS)

(219,221,227) which is thought to strengthen their association with caveolins at the plasma membrane (PM). Furthermore, cavin family members accumulate in large complexes at the PM suggesting that the cumulative effect of several weak interactions with PS might be important. The PS interaction site might be predicted to be the basic region which is conserved across all cavin family members (221). As such, SOCS3 binding at this site may act to disrupt the cavin complex and/or cavin-1 from the PM. The SOCS3 SOCS-box is unstructured domain that only becomes structured upon binding elonginBC *via* mainly hydrophobic interactions (77). As such, the presence of multiple hydrophobic LRRs might potentially implicate this region in binding cavin-1.

Analysis of the SOCS3-dependent ubiquitination of cavin-1 produced interesting results. Immunoprecipitation of the ubiquitinome resulted in the enrichment of ubiquitinated cavin-1 (Figure 6.9). However, the band enriched seemed to relate to a cavin-1 fragment. The reciprocal experiment replicated this result (Figure 6.10). However, in this case, in the presence of SOCS3-E3 there seemed to be a switch in the intensity of the ubiquitin smear from a high to a lower molecular weight focused around cavin-1 (~75kDa). The same result was replicated in the presence of only SOCS3 i.e. cavin-1 vs. cavin-1 and SOCS3 (Figure 6.13). Here, an enrichment of ubiquitinated protein below 75kDa might be attributed to ubiquitinated cavin-1 fragments while those above might be ubiquitinated full-length cavin-1. Interestingly, K48-specific polyubiquitination was also enhanced in the presence of SOCS3 within this same region. However, since SOCS3-L189A produces the same effect, it suggests that K48-polyubiquitination is *via* a non-SOCS3 mechanism. It may however support SOCS3 in the role of protecting cavin-1 K48-polyubiquitination. These data suggest that SOCS3 might somehow inhibit or negatively regulate polyubiquitination of cavin-1, possibly by out-competing other E3 ligases. Given that only lower molecular weight ubiquitination is enhanced in the presence of the SOCS3-E3, mono-or multi-ubiquitination might be involved. However, due to the enhanced detection of K48-polyubiquitination, K48-linked dimers or short chains are also a possibility. SOCS3 might therefore protect or preferentially ubiquitinate cavin-1 leading to this switch in the ubiquitin smear. However, this data does not explain the enrichment of specific cavin-1 bands. Aboulaich et al (222) found that cavin-1 contains three PEST domains and that it is also acetylated at the N-terminal methionine (Figure 6.9

Table 6.1), both of which are associated with protein stability. Since several cavin-1 fragments are likely observable in immunoblots (219,222), it might be possible that following cleavage of the N-terminal PEST domain, cavin-1 becomes less susceptible to proteolysis and is bound by SOCS3 which limits further proteolysis. This observation is supported by the full-length cavin-1 peptide array, which revealed that SOCS3 only weakly interacts with the N-terminal domain of cavin-1 (Table 6.1). Enrichment of a ubiquitinated, N-terminally truncated cavin-1 would also suggest that the K48-polyubiquitin-modified lysine residue is located further upstream. As such, it might be concluded that the enhanced ubiquitination signal is a consequence of the enrichment of the ubiquitinated cavin-1 fragments. It is not known whether the ubiquitin signal is SOCS3-dependent. However, since cavin-1 was found to be enriched in the presence but not absence of SOCS3 in the proteomics screen, it is expected that SOCS3 has some role in the regulation of cavin-1 ubiquitination.

It is of note that cavin-1 was not substantially enriched *via* immunoprecipitation. The small variations in the ubiquitin smear between test and control lanes have made interpretation of the data difficult. This is perhaps a consequence of not optimising the volume of the anti-cavin-1 antibody prior to performing immunoprecipitation. Optimisation was not performed because of the restrictive cost of the cavin-1 antibody, the recommended amount (1/250, ~200µg) for an immunoprecipitation was used. Cavin-1 is available as an N- or C-terminally-tagged GFP construct. As such, more informative results might be possible using anti-GFP antibody, which is much cheaper to optimise.

As control for cavin-1 ubiquitination assays, ubiquitination of SOCS3 was assessed in the presence or absence of the E3 ligase complex. SOCS3 has been shown to be degraded concomitantly with its substrates (11,12) suggesting that formation of an E3 ligase complex can destabilise SOCS3. In support of this, a SOCS3-SOCS-box deletion mutant or mutation of Lys6 of SOCS3 stabilises the protein (97) by disrupting the E3-SOCS3 interaction and by preventing SOCS3 ubiquitination respectively. As such, it was predicted that SOCS3 would be ubiquitinated in the presence but not absence of the E3 complex. Furthermore, no ubiquitin-mediated degradation was expected since cells were treated with the proteasome inhibitor MG132. However, the opposite ubiquitin profile was

detected i.e. SOCS3 was highly ubiquitinated in the absence of the E3 complex but less so in its presence. Furthermore, levels of SOCS3 were also reduced in the presence of the E3 complex suggesting that degradation took place. Components of the E3-complex are required in a 1:1 stoichiometry. Given that expression levels of the individual components were not optimised beforehand, reduced ubiquitination might be a consequence of incomplete formation of the E3-complexes. However, in this event, SOCS3 would have been predicted to be stabilised. As such, loss of SOCS3 might be occurring *via* an alternative route, possibly *via* a PEST-domain mediated route. Contrary to the destabilising effect of the E3-complex on SOCS3, disrupting the SOCS3-E3 interaction by tyrosine phosphorylation of Y²⁰⁴ and Y²²¹ within the SOCS-box has also been shown to destabilise SOCS3 *via* proteasome mediated degradation (100). Perhaps, while unbound to the E3 complex, SOCS3 is vulnerable to phosphorylation or other modifying events that might target it for non-proteasome-mediated degradation. SOCS3 was also shown to be ubiquitinated in the absence of the E3 complex. This was suggested to be *via* endogenous components of the E3 complex. However, the same result was seen using the SOCS3-L189A SOCS-box mutant (Figure 6.12) suggesting that SOCS3 is being ubiquitinated by a different E3 ligase. Currently, SOCS3 is thought to perform autoubiquitination on the formation of an E3-ligase complex and is degraded concomitantly with its substrates (11,12). Furthermore, cross-regulation between SOCS family members has been demonstrated (103) although this data has been disputed (102). No other E3 that targets SOCS3 is known. This data suggests that SOCS3 might be degraded *via* several mechanisms including proteasome and proteolysis-mediated routes.

SOCS3 was predicted to mediate K48-polyubiquitin-directed proteasomal degradation of cavin-1. As such, enhanced degradation of cavin-1 was expected in the presence of but not absence of SOCS3. The natural degradation of cavin-1 was first assessed with the aim of detecting a time-point after which cavin-1 is significantly degraded as to be detectable *via* immunoblotting. This time-point would be expected to be reduced in the presence of SOCS3. However, the natural degradation of cavin-1 could not be adequately detected (Figure 6.15). This prevented the functional analysis of SOCS3 using this technique from being performed. Co-expressing SOCS3 and cavin-1 might have produced more

meaningful data i.e. by potentially reducing the half-life of cavin-1. However, this was not done due to time constraints.

The role of SOCS3 in relation to cavin-1 is not understood. These data suggest that it might have role in the regulation of cavin-1 ubiquitination. In this role, SOCS3 might be induced and bind cavin-1 to regulate its function. Alternatively, cavin-1 might sequester SOCS3 to caveolae. Several PEST-domain-containing proteins have been found to be enriched in caveolae including cavin-1 and all its truncated forms (222). However, these truncated forms are not detected in the nucleus or cytosol suggesting that proteolysis occurred *in situ*. As such, there might be a connection between proteolytic regulation and targeting to caveolae (222). While SOCS3 was not detected in the same experiment, possibly since it is present at low basal levels, SOCS3 does contain a PEST domain and might be regulated in a similar fashion.

A further hypothesis is that cavin-1 sequesters SOCS3 to caveolae to support the ablation of cytokine and insulin signalling. The insulin receptor and cytokine receptors as well as their signalling components, insulin receptor substrate-1 (IRS-1) and JAK/STAT family members respectively, have been detected in caveolae (236,253). Furthermore, caveolin-1 has been described as a novel regulator of cytokine signalling due to its ability to inhibit prolactin-induced STAT5 signalling *via* a conserved pseudo-kinase domain (234) similar to that of SOCS1/3. Additionally, caveolin-1 knockout mice show prolonged activation of STAT3. Thus, caveolin-1 might be necessary for suppression of cytokine signalling in caveolae. Interestingly, siRNA knockdown of cavin-1 resulted in a reduction of SOCS3 levels (Paul Pilch, Boston University, personal communication) and so cavin-1 might therefore regulate SOCS3 stability in a similar way in which it regulates caveolin-1 (220). The impact of STAT3 signalling was not pursued but a loss of SOCS3 would also be expected to affect STAT3 signalling (70,95). Therefore, it might be possible that through stabilisation and/or sequestering to caveolae by cavin-1, SOCS3 works in concert with caveolin-1 to suppress cytokine signalling. Likewise, since SOCS3 regulates insulin signalling (9,159,160), a similar argument could be made.

6.4 Future prospects

SOCS3 is an important negative regulator of pro-inflammatory signalling events (130,131). However, SOCS3 has been shown to have context specific effects. As such, overexpression of SOCS3 is protective in the case of rheumatoid arthritis where it acts to suppress STAT3 signalling (130). However, the specific loss of SOCS3 in macrophages allows an IL6-mediated IL10-like anti-inflammatory response, possibly by the sustained activation of STAT3 (125). Due to the polar effects of SOCS3, it must be specifically targeted to be therapeutically beneficial. Therefore, the impact of SOCS3 on its candidate substrates must be assessed in various contexts to be of utility.

Ultimately, the aim would be to devise strategies to specifically target SOCS3 to either prolong or suppress its action. Due to the transient nature of SOCS3 expression, extending its action might be possible *via* inhibition of its regulators i.e. SOCS family members (103) or as yet unidentified E3 ligases or activation of cyclic-AMP/inhibition of phosphodiesterases (PDEs). Local delivery of SOCS3 cDNA *via* adenovirus or liposomes has already been shown to be successful in the treatment of mouse models of rheumatoid arthritis and endotoxic shock respectively (130,131). While inhibition of SOCS3 might be useful in certain situations i.e. in IL6 mediated inflammatory disorders where sustaining STAT3 signalling produces an anti-inflammatory response (125), it has not yet been explored. However, this might be achieved by the use of peptide or small molecule inhibitors aimed at the KIR and SOCS-box domains, although the global effect might be undesirable. Since SOCS3 is predicted to specifically interact with its substrates, targeting the E3-SOCS3-substrate interface might produce specific and desirable physiological effects. To do so would require the full understanding of the SOCS3-substrate interaction and its context specific role.

The preliminary experiments performed here have suggested roles SOCS3 in relation to cavin-1 while its effects on Hsc70 and other candidate substrates have yet to be fully explored. To further understand the role SOCS3 and its impact on its candidate substrates, further experimentation is necessary.

6.4.1 Cavin-1

It was suggested that ubiquitinated cavin-1 C-terminal-domain fragments are enriched by SOCS3 leading to an enhanced ubiquitin signal. SOCS3 was hypothesised to stabilise this truncated form of cavin-1. I would like to repeat the ubiquitination assays using an N-terminal-GFP-SOCS3 construct. If the enhanced ubiquitin signal is due to the enrichment of C-terminal-domain cavin-1 fragments, then a shift in the ubiquitin signal from 75kDa to the lower mass (~45kDa) would be expected. Alternatively, the same experiments could be performed using a series of cavin-1 N-terminal truncations. Since this data seems to dispute the ubiquitination of cavin-1 by SOCS3, *in vitro* ubiquitination assays should also be performed using purified components. Doing so would confirm such an event since it would be unaffected by outside agents.

I have also shown that SOCS3 can bind cavin-1 directly using a peptide array approach. A reciprocal experiment must now be performed after which, the additional information will aid in mutational analysis of either protein to identify important structural domains and residues involved in the interaction. Furthermore, SOCS3 binding sites on cavin-1 indentified by the peptide array suggest a role of SOCS3 in the localisation of cavin-1. It would therefore be of interest to perform co-localisation experiments in WT and SOCS3^{-/-} MEFs after treating with SOCS3-inducing stimuli. For example, caveolin-1, and presumably cavin-1 *via* its stabilising effect on caveolin-1, regulate several signalling events including cytokine (253), insulin (236), and eNOS signalling (254). It is hypothesised here that SOCS3 might be sequestered to caveolae in order to disrupt the cavin complex or ablate signalling events. Co-localisation experiments could therefore be extended to examine the effect of SOCS3 on caveolin-1/cavin-1 localisation, caveolae formation, and their impact on signalling events.

6.4.2 Project summary, conclusions, and perspectives

Using a global proteomics approach, I have been able to identify proteins that may potentially be targeted by SOCS3 for ubiquitination (Section 5.0). Of these, SOCS3 was found to interact with and regulate the ubiquitination of PTRF/cavin-1 (Sections 6.2.3, 6.2.4, 6.2.6). However, the mechanism by which SOCS3

regulates cavin-1 ubiquitination or its functional outcome is not understood. Most candidate substrates (Table 5.1, light grey/dotted box) were not found to interact with SOCS3 *via* a co-immunoprecipitation assay, while cDNA constructs were not available for the others.

The limited detection of candidate SOCS3 substrates can be attributed to inadequate experimental conditions. With hindsight, improvements could be made to all stages of the experimental procedure. This includes the use of different SILAC isotopes (R10K8 vs. R6K6), TAP elution strategy (reduced temperature, on-bead trypsin digestion), and MS data analysis. Furthermore, *via* this global proteomics screen, the enhancement of ubiquitination in the presence of SOCS3 was analysed. A better approach might have been to assess the stability of the proteome in the presence of SOCS3. This has previously been successfully accomplished using a similar experimental approach used here (215). Hör et al identified targets of an E3 ligase *via* MS analysis of isolated, SILAC-labelled membrane proteins. A similar study, if performed for SOCS3, would require analysis of the entire proteome. Given that down-regulation might occur *via* several mechanisms such as lysosomal and proteome-mediated degradation, this approach might have generated too many false-positives and was therefore not pursued. However, given that too few substrates were identified using the current approach, this modified technique might be of value. Furthermore, following this screen with a secondary stage of high-throughput analysis i.e. peptide array, yeast-2-hybrid, the list of candidates might be sufficiently reduced to generate a list of likely SOCS3 substrates

Given that most candidates have yet to be fully verified, improved validation techniques (Section 6.4.1) can be applied. The role of SOCS3-cavin-1 interaction can also be further investigated. First, the mode of cavin-1 ubiquitination should be clarified. *In vitro* ubiquitination assays performed in the presence or absence of purified SOCS3 and components of the E3-ligase should be sufficient to assess if SOCS3 can modify cavin-1. However, immunoprecipitation of a series of cavin-1 truncations might be able to verify if SOCS3, for whatever reason, binds and inhibits further ubiquitination of cavin-1 and potential cavin-1 fragments. The latter would suggest a novel role of SOCS3. As previously discussed, cavin-1 may act as a scaffold for SOCS3, targeting it to the caveolae so to regulate signalling

events. Equally likely is the role of SOCS3 to disrupt cavin complex although it is not seen how this could be beneficial. A study of the localisation of SOCS3 and cavin-1 could be performed using confocal microscopy and fluorescently labelled antibodies upon induction of SOCS3 in WT MEFs. A similar approach has been used to demonstrate an interaction between SOCS3 and the insulin receptor (160). Furthermore, information gained from full-length peptide arrays might enable the fabrication of cavin-1/SOCS3 mutants or peptide inhibitors that can be used to disrupt co-localisation and impact functionality. Recently, cavin-1 has been found to be downregulated in breast cancer (238), adenocarcinoma and squamous cell carcinoma (239), and prostate cancer cell lines PC3 and LNCaP (240). Moreover, expression of cavin-1 has been demonstrated to negatively regulate cell migration (241). As such, it would be important to assess how cavin-1 affects downstream signalling events and the role of SOCS3, if any, in these events. Furthermore, enhanced STAT3 signalling is associated with certain cancers such as prostate cancer (246) and loss of caveolae, due to loss of caveolin-1, increase JAK/STAT signalling (235). It would be of interest to assess how cavin-1/SOCS3 impact caveolae signalling. Multiple signalling complexes are recruited to caveolae such as gp130, the impact of SOCS3 on specific signalling events i.e. IL6, insulin, and eNOS signalling might be elucidated *via* a combination of immunoblotting cell lysates in the presence or absence of peptide inhibitors that disrupt the SOCS3-cavin-1 interaction.

7.0 References

1. Schienkiewitz, A., Mensink, G. B., and Scheidt-Nave, C. (2012) *BMC. Public Health* **12**, 658
2. Suganami, T., Nishida, J., and Ogawa, Y. (2005) *Arterioscler. Thromb. Vasc. Biol.* **25**, 2062-2068
3. Sun, S., Ji, Y., Kersten, S., and Qi, L. (2012) *Annu. Rev. Nutr.* **32**, 261-286
4. Weisberg, S. P., McCann, D., Desai, M., Rosenbaum, M., Leibel, R. L., and Ferrante, A. W., Jr. (2003) *J. Clin. Invest* **112**, 1796-1808
5. Roytblat, L., Rachinsky, M., Fisher, A., Greemberg, L., Shapira, Y., Douvdevani, A., and Gelman, S. (2000) *Obes. Res.* **8**, 673-675
6. O'Shea, J. J., Gadina, M., and Schreiber, R. D. (2002) *Cell* **109 Suppl**, S121-S131
7. Grote, K., Luchtefeld, M., and Schieffer, B. (2005) *Vascul. Pharmacol.* **43**, 357-363
8. Irandoust, M. I., Aarts, L. H., Roovers, O., Gits, J., Erkeland, S. J., and Touw, I. P. (2007) *EMBO J.* **26**, 1782-1793
9. Kawaguchi, T., Yoshida, T., Harada, M., Hisamoto, T., Nagao, Y., Ide, T., Taniguchi, E., Kumemura, H., Hanada, S., Maeyama, M., Baba, S., Koga, H., Kumashiro, R., Ueno, T., Ogata, H., Yoshimura, A., and Sata, M. (2004) *Am. J. Pathol* **165**, 1499-1508
10. Liu, E., Cote, J. F., and Vuori, K. (2003) *EMBO J.* **22**, 5036-5046
11. Orr, S. J., Morgan, N. M., Elliott, J., Burrows, J. F., Scott, C. J., McVicar, D. W., and Johnston, J. A. (2007) *Blood* **109**, 1061-1068
12. Orr, S. J., Morgan, N. M., Buick, R. J., Boyd, C. R., Elliott, J., Burrows, J. F., Jefferies, C. A., Crocker, P. R., and Johnston, J. A. (2007) *J. Biol. Chem* **282**, 3418-3422
13. Bruce Alberts, Alexander Johnson, Julian Lewis, Martin Raff, Keith Roberts, and Peter Walter (2008) *The Adaptive Immune System. Molecular Biology of the Cell* 5th edition, Garland Science, New York.
14. Bhoj, V. G. and Chen, Z. J. (2009) *Nature*. 2009. Mar. 26. ;458. (7237.):430. -7. **458**, 430-437
15. Janeway, C. A., Jr. and Medzhitov, R. (2002) *Annu. Rev. Immunol.* **20**, 197-216
16. Skaug, B., Jiang, X., and Chen, Z. J. (2009) *Annu. Rev. Biochem.* **78**, 769-796

17. Takeuchi, O., Hoshino, K., Kawai, T., Sanjo, H., Takada, H., Ogawa, T., Takeda, K., and Akira, S. (1999) *Immunity*. **11**, 443-451
18. Tedgui, A. and Mallat, Z. (2006) *Physiol Rev.* **86**, 515-581
19. Hunt, B. J. and Jurd, K. M. (1998) *BMJ*. **316**, 1328-1329
20. Schmid-Schonbein, G. W. (2006) *Annu. Rev. Biomed. Eng* **8**, 93-131
21. Mittendorfer, B. and Peterson, L. R. (2008) *Drug Discov. Today Ther. Strateg.* **5**, 53-61
22. Yang, X. F., Yin, Y., and Wang, H. (2008) *Drug Discov. Today Ther. Strateg.* **5**, 125-142
23. Esper, R. J., Nordaby, R. A., Vilarino, J. O., Paragano, A., Cacharron, J. L., and Machado, R. A. (2006) *Cardiovasc. Diabetol.* **5**, 4
24. Zhang, Y., Proenca, R., Maffei, M., Barone, M., Leopold, L., and Friedman, J. M. (1994) *Nature* **372**, 425-432
25. Fruhbeck, G. (2006) *Biochem. J.* **393**, 7-20
26. Lau, D. C., Dhillon, B., Yan, H., Szmitko, P. E., and Verma, S. (2005) *Am. J. Physiol Heart Circ. Physiol* **288**, H2031-H2041
27. Rott, D., Zhu, J., Zhou, Y. F., Burnett, M. S., Zalles-Ganley, A., and Epstein, S. E. (2003) *Atherosclerosis* **170**, 223-228
28. Watson, C., Whittaker, S., Smith, N., Vora, A. J., Dumonde, D. C., and Brown, K. A. (1996) *Clin. Exp. Immunol.* **105**, 112-119
29. Zhang, J., Alcaide, P., Liu, L., Sun, J., He, A., Luscinskas, F. W., and Shi, G. P. (2011) *PLoS. One.* **6**, e14525
30. Morin, C. L., Eckel, R. H., Marcel, T., and Pagliassotti, M. J. (1997) *Endocrinology* **138**, 4665-4671
31. Fried, S. K., Bunkin, D. A., and Greenberg, A. S. (1998) *J. Clin. Endocrinol. Metab* **83**, 847-850
32. Cao, Y. L., Hu, C. Z., Meng, X., Wang, D. F., and Zhang, J. (2008) *Diabetes Res. Clin. Pract.* **79**, 214-219
33. Lumeng, C. N., Maillard, I., and Saltiel, A. R. (2009) *Nat. Med.* **15**, 846-847
34. Karalis, K. P., Giannogonas, P., Kodela, E., Koutmani, Y., Zoumakis, M., and Teli, T. (2009) *FEBS J.* **276**, 5747-5754
35. Hirosumi, J., Tuncman, G., Chang, L., Gorgun, C. Z., Uysal, K. T., Maeda, K., Karin, M., and Hotamisligil, G. S. (2002) *Nature* **420**, 333-336
36. Mokdad, A. H., Ford, E. S., Bowman, B. A., Dietz, W. H., Vinicor, F., Bales, V. S., and Marks, J. S. (2003) *JAMA* **289**, 76-79

37. Danaei, G., Ding, E. L., Mozaffarian, D., Taylor, B., Rehm, J., Murray, C. J., and Ezzati, M. (2009) *PLoS. Med.* **6**, e1000058
38. Song, M. J., Kim, K. H., Yoon, J. M., and Kim, J. B. (2006) *Biochem. Biophys. Res. Commun.* **346**, 739-745
39. Baker, R. G., Hayden, M. S., and Ghosh, S. (2011) *Cell Metab* **13**, 11-22
40. Uysal, K. T., Wiesbrock, S. M., Marino, M. W., and Hotamisligil, G. S. (1997) *Nature* **389**, 610-614
41. Eckel, R. H. (1997) *Circulation* **96**, 3248-3250
42. POOLE, J. C. and FLOREY, H. W. (1958) *J. Pathol. Bacteriol.* **75**, 245-251
43. Hansson, G. K. (2005) *N. Engl. J. Med.* **352**, 1685-1695
44. Glass, C. K. and Witztum, J. L. (2001) *Cell* **104**, 503-516
45. Ross, R. (1999) *N. Engl. J. Med.* **340**, 115-126
46. Lovato, P., Brender, C., Agnholt, J., Kelsen, J., Kaltoft, K., Svejgaard, A., Eriksen, K. W., Woetmann, A., and Odum, N. (2003) *J. Biol. Chem.* **278**, 16777-16781
47. Barton, B. E. (2005) *Expert. Opin. Ther. Targets.* **9**, 737-752
48. Nash, P. T. and Florin, T. H. (2005) *Med. J. Aust.* **183**, 205-208
49. Schieffer, B., Selle, T., Hilfiker, A., Hilfiker-Kleiner, D., Grote, K., Tietge, U. J., Trautwein, C., Luchtefeld, M., Schmittkamp, C., Heeneman, S., Daemen, M. J., and Drexler, H. (2004) *Circulation* **110**, 3493-3500
50. Minamoto, S., Ikegame, K., Ueno, K., Narazaki, M., Naka, T., Yamamoto, H., Matsumoto, T., Saito, H., Hosoe, S., and Kishimoto, T. (1997) *Biochem. Biophys. Res. Commun.* **237**, 79-83
51. Johnston, J. A. (2004) *J. Leukoc. Biol* **75**, 743-748
52. Nalepa, G., Rolfe, M., and Harper, J. W. (2006) *Nat. Rev. Drug Discov* **5**, 596-613
53. Steinke, J. W. and Borish, L. (2006) *J. Allergy Clin. Immunol.* **117**, S441-S445
54. Fitzgerald, K. A. (2001) *The Cytokine FactsBook and Webfacts* (2nd Ed), Academic Press,
55. Heinrich, P. C., Behrmann, I., Haan, S., Hermanns, H. M., Muller-Newen, G., and Schaper, F. (2003) *Biochem. J.* **374**, 1-20
56. Muller-Newen, G., Kohne, C., Keul, R., Hemmann, U., Muller-Esterl, W., Wijdenes, J., Brakenhoff, J. P., Hart, M. H., and Heinrich, P. C. (1996) *Eur. J. Biochem.* **236**, 837-842

57. Matthews, V., Schuster, B., Schutze, S., Bussmeyer, I., Ludwig, A., Hundhausen, C., Sadowski, T., Saftig, P., Hartmann, D., Kallen, K. J., and Rose-John, S. (2003) *J. Biol. Chem.* **278**, 38829-38839
58. Bihl, M. P., Heinemann, K., Rudiger, J. J., Eickelberg, O., Perruchoud, A. P., Tamm, M., and Roth, M. (2002) *Am. J. Respir. Cell Mol. Biol.* **27**, 48-56
59. Yatsenko, O. P., Filipenko, M. L., Khrapov, E. A., Voronina, E. N., Kozlov, V. A., and Sennikov, S. V. (2004) *Cytokine* **28**, 190-196
60. Kimura, A. and Kishimoto, T. (2010) *Eur. J. Immunol.* **40**, 1830-1835
61. Borish, L. C. and Steinke, J. W. (2003) *J. Allergy Clin. Immunol.* **111**, S460-S475
62. Sommer, U., Schmid, C., Sobota, R. M., Lehmann, U., Stevenson, N. J., Johnston, J. A., Schaper, F., Heinrich, P. C., and Haan, S. (2005) *J. Biol. Chem.* **280**, 31478-31488
63. Brierley, M. M. and Fish, E. N. (2005) *J. Interferon Cytokine Res.* **25**, 733-744
64. Ihle, J. N. (1996) *Cell* **84**, 331-334
65. Bank, U., Kupper, B., Reinhold, D., Hoffmann, T., and Ansorge, S. (1999) *FEBS Lett.* **461**, 235-240
66. Ortiz-Munoz, G., Martin-Ventura, J. L., Hernandez-Vargas, P., Mallavia, B., Lopez-Parra, V., Lopez-Franco, O., Munoz-Garcia, B., Fernandez-Vizarra, P., Ortega, L., Egido, J., and Gomez-Guerrero, C. (2009) *Arterioscler. Thromb. Vasc. Biol.* **29**, 525-531
67. Narazaki, M., Yasukawa, K., Saito, T., Ohsugi, Y., Fukui, H., Koishihara, Y., Yancopoulos, G. D., Taga, T., and Kishimoto, T. (1993) *Blood* **82**, 1120-1126
68. Palvimo, J. J. (2007) *Biochem. Soc. Trans.* **35**, 1405-1408
69. Rytinki, M. M., Kaikkonen, S., Pehkonen, P., Jaaskelainen, T., and Palvimo, J. J. (2009) *Cell Mol. Life Sci.* **66**, 3029-3041
70. Sands, W. A., Woolson, H. D., Milne, G. R., Rutherford, C., and Palmer, T. M. (2006) *Mol. Cell Biol* **26**, 6333-6346
71. Muller-Newen, G., Kuster, A., Hemmann, U., Keul, R., Horsten, U., Martens, A., Graeve, L., Wijdenes, J., and Heinrich, P. C. (1998) *J. Immunol.* **161**, 6347-6355
72. Ungureanu, D., Vanhatupa, S., Kotaja, N., Yang, J., Aittomaki, S., Janne, O. A., Palvimo, J. J., and Silvennoinen, O. (2003) *Blood* **102**, 3311-3313

73. Boyle, K., Zhang, J. G., Nicholson, S. E., Trounson, E., Babon, J. J., McManus, E. J., Nicola, N. A., and Robb, L. (2009) *Cell Signal.* **21**, 394-404
74. Yoshimura, A., Ohkubo, T., Kiguchi, T., Jenkins, N. A., Gilbert, D. J., Copeland, N. G., Hara, T., and Miyajima, A. (1995) *EMBO J.* **14**, 2816-2826
75. Piessevaux, J., Lavens, D., Peelman, F., and Tavernier, J. (2008) *Cytokine Growth Factor Rev* **19**, 371-381
76. Alexander, W. S. (2002) *Nat. Rev Immunol.* **2**, 410-416
77. Babon, J. J., McManus, E. J., Yao, S., DeSouza, D. P., Mielke, L. A., Sprigg, N. S., Willson, T. A., Hilton, D. J., Nicola, N. A., Baca, M., Nicholson, S. E., and Norton, R. S. (2006) *Mol. Cell* **22**, 205-216
78. De, S. D., Fabri, L. J., Nash, A., Hilton, D. J., Nicola, N. A., and Baca, M. (2002) *Biochemistry* **41**, 9229-9236
79. Bos, J. L. (1998) *EMBO J.* **17**, 6776-6782
80. Kubo, M., Hanada, T., and Yoshimura, A. (2003) *Nat. Immunol.* **4**, 1169-1176
81. Elliott, J. and Johnston, J. A. (2004) *Trends Immunol.* **25**, 434-440
82. Seki, Y., Inoue, H., Nagata, N., Hayashi, K., Fukuyama, S., Matsumoto, K., Komine, O., Hamano, S., Himeno, K., Inagaki-Ohara, K., Cacalano, N., O'Garra, A., Oshida, T., Saito, H., Johnston, J. A., Yoshimura, A., and Kubo, M. (2003) *Nat. Med.* **9**, 1047-1054
83. Hilton, D. J., Richardson, R. T., Alexander, W. S., Viney, E. M., Willson, T. A., Sprigg, N. S., Starr, R., Nicholson, S. E., Metcalf, D., and Nicola, N. A. (1998) *Proc. Natl. Acad. Sci. U. S. A* **95**, 114-119
84. Wei, D. and Sun, Y. (2010) *Genes Cancer* **1**, 700-707
85. Bayle, J., Lopez, S., Iwai, K., Dubreuil, P., and De, S. P. (2006) *FEBS Lett.* **580**, 2609-2614
86. Babon, J. J., Sabo, J. K., Zhang, J. G., Nicola, N. A., and Norton, R. S. (2009) *J. Mol. Biol.* **387**, 162-174
87. Ungureanu, D., Saharinen, P., Junttila, I., Hilton, D. J., and Silvennoinen, O. (2002) *Mol. Cell Biol.* **22**, 3316-3326
88. Kamizono, S., Hanada, T., Yasukawa, H., Minoguchi, S., Kato, R., Minoguchi, M., Hattori, K., Hatakeyama, S., Yada, M., Morita, S., Kitamura, T., Kato, H., Nakayama, K., and Yoshimura, A. (2001) *J. Biol. Chem.* **276**, 12530-12538
89. De, S. P., Ilangumaran, S., and Rottapel, R. (2000) *J. Biol. Chem.* **275**, 14005-14008

90. Ryo, A., Suizu, F., Yoshida, Y., Perrem, K., Liou, Y. C., Wulf, G., Rottapel, R., Yamaoka, S., and Lu, K. P. (2003) *Mol. Cell* **12**, 1413-1426
91. Mansell, A., Smith, R., Doyle, S. L., Gray, P., Fenner, J. E., Crack, P. J., Nicholson, S. E., Hilton, D. J., O'Neill, L. A., and Hertzog, P. J. (2006) *Nat. Immunol.* **7**, 148-155
92. Kamio, M., Yoshida, T., Ogata, H., Douchi, T., Nagata, Y., Inoue, M., Hasegawa, M., Yonemitsu, Y., and Yoshimura, A. (2004) *Oncogene* **23**, 3107-3115
93. Zhang, J. G., Metcalf, D., Rakar, S., Asimakis, M., Greenhalgh, C. J., Willson, T. A., Starr, R., Nicholson, S. E., Carter, W., Alexander, W. S., Hilton, D. J., and Nicola, N. A. (2001) *Proc. Natl. Acad. Sci. U. S. A* **98**, 13261-13265
94. Boyle, K., Egan, P., Rakar, S., Willson, T. A., Wicks, I. P., Metcalf, D., Hilton, D. J., Nicola, N. A., Alexander, W. S., Roberts, A. W., and Robb, L. (2007) *Blood* **110**, 1466-1474
95. Croker, B. A., Krebs, D. L., Zhang, J. G., Wormald, S., Willson, T. A., Stanley, E. G., Robb, L., Greenhalgh, C. J., Forster, I., Clausen, B. E., Nicola, N. A., Metcalf, D., Hilton, D. J., Roberts, A. W., and Alexander, W. S. (2003) *Nat. Immunol.* **4**, 540-545
96. Chen, X. P., Losman, J. A., Cowan, S., Donahue, E., Fay, S., Vuong, B. Q., Nawijn, M. C., Capece, D., Cohan, V. L., and Rothman, P. (2002) *Proc. Natl. Acad. Sci. U. S. A* **99**, 2175-2180
97. Sasaki, A., Inagaki-Ohara, K., Yoshida, T., Yamanaka, A., Sasaki, M., Yasukawa, H., Koromilas, A. E., and Yoshimura, A. (2003) *J. Biol. Chem.* **278**, 2432-2436
98. Woelk, T., Sigismund, S., Penengo, L., and Polo, S. (2007) *Cell Div* **2**, 11
99. Kamura, T., Sato, S., Haque, D., Liu, L., Kaelin, W. G., Jr., Conaway, R. C., and Conaway, J. W. (1998) *Genes Dev.* **12**, 3872-3881
100. Haan, S., Ferguson, P., Sommer, U., Hiremath, M., McVicar, D. W., Heinrich, P. C., Johnston, J. A., and Cacalano, N. A. (2003) *J. Biol. Chem.* **278**, 31972-31979
101. Kamura, T., Maenaka, K., Kotoshiba, S., Matsumoto, M., Kohda, D., Conaway, R. C., Conaway, J. W., and Nakayama, K. I. (2004) *Genes Dev.* **18**, 3055-3065
102. Kiu, H., Greenhalgh, C. J., Thaus, A., Hilton, D. J., Nicola, N. A., Alexander, W. S., and Roberts, A. W. (2009) *Growth Factors* **27**, 384-393
103. Tannahill, G. M., Elliott, J., Barry, A. C., Hibbert, L., Cacalano, N. A., and Johnston, J. A. (2005) *Mol. Cell Biol* **25**, 9115-9126
104. Houslay, M. D., Baillie, G. S., and Maurice, D. H. (2007) *Circ. Res.* **100**, 950-966

105. Kaupp, U. B. and Seifert, R. (2002) *Physiol Rev.* **82**, 769-824
106. Tasken, K. and Aandahl, E. M. (2004) *Physiol Rev.* **84**, 137-167
107. de, R. J., Zwartkruis, F. J., Verheijen, M. H., Cool, R. H., Nijman, S. M., Wittinghofer, A., and Bos, J. L. (1998) *Nature* **396**, 474-477
108. Kawasaki, H., Springett, G. M., Mochizuki, N., Toki, S., Nakaya, M., Matsuda, M., Housman, D. E., and Graybiel, A. M. (1998) *Science* **282**, 2275-2279
109. Pham, N., Cheglakov, I., Koch, C. A., de Hoog, C. L., Moran, M. F., and Rotin, D. (2000) *Curr. Biol* **10**, 555-558
110. Amsen, E. M., Pham, N., Pak, Y., and Rotin, D. (2006) *J. Biol. Chem.* **281**, 121-128
111. Beene, D. L. and Scott, J. D. (2007) *Curr. Opin. Cell Biol.* **19**, 192-198
112. Cheng, X., Ji, Z., Tsalkova, T., and Mei, F. (2008) *Acta Biochim. Biophys. Sin. (Shanghai)* **40**, 651-662
113. Mayr, B. and Montminy, M. (2001) *Nat. Rev. Mol. Cell Biol.* **2**, 599-609
114. Borland, G., Smith, B. O., and Yarwood, S. J. (2009) *Br. J. Pharmacol.* 2009. Feb. 6.
115. Moore, A. R. and Willoughby, D. A. (1995) *Clin. Exp. Immunol.* **101**, 387-389
116. Kooistra, M. R., Corada, M., Dejana, E., and Bos, J. L. (2005) *FEBS Lett.* **579**, 4966-4972
117. Gasperini, S., Crepaldi, L., Calzetti, F., Gatto, L., Berlato, C., Bazzoni, F., Yoshimura, A., and Cassatella, M. A. (2002) *Eur. Cytokine Netw.* **13**, 47-53
118. Woolson, H. D., Thomson, V. S., Rutherford, C., Yarwood, S. J., and Palmer, T. M. (2009) *Cell Signal.* **21**, 1706-1715
119. Yarwood, S. J., Borland, G., Sands, W. A., and Palmer, T. M. (2008) *J. Biol. Chem* **283**, 6843-6853
120. Borland, G., Bird, R. J., Palmer, T. M., and Yarwood, S. J. (2009) *J. Biol. Chem.* **284**, 17391-17403
121. Wiejak, J., Dunlop, J., Gao, S., Borland, G., and Yarwood, S. J. (2012) *Mol. Pharmacol.* **81**, 657-668
122. Wiejak, J., Dunlop, J., Stoye, C., Lappin, G., Mcllroy, A., Pediani, J. D., Gao, S., and Yarwood, S. J. (2012) *Cell Signal.* **24**, 1690-1699
123. Babon, J. J., Kershaw, N. J., Murphy, J. M., Varghese, L. N., Laktyushin, A., Young, S. N., Lucet, I. S., Norton, R. S., and Nicola, N. A. (2012) *Immunity.* **36**, 239-250

124. Suzuki, A., Hanada, T., Mitsuyama, K., Yoshida, T., Kamizono, S., Hoshino, T., Kubo, M., Yamashita, A., Okabe, M., Takeda, K., Akira, S., Matsumoto, S., Toyonaga, A., Sata, M., and Yoshimura, A. (2001) *J. Exp. Med.* **193**, 471-481
125. Yasukawa, H., Ohishi, M., Mori, H., Murakami, M., Chinen, T., Aki, D., Hanada, T., Takeda, K., Akira, S., Hoshijima, M., Hirano, T., Chien, K. R., and Yoshimura, A. (2003) *Nat. Immunol.* **4**, 551-556
126. Pasterkamp, G. and Falk, E. (2000) *Journal of Clinical and Basic Cardiology* **3**, 81-86
127. Croker, B. A., Metcalf, D., Robb, L., Wei, W., Mifsud, S., DiRago, L., Cluse, L. A., Sutherland, K. D., Hartley, L., Williams, E., Zhang, J. G., Hilton, D. J., Nicola, N. A., Alexander, W. S., and Roberts, A. W. (2004) *Immunity.* **20**, 153-165
128. Ramgolam, V. S. and Markovic-Plese, S. (2011) *J. Signal. Transduct.* **2011**, 635721
129. Chen, Z., Laurence, A., Kanno, Y., Pacher-Zavisin, M., Zhu, B. M., Tato, C., Yoshimura, A., Hennighausen, L., and O'Shea, J. J. (2006) *Proc. Natl. Acad. Sci. U. S. A* **103**, 8137-8142
130. Shouda, T., Yoshida, T., Hanada, T., Wakioka, T., Oishi, M., Miyoshi, K., Komiya, S., Kosai, K., Hanakawa, Y., Hashimoto, K., Nagata, K., and Yoshimura, A. (2001) *J. Clin. Invest* **108**, 1781-1788
131. Fang, M., Dai, H., Yu, G., and Gong, F. (2005) *Cell Mol. Immunol.* **2**, 373-377
132. Jo, D., Liu, D., Yao, S., Collins, R. D., and Hawiger, J. (2005) *Nat. Med.* **11**, 892-898
133. Weitz-Schmidt, G. (2002) *Trends Pharmacol. Sci.* **23**, 482-486
134. Lazzerini, P. E., Lorenzini, S., Selvi, E., Capecchi, P. L., Chindamo, D., Bisogno, S., Ghittoni, R., Natale, M. R., Caporali, F., Giuntini, S., Marcolongo, R., Galeazzi, M., and Laghi-Pasini, F. (2007) *Clin. Exp. Rheumatol.* **25**, 696-700
135. Ikeda, M., Ikeda, A., and Longnecker, R. (2002) *Virology* **300**, 153-159
136. Koegl, M., Hoppe, T., Schlenker, S., Ulrich, H. D., Mayer, T. U., and Jentsch, S. (1999) *Cell* **96**, 635-644
137. Chau, V., Tobias, J. W., Bachmair, A., Marriott, D., Ecker, D. J., Gonda, D. K., and Varshavsky, A. (1989) *Science* **243**, 1576-1583
138. Bedford, L., Layfield, R., Mayer, R. J., Peng, J., and Xu, P. (2011) *Neurosci. Lett.* **491**, 44-47
139. Pan, Z. Q., Kentsis, A., Dias, D. C., Yamoah, K., and Wu, K. (2004) *Oncogene* **23**, 1985-1997

140. Nijman, S. M., Luna-Vargas, M. P., Velds, A., Brummelkamp, T. R., Dirac, A. M., Sixma, T. K., and Bernards, R. (2005) *Cell* **123**, 773-786
141. Sun, S. C. (2008) *Nat. Rev. Immunol.* **8**, 501-511
142. Reiley, W. W., Zhang, M., Jin, W., Losiewicz, M., Donohue, K. B., Norbury, C. C., and Sun, S. C. (2006) *Nat. Immunol.* **7**, 411-417
143. Hurley, J. H., Lee, S., and Prag, G. (2006) *Biochem. J.* **399**, 361-372
144. Wertz, I. E. and Dixit, V. M. (2010) *Cold Spring Harb. Perspect. Biol.* **2**, a003350
145. Maine, G. N., Mao, X., Komarck, C. M., and Burstein, E. (2007) *EMBO J.* **26**, 436-447
146. Wertz, I. E., O'Rourke, K. M., Zhou, H., Eby, M., Aravind, L., Seshagiri, S., Wu, P., Wiesmann, C., Baker, R., Boone, D. L., Ma, A., Koonin, E. V., and Dixit, V. M. (2004) *Nature* **430**, 694-699
147. Kovalenko, A., Chable-Bessia, C., Cantarella, G., Israel, A., Wallach, D., and Courtois, G. (2003) *Nature* **424**, 801-805
148. Doffinger, R., Smahi, A., Bessia, C., Geissmann, F., Feinberg, J., Durandy, A., Bodemer, C., Kenwrick, S., Dupuis-Girod, S., Blanche, S., Wood, P., Rabia, S. H., Headon, D. J., Overbeek, P. A., Le, D. F., Holland, S. M., Belani, K., Kumararatne, D. S., Fischer, A., Shapiro, R., Conley, M. E., Reimund, E., Kalhoff, H., Abinun, M., Munnich, A., Israel, A., Courtois, G., and Casanova, J. L. (2001) *Nat. Genet.* **27**, 277-285
149. Lee, E. G., Boone, D. L., Chai, S., Libby, S. L., Chien, M., Lodolce, J. P., and Ma, A. (2000) *Science* **289**, 2350-2354
150. Gerlach, B., Cordier, S. M., Schmukle, A. C., Emmerich, C. H., Rieser, E., Haas, T. L., Webb, A. I., Rickard, J. A., Anderton, H., Wong, W. W., Nachbur, U., Gangoda, L., Warnken, U., Purcell, A. W., Silke, J., and Walczak, H. (2011) *Nature* **471**, 591-596
151. Walczak, H., Iwai, K., and Dikic, I. (2012) *BMC. Biol.* **10**, 23
152. Vassilev, L. T., Vu, B. T., Graves, B., Carvajal, D., Podlaski, F., Filipovic, Z., Kong, N., Kammlott, U., Lukacs, C., Klein, C., Fotouhi, N., and Liu, E. A. (2004) *Science* **303**, 844-848
153. Willems, A. R., Schwab, M., and Tyers, M. (2004) *Biochim. Biophys. Acta* **1695**, 133-170
154. Swinney, D. C., Xu, Y. Z., Scarafia, L. E., Lee, I., Mak, A. Y., Gan, Q. F., Ramesha, C. S., Mulkins, M. A., Dunn, J., So, O. Y., Biegel, T., Dinh, M., Volkell, P., Barnett, J., Dalrymple, S. A., Lee, S., and Huber, M. (2002) *J. Biol. Chem.* **277**, 23573-23581
155. Tanaka, K. (2009) *Proc. Jpn. Acad. Ser. B Phys. Biol. Sci.* **85**, 12-36

156. Adams, J. (2003) *Cancer Treat. Rev.* **29 Suppl 1**, 3-9
157. Nalepa, G. and Wade, H. J. (2003) *Cancer Treat. Rev.* **29 Suppl 1**, 49-57
158. Stoiber, D., Kovarik, P., Cohney, S., Johnston, J. A., Steinlein, P., and Decker, T. (1999) *J. Immunol.* **163**, 2640-2647
159. Emanuelli, B., Peraldi, P., Filloux, C., Chavey, C., Freidinger, K., Hilton, D. J., Hotamisligil, G. S., and Van, O. E. (2001) *J. Biol. Chem.* **276**, 47944-47949
160. Emanuelli, B., Peraldi, P., Filloux, C., Sawka-Verhelle, D., Hilton, D., and Van, O. E. (2000) *J. Biol. Chem.* **275**, 15985-15991
161. Kolenko, V., Rayman, P., Roy, B., Cathcart, M. K., O'Shea, J., Tubbs, R., Rybicki, L., Bukowski, R., and Finke, J. (1999) *Blood* **93**, 2308-2318
162. Tanaka, Y., Tanaka, N., Saeki, Y., Tanaka, K., Murakami, M., Hirano, T., Ishii, N., and Sugamura, K. (2008) *Mol. Cell Biol.* **28**, 4805-4818
163. Ong, S. E., Blagoev, B., Kratchmarova, I., Kristensen, D. B., Steen, H., Pandey, A., and Mann, M. (2002) *Mol. Cell Proteomics* **1**, 376-386
164. Tuli, L. and Ressom, H. W. (2009) *Journal of Proteomics & Bioinformatics* **2**, 416-438
165. Ong, S. E., Kratchmarova, I., and Mann, M. (2003) *J. Proteome. Res.* **2**, 173-181
166. Scott, L., Lamb, J., Smith, S., and Wheatley, D. N. (2000) *Br. J. Cancer* **83**, 800-810
167. Olsen, J. V., Ong, S. E., and Mann, M. (2004) *Mol. Cell Proteomics.* **3**, 608-614
168. Meierhofer, D., Wang, X., Huang, L., and Kaiser, P. (2008) *J. Proteome. Res* **7**, 4566-4576
169. Bendall, S. C., Hughes, C., Stewart, M. H., Doble, B., Bhatia, M., and Lajoie, G. A. (2008) *Mol. Cell Proteomics.* **7**, 1587-1597
170. Cox, J. and Mann, M. (2008) *Nat. Biotechnol.* **26**, 1367-1372
171. Ong, S. E. and Mann, M. (2006) *Nat. Protoc.* **1**, 2650-2660
172. Van, H. D., Pinkse, M. W., Oostwaard, D. W., Mummery, C. L., Heck, A. J., and Krijgsveld, J. (2007) *Nat. Methods* **4**, 677-678
173. Bicho, C. C., de Lima, A. F., Chen, Z. A., Rappsilber, J., and Sawin, K. E. (2010) *Mol. Cell Proteomics.* **9**, 1567-1577
174. Puig, O., Caspary, F., Rigaut, G., Rutz, B., Bouveret, E., Bragado-Nilsson, E., Wilm, M., and Seraphin, B. (2001) *Methods* **24**, 218-229

175. Tagwerker, C., Flick, K., Cui, M., Guerrero, C., Dou, Y., Auer, B., Baldi, P., Huang, L., and Kaiser, P. (2006) *Mol. Cell Proteomics* **5**, 737-748
176. Cronan, J. E., Jr. (1990) *J. Biol. Chem.* **265**, 10327-10333
177. Glish, G. L. and Vachet, R. W. (2003) *Nat. Rev. Drug Discov.* **2**, 140-150
178. Yates, J. R., Ruse, C. I., and Nakorchevsky, A. (2009) *Annu. Rev. Biomed. Eng* **11**, 49-79
179. Gruhler, A., Olsen, J. V., Mohammed, S., Mortensen, P., Faergeman, N. J., Mann, M., and Jensen, O. N. (2005) *Mol. Cell Proteomics.* **4**, 310-327
180. Perkins, D. N., Pappin, D. J., Creasy, D. M., and Cottrell, J. S. (1999) *Electrophoresis* **20**, 3551-3567
181. Mahrouf, N., Redwine, W. B., Florens, L., Swanson, S. K., Martin-Brown, S., Bradford, W. D., Staehling-Hampton, K., Washburn, M. P., Conaway, R. C., and Conaway, J. W. (2008) *J. Biol. Chem.* **283**, 8005-8013
182. Liu, L. and Pilch, P. F. (2008) *J. Biol. Chem.* **283**, 4314-4322
183. Pelzer, C., Kassner, I., Matentzoglou, K., Singh, R. K., Wollscheid, H. P., Scheffner, M., Schmidtke, G., and Groettrup, M. (2007) *J. Biol. Chem.* **282**, 23010-23014
184. Kampinga, H. H., Kanon, B., Salomons, F. A., Kabakov, A. E., and Patterson, C. (2003) *Mol. Cell Biol.* **23**, 4948-4958
185. Boeddrich, A., Gaumer, S., Haacke, A., Tzvetkov, N., Albrecht, M., Evert, B. O., Muller, E. C., Lurz, R., Breuer, P., Schugardt, N., Plassmann, S., Xu, K., Warrick, J. M., Suopanki, J., Wullner, U., Frank, R., Hartl, U. F., Bonini, N. M., and Wanker, E. E. (2006) *EMBO J.* **25**, 1547-1558
186. Polo, S., Sigismund, S., Faretta, M., Guidi, M., Capua, M. R., Bossi, G., Chen, H., De, C. P., and Di Fiore, P. P. (2002) *Nature* **416**, 451-455
187. Klapisz, E., Sorokina, I., Lemeer, S., Pijnenburg, M., Verkleij, A. J., and van Bergen en Henegouwen PM (2002) *J. Biol. Chem.* **277**, 30746-30753
188. Nicassio, F., Corrado, N., Vissers, J. H., Areces, L. B., Bergink, S., Marteijn, J. A., Geverts, B., Houtsmuller, A. B., Vermeulen, W., Di Fiore, P. P., and Citterio, E. (2007) *Curr. Biol.* **17**, 1972-1977
189. Ardley, H. C., Scott, G. B., Rose, S. A., Tan, N. G., and Robinson, P. A. (2004) *J. Neurochem.* **90**, 379-391
190. Dubielecka, P. M., Ladwein, K. I., Xiong, X., Migeotte, I., Chorzalska, A., Anderson, K. V., Sawicki, J. A., Rottner, K., Stradal, T. E., and Kotula, L. (2011) *Proc. Natl. Acad. Sci. U. S. A* **108**, 7022-7027
191. Mosmann, T. (1983) *J. Immunol. Methods* **65**, 55-63

192. Smith, P. K., Krohn, R. I., Hermanson, G. T., Mallia, A. K., Gartner, F. H., Provenzano, M. D., Fujimoto, E. K., Goeke, N. M., Olson, B. J., and Klenk, D. C. (1985) *Anal. Biochem.* **150**, 76-85
193. Cox, J., Neuhauser, N., Michalski, A., Scheltema, R. A., Olsen, J. V., and Mann, M. (2011) *J. Proteome. Res* **10**, 1794-1805
194. Babon, J. J., Sabo, J. K., Soetopo, A., Yao, S., Bailey, M. F., Zhang, J. G., Nicola, N. A., and Norton, R. S. (2008) *J. Mol. Biol.* **381**, 928-940
195. Reijns, M. A., Bubeck, D., Gibson, L. C., Graham, S. C., Baillie, G. S., Jones, E. Y., and Jackson, A. P. (2011) *J. Biol. Chem.* **286**, 10530-10539
196. Bolger, G. B., Baillie, G. S., Li, X., Lynch, M. J., Herzyk, P., Mohamed, A., Mitchell, L. H., McCahill, A., Hundsrucker, C., Klusmann, E., Adams, D. R., and Houslay, M. D. (2006) *Biochem. J.* **398**, 23-36
197. Jimenez, A., Carrasco, L., and Vazquez, D. (1977) *Biochemistry* **16**, 4727-4730
198. Madjar, J. J., Frahm, M., McGill, S., and Roufa, D. J. (1983) *Mol. Cell Biol.* **3**, 190-197
199. Mohamed-Ali, V., Pinkney, J. H., and Coppack, S. W. (1998) *Int. J. Obes. Relat Metab Disord.* **22**, 1145-1158
200. Nicholson, S. E., De, S. D., Fabri, L. J., Corbin, J., Willson, T. A., Zhang, J. G., Silva, A., Asimakis, M., Farley, A., Nash, A. D., Metcalf, D., Hilton, D. J., Nicola, N. A., and Baca, M. (2000) *Proc. Natl. Acad. Sci. U. S. A* **97**, 6493-6498
201. Wolfler, A., Irandoust, M., Meenhuis, A., Gits, J., Roovers, O., and Touw, I. P. (2009) *Traffic.* **10**, 1168-1179
202. Lignitto, L., Carlucci, A., Sepe, M., Stefan, E., Cuomo, O., Nistico, R., Scorziello, A., Savoia, C., Garbi, C., Annunziato, L., and Feliciello, A. (2011) *Nat. Cell Biol* **13**, 412-422
203. Tagwerker, C., Zhang, H., Wang, X., Larsen, L. S., Lathrop, R. H., Hatfield, G. W., Auer, B., Huang, L., and Kaiser, P. (2006) *Yeast* **23**, 623-632
204. Heffetz, D., Bushkin, I., Dror, R., and Zick, Y. (1990) *J. Biol Chem* **265**, 2896-2902
205. Zick, Y. and Sagi-Eisenberg, R. (1990) *Biochemistry* **29**, 10240-10245
206. Tarcic, G., Boguslavsky, S. K., Wakim, J., Kiuchi, T., Liu, A., Reinitz, F., Nathanson, D., Takahashi, T., Mischel, P. S., Ng, T., and Yarden, Y. (2009) *Curr. Biol* **19**, 1788-1798
207. Uniprot - Protein Knowledgebase (2012) GAPDH - P04406 (G3P_HUMAN).

208. Berg, J. M., Tymoczko, J. L., and Stryer, L. (2002) *Biochemistry*, Fifth Ed. Ed., W. H. Freeman and Co, New York
209. Gevaert, K., Impens, F., Ghesquiere, B., Van, D. P., Lambrechts, A., and Vandekerckhove, J. (2008) *Proteomics* **8**, 4873-4885
210. Rybak, J. N., Scheurer, S. B., Neri, D., and Elia, G. (2004) *Proteomics*. **4**, 2296-2299
211. Holmberg, A., Blomstergren, A., Nord, O., Lukacs, M., Lundeberg, J., and Uhlen, M. (2005) *Electrophoresis* **26**, 501-510
212. Ziv, I., Matiuhin, Y., Kirkpatrick, D. S., Erpapazoglou, Z., Leon, S., Pantazopoulou, M., Kim, W., Gygi, S. P., Haguener-Tsapis, R., Reis, N., Glickman, M. H., and Kleifeld, O. (2011) *Mol. Cell Proteomics*. **10**, M111
213. Bell, A. W., Deutsch, E. W., Au, C. E., Kearney, R. E., Beavis, R., Sechi, S., Nilsson, T., and Bergeron, J. J. (2009) *Nat. Methods* **6**, 423-430
214. Colaert, N., Van, H. C., Degroeve, S., Staes, A., Vandekerckhove, J., Gevaert, K., and Martens, L. (2011) *Nat. Methods*
215. Hor, S., Ziv, T., Admon, A., and Lehner, P. J. (2009) *Mol. Cell Proteomics*. **8**, 1959-1971
216. Thakur, S. S., Geiger, T., Chatterjee, B., Bandilla, P., Frohlich, F., Cox, J., and Mann, M. (2011) *Mol. Cell Proteomics*. **10**, M110
217. Vinten, J., Johnsen, A. H., Roepstorff, P., Harpoth, J., and Trantum-Jensen, J. (2005) *Biochim. Biophys. Acta* **1717**, 34-40
218. Chidlow, J. H., Jr. and Sessa, W. C. (2010) *Cardiovasc. Res.* **86**, 219-225
219. Bastiani, M., Liu, L., Hill, M. M., Jedrychowski, M. P., Nixon, S. J., Lo, H. P., Abankwa, D., Luetterforst, R., Fernandez-Rojo, M., Breen, M. R., Gygi, S. P., Vinten, J., Walser, P. J., North, K. N., Hancock, J. F., Pilch, P. F., and Parton, R. G. (2009) *J. Cell Biol.* **185**, 1259-1273
220. Davalos, A., Fernandez-Hernando, C., Sowa, G., Derakhshan, B., Lin, M. I., Lee, J. Y., Zhao, H., Luo, R., Colangelo, C., and Sessa, W. C. (2010) *Mol. Cell Proteomics*. **9**, 2109-2124
221. Hansen, C. G. and Nichols, B. J. (2010) *Trends Cell Biol.* **20**, 177-186
222. Aboulaich, N., Vainonen, J. P., Stralfors, P., and Vener, A. V. (2004) *Biochem. J.* **383**, 237-248
223. Jansa, P., Mason, S. W., Hoffmann-Rohrer, U., and Grummt, I. (1998) *EMBO J.* **17**, 2855-2864
224. Razani, B., Woodman, S. E., and Lisanti, M. P. (2002) *Pharmacol. Rev.* **54**, 431-467
225. Sowa, G. (2012) *Front Physiol* **2**, 120

226. Liu, L., Brown, D., McKee, M., Lebrasseur, N. K., Yang, D., Albrecht, K. H., Ravid, K., and Pilch, P. F. (2008) *Cell Metab* **8**, 310-317
227. Hill, M. M., Bastiani, M., Luetterforst, R., Kirkham, M., Kirkham, A., Nixon, S. J., Walser, P., Abankwa, D., Oorschot, V. M., Martin, S., Hancock, J. F., and Parton, R. G. (2008) *Cell* **132**, 113-124
228. Engelman, J. A., Chu, C., Lin, A., Jo, H., Ikezu, T., Okamoto, T., Kohtz, D. S., and Lisanti, M. P. (1998) *FEBS Lett.* **428**, 205-211
229. Jasmin, J. F., Mercier, I., Sotgia, F., and Lisanti, M. P. (2006) *Trends Endocrinol. Metab* **17**, 150-158
230. Sedding, D. G., Hermsen, J., Seay, U., Eickelberg, O., Kummer, W., Schwencke, C., Strasser, R. H., Tillmanns, H., and Braun-Dullaeus, R. C. (2005) *Circ. Res.* **96**, 635-642
231. Salani, B., Briatore, L., Contini, P., Passalacqua, M., Melloni, E., Paggi, A., Cordera, R., and Maggi, D. (2009) *Biochem. Biophys. Res. Commun.* **380**, 489-492
232. Chen, S. F., Liou, J. Y., Huang, T. Y., Lin, Y. S., Yeh, A. L., Tam, K., Tsai, T. H., Wu, K. K., and Shyue, S. K. (2010) *J. Cell Biochem.* **109**, 356-362
233. Vassilieva, E. V., Gerner-Smidt, K., Ivanov, A. I., and Nusrat, A. (2008) *Am. J. Physiol Gastrointest. Liver Physiol* **295**, G965-G976
234. Park, D. S., Lee, H., Frank, P. G., Razani, B., Nguyen, A. V., Parlow, A. F., Russell, R. G., Hulit, J., Pestell, R. G., and Lisanti, M. P. (2002) *Mol. Biol. Cell* **13**, 3416-3430
235. Yuan, K., Huang, C., Fox, J., Gaid, M., Weaver, A., Li, G., Singh, B. B., Gao, H., and Wu, M. (2011) *J. Biol. Chem.* **286**, 21814-21825
236. Fagerholm, S., Ortegren, U., Karlsson, M., Ruishalme, I., and Stralfors, P. (2009) *PLoS. One.* **4**, e5985
237. Frank, P. G., Pavlides, S., Cheung, M. W., Daumer, K., and Lisanti, M. P. (2008) *Am. J. Physiol Cell Physiol* **295**, C242-C248
238. Bai, L., Deng, X., Li, Q., Wang, M., An, W., Deli, A., Gao, Z., Xie, Y., Dai, Y., and Cong, Y. S. (2012) *J. Cell Biochem.* **113**, 322-328
239. Gamez-Pozo, A., Sanchez-Navarro, I., Calvo, E., Agullo-Ortuno, M. T., Lopez-Vacas, R., Diaz, E., Camafeita, E., Nistal, M., Madero, R., Espinosa, E., Lopez, J. A., and Fresno Vara, J. A. (2012) *PLoS. One.* **7**, e33752
240. Gould, M. L., Williams, G., and Nicholson, H. D. (2010) *Prostate* **70**, 1609-1621
241. Hill, M. M., Daud, N. H., Aung, C. S., Loo, D., Martin, S., Murphy, S., Black, D. M., Barry, R., Simpson, F., Liu, L., Pilch, P. F., Hancock, J. F., Parat, M. O., and Parton, R. G. (2012) *PLoS. One.* **7**, e43041

242. Hartl, F. U. and Hayer-Hartl, M. (2002) *Science* **295**, 1852-1858
243. Shiota, M., Kusakabe, H., Izumi, Y., Hikita, Y., Nakao, T., Funae, Y., Miura, K., and Iwao, H. (2010) *Arterioscler. Thromb. Vasc. Biol.* **30**, 491-497
244. Ding, Y., Li, M., Zhang, J., Li, N., Xia, Z., Hu, Y., Wang, S., and Fan, G. H. (2006) *Mol. Pharmacol.* **69**, 1269-1279
245. Sarrio, S., Casado, V., Escriche, M., Ciruela, F., Mallol, J., Canela, E. I., Lluís, C., and Franco, R. (2000) *Mol. Cell Biol.* **20**, 5164-5174
246. Pierconti, F., Martini, M., Pinto, F., Cenci, T., Capodimonti, S., Calarco, A., Bassi, P. F., and Larocca, L. M. (2011) *Prostate* **71**, 318-325
247. Dammer, E. B., Na, C. H., Xu, P., Seyfried, N. T., Duong, D. M., Cheng, D., Gearing, M., Rees, H., Lah, J. J., Levey, A. I., Rush, J., and Peng, J. (2011) *J. Biol. Chem.* **286**, 10457-10465
248. Hayes, G. R. and Lockwood, D. H. (1987) *Proc. Natl. Acad. Sci. U. S. A* **84**, 8115-8119
249. Wilson, L. S., Baillie, G. S., Pritchard, L. M., Umana, B., Terrin, A., Zaccolo, M., Houslay, M. D., and Maurice, D. H. (2011) *J. Biol. Chem.* **286**, 16285-16296
250. Hunter, T. and Plowman, G. D. (1997) *Trends Biochem. Sci.* **22**, 18-22
251. Pilch, P. F., Souto, R. P., Liu, L., Jedrychowski, M. P., Berg, E. A., Costello, C. E., and Gygi, S. P. (2007) *J. Lipid Res.* **48**, 2103-2111
252. Aboulaich, N., Ortegren, U., Vener, A. V., and Stralfors, P. (2006) *Biochem. Biophys. Res. Commun.* **350**, 657-661
253. Sehgal, P. B. (2003) *Acta Biochim. Pol.* **50**, 583-594
254. Sowa, G., Pypaert, M., and Sessa, W. C. (2001) *Proc. Natl. Acad. Sci. U. S. A* **98**, 14072-14077